PROCEEDING

THE 2nd INTERNATIONAL CONFERENCE ON SCIENCE AND TECHNOLOGY

Science and Technology for Nation Prosperity

2019

Bengkulu, 6th -7th July 2019

RISTEKDIKTI

Faculty of Mathematics and Natural Sciences

UNIVERSITY OF BENGKULU

PROCEEDING

THE 2nd INTERNATIONAL CONFERENCE ON SCIENCE AND TECHNOLOGY

"SCIENCE AND TECHNOLOGY FOR NATION PROSPERITY"

Bengkulu, Indonesia
6th-7th July 2019

Editor

Nur Afandi, S.Si., M.Sc.
Nanang Sugianto, S.Si., M.Sc.
Deni Agustriawan, S.Si., M.Sc.
Santi Nurul Kamilah, S.Si., M.Si.
Dyah Setyo Rini, S.Si., M.Sc.
Suhendra, S.Si., MT.

Publisher

UNIB PRESS

Proceeding The 2nd International Conference on Science and Technology

Publisher
UNIB Press
LPPM UNIB
University of Bengkulu, WR Supratman street, Kandang Limun Bengkulu City 38371

Published in June 2020

Organizer
Faculty of Mathematics and Natural Sciences, University of Bengkulu
W.R. Supratman Street, Kandang Limun, Bengkulu City. 38371.

Proceeding The 2nd International Conference on Science dan Technology
Bengkulu 6th-7th July 2019
ISBN : 978-602-5830-19-8

ISBN 978-602-5830-19-8 (PDF)

9 786025 830198

FOREWORD

All praises be to the Almighty God, for all His grace and guidance, proceeding of the 2nd International Conference on Science and Technology with the theme "Science and Technology for Nation Prosperity" can be completed. This proceeding is a collection of papers held by the Mathematics and Natural Science, University of Bengkulu on 6th – 7th July 2019 at GRAGE Hotel Bengkulu.

Our highest gratitude and appreciation goes to the presenters and authors of the papers, as well as the executive committee who have worked hard so that this proceeding can be published. We also thank the Reviewer Board for reviewing all papers so that the quality of the contents of the paper can be maintained and accounted for. Do not forget to all parties who have provided support for the holding of the international conference and the preparation of this proceeding, we thank you.

We do hope that this conference would bring a great opportunity for all of us to strengthen our contribution to the advancement of our nation.

Finally, I hope this proceeding can provide benefits for all.

Bengkulu, June 2020

Publication Committee

COMMITTEE

THE 2nd INTERNATIONAL CONFERENCE ON SCIENCE AND TECHNOLOGY

"Science and Technology for Nation Prosperity"

Organized by Faculty of Mathematics and Natural Sciences, University of Bengkulu

Prof. Dr. Irfan Gustian, M.Si. (Conference General Chair)
Dr. Fanani Haryo Widodo, M.Sc. (Technical Program Chair)
Dr. M. Farid, MS. (Technical Program Chair)
Ramya Rachmawati, S.Si., M.Si., Ph.D. (General Secretary)
Dr. Riska Ekawita, S.Si., M.Si.
Pepi Novianti, S.Si., M.Si.
Suhendra, S.Si., MT.
Dr. Liza Lidiawati, S.Si., M.Si.
Santi Nurul Kamilah, S.Si., M.Si.
Dyah Setyo Rini, S.Si., M.Sc.
Nur Afandi, S.Si., M.Sc.
Nanang Sugianto, S.Si., M.Sc.
Dr. Risky Hadi Wibowo, M.Si.
Siska Yosmar, S.Si., M.Si.
Dr. Elfi Yuliza, S.Si., M.Si.
Ulfasari Rafflesia, S.Si., M.Si.
Drs. Hery Haryanto, M.Sc.
Etis Sunandi, S.Si., M.Si.
Idhia Sriliana, S.Si., M.Si.
Nori Wirahmi, S.Si., M.Farm, Apt.
Dian Agustina, S.Si., M.Sc.
Ashar Muda Lubis, S.Si., M.Sc., Ph.D.
Dr. Mulia Astuti, S.Si., M.Si.
Dr. Eng Asdim, S.Si., M.Si.
Drs. Choirul Muslim, SU., Ph.D.
Faisal Hadi, MT.
Fachri Faisal, S.Si., M.Si.
Zulfia Memi Mayasari, S.Si., M.Si.
Herlin Fransiska, S.Si., M.Si.
Dr. Arif Ismul Hadi, S.Si, M.Si.
Ghufira, S.Si., M.Si.

KEYNOTE SPEAKER

1. Prof. Sudarsanam (Sri Venkateswara University, INDIA),
2. Prof. Martianus Frederick Ezerman (Nanyang Technology University, SINGAPORE)
3. Bambang Sumintono, Ph.D. (Universiti Malaya, MALAYSIA)
4. Assoc. Prof. Dr. Oki Muraza (King Fahd University of Petroleum and Minerals, Dhahran, SAUDI ARABIA)

INVITED SPEAKER

Dr. Nampiah Sukarno (Bogor Agricultural University, INDONESIA)

TABLE OF CONTENTS

Biology

INTERNATIONAL PROCEEDING
The 2nd International Conference on Science and Technology (ICST)
ISBN: ISBN: 978-602-5830-19-8, June 2020

Secondary Particle-Based Radioisotope Production: Theoretical Approach

H Suryanto*, I Kambali

Center for Radioisotope and Radiopharmaceutical Technology, National Nuclear Energy Agency (BATAN), Puspiptek Area, Serpong, South Tangerang, Indonesia

*E-mail: harisur@batan.go.id

Abstract. Radioisotopes used in nuclear medicine are mostly produced by cyclotron or nuclear reactor using primary particle beams. In this work, we investigated a novel method for radioisotope production using secondary beam of particles. Proton beam was simulated as the primary beams to hit beryllium target. Using the TALYS 2017 software, the predicted nuclear reactions were studied. Based on the calculations, there were several secondary particles produced during the bombardment, including neutron (n), alpha (α), deuteron (d), triton (t), and ^{3}He. There secondary particles were found to have significantly high cross-section; thus, they could be used for medical radioisotope production. In this case, radioisotopes produced during proton bombardment of ^{9}Be were ^{9}B which was generated via ^{9}Be(p,n)^{9}B nuclear reaction, ^{6}Li as a result of ^{9}Be(p, α)^{6}Li reaction, ^{8}Be from ^{9}Be(p, d)^{8}Be reaction and ^{7}Be due to ^{9}Be(p,t)^{7}Be. Both ^{6}Li and ^{7}Li are stable isotopes whereas ^{7}Be is a long-lived radioisotope emitting γ at half-life of 53.12 days and ^{8}Be is α emitting radioisotope with half-life of 8.19×10^{-17} seconds. From the calculation it is clear that secondary particles such as n, α, d, t and ^{3}He resulted from ^{9}Be(p,n)^{9}B might be used for radioisotope production such as ^{177}Lu, ^{153}Sm and ^{211}At. These calculated data could be used as references for future radioisotope production should secondary particles are employed.

1. Introduction

Radioisotopes can be used in various fields including medical, industrial and agricultural applications. In nuclear medicine, radioisotopes such as ^{99m}Tc, ^{18}F, ^{64}Cu, ^{11}C, ^{123}I, ^{125}I, ^{99m}Tc and ^{201}Tl have been routinely produced and used for diagnosis of various diseases such as cancer imaging, brain imaging, stroke imaging, alzheimer's disease imaging, thyroid imaging, etc. [1-7]. Some radioisotopes such as ^{131}I, ^{177}Lu are employed in cancer therapy and thyroid disease therapy [8-10], while other radioisotopes such as ^{153}Sm, ^{32}P, ^{188}Re and ^{223}Ra are used for palliative therapy of bone meta states [11-15].

There are two most common ways of producing radioisotopes, either by neutron activation using nuclear reactor or charged particle bombardment using cyclotron or accelerator. Radioisotopes produced using nuclear reactors include ^{131}I, ^{125}I, ^{99m}Tc, ^{32}P, whereas radioisotopes produced using cyclotrons are ^{18}F, ^{64}Cu, ^{15}O, ^{11}O, ^{68}Ga and ^{111}In.

While there have been overwhelming uses of primary particles for radioisotopes production, there have been very limited references in secondary particle-based radioisotope production, particularly cyclotron-generated secondary particle. The use of secondary neutrons for ^{57}Ni and ^{57}Co have been reported experimentally by Suryanto, et al [16].

In this work, we aim at theoretically studying secondary particles generated from proton irradiated ^{9}Be. By bombarding ^{9}Be with high-energy protons from the cyclotron accelerator, several nuclear reaction modes may occur including reactions (p, n), (p,α), (p,d), (p,t), (p,^{3}He). Where proton beam (p) as primary particles and n, α, d, t, and ^{3}He as secondary particles which will be used for bombarding target to produce radioisotopes. So, with this method allows various medical radioisotopes can be produced. We employ TALYS 2017 software to predict secondary particles emitted by the interaction. As well, proposed radioisotope production by means of secondary particles is also highlighted.

2. Materials and Methods

Nuclear cross-sections for proton-irradiated 9Be were calculated using the TALYS 2017 codes for various nuclear reactions, including (p,n), (p,α), (p,d), (p,t) and (p,3He). The TALYS-Evaluated Nuclear Data Library 2017 (TENDL 2017) could be downloaded online [17]. The TALYS codes have been previously employed to compute the cross-sections of several nuclear reactions as can be found elsewhere [18-24]. Interaction between primary proton beam ranging from 0 to 50 MeV and 9Be target was analyzed from the nuclear cross-sections. Flow chart of the procedure employed in this work are ilustrated in Figure 1 below. The resulted isotopes and secondary particles derived from the TALYS 2017 calculations were also highlighted.

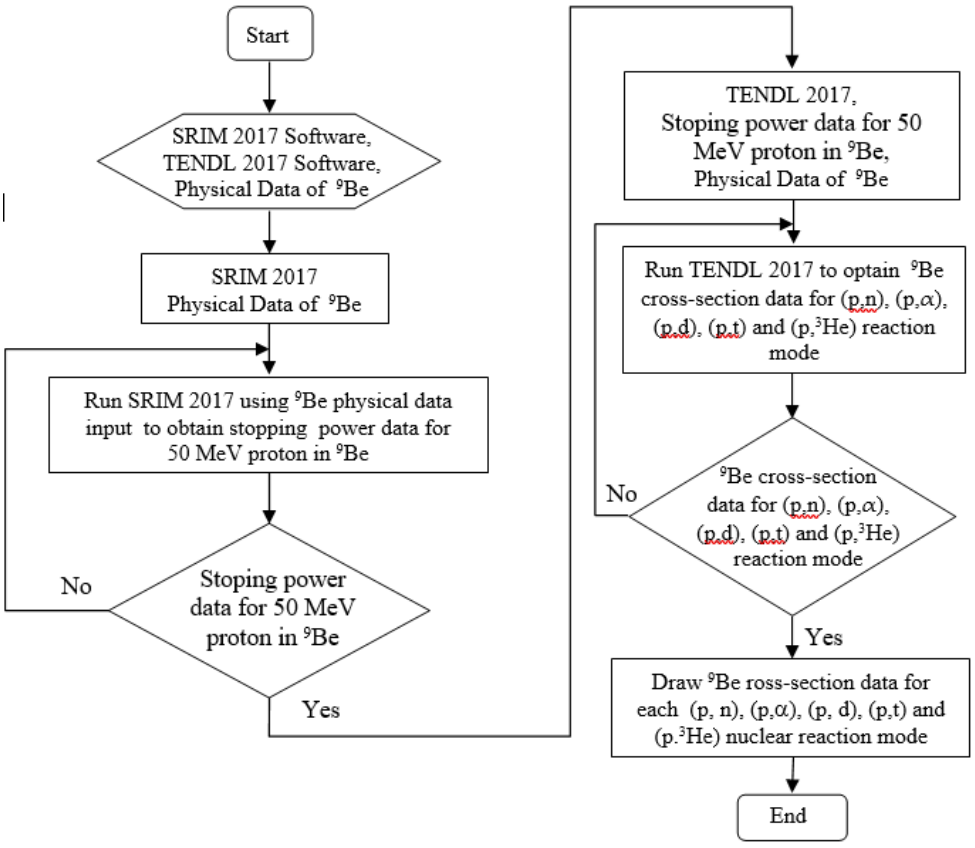

Figure 1. Flow chart of the procedure employed in this work

3. Results and Discussion

3.1. Interaction between Primary Proton Beam and Beryllium-9

High energy primary proton beam interacts with ^{9}Be target may create nuclear reactions; thus, secondary particle is possible generated from the interaction. According to the TALYS calculated nuclear cross-sections of several nuclear reactions such as (p,n), (p,α), (p,d), (p,t) and (p,^{3}He) as shown in Figure 2, the highest nuclear cross-section is (p,α) reaction (260 millibarn) which occurs at proton incident energy of 3 MeV. Meanwhile, the other nuclear reactions has lower nuclear cross-sections, for instance the nuclear cross-sections for (p,n), (p,d), (p,t) and (p,^{3}He) reactions are 240, 153, 33, and 37 millibarn, respectively.

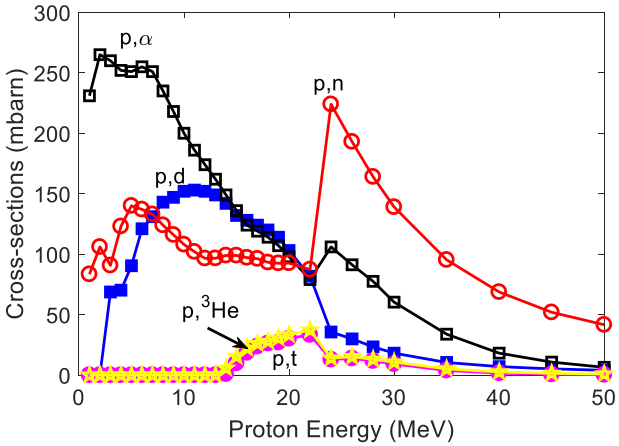

Figure 2. Talys – calculated nuclear cross-sections of (p,n), (p,d), (p,t) and (p, ^{3}He) nuclear reactions.

Five types of secondary particles significantly generated during proton bombardment of ^{9}Be target are n, α, d, t and ^{3}He. The secondary particles are produced at different proton threshold energies, for instance, neutron, alpha and deuteron particles begin to be generated at 0.001 MeV proton incident energy, whereas triton and ^{3}He particles start to be produced at 13.4 and 12.5 MeV proton incident energy, respectively.
During proton beam interaction with ^{9}Be target, several isotopes are generated as listed in Table 1. Radionuclide ^{9}B is produced as a result of ^{9}Be(p,n)^{9}B reaction which decays through p and α emission at half-life of 800x10^{-21} s. Stable ^{6}Li isotope is generated via ^{9}Be(p, α)^{6}Li, while α emitting ^{8}Be is produced due to ^{9}Be(p, d)^{8}Be reaction. Radionuclide ^{7}Be is generated by means of of ^{9}Be(p,t)^{7}Be reaction which decays by Electron Capture (EC) with half-life of 53.22 days. In addition, β emitting ^{6}He radionuclide is produced as a result of ^{9}Be(p,^{3}He)^{6}He reaction with half-life of 806.92 milliseconds.

Table 1. Various isotopes are predicted to be generated during proton bombardment of ^{9}Be target

Isotope	Nuclear reaction	Threshold energy (MeV)	Decay mode	Half life
^{9}B	^{9}Be(p,n)^{9}B	0.001	p, α	800x10^{-21} s
^{6}Li	^{9}Be(p, α)^{6}Li	0.001	-	stable
^{8}Be	^{9}Be(p, d)^{8}Be	0.001	α	8.19x10^{-17} s
^{7}Be	^{9}Be(p,t)^{7}Be	13.4	EC	53.22 d
^{6}He	^{9}Be(p,^{3}He)^{6}He	12.	β	806.92 ms

3.2. Proposed Radioisotope Production using Secondary Particles

As discussed in previous section, secondary particles such as neutrons, alpha, deuteron, triton and ^{3}He are generated as a result of proton-irradiated ^{9}Be target. In this work, we propose radioisotope production using secondary particles, particularly for medical applications.

(1) Neutron
Secondary neutrons can be employed to indirectly produce ^{177}Lu via ^{176}Yb (n,γ) ^{177}Yb→ ^{177}Lu nuclear reaction or directly to produce ^{177}Lu through ^{176}Yb (n,γ) ^{177}Lu nuclear reaction [25]. To the best of the authors' knowledge, there has been no ^{177}Lu radioisotope generated using cyclotron-produced secondary neutrons, though nuclear-reactor produced secondary neutrons have been widely used to produce ^{177}Lu radioisotope [26-27]. *Therefore,* we propose ^{177}Lu radioisotope production by means of cyclotron-produced secondary neutrons for future experiments. Other radioisotopes such as ^{131}I, ^{126}I, ^{32}P, ^{153}Sm and many others may be produce using cyclotron-produced secondary neutrons via (n, γ) nuclear reactions.

(2) Alpha
Secondary alpha particles may be used to produce ^{211}At through ^{209}Bi(α,2n)^{211}At nuclear reaction, though high alpha energy between 25 and 35 MeV would be optimum for ^{211}At production [19]. Radioisotope ^{211}At is useful for cancer therapy.

(3) Deuteron
Secondary deuteron particles can be employed for ^{177}Lu radioisotope production via ^{176}Yb(d,p)^{177}Yb →^{177}Lu and ^{176}Yb(d,n)^{177}Lu nuclear reactions as previously discussed elsewhere [20].

(4) Triton
Triton has been rarely used to produce radioisotopes. Current report on the application of secondary triton beam produced by D(d,t)^{3}He was employed for studying elastic scattering on gold [28]. Thus secondary triton particle may not be as much useful as the other particles for radioisotope production but for other studies such as elastic scattering.

(5) Helium-3 (^{3}He)
Secondary ^{3}He particle can be used to produce radionuclides such as ^{48}Sc, ^{48}V and ^{48}Cr. Using primary ^{3}He beam Szelecsenyi et al [29] recently reported production of ^{48}Sc, ^{48}V and ^{48}Cr radioisotopes which can be used in nuclear medicine. This result opens possibility of using Secondary ^{3}He particle for medical radioisotope production.

4. Conclusion

We have employed the TALYS 2017 codes to study secondary particles produced during primary proton beam irradiation of ^{9}Be. The TALYS calculated results indicated that the highest nuclear cross-section is (p,α) reaction (260 millibarn) which occurs at proton incident energy of 3 MeV while the other nuclear reactions has lower nuclear cross-sections, for instance the nuclear cross-sections for (p,n), (p,d), (p,t) and (p,3He) reactions are 240, 153, 33, and 37 millibarn, respectively. Five types of secondary particles significantly generated during proton bombardment of ^{9}Be target are n, α, d, t and ^{3}He. Four radioisotopes are predicted to be produced during the bombardment, i.e. ^{9}B, ^{8}Be, ^{7}Be and ^{6}He, which is stable isotope ^{6}Li is also produced. Secondary particles are suggested for radioisotopes production, including ^{177}Lu, ^{211}At, ^{48}Sc, ^{48}V, ^{48}Cr and many others. This work is expected to be used as a reference for future ^{186}Re production when proton beams of up to 50 MeV are employed. Other calculations will be done for some other radionuclides relevant in nuclear medicine applications.

Acknowledgments

This research project is fully supported by The Indonesian National Nuclear Energy Agency (BATAN). Discussion with Radioisotope Technology Division of BATAN staff is also greatly acknowledged.

5. References

[1] Kambali I, Parwanto, Suryanto H, Huda N, Listiawadi FD, Astarina H, Ismuha RR, Kardinah 2017 Physics Research International **2017** 1
[2] Kambali I, Suryanto H, Parwanto 2016 *Australas. Phys. Eng. Sci. Med.* **39** 403
[3] Singh N, Veronesa M, O'Doherty J, Sementa T, Bongarzone S, Cash D, Simmons C, Arcolin M, Marsden PK, Gee A, Turkheimer FE 2018 *Nuclear Medicine and Biology* **66** 32
[4] Guylas K, Toth M, Schain M, Airaksinen A, Vas A, Koskulas K, Lindstrom P, Hillert J, Haldin C 2012 *Journal of the Neurological* Sciences **320** 110
[5] Edison P, Archer HA, Gerard A, Hinz R, Pavese N, Turkheimer FE, Hammers A, Tai YF, Fox N, Kennedy A, Rossor M, Brooks DJ 2008 *Neurobiology of Disease* **32** 412
[6] Parente A, Garcia DV, Shoji A, Alves IL, Maas B, Ziljma R, Dierjkx RAJO, Buchpiguel C, Vries EF, Doorduin J 2017 *Nuclear Medicine and Biology* **49** 50
[7] Pan G, Li D, Wang YPT, Zuo C 2018 *Biochemical and Biophysical Research Communications* **504** 765
[8] Hromadik LK, Laura SRN *Journal of Radiology Nursing* **38** 28
[9] Heck MM, Tauber R, Schwaiger S, Retz M, D'Alessandria C, Maurer T, Gafita A, Wester HJ, Gschwend JE, Weber WA, Schwaiger M, Knorr K, Eiber M 2018 *European Urology* (in press)
[10] Chen L, Zhong X, Yi X, Huang M, Ning P, Liu T, Ge C, Chai Z, Liu Z, Yang K 2015 *Biomaterials* **66** 21
[11] Luz S, Balboni T, Jones J, Lo S, Petit J, Rich SE, Wong R, Hahn C 2017 *Practical Radiation* Oncology **7** 4
[12] Liberal FDCG, Tavares AAS, Tavares JMRS 2016 *Applied Radiation and Isotopes* **110** 87
[13] Jessome R *Journal of Medical Imaging and Radiation Sciences* **46** 156
[14] Erfani M, Rahmani N, Doroudi A, Shafiei M 2017 *Nuclear Medicine and Biology* **49** 1
[15] Poel HG 2007 *EAU-EBU Update Series* **5** 113
[16] Suryanto H, Kambali I 2018 *Atom Indonesia* **44** 81
[17] Koning A J et al 2017 https://tendl.web.psi.ch/tendl_2017/tendl2017.html
[18] Kambali 2018 *Journal of Physics: Conference Series* **1120** 012010
[19] Kambali I 2018 *Journal of Physics: Conference Series* **1116** 032013
[20] Kambali I 2018 *Journal of Physics: Conference Series* **1120** 012011
[21] Kambali I 2019 *Journal of Physics: Conference Series* **1153** 012106
[22] Kambali I 2017 *Makara J. Science* **21** 125
[23] Kambali I 2019 *Journal of Physics: Conference Series* **(in press)**
[24] Wibowo FA, Kambali I 2019 *Journal of Physics: Conference Series* **(in press)**
[25] Dash A, Raghavan M, Pillai A, Knapp Jr. FF, 2015 *Nuclear Medicine and Molecular Imaging* **49** 85
[26] Golabian A, Mosseini MA, Ahmadi M, Soleimani B, Rezfanifard M 2018 *Applied Radiation and Isotopes* **131** 62
[27] Duodu GO, Akaho EHK, Serfor-Armah Y, Nyarko BJB, Achoribo EA 2011 *Applied Radiation and Isotopes* **69** 588
[28] Policroniades R,Fernandez-Arnaiz J, Murillo G, Moreno G, Villasenor G, Mendez B, Chavez E, Ortiz-Salazar ME, Huerta A, Varela-Gonzalez A 2014 *Nuclear Instruments and Methods in Physics Research Section A: Accelerators, Spectrometers, Detectors and Associated Equipment* **747** 19
[29] Szelecsenyi F, Kovacs Z, Nagatsu K, Zhang MR, Suzuki K 2017 *Applied Radiation and Isotopes* **119** 94

INTERNATIONAL PROCEEDING
The 2nd International Conference on Science and Technology (ICST)
ISBN: 978-602-5830-19-8, June 2020

A preliminary study of the structure and electrical properties on transition metal incorporated in Li2CoSiO4 prepared from rice husk silica and cathode waste

A Riyanto[1*], S Sembiring[1], C Widyastuti[1], M T Rangga[1], Junaidi[1], and S Husain[2]

[1] Department of Physics, University of Lampung, Bandar Lampung, Indonesia
[2] Department of Physics, Lambung Mangkurat University, Banjarmasin, Indonesia

[*]Email: agus.riyanto@fmipa.unila.ac.id

Abstract. This work was conducted to study the potential of rice husk silica and lithium battery cathode waste as raw material for making transition metals incorporated in Li_2CoSiO_4. This study includes the phase analysis, element mapping, band gap energy, and electrical conductivity of the sample. The sample was prepared from fine rice husk silica powder and cathode waste powder with a mass ratio of 1:1 using a solid-state reaction method. It was sintered at 900 ^oC with a holding time of 12 hours at peak temperature. The results of the phase analysis show that Li_2CoSiO_4 dominates the phase in the sample, even though there is an impurity phase, i.e., Na_2SO_4. Elements mapping shows that transition metals in the form of Ni and Mn are incorporated evenly on the surface of the sample. It has band gap energy of around 1.4 eV and electrical conductivity around $6.26x10^{-5}$-$6.34x10^{-5}$ S/m at a range frequency of 1-1000 Hz. In further work, it is essential to study the phase, element mapping, and electrical properties of samples sintered at varying temperatures. Besides, electrochemical performance also needs to be tested.

1. Introduction

Dilithium cobalt silicate (Li_2CoSiO_4) compound is one of the polyanion silicate material families developed as a cathode on a lithium-ion battery. It has excellent thermal stability, high structural stability, and safety[1]. Besides, it also has a high theoretical capacity of 325 mAh/g, higher than other polyanion compounds based on phosphate, fluorophosphate, or borate[2]. However, like other polyanion silicate material, Li_2CoSiO_4 has an extremely low electrical conductivity and the slow diffusion rate of lithium ions. It causes the ion insertion/extraction into/from lattice difficult so that the electrochemical performance is not optimal[3]. The various method has been made to improve the performance of these materials, one of which is incorporating transition metals. According to Zhang et al. (2014), this technique has been shown to increase the defect concentration and electrical conductivity of polyanion silicate material so that the lithium-ion diffusion process rises[4].

One obstacle in developing Li_2CoSiO_4 materials incorporated with transition metals is the limitation of raw materials. This limitation can be overcome by utilizing lithium-ion battery cathode waste as a source of lithium, cobalt, and other transition metals. For example, the cathode of the Samsung SDI ICR18650-22F battery is made from a lithiated metal oxide (cobalt, nickel, manganese), which has the potential to be used as raw material. The composition of cobalt on the battery is 4-50%, while nickel and manganese are 0-25% and 0-15%, respectively. Many essential elements of the lithium battery

cathode can be recovered through the acid leaching method. For example, Shun-guan et al. (2012) succeeded in obtaining cobalt and lithium elements in the form of compounds $CoC_2O_4.2H_2O$ and Li_2CO_3 from $LiCoO_2$ cathode waste[5]. By dissolving the cathode $LiCoO_2$ into a solution of H_2SO_4 and H_2O_2, a leaching solution can be obtained. Addition $(NH_4)_2C_2O_4$ to leaching solution can precipitate $CoC_2O_4.2H_2O$ compounds, and the addition of Na_2CO_3 to the filtrate residue will precipitate Li_2CO_3. Meanwhile, silica, as one of the essential compounds in the formation of Li_2CoSiO_4, can be obtained from rice husk. Rice husk silica has a high purity level above 98%, amorphous, and reactive[6], [7]. These characteristics cause rice husk silica to be utilized in making silica-based materials. In our previous study, rice husk silica has been used successfully to produce some high purity ceramic materials, such as cordierite[8]–[10] and forsterite[11]. In other studies, rice husk silica has also been used in the manufacturing of mullite[12], borosilicate[13], and carbosil[14].

In the present work, we prepared transition metal incorporated in Li_2CoSiO_4 by utilizing recycling products from cathode waste of Samsung SDI ICR18650-22F batteries and silica from rice husks. The sample was synthesized using the solid-state reaction method and sintered at 900 ^oC. This study is purposed to analyze the potential of the waste as raw material to manufacture the cathode material. Specifically, this study is aimed to investigate functional groups, phases, elements mapping, band gaps, and electrical conductivity of the sample of transition metal incorporated in Li_2CoSiO_4.

2. Materials and Methods

Silica extraction from rice husk

Rice husk silica extraction refers to our previous studies[8]–[11]. As much as 50 g of rice husk in 500 ml of 5% NaOH solution was boiled to obtain silica sol. It was left at room temperature for 24 hours and then filtered to separate sol and remaining husk. To obtain silica gel, 10% HNO_3 solution was added by dropwise until the sol converts to the silica gel entirely. Furthermore, silica gel was cleaned using deionized water repeatedly and then dried at 110 ^oC for 4 hours until a solid was obtained. It was milled to obtain fine silica powder.

Decomposition of cathode waste

The decomposition process was carried out by adding 300 ml of NH_4OH 4 M solution to 20 g pieces of Samsung SDI ICR18650-22F battery cathode waste and then stirring at 60 °C for 1 hour. The deposits obtained from this process are filtered and then dried at 80 ^oC for 2 hours until the powder was obtained. As much as 10 g of the powder was dissolved in 92 ml of 4 M H_2SO_4 and 8 ml of 4% H_2O_2 under stirring at 70 ^oC for 2 hours. As much as 4 M NaOH solution was added to the solution to pH 7, and then 4 M Na_2CO_3 solution was added to obtain a paste with pH 11. The paste was washed using deionized water and then heated at 100 ^oC for 5 hours. The solid obtained from the heating was ground to get a fine powder (cathode waste powder).

Synthesis of transition metal incorporated in Li_2CoSiO_4

The preparation of transition metal incorporated in Li_2CoSiO_4 was carried out by the solid-state reaction method, namely by mixing 5 g of rice husk silica and 5 g of cathode waste powder. The mixture was then ground and sieved to obtain particles with a size of 250 meshes. Then, it was dissolved in 100 ml of 96% ethanol and stirred at room temperature for 6 hours following by stirring at 60 ^oC for 2 hours. Next, the sample was ground, and then as much as 1.5 g of sample powder was pressed with a pressure of 5 MPa to become a cylindrical pellet with a diameter of 2 cm and thickness 0.3 cm. It was calcined at a temperature of 300 ^oC with a holding time of 3 hours then continued with the sintering at 900 ^oC with a holding time of 12 hours at peak temperature.

Identification of functional groups

FTIR (Prestige 21 Shimadzu) was used to identify functional groups. The measurement was carried out by preparing a sample by grinding around 2 mg of metal incorporated in Li_2CoSiO_4 and 300 mg of

potassium bromide (KBr) in the mortar. The mixture was pressed to form the KBr pellet. The sample scanned at wavenumbers with a range of 4000-300 cm^{-1}.

Crystal structure analysis

Crystal structure analysis was carried out using an x-ray diffractometer (X'Pert Powder PANalytical PW 30/40) with CuKα radiation (λ = 0.15418 Å) produced at a voltage of 40 kV and an electric current of 30 mA. Diffractogram was recorded in the range 2θ 10°-100°.

Morphology investigation and mapping elements

The sample was characterized using SEM/EDS (Hitachi SU-3500) to evaluate the surface morphology and elemental composition.

Band gap calculation

Calculation of band gap values begins by measuring diffuse reflection using UV-Vis Spectrophotometer (Shimadzu 2450). The band gap was calculated using the Kubelka-Munk relation as shown in Equation 1

$$F(R) = K/S = (1-R)^2/2R \quad (1)$$

where S and K are the scattering and absorption coefficients respectively, $F(R)$ is the function of Kubelka-Munk, and R is the diffuse reflection. The band gap (E_g) and the absorption coefficient is related through the Tauc relation. Tauc relation to the direct band gap is given in Equation 2

$$(\alpha h\nu)^{1/n} = A\left(h\nu - E_g\right) \quad (2)$$

where α is the linear absorption coefficient, ν is the light frequency (Hz), A is the proportional constant, and $n = 1/2$ for the direct band gap. When incident radiation scatters are perfectly diffuse manner, the absorption coefficient K becomes equal to 2α. In this case, considering the scattering coefficient S as constant concerning wavelength, the Kubelka-Munk is proportional to the absorption coefficient α, applying Equation 1 can be obtained from the relation such as Equation 3

$$[F(R)h\nu]^2 = A\left(h\nu - E_g\right) \quad (3)$$

Electrical conductivity measurement

Electrical conductivity was measured using LCR meter (HIOKI 3520-52) in the range frequency of 1-1000 Hz. The value of electrical conductivity was calculated using Equation 4

$$\sigma = Gl/A \quad (4)$$

where G is conductance (S), l is length (m), and A is cross-sectional area (m^2).

3. Result and discussion

Figure 1 shows the infrared spectrum of a sample of transitions metal incorporated in Li_2CoSiO_4. The absorption peak observed at 3448 cm^{-1} is related to the stretching vibration of the O-H bond. This absorption band mostly arises from O-H bonds in silanol groups (Si-OH) and water molecules trapped in the sample[15]. The presence of silanol groups is supported by the presence of an absorption band at 1635 cm^{-1}, which is a characteristic peak of Si-OH bond[11]. In the spectrum, there is also the most absorption peak observed at 1111 cm^{-1}, which is related to the asymmetric vibrations of the Si-O-Si group. Meanwhile, the absorption peak at 794 cm^{-1} is associated with the stretching vibration of the Si-O-Si bond[16]. The peak at 1111 cm^{-1} is also related to the stretching vibration of the S-O bond[17]. The peak at 617 cm^{-1} is also associated with the bending vibration of the S-O bond[17]. Other influential absorption bands are at 470 cm^{-1}, which is related to the vibration of the Co-O group originating from CoO_4 bonds[18]. Besides, there are also absorption bands at 370 and 354 cm^{-1}, which are related to the vibration of the Li-O group originating from LiO_4[19].

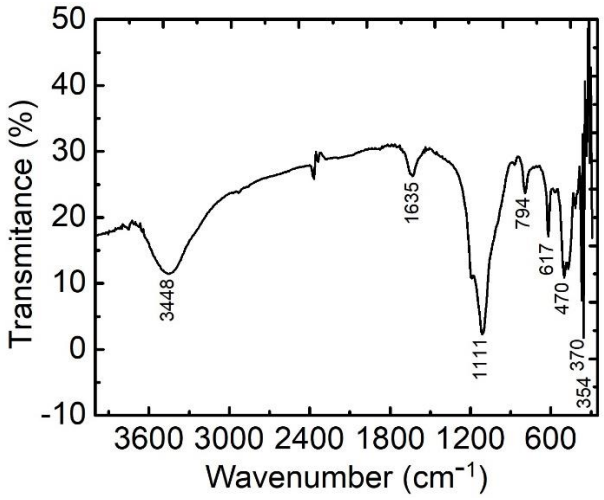

Figure 1 FTIR spectrum of a sample of transition metal incorporated in Li_2CoSiO_4

The diffraction pattern of the sample is shown in Figure 2. XRD qualitative analysis was conducted by comparing diffraction lines with PDF databases using the search-match method. Based on this method, the phase identified in Figure 2 shows the presence of the phase of Li_2CoSiO_4 with the most intense peak located at 2θ 21.73° (PDF 00-070-2351). The phase formation Li_2CoSiO_4 is in agreement with FTIR analysis, which shows the presence of Si-OH, Si-O-Si, Co-O, and Li-O groups. Besides Li_2CoSiO_4, there is also an impurity phase, Na_2SO_4, with the most intense peak located at 2θ 32.12° (PDF 00-036-0397). The impurity phase is predicted to be formed from the raw material used to prepare the sample. The formation of the Li_2CoSiO_4 and Na_2SO_4 phases is also in agreement with the results of the composition analysis on the sample surface, which shows the presence of several related elements, as shown in Figure 3. Figure 3(a) shows the morphology of the sample, which shows the form of dense and without clear grain boundaries. Silicon (Si), cobalt (Co), and oxygen (O) as the main elements forming the structure of Li_2CoSiO_4 are distributed evenly on the surface of the sample, as shown in Figure 3(b)-(d). Transition metal elements also appear to be quite uniformly distributed on the surface of the sample, as shown in 3(e)-(f). The presence of nickel (Ni) and manganese (Mn) in this sample shows that there are transition metals incorporated in the Li_2CoSiO_4 structure. The presence of the Na_2SO_4 phase was also confirmed in the distribution of the elements shown in Figure 3(g)-(h), which showed the presence of sodium (Na) and sulfur (S). However, these elements are in relatively small amounts compared to the constituent of transition metal incorporated in Li_2CoSiO_4.

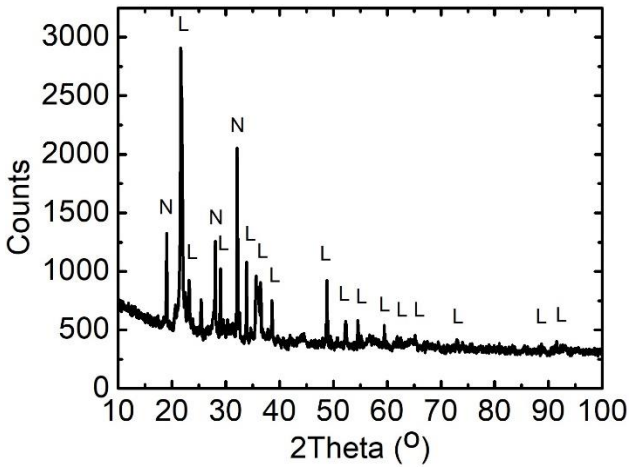

Figure 2 X-ray diffraction pattern of a sample transition metal incorporated in Li_2CoSiO_4, L = Li_2CoSiO_4, and N = Na_2SO_4 (impurity)

The band gap energy of transition metal incorporated in Li_2CoSiO_4 estimated using Tauc plots, as shown in Figure 4(a) shows a small enough value of around 1.4 eV. This small band gap is followed by a high electrical conductivity value, as shown in Figure 4(b). The electrical conductivity of the sample at room temperature in the frequency range 1-1000 Hz looks stable with the lowest value is $6.26x10^{-5}$ S/m, and the highest value is $6.34x10^{-5}$ S/m. This electrical conductivity is much more excellent when compared to the electrical conductivity of pristine Li_2CoSiO_4. The pristine Li_2CoSiO_4 produced from manufacturing raw materials generally only have electrical conductivity in the order of ~ 10^{-12} S/m[20]. The presence of transition metals in the sample has a significant effect on the electrical conductivity of the sample. It can be known from the value of electrical conductivity of transition metal incorporated in Li_2CoSiO_4, which is much higher than that of pure Li_2CoSiO_4. Not only increasing the concentration of defects, but the presence of transition metals Ni and Mn in the sample also triggers an increase in the density of free electrons[4]. As a result, the energy band gap of the sample incorporated with the transition metal becomes narrower, and its electrical conductivity is much higher than that of pure Li_2CoSiO_4. Based on the band gap value and electrical conductivity, the rice husk silica and cathode waste are very potential to be used as a raw material for making transition metal incorporated in Li_2CoSiO_4 for cathode applications.

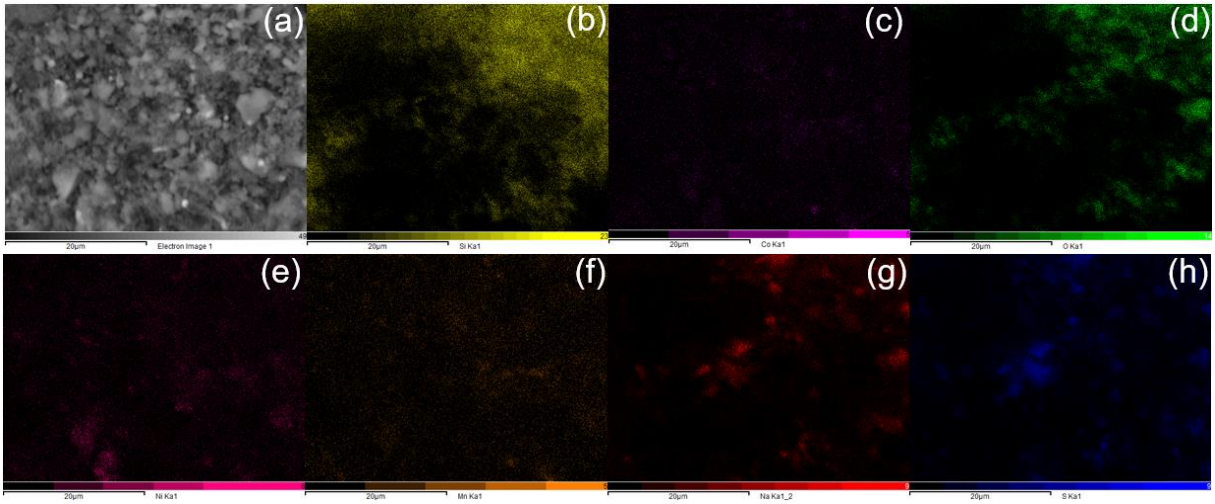

Figure 3 Morphology and elements mapping in a sample transition metal incorporated in Li_2CoSiO_4, (a) morphology of sample, (b) Si, (c) Co, (d) O, (e) Ni, (f) Mn, (g) Na, and (h) S

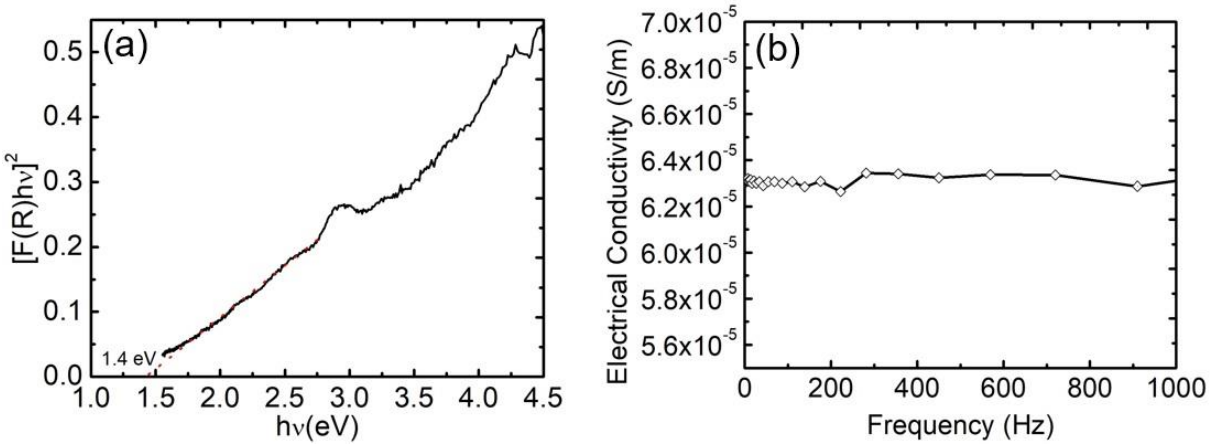

Figure 4 Electrical characteristic of transition metal incorporated in Li_2CoSiO_4, (a) the Tauc plot of band gap energy, and (b) electrical conductivity at a different frequency

4. Conclusion

The functional group identification, phase analysis, and element mapping show that the rice husk silica and cathode waste are very potential used as a raw material to produce a transition metal incorporated in Li_2CoSiO_4, even though still accompanied by impurity. This material also has a small band gap around 1.4 eV and very stable electrical conductivity in room temperature in the range $6.26x10^{-5}$-$6.34x10^{-5}$ S/m in the frequency region 1-1000 Hz. This characteristic makes it very suitable for a cathode of lithium battery application. For further studies, an electrochemical performance test of this sample needs to be carried out. Besides, the phases, element mapping, electrical characteristics, and electrochemical performance of these samples, which sintered at different temperatures, also need to be studied.

Acknowledgement

The author would like to thank University of Lampung for providing financial support for the implementation of this research activity through grants with contract numbers 1449/UN26.21/PN/2018.

5. References

[1] Devaraju M K, Truong Q D, Tomai T, Honma I 2014 Supercritical Fluid Methods for Synthesizing Cathode Materials Towards Lithium Ion Battery Applications. *Royal Society of Chemistry Advances* 4(**52**): 27452–27470

[2] Gong Z, Yang Y 2011 Recent Advances in the Research of Polyanion-type Cathode Materials for Li-ion batteries. *Energy & Enviromental Science* 4: 3223–3242

[3] Thayumanasundaram S, Rangasamy V S, Seo J W, Locquet J P 2018 Effect of Doping Functionalized MWCNTs on the Electrochemical Performances of Li_2CoSiO_4 for Lithium-ion Batteries. *Ionics* 24(**5**): 1–9

[4] Zhang L, Duan S, Yang X, Liang G, Huang Y, Cao X, Yang J, Ni S, Li M 2014 Systematic Investigation on Cadmium-incorporation in Li_2FeSiO_4/C Cathode Material for Lithium-ion Batteries. *Scientific Reports* 2014(**4**): 1–9

[5] Shu-guang Z H U, Wen-zhi H E, Guang-ming L I, Xu Z, Xiao-jun Z, Ju-wen H 2012 Recovery of Co and Li from Spent Lithium-ion Batteries by Combination Method of Acid Leaching and Chemical Precipitation. *Transactions Nonferrous Metal Society of China* 22(**9**): 2274–2281

[6] Bakar R A, Yahya R, Gan S N 2016 Production of High Purity Amorphous Silica from Rice Husk. *Procedia Chemistry* 19(**2016**): 189–195

[7] Fernandes I J, Calheiro D, Sánchez F A L, Camacho A L D, Rocha T L A C, Moraes C A M, Sousa V C 2017 Characterization of Silica Produced from Rice Husk Ash: Comparison of Purification and Processing Methods. *Mater. Res.* 20(**2**): 512–518

[8] Sembiring S, Simanjuntak W, Situmeang R, Riyanto A 2016 Preparation of Refractory Cordierite Using Amorphous Rice Husk Silica for Thermal Insulation Purposes. *Ceramic International* 42(**7**): 8431–8437

[9] Sembiring S, Simanjuntak W, Situmeang R, Riyanto A, Karo-Karo P 2017 Effect of Alumina Addition on the Phase Transformation and Crystallisation Properties of Refractory Cordierite Prepared from Amorphous Rice Husk Silica. *Journal of Asian Ceramic Societies* 5(**2**): 186–192

[10] Sembiring S, Simanjuntak W, Situmeang R, Riyanto A, Junaidi 2018 Structural and Physical Properties of Refractory Cordierite Precursors Prepared from Rice Husk. *Ceramic Silikaty* 62(**2**): 163–172

[11] Sembiring S, Riyanto A, Simanjuntak W, Situmeang R 2017 Effect of MgO-SiO_2 Ratio on the Forsterite (Mg_2SiO_4) Precursors Characteristics Derived from Amorphous Rice Husk Silica. *Oriental Journal of Chemistry* 33(**4**): 1828–1836

[12] Sembiring S, Simanjuntak W 2012 X-ray Diffraction Phase Analyses of Mullite Derived from Rice Husk Silica X-ray Diffraction Phase Analyses of Mullite Derived from Rice Husk Silica. *Makara Journal of Science*16(**2**): 77–82

[13] Sembiring S 2011 Synthesis and Characterization of Rice Husk Silica Based Borosilicate (B_2SiO_5) Ceramic by Sol-Gel Routes. *Indonesia Journal of Chemistry* 11(**1**): 85–89

[14] Simanjuntak W, Sembiring S, Sebayang K 2012 Effect of Pyrolysis Temperatures on Composition and Electrical Conductivity of Carbosil Prepared from Rice Husk. *Indonesia Journal of Chemistry* 12(**2**): 119–125
[15] Kalapathy U, Proctor A, Shultz J, 2000 A Simple Method for Production of Pure Silica from Rice Hull Ash. *Bioresource Technology* 73(**3**): 257–262
[16] Ghorbani F, Sanati A M, Maleki M 2015 Production of Silica Nanoparticles from Rice Husk as Agricultural Waste by Environmental Friendly Technique. *Environmental Studies Persian Gulf* 2(**1**): 56–65
[17] Vidya Y S, Lakshminarasappa B N 2013 Preparation, Characterization, and Luminescence Properties of Orthorhombic Sodium Sulphate. *Physics Research International* 2013: 1–7
[18] Julien C, Massor M 2002 Spectroscopic Studies of the Local Structure in Positive Electrodes for Lithium Batteries. *Physical Chemistry Chemical Physics* 2002(**4**): 4226–4235
[19] Jayaprakash N, Kalaiselvi N, Periasamy P, 2008 A preliminary Investigation into the New Class of Lithium Intercalating $LiNiSiO_4$ cathode material. *Nanotechnology* 19(**2**): 1–5
[20] Świętosławski M, Molenda M, Natkański P, Kuśtrowsk P, Dziembaj R 2014 Sol–gel Synthesis, Structural and Electrical Properties of Li_2CoSiO_4 Cathode Material. *Functional Materials Letters* 7(**6**): 1–4

INTERNATIONAL PROCEEDING
The 2nd International Conference on Science and Technology (ICST)
ISBN: 978-602-5830-19-8, June 2020

Measurement of Position and Groundwater Quality Around the Palm Oil Plantation by Using Geo-Electric Method

M Farid[1*], M L Firdaus[2], D Alfina S[3]

[1]Department of Physics, Mathematics and Natural Science Faculty, University of Bengkulu, Indonesia
[2]Graduate School of Science Education, University of Bengkulu, Indonesia
[3]Department of Education, Ratu Samban University, Indonesia

[*]Email: mfarid@unib.ac.id

Abstract. Palm oil trees are classified as trees that use a lot of water for their survival. If palm oil trees are planted at the plantation level, it is possible that they will suck up the water around the plantation. As a result of continuous water extraction around the plantation, it is presumed that there will be a decrease in water quality which had been consumed by the public. The decrease in water quality will disrupt health and intelligence of the people around the plantation. This study aimed to investigate: (1) the position of groundwater level around palm oil plantation, and (2) the quality of the groundwater. Geo-electric method was applied to determine the position of the groundwater, while to find out the water quality the analytical method was used. The results of the study revealed that the position of the groundwater level was between 2-3 meters from the surface, while the water quality was very poor based on the pH test, turbidity and iron content. Water pH was ranging from 5.7 to 6.0, the turbidity was between 19 to 54 NTU, while the iron content was between 0.0012 to 0.0022 mg/liter. The results of the study lead to a conclusion that the position of the groundwater around the palm oil plantation are still relatively shallow, but the water quality is already above the threshold in the measurement of health standards.

1. Introduction

Water is a natural substance that plays an important role for the life of human beings, animals and plants [1]. In another study it was stated, that in terms of quantity, ground water will decrease in supply capacity if the amount used exceeds its availability. [2]. In terms of quality, the water has a requirement that it should be tasteless, odorless and total of certain dissolved solids, color, turbidity, and temperature do not exceed the threshold. Water quality is also determined by the quality of the chemicals, which refers to the content of certain elements of both organic and inorganic. The content of these elements should not be less than the minimum limit or does not exceed the maximum limit [3].

The rapid development of palm oil plantations and the number of absorbed waters needs, should be a concern as an environmental issue, especially related to the disruption of the water system. Palm oil plantations that are a monoculture are rated as the cause of the reduced availability of groundwater and can lower the groundwater level [4]. Based on the data obtained from PPKS of Kabun Kalianta Riau sub-unit, at the palm oil plantation area, the pattern of decrease in groundwater level occurred in the period of April-September. The study of groundwater potential can be determined by measuring the alleged points by using *resistivity-meter* tool with geo-electric method.

The geo-electric method does not damage the medium and the surrounding environment, but the results can be analyzed to determine the presence of the groundwater layer. The magnitude of the potential for groundwater can be characterized by the presence of a thick aquifer zone. Resistivity-meter tool is capable of measuring the groundwater level up to a depth**, o**f 60 meters and is easy to use as well as has high enough accuracy [5]. Alile et al (2010), revealed that the electrical resistivity method is one of the most useful technique in geophysical exploration of underground water due to the resistivity of the rocks is extremely sensitive to water content [6]. In another study the results were obtained that the rock resistivity layer ranged from 63 Ohm to 333 Ohm with around 85% of the area in it having medium groundwater potential (100-250 Ohm) and high potential groundwater (> 250 Ohm). Resistivity method is one of the active geoelectric methods used to determine the resistivity value of layers or rocks which is very useful to determine the possibility of the existence of aquifer layers, which are water-bearing rock layers [7]. Geo-electric measurement method is performed by injecting electric current through two current-electrodes and measures the results of the voltage difference at two potential electrodes which are driven into the ground [8]. The magnitude of the radial currents can be measured in terms of the potential difference at a particular place at ground level, so that it will be obtained information about subsurface rock resistivity [9].

Measurement of groundwater levels with geo-electric method in the area around the Aguobiri Southern Nigeria found that groundwater can still be consumed and has not been contaminated by oil [10]. It is in contrast to the results of research by Carlson, et al (2013) which states that there is a threat of water sources pollution that become public consumption **[11]**. To find out the quality of the water, whether it is contaminated or not, a test must be conducted.

Water quality testing is required to determine water quality. Water has the nature of the physics, chemistry and biology. According to Suripin (2002) physical characteristics that affect water quality are determined by the color, temperature, and turbidity, while the chemical characteristics of water cover pH, alkalinity and hardness; and biological characteristic is in the form of a wide range of living organisms **[12]**. The data measuring groundwater levels and water quality testing further is correlated to the relationship between the two variables.

2. Theoretical Framework

Geo-electric is a method in geophysics that studies the nature of electricity current in the earth and how to detect them in the earth's surface. This detection includes measuring the potential difference, currents, and electromagnetic that occurs naturally or as a result of currents injection into the earth [13]. The work steps of geo-electric method are written as follows:

The potential difference at the point P1 as a result of the electrode flow of C1 is

$$\boldsymbol{\rho_a = K\frac{\Delta V}{I}} \quad (1)$$

In equation (1) $\rho_a$is the resistivity, K is a geometric factor, ΔV is the potential difference between the points P_1andP_2, $I$is the electricityflow that flows through P_1andP_2.
$\boldsymbol{K}$value is formulated as set forth in equation (2).

$$\boldsymbol{K = 2\pi a} \quad (2)$$

In equation (2) $a$is the distance between the electrodes.

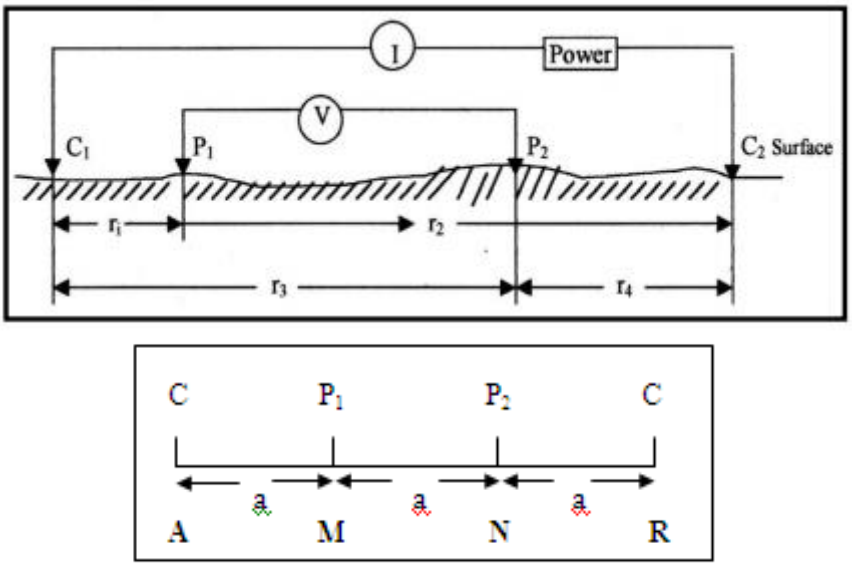

Figure 1. Two pairs of flow and potential electrodes on the surface of a homogeneous isotropic medium with resistivity

3. Methods

Measurement of water quality and groundwater levels was conducted at Dusun Simpang Beliben of Pondok Kelapa Village of Bengkulu Tengah. Water sampling from wells was determined around the points of which the groundwater level is measured. There are four measurement locations that have been determined through a survey. Wells water quality testing was conducted in the laboratory of University of Bengkulu. Variables that are physically and chemically tested were pH, levels of iron (Fe) and turbidity of the samples. pH testing was performed by using a pH meter, iron content testing was done by using a spectrophotometer, and turbidity testing was performed by using a turbidity-meter. The test results of the samples were subsequently analyzed with reference to the list of water quality for each allotment according to the Indonesian government regulation No.20 of 1990.

Groundwater level measurement in this study was done by using a GE GL-4200 type *Resistivity Meter*, geo-electric method was performed with Wenner electrode configuration. Geo-electric appliance parts consisted of Current transmitter, voltmeter, ampere-meter, Connection test, ADC, and PC controller Current Transmitter. Supporting tools in the groundwater level measurements were compass, two-way communication tool, GPS, camera, 4 rolls of cable, 4 pieces of electrode and 20 pieces of stick. The required data to measure groundwater quality include the distance between two AB current electrodes, the distance between two MN potential electrodes, electric current (I), potential difference (ΔV) guided by stacking chart, then obtained the geometry correction factor price (K) and the value of the resistance type (ρ).

Groundwater measurements are carried out by injecting an electric current using 2 pieces of A and B current electrodes which are plugged into the ground at a certain distance. The electrical voltage that occurs at groundwater level is measured by using a multi-meter that is connected through 2 pieces of "voltage electrodes" M and N whose distances are shorter than the distance of the AB electrode. If the position of the distance of the AB electrode is changed to be greater than the electrical voltage that occurs at the MN electrode changes according to the information on the type of rock which is also injected with the electric current at a greater depth **[14].** The final result of the calculation is entered into the RES2dinv software to describe the resistivity values that exist within the earth's surface in the form of a contour map of the layers contained in it.

4. Results and Discussion

The results of physical and chemical water quality testing of well water samples from the laboratory are shown in Table 1 below.

Table 1. Results of sample test analysis

Samples	Parameter Analysis		
	pH	Iron (mg/L)	Turbidity (NTU)
Sample 1	6.0	0.0021	54.16
Sample 2	6.0	0.0022	37.12
Sample 3	5.8	0.0021	35.65
Sample 4	5.7	0.0011	19.02

Analysis of pH values in the water quality test sample in Table 1 shows that the water sample is acidic with a pH of 5.7–6. According to the government regulations of the Republic of Indonesia No.20 of 1990, the pH of groundwater of Group A allowed is 6.5-8.5. This shows that samples of well water can be said to be polluted and not suitable for consumption.

Analysis of iron (Fe) levels in water quality sample test showed the content of 0.0011–0.00022 mg/L. According to the government regulation of the Republic of Indonesia No.20 of 1990, the metal content of iron (Fe) in Group A allowed is 0.3 mg/L. This shows value is very far from the permissible limit of 0.3, therefore, the well water sample can be said not to contain iron (Fe) metal.

Analysis of the turbidity level in the water quality sample test shows a range of 19.02–54.16. According to the government regulations of the Republic of Indonesia No.20 of 1990, the maximum turbidity level allowed in Group A is 5 NTU. This is showed that a value that very far from the permissible limit of 5 NTU, therefore, well water samples can be said to have very high turbidity levels. The turbidity can be caused by solids such as sand, silt, clay and organic content.

Groundwater measurement data using the geo-electric method after processing to obtain a type of resistivity value, then with the Res2dinv software. The results of processing the data are in the form of the actual resistivity distribution of cross-sections below the surface of the soil. Based on this geo-electric cross-section, it can be known the depth and structure of the soil layers visualized by a particular color. On track 1, the results of processing data are shown in Figure 1 below:

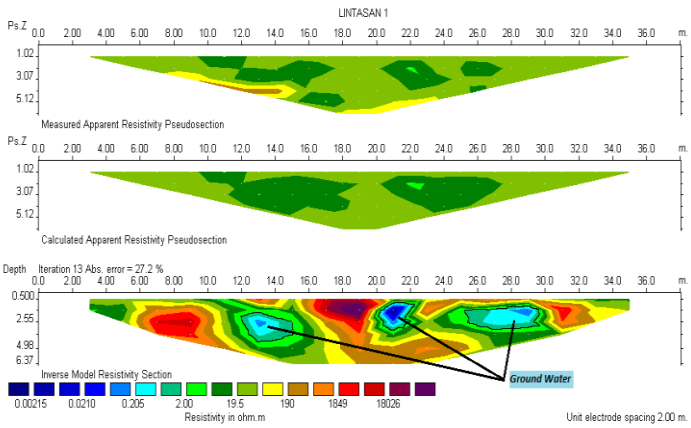

Figure 1. Layers of groundwater on the track 1

Based on Figure 1, there is shown a potential spread of groundwater, the resistivity of groundwater is shown in blue which ranges between 0.00215–0.206 Ωm with an average depth of 1,967m.
In track 2, the results of processing data are shown in Figure 2 below:

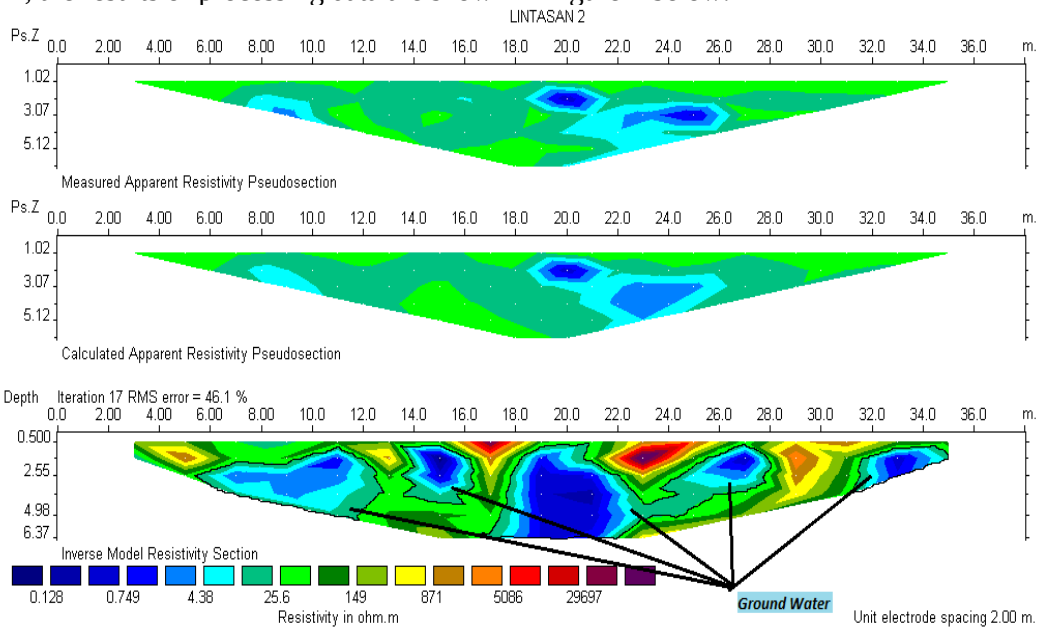

Figure 2. Layers of groundwater on the track 2

Based on Figure 2 there is also shown a potential spread of groundwater, the resistivity of groundwater is shown in blue which ranges between 0.128–4.38 Ωm with an average depth of 2,935 m.
In track 3, the results of processing data are shown in Figure 3 below:

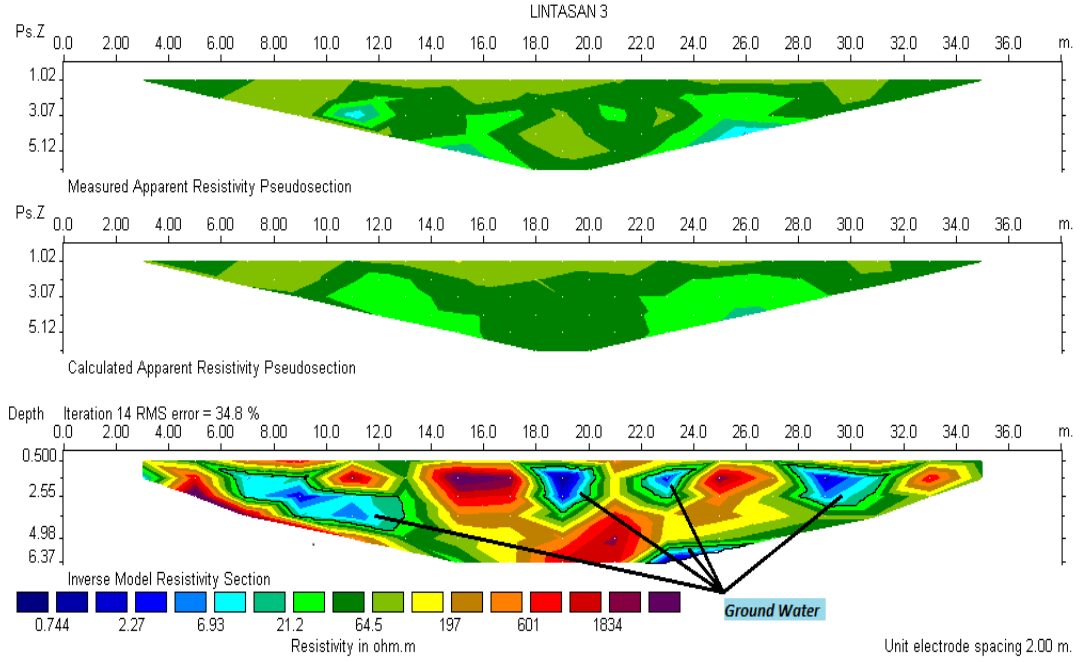

Figure 3. Layers of groundwater on the track 3

Based on Figure 3 there is also shown a potential spread of groundwater, the resistivity of groundwater is shown in blue which ranges between 0.744– 6.93 Ωm with an average depth of 2,240m.
In track 4, the results of processing data are shown in Figure 4 below:

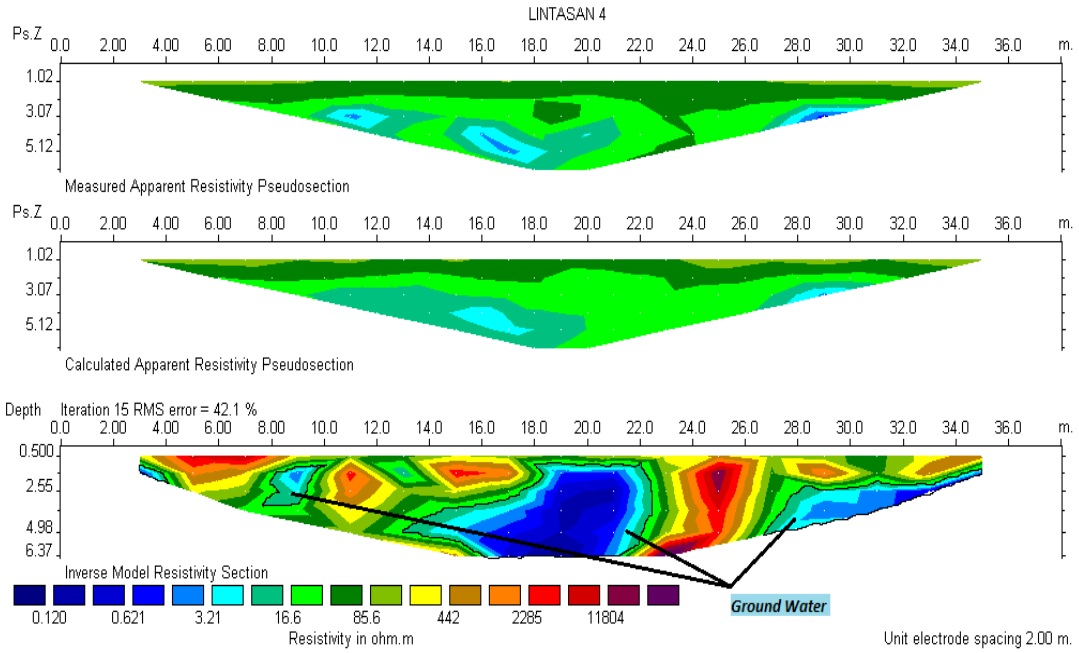

Figure 4. Layer groundwater on track 4

Based on Figure 4 there is also shown a potential spread of groundwater, the resistivity of groundwater is shown in blue which ranges between 0.120 to 3.21 Ωm with an average depth of 2,679 m. The four measurement tracks obtained that the depth of the groundwater level varies for each track. Hypothesis testing of the relationship between water quality and groundwater depth was carried out using product moment correlation which is indicating that there was no tendency for the relationship between pH and iron (Fe) to groundwater level.

However, there is a tendency for an inverse relationship between turbidity and groundwater. This inverse relationship is defined as that the closer/shorter the distance of the groundwater level from the ground surface, then the level of turbidity is getting higher/bigger. This is in line with the research of Carlson, et al., from Stanford University and the University of Minnesota (2013) who conducted research in Ketapang Regency on the southern coast of West Kalimantan Province, revealed that water quality was significantly eroded and the risks associated with oil palm plantations. The impact that occurred, starting from the decreasing of water quality with marked by the turbidity has occurred between 40-713 NTU.

5. Conclusion

Based on research that has been conducted, it can be concluded that the quality of the four wells in terms of pH indicates that the water is acidic with pH range between 5.7–6, the content of iron (Fe) ranges between 0.0011–0.0022 mg/L indicate that the well water contains trace metal iron (Fe), and turbidity ranges from 19.02–54.16 NTU, which means that the well water turbidity is very high. The depth of the groundwater level which carried out by Wenner's geo-electric configuration measurement shows that track 1 has an average depth of groundwater of 1,967 m, track 2 has an average depth of 2,935 m, track 3 has an average depth of 2,240 m, and track 4 the average depth is 2.679 m. The relationship between the water quality in terms of turbidity with a depth of groundwater depth has a "strong" relationship, so as it can be said that there is a tendency for the inverse relationship between water quality and groundwater in terms of turbidity.

6. Refferences

[1] Dyah A, Setia BS dan Sudarmo 2012 Analisis Kualitas Air dan Strategi Pengendalian Pencemaran Air Sungai Blukar Ka, bupaten Kendal. *Jurnal Presipitasi* 9 (2) 1907-187.

[2] Purnama 2007. Sistem Akuifer dan Potensi Air tanah Daerah Aliran Sungai (DAS) Opak. *Forum Geografi, Fakultas Geografi Universitas Gadjah Mada, Yogyakarta* 21 (2).

[3] Lawrence A O and Ojo TA 2012. The use of Combined Geophysical Survey Methods for Groundwater Prospecting in a Typical Basement Complex Terrain: Case Study of Ado-Ekiti Southwest Nigeria, *Research Journal in Engineering and Applied Sciences* 1(6) 362-376.

[4] Sandhyavitri, Ari 201 4. Kajian Upaya Pelestarian Sumber Daya Air Tanah Kemungkinan Akibat Pembangunan Kebun Kelapa Sawit di Provinsi Riau.

[5] Anomohanran O 2011. Determination of groundwater potential in Asaba Nigeria using surface geoelectric sounding. *International Journal of the Physical Sciences*, 6(33).

[6] Alile, OM., O. Unjabi, I.A Evbuomwan. 2010. Geoelectric investigation of groundwater in Obaretin – Iyanomon locality, Edo state, Nigeria. *Journal of Geology and Mining Research* 3(1) 13-20.

[7] Oyediran IA1 and Falae PO 2018. Integrated Geophysical and Geotechnical Methods for Pre-Foundation, Investigations. *Journal of Geology & Geophysics* 8(1).

[8] Loke, M.H. 1990. RES2MOD, Rapid 2D Resistivity Forward Modeling Using Finite- Difference and Finite-Element Methods.Malaysian:Penang.

[9] Hartantya, E., 2000, Survai Elektromagnetik, UGM, Yogyakarta.

[10] Egai, A.O 2013.Geoelectric Characterization of Subsurface Crude Oil Leachate Plume in Aguobiri, Southern Nigeria. Research Journal in Engineering and Applied Science 2 (6) 427-433.

[11] Carlson KM, Lisa MC, Alexandra GPG, Dessy R, Ruspita, NL, Yadi P, Kate A. Brauman, and Peter AR 2014. Influence of watershed-climate interactions on stream temperature, sediment yield, and metabolism along a land use intensity gradient in Indonesian Borneo. *Journal of Geophysical Research*.

[12] Suripin, 2002. Pelestarian Sumber Daya Tanah.

[13] Kanata, Bulkis dan Zubaidah. 2008. Pemodelan Fisika Aplikasi Metode Geolistrik Konfigurasi Schlumberger untuk Investigasi Keberadaan Air Tanah. Jurnal 7 (1).

[14] Broto S dan Afifah SR 2008.Pengolahan Data Geolistrik dengan Metode Schlumberger. *Teknik*-29 (2).

INTERNATIONAL PROCEEDING
The 2nd International Conference on Science and Technology (ICST)
ISBN: 978-602-5830-19-8, June 2020

Formulation Gel Mask Peel Off From Palm Shell *(Elaeis quinemis Jacq)* Activated Charcoal as Facial Cleanser With Polyvinyl Alcohol (PVA)

U Lestari [1*], Y A J Limbong[1], Muhaimin[2]
[1]Department of Pharmaceutical, Faculty of Science and Technology University of Jambi, Indonesia
[2] Department of Chemistry, Faculty of Science and Technology University of Jambi, Indonesia

[*]Email: ucelestari@unja.ac.id

Abstract. Palm oil shells are one of the palm oil waste that has the potential to be processed into activated charcoal. Activated charcoal is a carbon compound that has been processed by means of activation so that the compound has a pore and a very large surface area in order to increase the absorber power to the dirt on the face as a facial cleanser. The purpose of this research is to look for alternative utilization of waste to be activated charcoal which can give added value so that can be made into face cleansing mask in gel peel off form. To create a peel-off gel mask requires an appropriate gel-forming agent such as polyvinyl Alcohol (PVA). PVA is used because PVA will form an elastic and strong peel off coating so that contact with the skin is good as well as easy to dry without any help of other materials. The gel mask of peel off charcoal is actively tested for its physical stability. Evaluation of the physical properties performed is organoleptic examination, homogeneity, pH, viscosity and flow properties, scatter test, dry time test, stickiness test, irritation test, favorite test, and stability test by cycling test method. The results showed that the physical properties of the third formula has good physical properties, then tested the effectiveness in cleaning the dirt. Effectiveness testing using a digital camera shows that the surface structure of the volunteer skin becomes smoother and the blackish stains on the skin look faded after the use of the test preparation when compared to the skin control structure without the use of a test gel mask

Keywords: Palm oil shells, activated charcoal, PVA, Gel Mask Peel Off

1. Introduction

In Indonesia, the area of oil palm plantations in 2014 reached 11 million hectares capable of producing 30.9 million tons of palm oil. In Jambi province itself has a plantation area of 1.8 million ha with palm oil production of 688 thousand tons [1]. One of the wastes generated from the processing of oil palm is shell. Palm oil shells formerly used only as a hardener especially in palm factory and as a mixture of animal feed, with the existence of science and technology, the palm shell can be processed into products that have high economic value, such as activated charcoal oil palm shells [2].

Widely active charcoal can be used for color removal, deodorizing, deodorizing, and as an industrial purifying agent. Activated charcoal is a charcoal with carbon atom configuration is released from bondage with other elements, and pores are cleaned from other compounds so that the surface and the active center become widespread resulting in increased adsorption power [3]. The purpose of this research is to look for alternative utilization of waste to be activated charcoal which can give added value so that can be

made into face cleansing mask in gel peel off form. Gel Mask Peel Off is a vinyl base preparation. The Gel Mask Peel Off has several advantages, namely easy to use, and easy to clean [4], to make a peel-off gel mask requiring an appropriate gel-forming agent such as Polivinil Alcohol (PVA). PVA on mask preparations will form a strong and elastic peel off coating so that contact with the skin is good as well as easy to dry without any help of other materials [5].

The physical quality of the gel preparation of the Gel Mask Peel Off is influenced by the composition of the ingredients used, particularly the polyvinyl alcohol (PVA) composition and other polymers used [5]. To obtain a good and standardized preparation, evaluation of gel preparation of peel-off gel includes organoleptic evaluation, viscosity evaluation and flow properties, pH evaluation, spreading power evaluation and evaluation of the dosage time to dry, evaluating the effectiveness of gel peel off mask clean up the dirt. The purpose of this research is to look for alternative utilization of waste to be activated charcoal which can give added value so that can be made into face cleansing mask in gel peel off form.

2. Method

2.1. Materials Research

The materials used in this research are Palm-free fruit shell, polyvinyl alcohol (PVA), propylene glycol, polyvinyl pyrrolidone PVP K30, propyl paraben, methyl paraben, ethanol, Aqua Rosae, aquadest, Iodine, KI, sodium thiosulfate, Methylene blue

2.2. Equipment

The tools used in this study include stirring rod, porcelain cup, beaker glass, measuring cylinder, dropper, pH meter, spoon, digital scales, Oven, Furnace, grinder machine, test tube, tube rack.

2.3. Sample Preparation

Sample of waste of palm shell obtained from PT. Sumbertama Nusa Pertiwi Sungai Gelam, Jambi. Shell is separated from the kernel and other impurities, the sample weighed 2 kg then washed with running water and then dried until the weight is constant [2,3].

2.4. Charcoal Making

Palm shells that have been dried and then carbonized by burning with free fire to charcoal. charcoal is cooled and grinded into charcoal powder, then sieved with a 200 mesh sieve. Then the charcoal yield is calculated [2,3].

2.5. Activated Charcoal with Physical Activation

Charcoal is activated physically. The activated charcoal powder is fed into the vapor plate and then put in the furnace at 750ºC for 3 hours [2,3].

2.6. Determination of absorption test Charcoal that actively qualitative with methylene blue

To determine the adsorption ability of activated carbon, the step done by adsorption test with methylen blue. The active charcoal as much as 0.1 gram was then added 100 ml methylene solution 100 ppm as much as 20 mL then placed in a 50 ml erlenmeyer and covered with aluminum foil, the sample stirred using a magnetic stirrer for 15 min and stirred for 30 min at 100 rpm, then filtered, and seen the color changes that occur [6].

2.7. Determination of absorption test the activated charcoal quantitatively with iodine

The active char of 0.25 g was introduced into the erlenmeyer, then 25 ml of 0.2 N of solution was added, then shake for 15 minutes at room temperature and then filtered. The filtrate of 10 mL was titrated with 0.1 N sodium thiosulfate (Na2S2O3) solution until light yellow and then given a few drops of 1% starch solution and the titration was continued until the right color disappeared. Good Iodine Absorption Capability 750 mg / g [6].

2.8. Gel mask Peel Off Formulation Design

Table 1. Gel Mask Formula

Material	Concentration (%)				Function
	F1	F2	F3	F4	
Activated charcoal	1.5	1.5	1.5	1.5	Dirt cleaner
PVA	5	10	15	20	Gelling Agent
PVP	5	5	5	5	Plasticizer
Propylenlicol	10	10	10	10	Humectan
Methyl Paraben	0.2	0.2	0.2	0.2	Preservative
Propyl Paraben	0.1	0.1	0.1	0.1	Preservative
Ethanol	15	15	15	15	Solvent
Aquadest	Ad 100	Ad 100	Ad 100	Ad 100	Solvent

2.9. Preparation of Gel Peel-Off Gel Activated Charcoal Activated Palm Shell

The preparation of a peel-off face mask begins with the development of PVA (Mass A) in a container with warm aquadest (80ºC), then in another place PVP (Mass B) is developed in a cold water to expand. Methyl paraben and propyl paraben are dissolved into propylene glycol (Mass C). Mass B and Mass C are consecutively inserted into Mass A and then stirred until homogenous. Activated charcoal powder is added bit by while stirring constantly, then 96% ethanol is added and the deodorizer, stirring again, and put into the container.

2.10. Evaluation of Gel Mask Peel Off

Organoleptic examination

Includes visual examination of shapes, smells and colors. The gel is usually clear with a semi-solid concentration [7].

Homogeneity check

With a little sample of gelatin gel compound formulas peel off activated charcoal and then placed a little gel on the glass object. A rough particle or nonhomogeneous array is observed, then recorded. The preparation is said to be homogeneous if there is no visible coarse grain [8].

pH Examination

Performed by using a pH meter dipped into the sample. The pH of the preparation meets the criteria according to the pH of the skin is in the interval 4.5-6.5 [9].

Viscosity Test

Determination of viscosity and flow properties was performed with a Brookfield viscometer. The preparations are put into a 250 ml beaker glass, then the spindle is lowered into the preparation to the specified limit. Good gel viscosity grades ranged from 7100 - 83144 cps [10].

Flow properties test

Flow properties are generated from viscosity testing. Created curve between shear stress and shear rate. In pharmaceutical preparations more often found non-Newton flow properties are plastic, pseudoplastis, or dilatan [11].

Power spread test

Spreading power checks are performed by calculating the spread of the gel after a given load. A preparation of 0.5 g is carefully placed on transparent coated transparent graph paper, allowed for a moment (15 seconds). Then weighed up to 150 g. Good dispersion for gelatin gel mask preparations that have a diameter between 3-5 cm [12].

Drying time Test

The test was performed by applying 1 gram of each dosage form to the back of the hand with a size of about 7 cm x 7 cm, then viewed using the stopwatch time required by the dosage to dry, ie until the preparation of the film form (Pertiwi, 2012). Dry time Gel Mask Peel Off is good that is between 15-30

minutes [13].

Stickness power test
1 gram gel is placed on top of the object glass. The object glass is placed on top of the gel, then pressed with a 1 kg load for 5 minutes. The load is released and recorded until the two glass objects are released. A good gel has a fixed adhesion that, the adhesive power test requirement should not be less than 0.07 minutes or 4 seconds [11] or preferably more than 1 second [14].

Irritation test
Test were done with patch test method, by attaching the mask to the skin with a piece of wattman paper coated with polyethylene film. The patch test is performed on the back skin of the body for 48 hours, after which it is lifted and then marked. Results are assessed 25 - 30 minutes after appointment. Observed an irritant reaction of heat, itching, or sore [15].

Hedonic Test
The analysis according to the preferred test (aroma parameter, skin sensation, and color of preparation) using 20 panels presented with sample of gel mask gel preparation peel off activated charcoal [15].

Stability Test of cycling test method
The gel samples were stored at 4ºC for 24 hours then transferred into an oven with temperature 40ºC ± 2ºC for 24 hours (one cycle), then the test was carried out for 6 cycles and observed the physical changes of the gel. The condition of the preparation was compared after the experiments with the previous dosage conditions [6].

Effectiveness of Gel Mask Peel Off on Cleaning Dirt test
The effectiveness test is performed to observe any changes occurring in the natural structure of the skin after the gluing of the Gel Mask Peel Off actively activates the palm shell. This test was performed on 15 volunteers for 28 days. The test method was the back of volunteer hand photographed with a digital camera to observe the initial condition of the skin surface, then the dosage applied on the back of the right hand of the volunteers. The back of the left hand is dwarfed as a control. After 4 weeks volunteer hand is photographed again. Then the results are compared before and after the test, see if the blackish stains fade [7].

3. Results and Discussion

3.1. Activated Charcoal preparation
This step is done by burning with free fire to become charcoal. The finished charcoal was cooled and grinded into charcoal powder, then sieved with 200 sieves. The yield was 42.7%. the high rendemen in the production of carbonization is influenced by several factors such as climate, season, plant elements, soil conditions, raw materials, and combustion. The speed of the frying process affects the amount of smoke produced [16].

3.2. Charcoal Making with Physical Activation
The carbonated charcoal was continued at the physics activation stage using furnace at 750ºC for 3 hours. Researchers choose the activation of charcoal physically because the active charcoal will be made gel preparations peel off gel that applied on the face, in addition to the use of chemicals can cause irritation, it that activate charcoal chemically , its pH 3 and a bit difficult to neutralize it [2,3].The yield of activated charcoal of oil palm shell is 39.8%. The determination of active charcoal yield is performed to determine the amount of activated charcoal produced after the activation process. The longer activation time causes the active charcoal yield to be lower [17].

3.3. Qualitative Absorption Power Test Against Methylene Blue
This test is conducted with the aim to find out how much the absorption of activated carbon qualitatively, that is, only by seeing the color change occurs in metilen blue that has been dissolved with active charcoal powder. From the research that has been done, the blue color of methylene blue fades after dissolved with active charcoal powder. According to Jawnkoska the absorption capacity of activated charcoal against

methylene blue indicates the ability of activated charcoal adsorbents for molecular molecules that have metallic-resembling size [2,3].

3.4. Quantitative Absorption Power Test Against Iodine

The parameter that can show the quality of the activated charcoal is the adsorption power to the Iodine solution. The larger the number of iodnya the greater the ability to adsorb the adsorbate or solute. Therefore, the absorption capacity of iodine is an important indicator in assessing activated charcoal [18]. The addition of iodine solution serves as its adsorbate to be absorbed by activated charcoal as an adsorbent. The absorption of iodine solution is indicated by the reduced concentration of iodine solution. Measurement of residual iod concentration can be done by adjusting the color of the filtrate from iod solution with a series of iodine solutions that have been made with known concentration. The result of iodine absorption power analysis resulting from the size of activated charcoal particles of oil palm shell is 766.443 mg / g, so that the absorption of activated charcoal oil palm shell has absorptive capacity that meets the Indonesian National Standard that is more than 750mg / g [19].

3.5. Evaluation of mask preparations

Examination of Organoleptis

The organoleptic test is performed by observing the consistency, smell, and color of the preparations. The gel is usually clear with a semi-solid concentration [7].

Table 2. Organoleptic observation result

Gel Formula	Form	Odor	Color
1	Slightly	Distinctive smell	Black
2	Thick	Distinctive smell	Black
3	Thick	Distinctive smell	Black
4	Thick	Distinctive smell	Black

The results obtained show similar shapes and colors that are black and distinctive smell, but on the four bases there is a consistency difference which in formula 1 and formula 2 is somewhat diluted, whereas in the gel formulas 3 and 4 the consistency is thick, indicating that the formula matches parameter. Here also can be concluded the greater the consistency of PVA hence the thicker consistency in the preparation.

Homogeneity test

Homogeneity test was performed to see the uniformity of gel particles. Evenly dispersed particles prove that the active substance is evenly dispersed in the preparation. The preparation should be homogeneous and no visible coarse grain [8].

Table 3. Homogeneity test result

Gel Formula	Homogenity
1	Homogeneous
2	Homogeneous
3	Homogeneous
4	Non homogeny

From the homogeneity examination on the gel preparation of the active charcoal peel off indicated that formula 1, formula 2, and formula 3 show the absence of coarse grains on transparent glass. This shows that the prepared preparation has a homogeneous arrangement [19], whereas in formula 4 there are unsolved clumps, due to large PVA concentrations. From the results obtained can be seen that the concentration of PVA affects the homogeneity of the formula.

Power Spreads Test

Measurement of scattering power is done to know the ability of spread gel on the surface of skin. The spreading power response is selected in the range of 3 - 5 cm [12], because in that range the perceived power is suitable for the area of the skin whose area is not very wide and its distribution allows the gel to have longer contact with the skin so that the absorbs is more optimal.

Table 4. Power spread test result

Gel Formula	Examination result
1	8.20 cm
2	7.24 cm
3	4.34 cm
4	3.13 cm

Seen from the table that the third and fourth formulas have a scattering force between 3.13 cm and 4.34 cm which means meeting the desired scattering criteria, ie 3 - 5 cm [12]. where the increase of PVA concentration on base of gel mask can cause decreasing of spread power [20]

pH Examination

The pH test was performed using pH meter. The pH of the dosage recommended for gel preparation does not irritate the skin should be in accordance with the pH of the skin is 4.5-6.5 [9].

Table 5. pH examination result

Gel Formula	Examination result
1	5.62
2	5.75
3	5.87
4	5.87

From the data obtained shows the pH of all formulations ranging from 5.62 to 5.87. From the pH evaluation test at table 6 it can be concluded that the pH of the preparation is influenced by the concentration of gelling agent PVA 4,5-6,5 [21]. so that all the formula is in accordance with physiological pH of the skin and is expected not to irritate the skin for the wearer. For topical preparations to be used on the skin if it has a pH smaller than 4.5 may cause irritation to the skin whereas if a pH greater than 6.5 can cause scaly skin [20].

Viscosity Testing

Viscosity is the main characteristic associated with the ease of use of the preparation in the formulation. The viscosity in the gel is influenced by increased concentrations of humectants and gelling agents [12]. The gel preparation with the optimum viscosity will be able to withstand the active substance to remain dispersed on the gel basis and to increase the gel concentration [22]. The viscosity of the gel preparation should be in the range 7100 - 83144 cps [10]. Excessive viscosity can be difficult at the time of packaging and packaging removal, the viscosity is too low will be difficult when the application on the skin of course the supply will flow from the face.

Table 6. Viscosity test result

Gel Formula	Viscosity level
1	2343.3 cps
2	3891.67 cps
3	46250cps
4	189000 cps

From the research that has been done can be seen the greater the concentration of PVA added in the formula will enlarge the viscosity gel mask gel preparation peel off. So it can be seen that the third formula is eligible.

Flow properties

The results (Figure 1) show the flow properties of all gel formulas having pseudoplastic flow properties. It is called pseudoplastic flow when the flow curve passes (0,0), in contrast to the plastic stream so that the pseudoplastic flow has no yield value. The viscosity of pseudoplastic substances decreases with increasing rate of shear. The pseudoplastic system is also called a diluted shear system because by increasing the viscosity shear pressure downward.

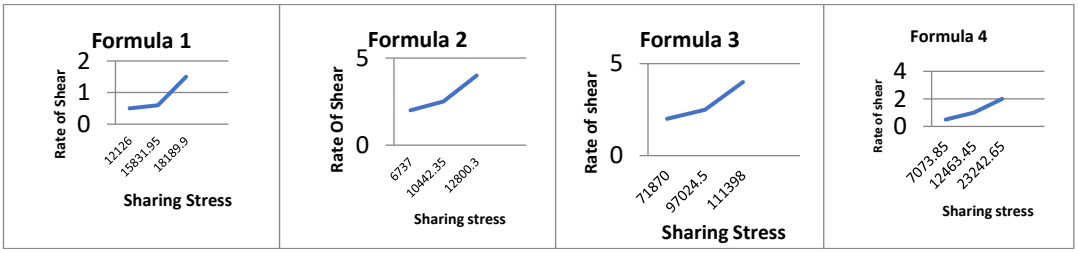

Figure 1. Flow properties of peel off gel activated charcoal from oil palm shells

Drying Time Test

The dry-time test of the preparation is carried out by observing the time it takes for the preparation to dry, ie the time from which the dosage begins to be applied to the skin to a completely dry layer. After the preparation dries, then the preparations are removed from the skin surface by exfoliation. The requirements for drying dosage time are for 15 - 30 minutes [7].

Table 7. Drying time test result

Gel Formula	Examination result
1	29.35 minute
2	21.37minute
3	15.14 minute
4	13.55 minute

The results showed that the dried time of the formula made ranged from 13.55 minutes to 29.35 minutes, so the four formulas were in accordance with the parameters. From the research results obtained concluded along with the increasing concentration of PVA then the preparation becomes more easily removed [5].

The most significant factor in dry time is the ethanol concentration in the formulation, because ethanol has a higher volatility level compared to pure water (Beringhs et al 2013). PVA is also one of the factors that affect dry time [20], where single PVA is more dominant in determining drying speed when compared with single CMC-Na or CMC-Na interaction with PVA.

Stickness power test

Stick test is done to determine the ability of gel to adhere to the skin. Condensed power test requirements should not be less than 0.07 minutes or 4 seconds [23]. According [14], good adhesiveness is over one second.

Table 8. Stickness power test result

Gel Formula	Examination result
1	00.43 second
2	03.09 minute
3	More than 30 minutes
4	More than 30 minutes

Based on the data obtained all the gel has different adhesive ability. This is due to the higher gelling agent used ie PVA will increase the consistency of gel and greater adhesiveness. So it can be seen from the table above that the first formula and the second formula are not eligible. While the third and fourth formulas meet the requirements of more than 1 second or more than 4 seconds. A good gel has high adherence. The greater the adhesion force the greater the diffusion of the drug because of the bonding that occurs between the gel and the longer the skin [20].

Irritation Test

Irritation test was conducted on 12 panelists. Testing is done by open patch test (patch test). Positive irritant reactions are characterized by redness, itching, or swelling on specially treated skin.

Table 9. Irritation test result on panelist's skin

Parameter	Formula	Irritation test result
Redness	F1	0%
	F2	0%
	F3	0%
	F4	0%
Itchiness	F1	0%
	F2	0%
	F3	0%
	F4	0%
Swollen	F1	0%
	F2	0%
	F3	0%
	F4	0%

Skin irritation test conducted to prevent the occurrence of side effects of skin preparations. The results of the irritation test on the skin of the above volunteers showed that all volunteers gave negative results on the irritant reaction parameters on all gel formulas peel off activated charcoal of oil palm shells [20].

Hedonic Test

The favorite test is performed to see the consumer's preference in terms of color, odor, viscosity, comfort sensation when worn on the skin, and gel potential in causing itching and redness of the skin after 5 minutes of application [20].

In this favorite test, respondents were given a brief explanation of the active peel off charcoal gel. Then, by the respondent, the gel provided is then applied to the back of the hand to assess the gel from the side color, odor, and ease of polishing, comfort when worn and gel potential in causing itching and redness on the skin after smeared for 5 minutes.

Table 10. Hedonic test result

Gel Formula	Odor	Skin sensation	Color
1	67%	28%	74.6%
2	83.3%	61%	88%
3	85.3%	97%	92%
4	83.3%	53%	86%

From the results, most volunteers liked formula 3

Stability Test by Cycling Test method

Test the stability of the cycling test method on the gel to test whether there is any change in the preparation. A stable preparation is a preparation which is still within acceptable limits during storage and use, whereby its properties and characteristics are similar to those at the time of manufacture. In terms of organoleptis, stability test results of cycling test method showed no difference between before and after test. the resulting organoleptic properties are black with distinctive smell and semi-solid shape. This indicates that the resulting organoleptic preparations are stable against storage [23].

The pH value after the stability test has increased. The change in pH of the preparation is due to a stability test that uses the effect of temperature in its storage at a temperature of 4 ° C and 40 ° C. Changes in the pH value will be affected by the media decomposed by the temperature at which the storage generates acids or bases. In this study the changes that occur more towards the base so as to produce an increase in pH value. Changing the pH value of the dosage indicates a lack of stabilization of the preparation during storage. However, the pH changes that occur still meet the physiological pH range of the skin [9].

Table 11. pH test result

Gel Formula	pH level before the *cycling test*	pH level after *cycling test*
1	5.62	5.55
2	5.75	5.78

3	5.87	5.83
4	5.87	5.80

The results of the spreading power test showed that there was an increase in the spread of the seeds in each dosage after the stability test was performed, due to the temperature changes during the test that caused the preparation to be more dilute than before. This will affect the stockpile distribution. So the scattering power after the stability test on the formula 3 and 4 is said to meet the good scattering power.

Table 12. Power spread test after the cycling test result

Formula	Examination result	
	Before the *Cycling test*	After the *Cycling test*
1	8.20	8.40
2	7.24	7.64
3	4.34	4.70
4	3.13	3.40

The results of the stability test of the cycling test method in terms of adherence have good adhesion to the third and fourth formulas, but there is a decrease in adherence time in formula 1 and formula 2. This is because the consistency of the dosage produced is more dilute after the stability test is done so causing a decrease in adhesiveness.

Table 13. Sticknes spower test after the cycling test result

Formula	Examination result	
	Before *Cycling test*	After the *Cycling test*
1	00.43 second	00.28 secon
2	03.09 minute	02.34 minute
3	More than 30 minutes	More than 30 minutes
4	More than 30 minutes	Motre than 30 minutes

3.6. Effectiveness Test of Gel Mask Peel Off on dirt cleaning

The gel formula tested is the third formula. Effectiveness testing using a digital camera shows that the surface structure of the volunteer skin becomes smoother and the spots or blackish stains on the skin appear to fade after the use of the test preparation when compared to the control skin structure without the use of gel masks, as shown in Figure 2

(a) (b)

Figure 2. (a). Comparison of dirt cleaning results before given gel mask peel off activated charcoal palm shells and Bioaqua. (b) Comparison of dirt cleaning results after given gel mask peel off activated charcoal palm shells and Bioaqua

4. Conclusion

The conclusions that can be drawn based on the results of research conducted are activated charcoal from palm shell can be made into gel preparation gel peel off. Formula of Gel Mask Peel Off active mask that has the best physical properties is in the third formula that is by using PVA as much as 15%. Testing the effectiveness of using a digital camera shows that the surface structure of the panelist skin becomes smoother and the spots or blackish stains on the skin look faded after the use of the test preparation when compared to the skin control structure without the use of gel mask

5. References

[1] Anonim. 2014. *Indonesian palm oil pantation statistics for 2011-2013*. Directorate General of

Plantations, Ministry of Agriculture. Jakarta.
[2] U. Lestari, F. Farid., And P.M. Sari, 2017. Formulation and Physical Properties Test of Active Body Scrub Body Scrub from Palm Oil Shell As Detoxification. *Journal of Science and Technology*, 19 (1).
[3] U. Lestari, et all, 2017. Formulation and Physical Properties Test of Active Charcoal Tablets from Waste of Palm Shells (Elaeis guineensis Jacg) as Antidiarrhea Agents. *Journals of science and technology of pharmacy* 19 (1) 27-30
[4] Harry, R.G. 1973. *Harry's Cosmetology*, Edisi 6, Chemical Publishing, New York.
[5] Birck C, Degoutin S, Tabary N, Miri V, Bacquet M. New, 2014 crosslinked cast films based on poly (vinyl alcohol): preparation and physico-chemical properties. Express Polymer Letters ;8(12):941–952.
[6] Anonim, 1985. *Indonesian cosmetics formulary*, Departement Health RI , Jakarta.
[7] Septiani, S., N. Wathoni., dan S.R Mita. 2011. *Formulations and antioxidant gel Mask from Melinjo Seed Extract* (Gnetun Gnemon Linn). *Journal University padjajaran*. 1(1):4-24
[8] Kuncari, E.S., Iskandarsyah, dan Praptiwi. 2014. Evaluation of Physical Stability Test And Sineresis of Gel Preparations Containing Monoksidil, Apigenin and Celery Herbal Juice (*Apium graveolens* L.). *Health Research Bulltetin*. Vol. 42: 213-222.
[9] R.I. Trenggono, and F. Latifah, 2007. Cosmetic Introductory Handbook. Jakarta: PT Gramedia Public Library.
[10] Chandira R.M., Pradeep., A. Pasupathi., D. Bhowmik., B. Chiranjib., K.K. Jayakar., K.P. Tripathi., S. Kumar. 2010. Design, Development and Formulations of Antiacne Dermatological Gel. *J.Chem. Pharm. Research*. 2(1): 401-414.
[11] Voight, R. 1994. *Translated Pharmaceutical Technology Textbooks*. UGM Press, Yogyakarta.
[12] Yuliani, S. H. 2010. Optimization Mixed Combination Sorbitol, Gliserol, dan Propilenglikol in Gel Sunscreen Ethanol Extract *Curcuma manggai*. *Indonesian Pharmaceutical Magazine*. 21 (2): 83-89.
[13] Vieira, R.P., A.R. Fernandes., T.M. Kaneko., V.O. Consiglieri., C.A. Pinto., C.S.C. Pereiera., A.R. Baby., and M.V. Velasco. 2009. Physical and Physiochemical Stability Evaluation of Cosmetic Formulation Containg Soybean Extract Fermented by Bifidobacterium Animalis. *Brazilian Journal of Pharmaceutical Sciences*, Vol. 45
[14] Lieberman, A.H., M.M. Rieger., and S.G. Banker. 1998. *Pharmaceutical Dosage Forms: Disperse System*, Vol 3, Second Edition, Revised and Expanded, Marcel Dekker, Inc, New York.
[15] T. Novianti, *The Effect of lotion preparation formulations on the effectiveness of red fruit oil as a sunscreen compared to sunscreen preparations containing antioxidants*, Essay. FMIPA Departemen Pharmaceutical University Indonesia. Depok, 2008.
[16] Rangari P.J dan P. Chavan. *A Review on Preparation of Activated Carbon from Coconut Shell*. 2017. 5(4). DOI : 10.15680/IJIRSET.2017.0604197.
[17] Pari, G., Nurhayati, T dan Hartoyo. 2000. *Possibility of Active Use of Bark Acacia mangium Willd for Refining Palm Oil*. 8(1): 40 - 53. Center for Forest Product Research and Development, Bogor
[18] Ademiluyi, F.T dan E.O.D. West. *Effect of Chemical Activated on the Adsoption of Heavy Metals Using Activated Carbons from Wate Materials*. 2012. DOI:10.5402/2012/674209.
[19] Anonymous. Indonesian National Standard (SNI). National standardization board. Jakarta, 1996.
[20] Rahmawanty, D., N. Yulianti., dan M, Fitriana. 2015. *Formulation and Evaluation of Peel Off Facial Mask Containing Quercetin With Various Concentration of Gelatin dan Gliserin*. *Pharmaceutical media.* 12 (1): 17-32.
[21] Rowe, R.C., P.J. Sheskey., dan Owen. *Handbook of Pharmaceutical Excipients,6th Edition,* Pharmaceutical Press: London. 2009.
[22] Butler, H. 2000. *Poacher's Perfumes, cosmetics and Soap*,10th Edition, Kluwer Academic Publishers, London.
[23] R. Voight, An Introduction to Pharmaceutical Technology Books. Gaja Mada University Press. Yogyakarta, 1994.

INTERNATIONAL PROCEEDING
The 2nd International Conference on Science and Technology (ICST)
ISBN: 978-602-5830-19-8, June 2020

Photochemistry of Chloroplatinate Anions

I H Silalahi[1,2*] and D W Bruce[2]

[1]Department of Chemistry, FMIPA, University of Tanjungpura, Pontianak, Indonesia
[2]Department of Chemistry, University of York, Heslington, YORK YO10 5DD UK

[*]Email: imelda.h.silalahi@chemistry.untan.ac.id

Abstract. A Zeise's salt analogue, the dinuclear, butadiene-bridged complex, *trans*-η^2:η^2-1,3-butadiene-bis(trichloroplatinate(II)) has been formed when tetrabutylammonium hexachloroplatinate(IV) was refluxed in acetone as well as in dichloromethane. The reaction proceeds under ambient light, but under UV illumination the reaction is complete in a matter of hours, while in a rigorously dark condition, no product was observed suggesting a photochemical reaction. Activation of hydrocarbons by hexachloroplatinate(IV) complex was reported but the importance of light in the reaction appears to be less clear. Thus, the photochemistry of chloroplatinate anions was discussed in this paper.

1. Introduction

Preparation of nanoparticle-doped, mesoporous silicas, through liquid crystal template and two different metal precursors has been reported [1, 2]. It was observed that nanoparticles contained PtCo were formed inside the pores exhibiting a ferromagnetic response but the metal insertion shown in a wide range of compositions [3]. In then thinking about well-defined, heterobimetallic precursors that might lead to bimetallic nanoparticles of, defined composition, uniformly, we reported on the preparation of the mixed-metal, heterobi nuclear anion $[Cl_2Pd(\mu\text{-}Cl)_2PtCl_2]^{2-}$, obtained by reaction of $[PtCl_4]^{2-}$ and $[PdCl_4]^{2-}$ as their $[K(18\text{-crown-}6)]^+$ salts. In seeking analogous complexes, $[PtCl_4]^{2-}$ was reacted with $[AuCl_4]^-$ leading immediately to oxidation to Pt^{IV} and reduction to Au^I. As part of the further investigation of this reaction, Bu_4N^+ salts were employed and on one occasion crystals were isolated that were identified as the dinuclear, butadiene-bridged complex *trans*-η^2:η^2-1,3-butadiene-bis(trichloroplatinate(II)) (**I**) (Figure **1**) [4].

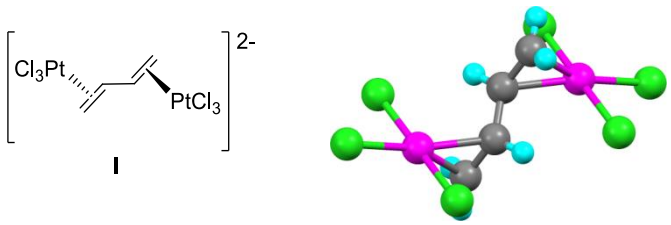

I

Figure 1: Molecular structure of the $[Cl_3Pt(\mu^2\text{:}\mu^2\text{-}1,3\text{-butadiene})PtCl_3]^{2-}$ dianion [4].

It then became clear that the role of the gold (III) salt was simply to oxidise the platinum (II) to platinum (IV) and so it was established that simple reaction of $[^nBu_4N]_2[PtCl_6]$ in acetone or dichloromethane led to the formation of the product. Ambient light can drive the reaction, but under

photolysis, the consumption of hexachloroplatinate(IV) occurred much faster, monitored by using $^{195}Pt\{^{1}H\}$ NMR spectroscopy. $^{195}Pt\{^{1}H\}$ NMR spectrum of the reaction mixture also revealed the existence of $[PtCl_4]^{2-}$ anion. Shul'pin and co-workers reported the reaction of hydrocarbons with $[PtCl_6]^{2-}$ under irradiation as well as thermally [5-8] but the importance of light in the activation of $^{n}Bu_4N^{+}$ cation was unexpected. Therefore, the photochemistry of $[^{n}Bu_4N]_2[PtCl_6]$ as well as the product: complex $\eta^2:\eta^2$-1,3-butadiene-bis(trichloroplatinate(II)) and $[^{n}Bu_4N]_2[PtCl_4]$ were studied as a part of the investigation of the reaction.

The photochemistry of the tetrachloroplatinate(II) and hexachloroplatinate(IV) anions has been reported [9-15]. Taube and Rich reported photo-properties of $[PtCl_4]^{2-}$ and $[PtCl_6]^{2-}$ observed in an isotopic labelling experiment [9]. Under irradiation (open window on a sunny day) in an aqueous solution of HNO_3 and NaCl at 25 °C, a chlorine exchange occurs between $[PtCl_6]^{2-}$ with Cl^- in the solution. It was reported that the exchange is also observed under dark conditions but with only 20% of the exchange compared to a complete exchange when the reaction was carried out under light, suggesting a photo-enhanced reaction. In the presence of reducing agents such as $[Fe(CN)_6]^{2-}$, and $[IrCl_6]^{2-}$, the reaction is halted, thus demonstrating a chain reaction type. The reaction is also inhibited by Cl_2, ruling out the possibility of elemental chlorine as a catalyst. Therefore, the reaction is believed to be catalysed by a radical suggesting a paramagnetic Pt^{III} species generated from the irradiation of $[PtCl_6]^{2-}$. A proposed mechanism suggested the initiation step generates the catalyst, $[Pt^{III}Cl_5]^{2-}$, and a chlorine radical followed by a chloride ion substitution. The propagation step proceeds after the generation of the catalyst, Pt^{III}, while the exchange of $[PtCl_6]^{2-}$ with the chloride ion is taking place. The chloride exchange step involves an inner-sphere electron transfer [16]. The photochemistry of $[PtCl_4]^{2-}$ appears to be quite different from that of $[PtCl_6]^{2-}$. Thus, when $[PtCl_4]^{2-}$ is illuminated under the same conditions as $[PtCl_6]^{2-}$, an exchange reaction takes place slowly but addition of an oxidant, Ce^{IV}, induces the reaction. It was proposed that the initiation step proceeds through a one-electron oxidation of Pt^{II} by Ce^{IV} generating Ce^{III} and the active species Pt^{III}. Further steps proceed on the same basis as that of the $[PtCl_6]^{2-}$ reaction [9]. The observations imply that $[PtCl_4]^{2-}$ is not an effective precursor for the paramagnetic species, Pt^{III}, under light.

Furthermore, oxidation of alcohols to afford aldehyde and ketone products in the presence of $H_2[PtCl_6]$ under irradiation was reported [10]. The reaction is catalytic where $H_2[PtCl_6]$ is the precursor to generate a photo-catalyst, Pt^{III} species. The catalytic reaction required co-catalysts, $CuCl_2$ and O_2, for regeneration of the precursor, as in the absence of the co-catalysts the organoplatinum product was obtained stoichiometrically ending the catalytic cycle. It was also reported that the reaction is hampered in the absence of $H_2[PtCl_6]$ even though $CuCl_2$ and/or O_2 are added to the reaction [10]. Experimental results suggest the photoreaction of alcohols undergoes a chain-type reaction. The fact that $CuCl_2$ is unable to oxidise $[PtCl_4]^{2-}$ to $[PtCl_6]^{2-}$, excludes the possible role of the Pt^{II} and leads to the idea of the existence of Pt^{III} as Taube and Henry [9] reported earlier. Thus the $CuCl_2$ is proposed to be the charge-transfer mediator by one-electron oxidation of Pt^{III} to Pt^{IV}, while reduction of Cu^{II} to Cu^{I} allows the reaction to take place in a catalytic cycle.

A set of experiments to study solvent participation in the photoactivation of $[PtCl_6]^{2-}$ were reported [12]. Under light with a metal present, solvent can act as a substrate undergoing charge transfer to solvent (CTTS) states and becoming an active species [12]. The CTTS state denotes an electron excitation from the metal complex to an appropriate orbital of the solvent molecule. The state commonly occurs in the UV region, thus for example, when a photoreaction does not proceed under visible light but proceeds under UV irradiation, the CTTS state can be responsible for the reaction. Monreal, *et.al* reported the photoreduction of $(Bu_4N)_2[PtCl_6]$ in $CHCl_3$ under 297 nm light and attributed the reaction to a metal-centred process [13]. The involvement of chloroform was suggested but definite evidence to distinguish the metal-centred state from the solvent state was not provided.

An extension of the role of $[PtCl_6]^{2-}$ under light was reported by Shul'pin in an activation of alkanes [5]. Reaction conditions are similar to the Shilov system but it is photochemical at room temperature with an absence of $[PtCl_4]^{2-}$. For example, irradiation of hexane with hexachloroplatinate(IV) affords hexene

coordinated *via* a π-bond to a reduced platinum(II) complex [5]. It suggests a C–H activation that appears to be followed by a β-hydride eliminiation and reductive elimination giving the alkene product coordinated to Pt^{II}. Mechanistic results regarding the photoactivation of alkanes using $[PtCl_6]^{2-}$ were reported by Shul'pin and co-workers [6-8]. The paramagnetic, platinum(III) species is detected in the reaction using electron paramagnetic resonance (EPR) spectroscopy where a *g* value of about 2.40 was found, which is common for transition metal radicals [17]. The same peak is also observed when acetone is irradiated with $[PtCl_6]^{2-}$ present [7]. Moreover, a σ-alkyl-platinum(IV) complex was synthesised separately from a photoreaction of $[PtCl_6]^{2-}$ with metal tetraalkyls of Sn and Ge, which was stable enough to be detected by nuclear magnetic resonance (NMR) spectroscopy. The reaction takes place through an electron substitution mechanism with involvement of an electron transfer from the tetraalkyl metal to the platinum(IV) complex. Further photolysis of the σ-alkyl-platinum(IV) complex affords the π-alkene-platinum(II) complex [17]. Similarly, the authors assumed that the formation of the π-alkene-platinum(II) complex in the irradiation of alkane with $[PtCl_6]^{2-}$ may proceed *via* the σ-alkyl-platinum(IV) intermediate [17].

2. Method

UV-visible spectra were recorded in solution on a Shimadzu UV–2401PC Spectrophotometer using quartz cuvettes of 1 cm path length and a spectral window between 190 nm and 800 nm.

^{1}H NMR spectra were recorded using Jeol ECS400 and Jeol ECX400 spectrometers operating at 400 MHz (^{1}H) and ^{1}H at 500 MHz, $^{195}Pt\{^{1}H\}$ NMR spectra were recorded on Bruker Avance 500 spectrometer using Topspin software. The resonance frequencies applied for $^{195}Pt\{^{1}H\}$ nuclear was 107 MHz. The processing of all spectra was carried out using MestreNova software. For ^{1}H-NMR, the residual protic solvent was used as the internal standard ($CDCl_3$: 7.26 ppm, CD_2Cl_2: 5.32 ppm, CD_3COCD_3: 2.04 ppm), for the ^{195}Pt-NMR spectra were referenced to $K_2[PtCl_6]$ in D_2O. Tetrabutylammonium hexachloroplatinate(IV), tetrabutylammonium tetrachloroplatinate(II) and 1,3-butadiene-bis(trichloroplatinate(II)) were prepared as reported by Silalahi, *et al*., 2018 [4].

3. Results and Discussion

Shul'pin and co-workers reported the reaction of hydrocarbons with $[PtCl_6]^{2-}$ under irradiation as well as thermally [5-8] but the importance of light in the activation of $^{n}Bu_4N^{+}$ cation was unexpected. Therefore, the photochemistry of $[^{n}Bu_4N]_2[PtCl_6]$ was studied and to begin, UV-vis spectra of the chloroplatinate anions were recorded, followed by irradiation under a variety of wavelengths to determine the wavelength necessary to activate $[PtCl_6]^{2-}$ in the formation of the butadiene-platinum(II) complex.

A UV-vis spectrum (Figure 2) of a solution of tetrabutylammonium hexachloroplatinate(IV) in acetone showed an absorption with λ_{max} = 324 nm with a shoulder at about 370 nm; a weak, longer wavelength absorption was also seen at 470 nm. The UV-vis spectrum of pure acetone is shown for reference. To define the viable wavelength responsible for the activation of $(^{n}Bu_4N)^{+}$ by $[PtCl_6]^{2-}$ photolysis of the complex in acetone at a variety of wavelengths was carried out.

Using the UV-vis spectra as a guide, the irradiations were conducted at each of 495, 435, 345 and 305 nm for 10 minutes. The $^{195}Pt\{^{1}H\}$ NMR spectra demonstrated consumption of $[^{n}Bu_4N]_2[PtCl_6]$ on irradiation at wavelengths shorter than 495 nm, with higher rates at 345 and 305 nm where 45% conversion was obtained compared to only about 3% consumption on irradiation at 435 nm. The platinum consumption was in accordance with the ^{1}H-NMR spectra in which on irradiation at 345 and 305 nm, a peak in the olefinic region at 4.3 ppm was seen. Therefore, experiments to investigate the photoreaction of $[PtCl_6]^{2-}$ with $(^{n}Bu_4N)^{+}$ cation were conducted under the irradiation of $h\nu > 305$ nm.

Light can be considered as an energy source for a homolytic reaction. Red light has an energy of 167 kJ mol^{-1} (λ = 715 nm), blue light (λ = 408 nm) corresponds to energy of 293 kJ mol^{-1}. Ultraviolet radiation (λ = 205 nm) corresponds to an energy of 586 kJ mol^{-1} which theoretically is able to cleave a C–H bond (435 kJ mol^{-1}) [18]. In the activation of the $(^{n}Bu_4N)^{+}$ cation, the substantial role of light as only a radical

initiator through a radical chain reaction was considered. However, irradiation of $^{n}Bu_4NCl$ compound in acetone did not activate the ammonium ion as confirmed by ^{1}H-NMR spectroscopy implying an important role of platinum(IV) complex in activation of NBu_4^+ cation.

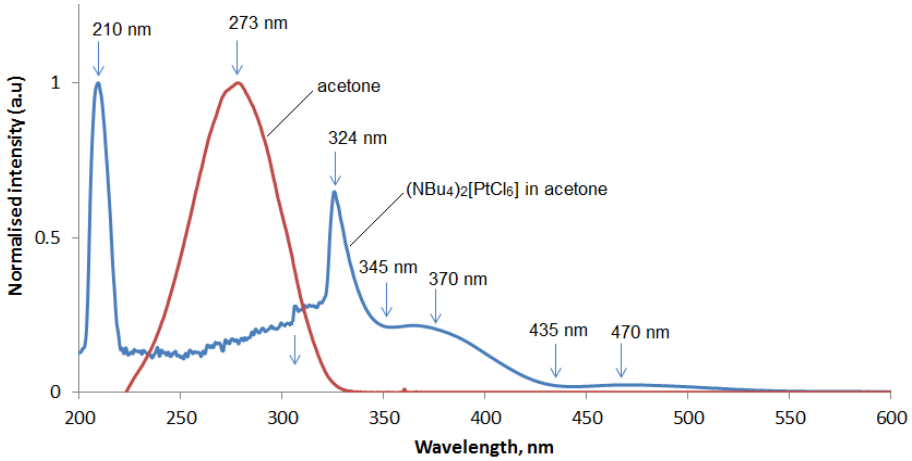

Figure 2. The UV-vis spectra of acetone and $[^{n}Bu_4N]_2[PtCl_6]$ in acetone

UV-vis spectra of the starting material, $[^{n}Bu_4N]_2[PtCl_6]$ as well as the observed products, $[^{n}Bu_4N]_2[PtCl_4]$ and $[^{n}Bu_4N]_2[\eta^2\text{-}Cl_3Pt(C_4H_6)\text{-}\eta^2\text{-}PtCl_3]$, **I**, in acetone and in dichloromethane were recorded, and molar absorptivity of those complexes were determined. Data of the molar absorptivity of those complexes are tabulated in Table 1. As mentioned earlier, in acetone $[^{n}Bu_4N]_2[PtCl_6]$ absorbs light strongly at 210 nm and 324 nm in which the magnitude of molar extinction coefficient suggests the absorption bands contributed to electronic transitions which are MLCT and LMCT. A weak band observed at 370 nm suggests electronic transitions of spin allowed but Laporte forbidden. The pattern is similar with the spectra of $[^{n}Bu_4N]_2[PtCl_4]$ and $[^{n}Bu_4N]_2[\eta^2\text{-}Cl_3Pt(C_4H_6)\text{-}\eta^2\text{-}PtCl_3]$ as shown in Figure 3. The absorptivity of $[^{n}Bu_4N]_2[\eta^2\text{-}Cl_3Pt(C_4H_6)\text{-}\eta^2\text{-}PtCl_3]$ at 210 nm was about 10 times higher than that of $[PtCl_4]^{2-}$ and $[PtCl_6]^{2-}$, but clearly, at 324 nm the absorptivity of $[^{n}Bu_4N]_2[PtCl_6]$ was higher than that of the products. Thus, when the $[^{n}Bu_4N]_2[PtCl_6]$ in acetone was irradiated at $\lambda \geq 305$ nm, the products were expected to be fairly stable. This was confirmed on the ^{1}H NMR spectra when the butadiene-platinum(II) complex alone was irradiated, in which decomposition appeared to be started on longer than 40-minute illumination introduced by an isomerisation.

Table 1. Molar absorptivity of chloroplatinate complexes in different solvents and wavelengths.

Complexes	Solvent	ε, $mol^{-1}\ dm^3\ cm^{-1}$
$[^{n}Bu_4N]_2[PtCl_6]$	DCM	370 nm: $0.40.10^3$
	Acetone	370 nm: $0.45.10^3$ 324 nm: $1.29.10^3$
$[^{n}Bu_4N]_2[PtCl_4]$	DCM	336 nm: $0.07.10^3$ 404 nm: $0.06.10^3$
	Acetone	336 nm: $0.08.10^3$ 404 nm: $0.06.10^3$
$[^{n}Bu_4N]_2[\eta^2\text{-}Cl_3Pt(C_4H_6)\text{-}\eta^2\text{-}PtCl_3]$	DCM	310 nm: $0.86.10^3$ 227 nm: $7.50.10^3$
	Acetone	325 nm: $0.37.10^3$ 210 nm: $0.53.10^3$

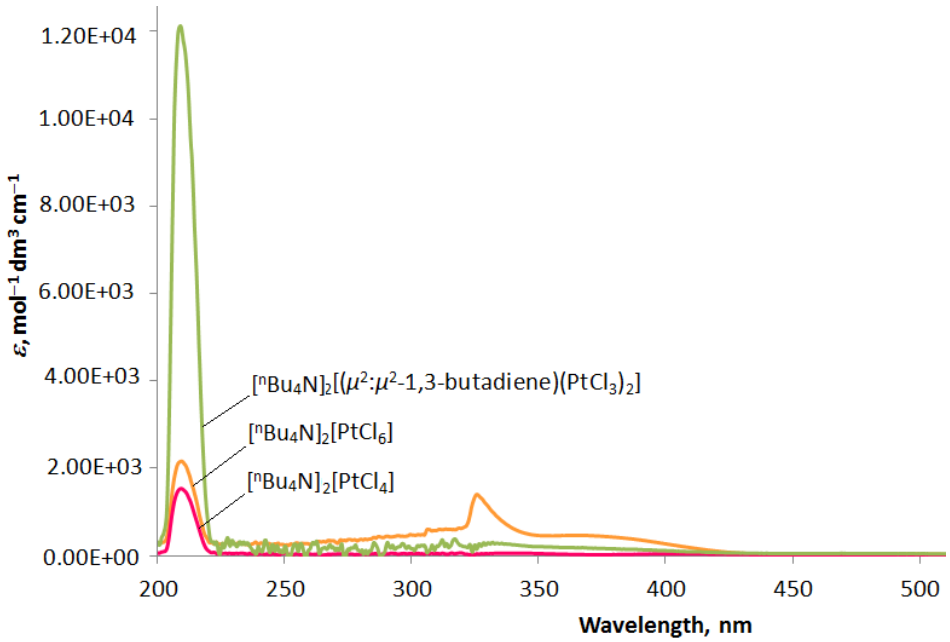

Figure 3. The UV spectra of the chloroplatinate complexes in acetone.

The absorption spectrum of $[^nBu_4N]_2[PtCl_6]$ in dichloromethane (Figure 4) is different where the main peak is at 269 nm, shorter wavelength than the wavelength observed in acetone although the weak signal at 370 nm was also seen. The pattern is also different from the spectra of $[^nBu_4N]_2[PtCl_4]$ and $[^nBu_4N]_2[\eta^2\text{-}Cl_3Pt(C_4H_6)\text{-}\eta^2\text{-}PtCl_3]$ while the molar absorptivity of $[^nBu_4N]_2[PtCl_6]$ at the wavelength lower than 305 nm appeared lower than the that of the products. The pattern of the spectrum as well as the absorptivity of $[^nBu_4N]_2[PtCl_6]$ perhaps contributes to low rate of $[PtCl_6]^{2-}$ consumption so the low yield of the photolysis in dichloromethane.

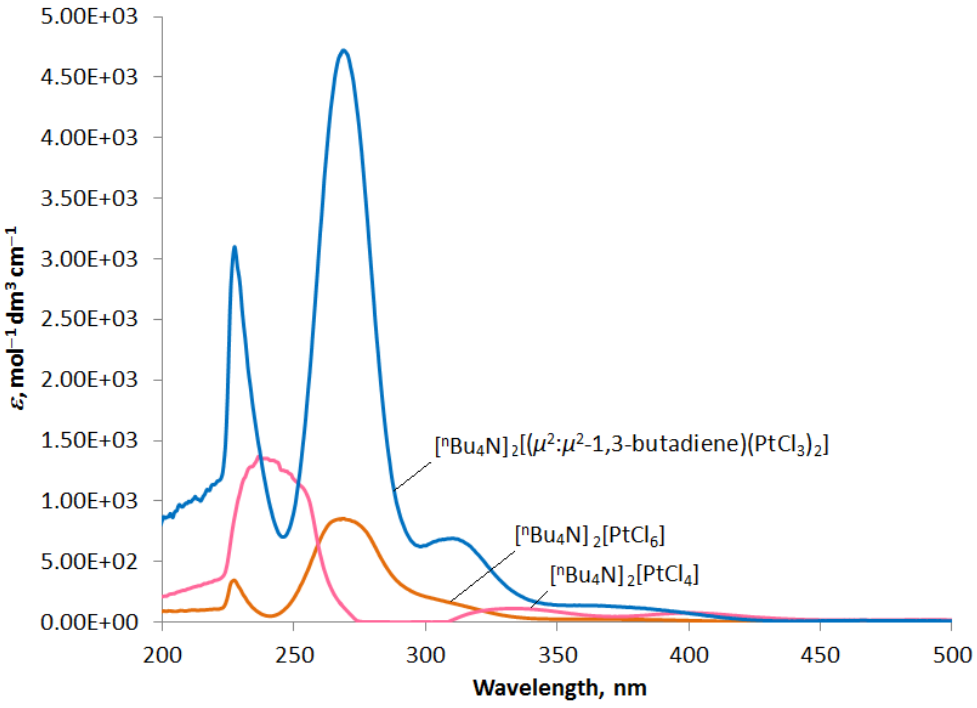

Figure 4. The UV spectra of the chloroplatinate complexes in dichloromethane.

The activation of tetrabutylammonium cation clearly proceeded under ambient light as has shown on the early observation, but the reaction was driven fast under UV light. We have reported a calculation using time-dependent density functional theory (TDDFT) to investigate the electronic structure of $[PtCl_6]^{2-}$ excited state. [4] The study showed an agreement with the experimental UV-vis spectra, in which the absorption at 207 nm demonstrates a mixed of MLCT with ligan-to-ligan charge transfer (LL'CT), whereas the peak at 324 nm represents two transitions of LL'CT and LMCT, the opposite of electron transfer direction at 207 nm. The study also suggests that the excited state of $[PtCl_6]^{2-}$ that activate tetrabutylammonium cation exists at the lowest excited triplet state (T_1) as the complex contains a heavy Pt atom allowing spin – orbit coupling (SOC) that attributes to fast singlet-triplet states intersystem-crossing (ISC).[4]

Acknowledgement
IHS thanks the Higher Education Ministry of Republic of Indonesia for a scholarship.

5. References

[1] C. M. A. Parlett, D. W. Bruce, N. S. Hondow, A. F. Lee and K. Wilson, *ACS Catalysis*, 2011, **1**, 636-640.
[2] C. M. A. Parlett, P. Keshwalla, S. G. Wainwright, D. W. Bruce, N. S. Hondow, K. Wilson and A. F. Lee, *ACS Catalysis*, 2013, **3**, 2122-2129.
[3] N. C. King, R. A. Blackley, M. L. Wears, D. M. Newman, W. Zhou and D. W. Bruce, *Chem. Commun.*, 2006, DOI: 10.1039/b607471e, 3414-3416.
[4] I. H. Silalahi, N. K. Sethi, M. Z. Shafikov, V. Chechik, A. C. Whitwood and D. W. Bruce, *Chem. Commun.*, 2018, **54**, 13682-13685.
[5] G. B. Shulpin, G. V. Nizova and A. E. Shilov, *J. Chem. Soc., Chem. Commun.*, 1983, DOI: 10.1039/c39830000671, 671-672.
[6] M. V. Serdobov, G. V. Nizova and G. B. Shulpin, *J. Organomet. Chem.*, 1984, **265**, C12-C14.
[7] G. V. Nizova, M. V. Serdobov, A. T. Nikitaev and G. B. Shulpin, *J. Organomet. Chem.*, 1984, **275**, 139-144.
[8] A. N. Kitaigorodskii, V. M. Nekipelov, A. T. Nikitaev and G. B. Shulpin, *J. Organomet. Chem.*, 1984, **275**, 295-301.
[9] R. L. Rich and H. Taube, *J. Am. Chem. Soc.*, 1954, **76**, 2608-2611.
[10] R. E. Cameron and A. B. Bocarsly, *J. Am. Chem. Soc.*, 1985, **107**, 6116-6117.
[11] R. E. Cameron and A. B. Bocarsly, *Inorg. Chem.*, 1986, **25**, 2910-2913.
[12] P. E. Hoggard, *Coord. Chem. Rev.*, 1997, **159**, 235-243.
[13] O. Monreal, T. Esmaeili and P. E. Hoggard, *Inorg. Chim. Acta*, 1997, **265**, 279-282.
[14] P. E. Hoggard and A. Vogler, *Inorg. Chim. Acta*, 2003, **348**, 229-232.
[15] P. E. Hoggard, A. J. Bridgeman, H. Kunkely and A. Vogler, *Inorg. Chim. Acta*, 2004, **357**, 639-643.
[16] M. Chanon, *Acc. Chem. Res.*, 1987, **20**, 214-221.
[17] G. B. Shulpin, G. V. Nizova, A. N. Kitaigorodskii and M. V. Serdobov, *J. Organomet. Chem.*, 1984, **275**, 273-282.
[18] N. G. Jonathan Clayden, and Stuart Warren, *Organic Chemistry*, Oxford University Press, Oxford, Second edn., 2012.

INTERNATIONAL PROCEEDING
The 2nd International Conference on Science and Technology (ICST)
ISBN: 978-602-5830-19-8, June 2020

Enzymatic Conversion of Potato Starch into Glucose using the purified α-Amylase Enzyme from Locale Isolate Bacteria Bacillus subtillis ITBCCB148

S Karlinasari[1], T Suhartati[2], H Satria[2], S Hadi[2] and Yandri[2*]

[1]Master Program in Chemistry, Department of Chemistry, Faculty of Mathematics and Natural Science, University of Lampung, Bandar Lampung 35145 (Indonesia).
[2]Department of Chemistry, Faculty of Mathematics and Natural Science, University of Lampung, Bandar Lampung 35145 (Indonesia).

[*]Email: yandri.as@fmipa.unila.ac.id

Abstract. The objective of this study was to determine the ability of the purified α-amylase enzyme to convert potato starch into glucose. For this objective, we isolated and purified α-amylase from locale bacteria isolate *Bacillus subtillis* ITBCCB148. The isolation of the extracellular α-amylase was conducted by the use of cold centrifuge method which was carried out to separate the enzyme from the cells. The purification of α-amylase was examined by fractionation using ammonium sulphate followed by dialysis. The activity of α-amylase was determined using the Fuwa method and Mandels while the protein content was determined using the Lowry method. The purified α-amylase obtained from 20–80% of saturated ammonium sulphate has specific activity of 11312.64 $U.mg^{-1}$. Based on the purity, it was increased to 6.41 times compared to the crude enzyme (1765.25 $U.mg^{-1}$). Furthermore, the purification in dialysis step was able to increse the specific activity at 28834.13 $U.mg^{-1}$, where the purity rose to 16.33 times higher than the crude enzyme. The purified enzyme had an optimum pH at 5 and optimum temperature at 65°C. The purified amylase from dialysis step was then applied for enzymatic conversion with various concentrations of potato starch 0.1; 0.2; 0.4; 0.6 and 0.8 % respectively to produce glucose. These starch concentration was able to produce glucose at 0.14; 0.33; 0.49; 0.72 and 0.71 $mg.mL^{-1}$, respectively. The activity of α-amylase in the conversion of starch potato were 26.54; 60.51; 91.18; 133.33 and 131.72 $U.mL^{-1}$ respectively. In conclusion, the purified α-amylase enzyme was able to convert potato starch to glucose with an optimum concentration of potato starch 0.6%.

Keywords: Palm oil shells, activated charcoal, PVA, Gel Mask Peel Off

1. Introduction

Many microorganisms are known as sources of α-amylase including bacteria and fungi. It also has also been studied and widely applied in many industrial sectors that they have been used in many large scale production of α-amylase [1]. Bacterial α-amylases which have novel properties, have been the major extent of recent research. [2]. *B. subtilis* is a rod-shaped gram-positive bacterium, members of the genus *Bacillus*. It can form endospore, to persist dangerous ecological surroundings of radiation, solvents, temperature and extreme pH, the endospore is considered at times of nutritional stress, allowing the organism to persist in the environment until the conditions become favorable [3]. In the field of biotechnology, *B. subtilis* is microorganism which could produce some type of enzymes such as proteases

and amylase that high product yields (20 to 25 gram per litre) with excellent fermentation properties [4].

Amylase, a starch degrading enzyme, is an important enzymes that widely used in industry and accounts for high proportion of the enzyme market [5]. The α-amylase (E.C. 3.2.1.1) has been applied as catalysts for enzymatic hydrolysis of materials with high content of starch [6]. α-amylases act on starch (polysaccharide) as the main substrate and yield small units of glucose (monosaccharide) and maltose (disaccharide). Starch is made of two glycose polymers, amylose and amylopectin, which comprise glucose molecules that are connected by glyosidic bonds. Both polymers have different structures and properties. A linear polymer of amylose has a maximum of 6000 glucose units linked by α-1,4 glycosidic bonds, whereas amylopectin is composed of α-1,4-linked chains of 10–60 glucose units with α-1,6-linked side chains of 15–45 glucose units [7]. Enzymatic hydrolysis generates a glucose solution which can be used without further treatments [8].

Glucose, an important industrial product of starch hydrolysis finds application as sweetener in the food and pharmaceutical industries [9]. Starchy substrates are good source of sugar, this study was designed to develop a suitable technology (by optimizing an enzymatic process) for conversion of locally available and cheaper starchy substrates. Starch hydrolysates containing glucose can be obtained from potato, sweet potato, corn, wheat, sorghum, sugarcane, sugar beet and cassava starch into fermentable sugars and bio-etanol [10,11]. Carbohydrates based agricultural products like starch from potato occur abundantly and can be used as a raw material for the production of energy. Interestingly, it is reported that after completion of saccharification process, glucose is found to the main hydrolysis product of potato and sweet potato starch [12].

Several industrial processes are carried out using whole cells as the source of enzymes but the efficiency can be improved using isolated and purified enzymes. However, the criteria for selection of a particular method of isolation and purification depend on its end use. Various steps of ammonium sulphate precipitation are followed by dialysis for partial purification of crude enzyme. The partial purification and characterization of the enzyme from locale bacteria isolate *B. subtillis* ITBCCB148 are presently reported. Thus based on the background above, the objective of this study is to determine the characteristics of the purified α-amylase to convert potato starch into glucose.

2. Research Method

2.1. α-Amylase production

Inoculum Preparation.

The stock culture of *Bacillus subtillis* ITBCCB148 was grown in Nutrient agar (NA) medium with 0.5 % soluble starch in order to obtain fresh isolates. The inoculum preparation was then inoculated in the production medium with the inoculum medium used by (Yandri *et al*., 2010) [13] consisting of 0.5% soluble starch, 0.5% yeast extract, 0.01% $CaCl_2$, 0.02% $MgSO_4$,$7H_2O$ and 0.08% KH_2PO_4. The pH of medium was seted up to 6.5. Then the medium was sterilized at 121 °C, pressure 1 atm for 15 minute by using autoclave.

Production of α-amylase Enzymes. The composition of the production medium was equal to the composition of the inoculum medium. The active inoculum (2%) was iinoculated into an Erlenmeyer containing the production medium, incubated in a shaker incubator with an agitation speed at 200 rpm for 72 hours at room temperature [13]. The centrifugation was then conducted at 6000 rpm for 20 minutes. The supernatant obtained was a crude extract of α-amylase enzyme.

2.2. Activity test of a-amylase and determination of protein content

α-Amylase assay

α-amylase activity was measured by determination the liberated reducing sugars as end products according to Fuwa [14] and Mandels method [15].

Protein determination

Lowry [16] method was used to determine the protein content.

2.3. Purification of α-amylase Enzymes

Fractionation.

The crude extract enzyme obtained was purified by fractionation using ammonium sulphate. The crude enzyme was added by solid ammonium sulphate with continuous overnight stirring and separation into the following saturation ranges: (0-20)%; (20-40)%;(40-60)%; (60-80)%; and (80-100)% respectively [17]. The precipitates collected by centrifugation (10,000 g for 20 min) were dissolved in 0.1M phosphate buffer, pH 6.0.

Dialysis

The fractionated ammonium sulphate enzyme with the highest activity was purified by dialysis in the cellophane pouch with the extraction buffer for 24 h at 4 °C. Dialysis of the α-amylase enzyme was used to partially hydrolyze the potato starch into glucose.

2.4. Effect of pH on α-amylase activity and stability

Effect of pH on α-amylase activity was determined by performing enzyme assay at various pH value (4.5; 5.0; 5.5; 6.0; 6.5; 7.0; 7.5 and 8.0) using 0.1 M phosphate buffer.

2.5. Effect of Temperature on α-amylase activity and stability

To determine the optimum incubation temperature for maximum α-amylase activity, the reaction was carried out at various incubation temperatures (55; 60; 65; 70; 75 and 80^{o}C) for 30 min. The reaction mix comprising the purified amylase and 0.1% of potato starch solution was incubated at different temperatures at pH optimum.

2.6. Enzymatic Conversion of Potato Starch into Glucose

The purified amylase from dialysis step with the optimum pH and Temperature was then applied for enzymatic conversion with various concentrations of potato starch 0.1; 0.2; 0.4; 0.6 and 0.8 % respectively to produce glucose.

3. Result and Discussion

3.1.1. *Purification of α-amylase enzymes*

Fractionation.

The crude extract enzyme obtained was purified by fractionation using ammonium sulphate. The crude sample was fractionated into five groups i.e. (0-20)%; (20-40)%;(40-60)%; (60-80)%; and (80-100)% based on the saturation of ammonium sulphate (Figure 1).

Figure 1 showed that the highest specific activity of α-amylase was obtained at fraction of 40-60% ammonium sulphate saturation in amount of 6519.51 U.mg^{-1}, whereas in the fraction 0-20; 20-40; 60-80; and 80-100% of saturated ammonium sulphate have unit activity 465.213; 4769.22; 1071.76; and 144.32 U.mg^{-1}, respectively. These results indicated that the presence of enzymes deposited on these fractions. For the next process, fractionation was carried out in 2 levels of saturated ammonium sulphate, i.e. 0-20 and 20-80%. The division of fractions into 2 levels was aimed to increase the yield of enzyme so that there is no loss of enzymes when the fractionation process takes place and to increase the acquisition of considerable enzyme activity.

The specific activity showed a purity level of amylase enzyme. The more pure amylase enzyme obtained, the more value of specific activity increased. Figure 2 shows that purified α-amylase obtained from 20–80% of ammonium sulphate saturation has specific activity 11312.64 U.mg^{-1}. Regarding the purity, it was increased to 6.41 times compared with the crude one (1765.25 U.mg^{-1}). The results of this fraction were used for the next purification stage, namely dialysis.

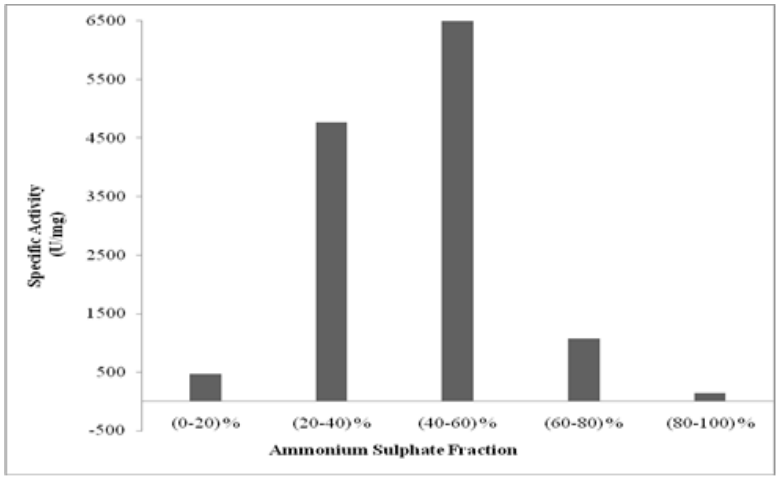

Figure 1 Effect of enzyme fraction at various levels of ammonium sulphate saturation on specific activity of the precipitates.

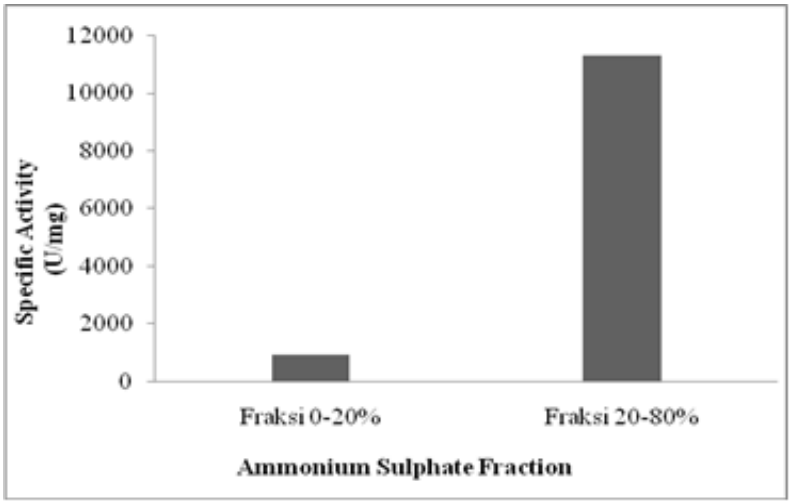

Figure 2 Effect of enzyme fraction at 2 levels of ammonium sulphate saturation on specific activity of the precipitates.

Dialysis

The membrane has pores that will permit small molecules such as ammonium and sulphate ions to cross, and hence equilibrate in the larger volume of buffer outside, while not permitting large protein molecules to cross. If the buffer is changed several times, allowing several hours each time for the ammonium sulphate to equilibrate, more or less all of it will be removed from the protein solution. Dialysis will increase the volume of the enzyme solution [18].

Table 1 The α-amylase purification scheme from *B. subtilis* ITBCCB148

Steps	Enzyme Volume (mL)	Unit Activity ($U.mL^{-1}$)	Protein Levels ($mg.mL^{-1}$)	Specific Activity ($U.mg^{-1}$)	Total Activity (U)	Yield (%)	Fold Purification
Crude Extract	3500	138.65	0.07854	1765.25	485272.20	100	1

Fractionation (20-80)% ammonium sulphate salt	165	1358.25	0.12007	11312.64	224111.99	46.18	6.41
Dialysis	203	1096.53	0.03803	28834.13	222596.16	45.87	16.33

From Table 1, it can be clearly seen that the specific activity of crude extract amylase unit is 1765.25 $U.mL^{-1}$ with a protein content of 0.07854 $mg.mL^{-1}$. Ammonium sulphate fractionated amylase obtained from dialysis has a specific activity of 28834.13 $U.mL^{-1}$ with a protein content of 0.03803 $mg.mL^{-1}$, thus ammonium sulphate fractionated enzyme from dialysis was 16.33 times and the purity of crude extract enzymes was 45.87 %. The purification of the enzyme was carried out in two stages namely fractionation with ammonium sulphate and dialysis.

3.2. Effect of pH on α-amylase activity and stability

Effects of pH on amylase activity were observed by conducting amylase assay with phosphate buffer at different pH (4.5–8.0) in which 0.1% soluble starch solutions were prepared. The pH stability of amylase was incubated at 60°C, as previously described in Table 2.

Table 2 Effect of pH of reaction on amylase activity

pH	**Unit Activity ($U.mL^{-1}$)**	**Relative Activity (%)**
4.5	34.96	82.64
5.0	42.31	100
5.5	37.37	88.34
6.0	37.20	87.92
6.5	34.65	81.90
7.0	33.86	80.03
7.5	26.99	63.80
8.0	33.36	78.87

It was found that the purified α-amylase produced by *B. subtilis* ITBCCB148 has an optimum pH at 5.0 with unit activity 42.31 $U.mL^{-1}$ and stable at 4.5-8.0 of pH. Activity of *α*-amylase at low pH range is very important for industrial applications. The application of liquefying amylases that are active and stable around the saccharification pH is attractive to avoid or reduce the use of acid to lower the pH from liquefying to saccharifying range and also to simplify the procedures during downstream processing [17].

3.3. Effect of temperature on α-amylase activity and stability

The effect of temperature on enzyme activity was measured by incubating the enzyme at different temperatures. The effect of temperature of reaction on amylase activity is shown in Table 3.

Table 3 Effect of temperature of reaction on amylase activity

Temperature (ºC)	**Unit Activity (U/mL)**	**Relative Activity (%)**
55	34.43	78
60	37.19	84

65	44.13	100
70	41.74	95
75	38.39	87
80	25.75	58

The purified enzyme has an optimum temperature at 65°C with unit activity 44.13 U.mL^{-1}. The purified amylase also still have high activity between 55-75°C.

3.4. Enzymatic conversion of potato starch into glucose

The purified amylolytic preparation was observed to exhibit α-amylase activities on potato starch. The α-amylase activity in various of substrate concentration is shown in **Figure 3.** The purified amylase from dialysis was able to convert potato starch to glucose with an optimum concentration of potato starch 0.6% and could produce glucose at 0.72 mg.mL^{-1} with unit activity 133.33 U.mL^{-1}. Enzymatic conversion with various concentrations of potato starch: 0.1; 0.2; 0.4 and 0.8% was able to produce glucose as follows 0.14; 0.33; 0.49; and 0.71 mg.mL^{-1}, respectively with unit activity of α-amylase 26.54; 60.51; 91.18 and 131.72 U.mL^{-1} respectively.

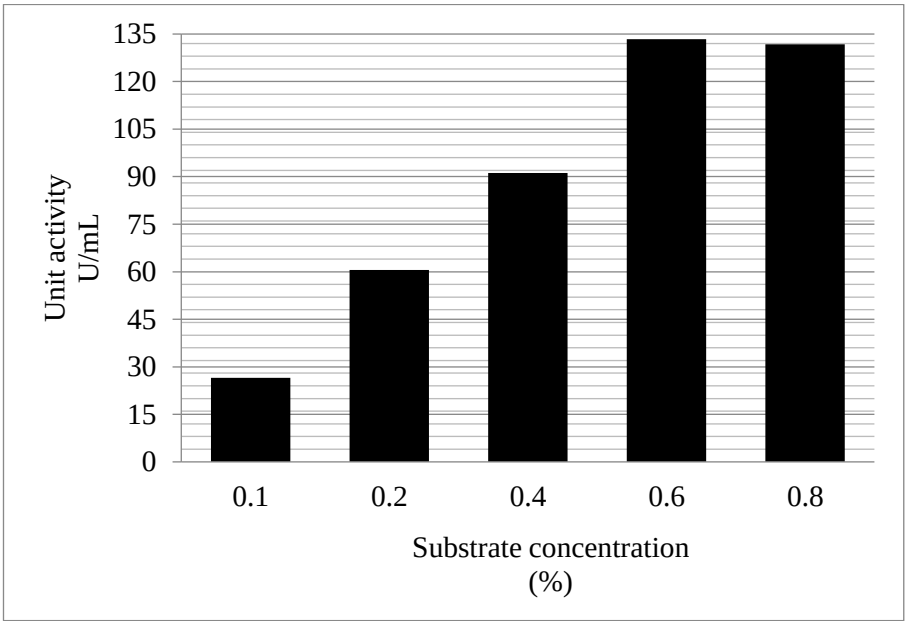

Figure 3. The α-amylase enzyme activity in various of substrat concentration

4. Conclusion

The locale isolate of bacteria (*B. subtillis* ITBCCB148) was proven to be able to produce α-amylase, which is not only stable at low pH, but also still active in wide pH ranges (4.5-8.0). The purified amylase as exepcted still have high activity at temperature between 55-75°C. The result of test indicated that the enzymatic conversion of potato starch was optimum at pH and temperature of 5.0 and 65° C, respectively. Moreover, it is also observed the best concentration of substrate is 0.6% that is able to produce the highest glucose. These properties are considered to be very important for industrial starch liquefaction.

Acknowledgement

The author would like to thank the Directorate of Research and Community Services, Directorate General of Strengthening Research and Development at the Ministry of Research, Technology and Higher Education For financial support in the form of Basic Research with a contract number: 065/SP2H/LT/DRPM/2019.

5. References

[1] Simair, A. A., Qureshi, A. S., Khushk, I., Ali, C. H., Lashari, S., Bhutto, M. A., & Lu, C. 2017. Production and partial characterization of α-amylase enzyme from bacillus sp. bcc 01-50 and potential applications. *BioMed research international* pp 1-9.

[2] Trabelsi S, Mabrouk S B, Kriaa M, Ameri R, Sahnoun M, Mezghani M, Bejar S 2019 The optimized production, purification, characterization, and application in the bread making industry of three acid-stable alpha-amylases isoforms from a new isolated *Bacillus subtilis* strain US586. *J Food Biochem*. e12826.

[3] Yu, AC, Loo JF, Yu S, Kong SK, Chan TF 2014 Monitoring bacterial growth using tunable resistive pulse sensing with a pore-based technique. *Applied Microbiology and Biotechnology*. 98 (2): 855–62.

[4] Van Dijl, JM, Hecker M 2013 Bacillus subtilis: from soil bacterium to super-secreting cell factory. *Microbial Cell Factories*. 12 (3): 3.

[5] Singh, R., Kumar, M., Mittal, A., & Mehta, P.K. 2016 Microbial enzymes: industrial progress in 21st century. *Biotech* **6** 2 174

[6] Lo´ pez, C., Torrado, A., Fucin˜ os, P., Guerra, N. P., & Pastrana, L. 2006. Enzymatic inhibition and thermal inactivation in the hydrolysis of chestnut pure´e with an amylases mixture. *Enzyme and Microbial Technology* 39: 252–258.

[7] Gopinath S.C.B., Anbu P., Arshad M. K. Md., Lakshmipriya T., Voon C.H., Hashim U., and Chinni C.V. 2017 Biotechnological Processes in Microbial Amylase Production. *BioMed Research International* Vol 2017 p 9

[8] Vázquez, M., Delgadob, R., and Castrob, A. J. 2009. Modelling of the Enzymatic Hydrolysis of Potato (*Solanum tuberosum*) Using Response Surface Methodology. *Starch/Stärke* (**61)**: 601–609.

[9] Majumder, C B. and Yadav P. 2017. Production of glucose syrup by the hydrolysis of starch made from rotten potato. *J Integr Sci Technol*, 5(**1**), 19-22.

[10] Luo L, Van Der Voel E and Huooes, G. 2009. Life cycle assessment and life cycle costing of bioethanol from sugarcane in Brazil. *Renewable and Sustainable Energy Rev*, 13, oo. 1613-1619.

[11] Mohanty, S.K, Behera, S., Swain, M.R., and Ray, R.C. 2009 Biotechnology production from mahula (Madhuca latifolia L.) flowers by solid-state fermentation. *Appl. Energy*, 86:640-644.

[12] Kumar A, Duhan J S, Saharan P, Surekhaa. 2012 Process optimization for the production of sugar from potato and sweet potato starch for bio-ethanol industry. Process optimization for the prodttction of sugar from potato.

[13] Yandri, Suhartati T. and Hadi S. 2010. Purification and Characterization of Extracellular α-Amilase Enzyme from Locale Bacteria Isolate *Bacillus subtilis* ITBCCB148. *Eur. J. Sci. Res.* **39**: 64-74.

[14] Fuwa H. 1954. A new method for microdetermination of amylase activity by the use of amylase as the substrate. *J. Biochem.* (Tokyo), **41**: 583-603.

[15] Mandels M., Raymond A. and Charles R. 1976. Measurment of saccharifying cellulose. *Biotech & Bioeng. Symp*. No 6. John Wiley & Sons Inc.

[16] Lowry O.H., Rosebrough N.J., Farr A.L. and Randall R.J. 1951. Protein measurement with the folin phenol reagen, *J. Biol. Chem*., 193-269.

[17] Singh R, Kumar V, and Kapoor V. 2014. Partial Purification and Characterization of a Heat Stable *α*-Amylase from a Thermophilic Actinobacteria, *Streptomyces* sp. MSC702. *Enzyme Research* Volume 2014, Article ID 106363, p 8.

[18] Shinde S and Soni R 2014. Production and Partial Purification of α-Amylase from Bacterial Strains. *International Journal of Genetic Engineering and Biotechnology.*1 (**5**), pp. 57-62.

INTERNATIONAL PROCEEDING
The 2nd International Conference on Science and Technology (ICST)
ISBN: 978-602-5830-19-8, June 2020

Solid Fixed Charge Transportation Problem and Its Paradox

E Sulistyono, B P Silalahi* and F Bukhari

Department of Mathematics, IPB University, Bogor, Indonesia

*Email: bibparuhum@gmail.com

Abstract. The solid fixed charge transportation problem is a problem of shipping products to minimize the shipping cost. This problem has 3 types of constraints, namely the supply of products, the demand for products, and other constraints that can be the type of products or vehicles. In the transportation problem, there is a case called a transportation paradox. Transportation paradox is a case when the number of products shipped increases but the shipping cost is smaller than before. This research aims to determine the sufficient condition of paradox, namely the conditions that must be met so that a paradox occurs. Besides that, it is formed the solid fixed charge transportation problem algorithm namely the steps to obtain a paradox until that paradox doesn't happen again. Furthermore, an illustration of the solid fixed charge transportation problem is given.

1. Introduction

Optimization is a part of mathematics that is studying and applying methods for finding the best solution. Some theories and applied optimization papers can be seen in [1-11]. The transportation problem is an optimization problem. The transportation problem was first formulated by Hitchcock in 1941 [12]. Generally, the transportation problem is a problem of shipping products from locations to other locations by minimizing shipping cost. The transportation problem has developed into various types of problems. Some of them are transportation problem with fuzzy [13], multi-objective transportation problem [14], and fixed charge transportation problem [15].

In the transportation problem, it is common if adding the product in shipping, the amount of the costs incurred increases. However, there is a condition when adding goods in shipping, the amount spent is actually reduced. This case is often also called transportation paradox [16].

Many researchers have worked on the transportation paradox. Some of them have researched about the paradox in fixed charge transportation problem. In 2000, Arora has researched about the paradox in a fixed charge transportation problem [17]. In 2015, Acharya has developed an algorithm of finding paradox in fixed charge transportation problem [18]. This research explained the condition needed so that a paradox can occur. The requirements need are usually called sufficient condition paradox. The transportation problem in previous research focused on two constraints, namely supply and demand of the product. The problem may have other constraints, like the type of product or type of vehicle. So the transportation problem may have three constraints, which is called a solid fixed charge transportation problem.

This paper is divided into 5 sections. Section 1 is an introduction, section 2 discuss the formulation of a solid fixed charge transportation problem. The sufficient condition occurrence paradox is explained in this section. In section 3, the algorithm paradox in a solid fixed charge transportation

problem is presented. Section 4 contains an example to support the previous theory. The last section is the conclusions.

2. Formulation of Solid Fixed Charge Transportation Problem

In this article, constraints consist of the supply of products, the demand of products and types of products. The objective function of solid fixed charge transportation problems is as follows:

$$\sum_{i=1}^{l}\sum_{j=1}^{m}\sum_{k=1}^{n} c_{ijk}x_{ijk} + \sum_{i=1}^{l}\sum_{k=1}^{n} F_{ik}$$

subject to

$$\sum_{j=1}^{m}\sum_{k=1}^{n} x_{ijk} \le a_i\,, \qquad i = 1,2,\dots,l$$

$$\sum_{i=1}^{l}\sum_{k=1}^{n} x_{ijk} = b_j\,, \qquad j = 1,2,\dots,m$$

$$\sum_{i=1}^{l}\sum_{j=1}^{m} x_{ijk} \le d_k\,, \qquad k = 1,2,\dots,n$$

$$x_{ijk} \ge 0, \qquad i = 1,2,\dots,l, \qquad j = 1,2,\dots,m, \qquad k = 1,2,\dots,n$$

with

$$\sum_{i=1}^{l} a_i = \sum_{k=1}^{n} d_k > \sum_{j=1}^{m} b_j,$$

x_{ijk} = the amount of k-th type of product that sent from the i-th origin to the j-th destination.
c_{ijk} = the cost of k-th type of product that sent from the i-th origin to the j-th destination.
F_{ik} = fixed cost of k-th type of product that sent from i-th origin.
a_i = supply of product in i-th origin.
b_j = demand of the product in j-th destination.
d_k = the amount of k-th type of product.

Let F_{ik} has q-step, so the formulation for F_{ik} is as follows:

$$F_{ik} = \sum_{p=1}^{q} \delta_{ikp} F_{ikp}$$

with

$$\delta_{ikp} = \begin{cases} 1\,; \sum_{j=1}^{m} x_{ijk} > A_{ikp} \\ 0\,; \text{others.} \end{cases}$$

A_{ikq} is constant that meet the condition $0 = A_{ik1} < A_{ik2} < \cdots, < A_{ikq}$. F_{ikp} is fixed cost.

Solid fixed charge transportation problem can be added with slack variable, so solid fixed charge transportation problem can be written as follows:

$$\sum_{i=1}^{l}\sum_{j=1}^{m+1}\sum_{k=1}^{n} c_{ijk}x_{ijk} + \sum_{i=1}^{l}\sum_{k=1}^{n} F_{ik}$$

subject to

$$\sum_{j=1}^{m+1}\sum_{k=1}^{n} x_{ijk} = a_i\,, \qquad i = 1,2,\dots,l$$

$$\sum_{i=1}^{l}\sum_{k=1}^{n} x_{ijk} = b_j\,, \qquad j = 1,2,\dots,m,m+1$$

$$\sum_{i=1}^{l}\sum_{j=1}^{m+1} x_{ijk} = d_k\,, \qquad k = 1,2,\dots,n$$

$$x_{ijk} \geq 0$$

$$i = 1,2,\dots,l, \qquad j = 1,2,\dots,m,m+1, \qquad k = 1,2,\dots,n$$

with

$$\sum_{i=1}^{l} a_i = \sum_{k=1}^{n} d_k = \sum_{j=1}^{m+1} b_j.$$

We know from [19], the optimality condition from solid fixed charge transportation problem must meet the condition as follows:

$$u_i + v_j + w_k = c_{ijk}, \qquad \forall (i,j,k) \notin B$$
$$u_i + v_j + w_k, \leq c_{ijk}, \qquad \forall (i,j,k) \in B$$

with u_i, v_j, w_k are dual variable and B is an index set of basis solution.

Theorem 1 The sufficient condition for paradox in solid fixed charge transportation problem is if there is at least one index$(r,s,t) \notin B$ with a_r, b_s, d_t are replaced by $a_r + \theta, b_s + \theta, d_t + \theta$, where $u_r + v_s + w_t + \Delta F < 0$. Variables u_r, v_s, w_t are dual variable and ΔF is fixed cost.

Proof. Let Z^0 be the value of objective function that corresponds with optimal solution x_{ijk}^0, $\sum_{i=1}^{l}\sum_{k=1}^{n} F_{ik}$ is given fixed cost. The dual variable is given with $u_i + v_j + w_k = c_{ijk}$ for each $(i,j,k) \notin B$, so

$$\begin{aligned}
Z^0 &= \sum_{i=1}^{l}\sum_{j=1}^{m}\sum_{k=1}^{n} c_{ijk}x_{ijk}^0 + \sum_{i=1}^{l}\sum_{k=1}^{n} F_{ik}^0 \\
&= \sum_{i=1}^{l}\sum_{j=1}^{m}\sum_{k=1}^{n} (u_i + v_j + w_k)x_{ijk}^0 + \sum_{i=1}^{l}\sum_{k=1}^{n} F_{ik}^0 \\
&= \sum_{i=1}^{l}\left(\sum_{j=1}^{m+1}\sum_{k=1}^{n} x_{ijk}^0\right)u_i + \sum_{j=1}^{m+1}\left(\sum_{i=1}^{l}\sum_{k=1}^{n} x_{ijk}^0\right)v_j + \sum_{k=1}^{n}\left(\sum_{i=1}^{l}\sum_{j=1}^{m+1} x_{ijk}^0\right)w_k + \sum_{i=1}^{l}\sum_{k=1}^{n} F_{ik}^0 \\
&= \sum_{i=1}^{l} a_i\, u_i + \sum_{j=1}^{m+1} b_j\, v_j + \sum_{k=1}^{n} d_k w_k + \sum_{i=1}^{l}\sum_{k=1}^{n} F_{ik}^0
\end{aligned}$$

Next, given at least one index $(r,s,t) \notin B$ with a_r, b_s, d_t are replaced by $a_r + \theta, b_s + \theta, d_t + \theta$ respectively $(\theta > 0)$. Then suppose $\hat{Z}$ is the value of the objective function that corresponds with an optimal solution $\hat{x}_{ijk}$ after increase θ, $\sum_{i=1}^{l}\sum_{k=1}^{n}\hat{F}_{ik}$ is fixed cost, θ and ΔF is the increase fixed cost after the increase θ. The value objective function $\hat{Z}$ is as follows:

$$\hat{Z} = \sum_{i=1}^{l}\sum_{j=1}^{m}\sum_{k=1}^{n} c_{ijk}\hat{x}_{ijk} + \sum_{i=1}^{l}\sum_{k=1}^{n}\hat{F}_{ik}$$
$$= \sum_{i=1}^{l}\sum_{j=1}^{m}\sum_{k=1}^{n}(u_i + v_j + w_k)x_{ijk}^{0} + \sum_{i=1}^{l}\sum_{k=1}^{n}\hat{F}_{ik}$$
$$= \sum_{i=1}^{l} a_i\, u_i + \sum_{j=1}^{m+1} b_j\, v_j + \sum_{k=1}^{n} d_k w_k + \sum_{i=1}^{l}\sum_{k=1}^{n}\hat{F}_{ik}$$
$$= \sum_{\substack{i=1\\ i\neq r}}^{l} a_i\, u_i + a_r u_r + \sum_{\substack{j=1\\ j\neq s}}^{m+1} b_j\, v_j + b_r v_r + \sum_{\substack{k=1\\ k\neq t}}^{n} d_k w_k + d_t w_t + \sum_{i=1}^{l}\sum_{k=1}^{n} F_{ik}^{0} + \Delta F$$
$$= \sum_{i=1}^{l} a_i\, u_i + \sum_{j=1}^{m+1} b_j\, v_j + \sum_{k=1}^{n} d_k w_k + \sum_{i=1}^{l}\sum_{k=1}^{n} F_{ik}^{0} + \theta(u_r + v_s + w_t) + \Delta F$$
$$= Z^0 + (u_r + v_s + w_t) + \Delta F$$

We know that $(u_r + v_s + w_t) + \Delta F$ is negative and Z^0 is the value of the objective function, so the value of $\hat{Z}$ is lower than Z^0, hence paradox occurs. ■

3. Algorithm

1. Determining paradoxical pair (Z^0, F^0), where Z^0 is the value of the objective function and F^0 is the amount of products that sent for the optimal solution X^0.
2. Determining $i = 1$.
3. Finding index$(r,s,t) \notin B$ that meet the condition $(u_r + v_s + w_t) + \Delta F < 0$ if it exists, otherwise go to step 8.
4. Determining $F^i = F^{i-1} + 1$.
5. Determining new paradoxical pair (Z^i, F^i).
6. Determining $i = i + 1$.
7. Go to step 3.
8. Write the best paradoxical pair $(Z^*, F^*) = (Z^i, F^i)$ for optimal special $X^* = X^i$.

Numerical example
Consider the following problem in Figure 1.

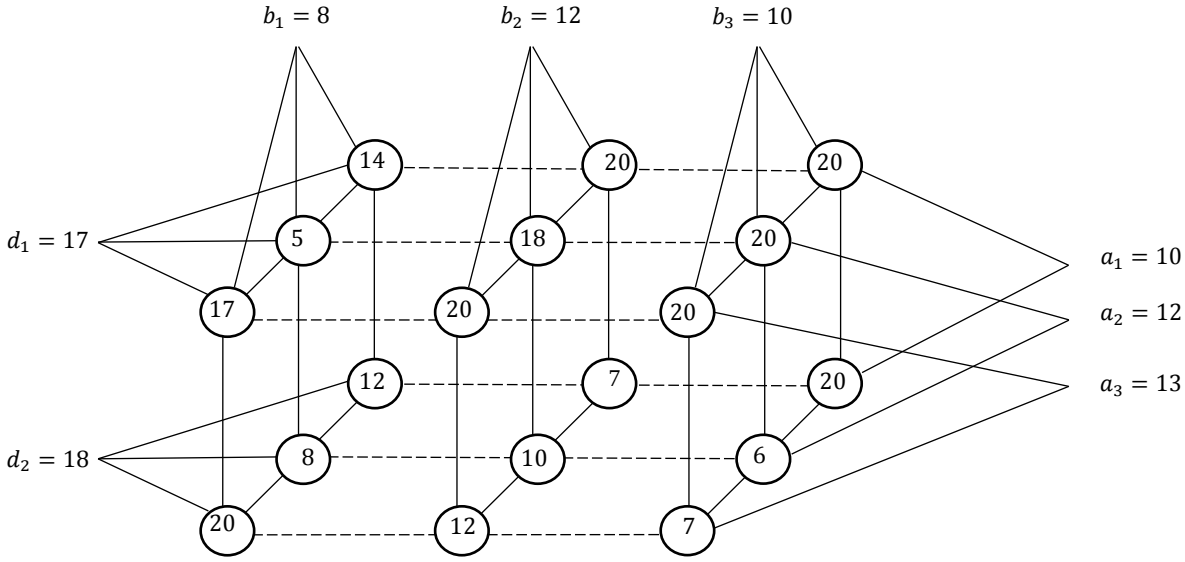

Figure 1

The fixed cost are

$$\begin{array}{lll} F_{111} = 15, & F_{112} = 7, & F_{113} = 5, \\ F_{121} = 12, & F_{122} = 4, & F_{123} = 2, \\ F_{211} = 11, & F_{212} = 7, & F_{213} = 3, \end{array}$$

$$\begin{array}{lll} F_{221} = 15, & F_{222} = 8, & F_{223} = 4 \\ F_{311} = 15, & F_{312} = 12, & F_{313} = 8 \\ F_{321} = 8, & F_{322} = 5, & F_{323} = 3 \end{array}$$

with

$$F_{I_2,I_3} = \sum_{j=1}^{3} \delta_{I_2,I_3,j}\, F_{I_2,I_3,j}$$

$$\delta_{I_2,I_3,1} = \begin{cases} 1\,; \sum_{I_1=1}^{3} x_{I_1,I_2,I_3} > 0 \\ 0\,; \text{others} \end{cases}$$

$$\delta_{I_2,I_3,2} = \begin{cases} 1\,; \sum_{I_1=1}^{3} x_{I_1,I_2,I_3} > 5 \\ 0\,; \text{others} \end{cases}$$

$$\delta_{I_2,I_3,3} = \begin{cases} 1\,; \sum_{I_1=1}^{3} x_{I_1,I_2,I_3} > 9 \\ 0\,; \text{others}\,. \end{cases}$$

Solid fixed charge transportation problems can be added with slack variables so that the solution to the problem is as follows (Figure 2).

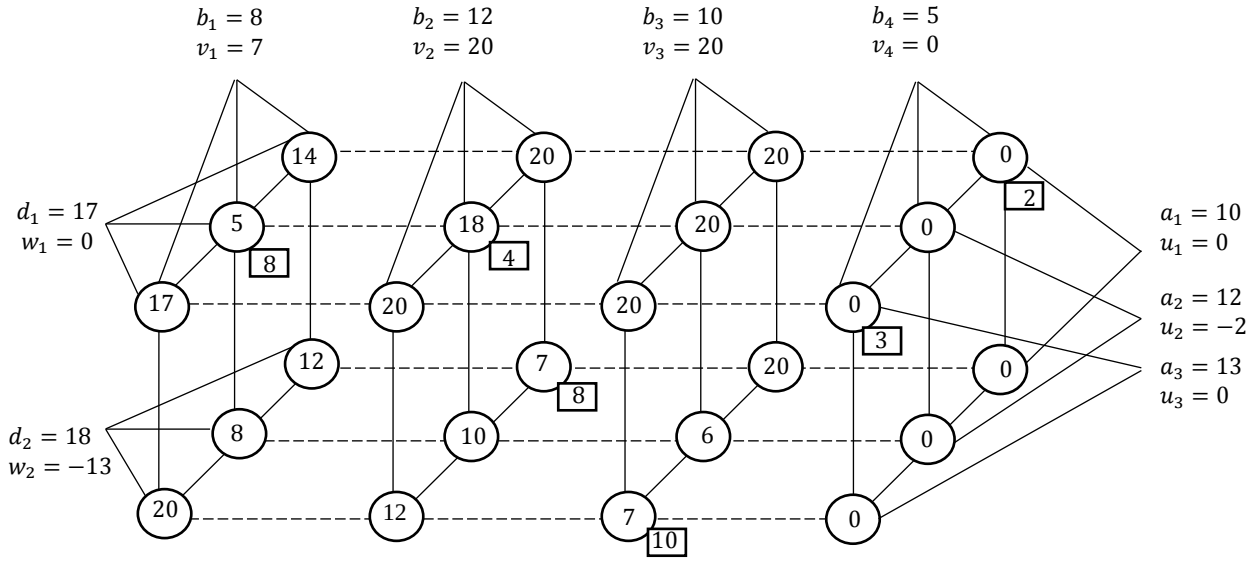

Figure 2

The fixed cost $\sum_{i_2,i_3} F^0_{i_2,i_3} = 53$, value of the objective function $Z^0 = 291$ and the amount of product that sent $F^0 = 30$, so the paradoxical pair $(Z^0, F^0) = (291,30)$.

Next by doing step 2, 3, and 4, selected index $(3,1,2) \notin B$ and increasing one item of product to the constraints, we have a new problem. The problem and the solution depicted in Figure 3.

The new fixed cost is $\sum_{i_2,i_3} F^1_{i_2,i_3} = 55$. To check the occurrence of paradox in this case, the condition in Theorem 1 must be fulfilled. The value of $\Delta F = 55 - 53 = 2$, then take the dual variable u_3, v_1 and w_2, so

$$u_3 + v_1 + w_2 + \Delta F = 0 + 7 + (-13) + 2 = -1 < 0.$$

A paradox occurs in this case because the dual variable and ΔF meet the Theorem 1. Next, by applying steps 5 and 6, the new paradox pair is obtained $(Z^1, F^1) = (287,31)$ and the value i = 2. After adding one unit item transported, there is a reduction in the objective function value by 4.

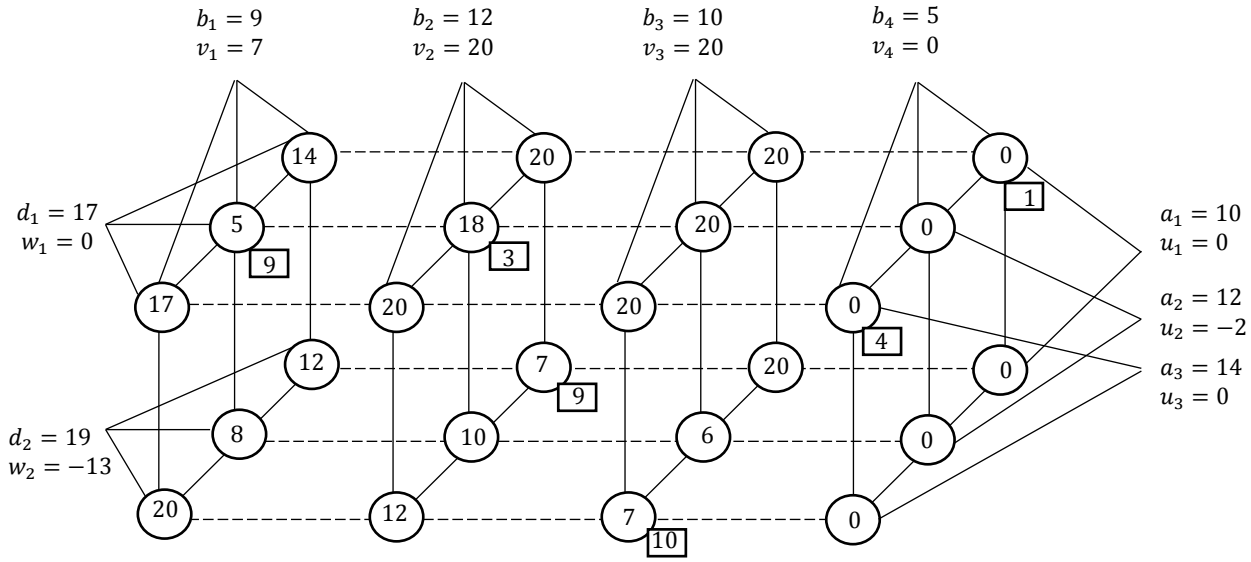

Figure 3

Back applying steps 3 to 6, the following results as in Figure 4 is obtained. The new fixed cost is $\sum_{i_2,i_3} F^2_{i_2,i_3} = 55$ and the new paradox pair is $(Z^2, F^2) = (281,32)$.

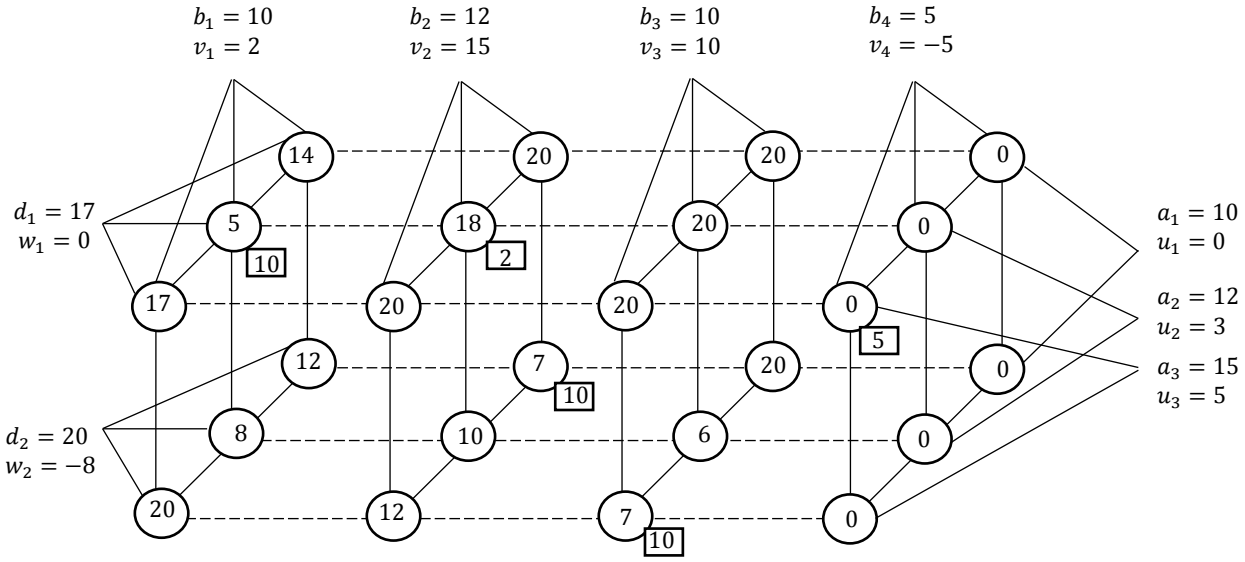

Figure 4

Again, applying steps 3 until 6, we obtain results as in Figure 5. The new paradox pair is $(Z^*, F^*) = (280, 33)$. This is the best paradox since there is no dual variable that satisfies Theorem 1. In this circumstance, it is no longer possible adding more products transported and the cost becomes lower.

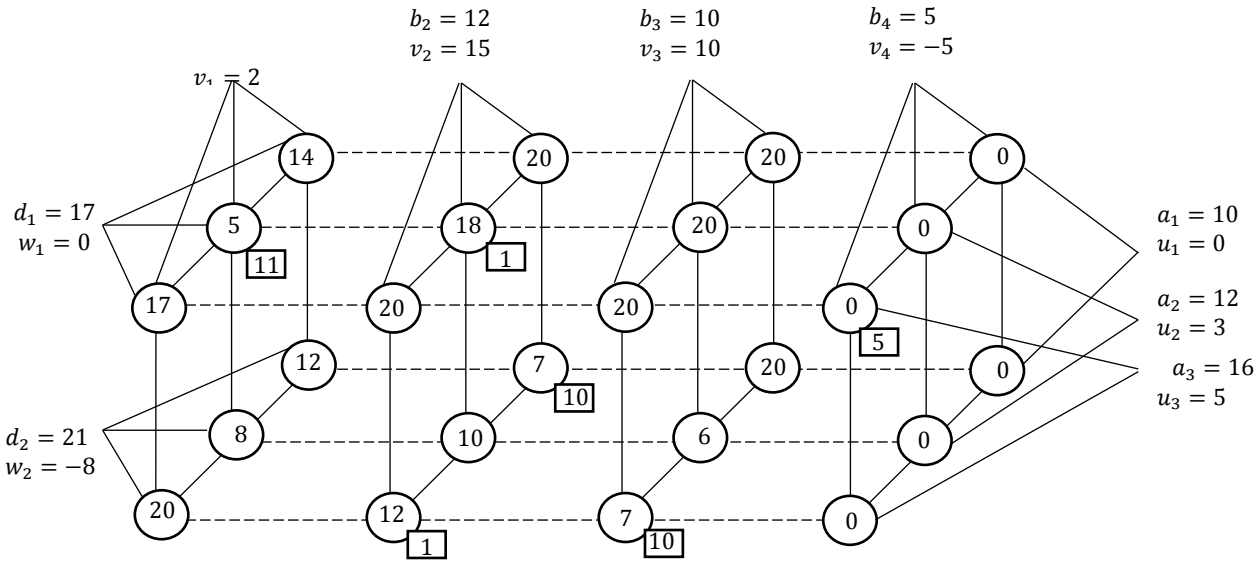

Figure 5

Acknowledgments
This paper is part of research that was supported by Direktorat Riset dan Pengabdian Masyarakat, Direktorat Jenderal Penguatan Riset dan Pengembangan Kementerian Riset, Teknologi, dan Pendidikan Tinggi Republik Indonesia No. 3/E1/KP.PTNBH/2019. We are very thankful.

References

[1] Desylvia SN, Buono A, Silalahi BP 2017 Modeling Text Independent Speaker Identification with Vector Quantization *Telkomnika* **15**(1): 322-327
[2] Krisnawijaya NN, Herdiyeni Y, Silalahi BP 2017 Parallel technique for medicinal plant identification system using fuzzy local binary pattern *Journal of ICT Research and Applications* **11**(1): 77-90
[3] Mayyani H, Silalahi BP, Aman A 2017 Frequency determination of bus rapid transit (BRT) applied on service system of trans mataram metro bus to minimize the operational cost *International Journal of Engineering and Management Research* (IJEMR) **7**(6): 134-140
[4] Saifudin MA, Silalahi BP, Sitanggang IS 2015 Star Catalog Generation for Satellite Attitude Navigation Using Density Based Clustering *Journal of Computer Science*, **11**(12): 1082-1089
[5] Silalahi BP 2014 Sharper analysis of upper bound for the iteration complexity of an interior-point method using primal-dual full-Newton step algorithm *Far East Journal of Mathematical Sciences* **95**(1): 69-80
[6] Silalahi BP 2019 Evaluation of interior-point method in scilab *IOP Conference Series: Earth and Environmental Science* **299**(1): 012040
[7] Silalahi BP, Bukhari F, Aman A, Khatizah E, Fahlevi NA 2019 Comparison of Interior Point Method Execution Time in Solving Linear Optimization Problems using MATHEMATICA and SCILAB. *International Journal of Statistics and Economics* **20**(4): 74-81
[8] Silalahi BP, Dewi MS 2014 Comparison of sensitivity analysis on linear optimization using optimal partition and optimal basis (in the simplex method) at some cases *IndoMS International Conference on Mathematics and Its Applications* pages 82–90
[9] Silalahi BP, Laila R, Sitanggang IS 2017 A combination method for solving nonlinear equations *IOP Conference Series: Materials Science and Engineering* **166**(1): 012011
[10] Silalahi BP, Wungguli D, Guritman S 2015 Steepest descent method with new step sizes *World Academy of Science, Engineering and Technology, International Journal of Mathematical, Computational, Physical, Electrical and Computer Engineering* **9**(7): 378–384
[11] Wihartiko FD, Buono A, Silalahi BP 2017 Integer programming model for optimizing bus timetable using genetic algorithm. *IOP Conference Series: Materials Science and Engineering* **166**(1): 012016
[12] Chvatal V 1983 *Linear Programming* (New York, US: W.H.Freeman and Company)
[13] Amit K, Amarpreet K 2011 Application of Classical Transportation Methods for Solving Fuzzy Transportation Problems *Journal of Transportation System Engineering and Information Technology* **11**(5): 68-80
[14] Rizk MRA, Hassanien AE, Elhoseny M 2018 A Multi-Objective Transportation Model Under Neutrosophic Environment *Computers and Electrical Engineering* pp:1-15
[15] Safi MR, Razmjoo A 2013 Solving Fixed Charge Transportation Problem with Interval Parameters *Applied Mathematical Modelling* **37**: 8341-8347
[16] Kautsar MMA, Silalahi BP, Guritman S 2018 Paradox In a d-Dimensional Transportation Problem *International Journal of Pure and Applied Mathematics* **118**(3): 547-557
[17] Arora SR, Ahuja A 2000 A Paradox In a Fixed Charge Transportation Problem *Indian Journal of Pure and Applied Mathematics* **31**(7): 809-822
[18] Acharya DP, Basu M, Das A 2015 The Algorithm of Finding all Paradoxical Pairs in a Fixed Charge Transportation Problem *Journal of Computer and Mathematical Sciences* **6**(6): 344-

352
[19] Das A, Acharya DP, Basu M 2015 More-for-Less Paradox in a Solid Transportation Problem *Journal of Information and Computing Science* **10**(4): (271-276)

INTERNATIONAL PROCEEDING
The 2nd International Conference on Science and Technology (ICST)
ISBN: 978-602-5830-19-8, June 2020

Transportation Paradox in Multi-objective Transportation Problem of *d*-Dimensional Case

I Husniah, B P Silalahi* and F Bukhari

Department of Mathematics, IPB University, Bogor, Indonesia

*E-mail: bibparuhum@gmail.com (corresponding author)

Abstract. The *d*-dimensional multi-objective transportation problem is a generalization of the classical transportation problem in a higher dimension with more than 1 objective function. A paradox in a transportation problem occurs when the optimum total cost becomes lower by shipping larger amount of goods over the same routes. In this paper, a sufficient condition for the existence of paradox will be established through its primal and dual. An algorithm to find all the paradoxical pairs will be discussed. A numerical example will be illustrated also in support of the theory.

1. Introduction

The transportation problem is one of the special class of linear optimization problems, which deals with shipping commodities from sources to destinations in order to minimize the total shipping cost [1]. This problem is first formulated by Hitchcock in 1941, then Dantzig in 1951 gave the standard linear optimization formulation and applied the simplex method to solve it [2]. Generally, in a transportation problem, shipping larger amount of goods will increase the total transportation cost. But, in some cases, it is possible to find a cheaper total cost than the optimal one by shipping more products over the same routes. This case is called transportation paradox.

In previous researches, Charnes and Klingman [3], Szwarc [4], and Storoy [2] considered the paradoxical transportation problem. Basu *et al.*[5] developed an algorithm to find all paradoxical pairs in a classical transportation problem and analyze the sufficient condition of the paradox, Das *et al.*[6] discussed paradox in a solid transportation problem, Kautsar *et al.*[7] developed an algorithm to find a paradoxical solution in *d*-dimension.

The classical transportation problem can be said as 2-dimensional transportation problem, because it only has 2 vector constraints. This problem also only has 1 objective function, which is to minimize the total cost of shipping goods. But, in real life, transportation problems also occur in higher dimensions and the objective function can be more complex such as minimizing the total cost of fuel consumption, minimizing the total delivery time, and more [8]. Therefore, in this paper, we will analyze a sufficient condition for the existence of paradox in multi-objective transportation problem of d-dimensional case, an algorithm to find paradoxical pairs will be discussed, and we will also illustrate a numerical example. Some other works of optimization can be seen in [9-19].

2. The *d*-dimensional Multi-objective Transportation Problem

The *d*-dimensional multi-objective transportation problem is a transportation problem that considers the existence of more than 1 objective function with *d* vector constraints. The formulation of this problem is as follows:

$$\text{minimize} \qquad Z^L = \sum_{i_1,i_2,\dots,i_d} c^L_{i_1,i_2,\dots,i_d} x_{i_1,i_2,\dots,i_d} \qquad L = 1,2,\dots,m$$

$$\text{subject to} \qquad \sum_{\substack{i_1,i_2,\dots,i_d \\ i_k=I}} x_{i_1,i_2,\dots,i_d} = a_I(k), \quad 1 \le k \le d;\ 1 \le I \le n_k$$

$$x_{i_1,i_2,\dots,i_d} \ge 0,$$

$a_I(k)$: I-th element of k-th vector constraints

$c^L_{i_1,i_2,\dots,i_d}$: the cost per unit amount corresponding to L-objective.

3. Dual of the *d*-dimensional Multi-objective Transportation Problem

First, we need to formulate the dual problem of the *d*-dimensional multi-objective transportation problem. By multiplying each constraint with a dual variable will have the following result:

$$\sum_{\substack{i_1,i_2,\dots,i_d \\ i_k=I_k}} u^L_{i_k}(k) x_{i_1,i_2,\dots,i_d} = a_{I_k}(k) u^L_{i_k}(k), \ \ 1 \le k \le d;\ \ 1 \le I_k \le n_k;\ L = 1,2,\dots,m,$$

by adding all the constraints above, we have:

$$\sum_{i_1,i_2,\dots,i_d} \Big(\sum_{k=1}^{d} u^L_{i_k}(k)\Big) x_{i_1,i_2,\dots,i_d} = \sum_{i_k=1}^{n_k} \sum_{k=1}^{d} a_{I_k}(k) u^L_{i_k}(k).$$

Because the dual of a minimization problem is a lower bound of its primal, the following condition must hold

$$\sum_{k=1}^{d} u^L_{i_k}(k) \le c^L_{i_1,i_2,\dots,i_d}.$$

So, the dual problem of the *d*-dimensional transportation problem can be written as

$$\text{maximize} \sum_{I_1}^{n_1} u^L_{i_1}(1)\, a_{I_1}(1) + \sum_{I_2}^{n_2} u^L_{i_2}(2)\, a_{I_2}(2) + \cdots + \sum_{I_d}^{n_d} u^L_{d}(d)\, a_{I_d}(d)$$

subject to

$$u^L_{i_1}(1) + u^L_{i_2}(2) + \cdots + u^L_{d-1}(d-1) + u^L_{d}(d) \le c^L_{i_1,i_2,\dots,i_d},$$
$$I_t = 1,2,\dots,n_t, t = 1,2,\dots d$$
$$L = 1,2,\dots,m.$$

4. Sufficient Condition of The Optimality

From the strong duality theorem in [20], if the primal has an optimal solution then the dual has an optimal solution with the same optimal value such that:

$$\sum_{i_1,i_2,\dots,i_d} \Big(\sum_{k=1}^{d} u^L_{i_k}(k)\Big) x_{i_1,i_2,\dots,i_d} = \sum_{k=1}^{d} \sum_{I_k}^{n_k} u^L_{i_k}(k)\, a_{I_k}(k) = \sum_{i_1,i_2,\dots,i_d} c^L_{i_1,i_2,\dots,i_d} x_{i_1,i_2,\dots,i_d}$$

We know that if $i_1, i_2, \dots, i_d \in B$, where B is the set of the optimal basic feasible solutions, then $x_{i_1,i_2,\dots,i_d} \ge 0$ and if $i_1, i_2, \dots, i_d \notin B$, then $x_{i_1,i_2,\dots,i_d} = 0$.

Therefore the sufficient for the optimality of the *d*-dimensional multi-objective transportation problem is as follow:

$$\sum_{k=1}^{d} u_{i_k}^{L}(k) = c_{i_1,i_2,\dots,i_d}^{L}, \qquad \forall i_1, i_2, \dots, i_d \in B$$

$$\sum_{k=1}^{d} u_{i_k}^{L}(k) \le c_{i_1,i_2,\dots,i_d}^{L}, \qquad \forall i_1, i_2, \dots, i_d \notin B$$

5. SufficientCondition of Paradox

Theorem 1. *Let* $p_1, p_2, \dots, p_d$ *with* $1 \le p_1 \le n_1, 1 \le p_2 \le n_2, \dots, 1 \le p_d \le n_d$, *so that*

$$u_{p_1}^{L}(1) + u_{p_2}^{L}(2) + \cdots + u_{p_d}^{L}(d) < 0.$$

If there is a $\theta > 0$ *so that if constraints* $a_{p_1}(1), a_{p_2}(2), \dots, a_{p_d}(d)$ *are replaced by* $\hat{a}_{p_1}(1) = a_{p_1}(1) + \theta, \hat{a}_{p_2}(2) = a_{p_2}(2) + \theta, \dots, \hat{a}_{p_d}(d) = a_{p_d}(d) + \theta$, *the optimal basic feasible solution can be found and have the set of optimal basic feasible solution remains the same, then the paradox will occur.*

Proof. Let $p_1, p_2, \dots, p_d$ with $1 \le p_1 \le n_1, 1 \le p_2 \le n_2, \dots, 1 \le p_d \le n_d$ and $u_{p_1}^{L}(1) + u_{p_2}^{L}(2) + \cdots + u_{p_d}^{L}(d) < 0$. Because of all the constraints replaced by $\hat{a}_{p_1}(1) = a_{p_1}(1) + \theta, \hat{a}_{p_2}(2) = a_{p_2}(2) + \theta, \dots, \hat{a}_{p_d}(d) = a_{p_d}(d) + \theta;\ \theta > 0$ and supposethe set optimal basic feasible solution remains the same, so the dual variables may remain the same. The change of the dual optimal value can be written as follows:

$$\begin{aligned}
Z^{L}(\hat{\boldsymbol{a}}_{\boldsymbol{I}}(\boldsymbol{k}), C^{L}) &= \sum_{I_1}^{n_1} u_{I_1}^{L}(1)\,\hat{a}_{I_1}(1) + \sum_{I_2}^{n_2} u_{I_2}^{L}(2)\,\hat{a}_{I_2}(2) + \cdots + \sum_{I_d}^{n_d} u_{I_d}^{L}(d)\,\hat{a}_{I_d}(d) \\
&= \sum_{\substack{I_1 \\ I_1 \neq p_1}}^{n_1} u_{I_1}^{L}(1)\,a_{I_1}(1) + u_{p_1}^{L}(1)\big(a_{p_1}(1) + \theta\big) + \sum_{\substack{I_2 \\ I_2 \neq p_2}}^{n_2} u_{I_2}^{L}(2)\,a_{I_2}(2) \\
&\quad + u_{p_2}^{L}(2)\big(a_{p_2}(2) + \theta\big) + \cdots + \sum_{\substack{I_d \\ I_d \neq p_d}}^{n_d} u_{I_d}^{L}(d) a_{I_d}(d) + u_{p_d}^{L}(d)\big(a_{p_d}(d) + \theta\big) \\
&= \sum_{\substack{I_1 \\ I_1 \neq p_1}}^{n_1} u_{I_1}^{L}(1)\,a_{I_1}(1) + u_{p_1}^{L}(1) a_{p_1}(1) + u_{p_1}^{L}(1)\theta + \sum_{\substack{I_2 \\ I_2 \neq p_2}}^{n_2} u_{I_2}^{L}(2)\,a_{I_2}(2) \\
&\quad + u_{p_2}^{L}(2) a_{p_2}(2) + u_{p_2}^{L}(2)\theta + \cdots + \sum_{\substack{I_d \\ I_d \neq p_d}}^{n_d} u_{I_d}^{L}(d) a_{I_d}(d) + u_{p_d}^{L} a_{p_d}(d) + u_{p_d}^{L}(d)\theta \\
&= \sum_{I_1}^{n_1} u_{I_1}^{L}(1)\,a_{I_1}(1) + u_{p_1}^{L}(1)\theta + \sum_{I_2}^{n_2} u_{I_2}^{L}(2)\,a_{I_2}(2) + u_{p_2}^{L}(2)\theta + \cdots \\
&\quad + \sum_{I_d}^{n_d} u_{I_d}^{L}(d)\,a_{I_d}(d) + u_{p_d}^{L}(d)\theta \\
&= \sum_{I_1}^{n_1} u_{I_1}^{L}(1)\,a_{I_1}(1) + \sum_{I_2}^{n_2} u_{I_2}^{L}(2)\,a_{I_2}(2) + \cdots + \sum_{I_d}^{n_d} u_{p_d}^{L}(d)\,a_{I_d}(d) \\
&\quad + \Big(u_{p_1}^{L}(1) + u_{p_2}^{L}(2) + \cdots + u_{p_d}^{L}(d)\Big)\theta \\
&= Z^{L}(\boldsymbol{a}_{\boldsymbol{I}}(\boldsymbol{k}), C^{L}) + \Big(u_{p_1}^{L}(1) + u_{p_2}^{L}(2) + \cdots + u_{p_d}^{L}(d)\Big)\theta.
\end{aligned}$$

We have that $u^L_{p_1}(1) + u^L_{p_2}(2) + \cdots + u^L_{p_d}(d) < 0$ and $\theta > 0$, so $\left(u^L_{p_1}(1) + u^L_{p_2}(2) + \cdots + u^L_{p_d}(d)\right)\theta < 0$, which implies $Z^L(\widehat{\boldsymbol{a}}_{\boldsymbol{I}}(\boldsymbol{k}), C^L) < Z^L(\boldsymbol{a}_{\boldsymbol{I}}(\boldsymbol{k}), C^L)$.

■

6. Algorithm for Finding Paradoxical Pairs

Step 1: Find the initial optimal solutions X_0 to the *d*-dimension multi-objective transportation problem, and write them as a pair of optimal value and the total product (Z_0, F_0).
Step 2: Fix $i = 1$.
Step 3: Find index $p_1, p_2, \ldots, p_d \notin B$ so that $u^L_{p_1}(1) + u^L_{p_2}(2) + \cdots + u^L_{p_d}(d) < 0$ with the same basic feasible solutions, if there aren't any, go to step 8.
Step 4: Increase the total shipment by 1 unit at each constraint corresponding to step 3.
Step 5: Write (Z_i, F_i).
Step 6: $i = i + 1$.
Step 7: Return to step 3.
Step 8: Write the paradoxical pair $(Z_*, F_*) = (Z_i, F_i)$ for an optimal solution $X_* = X_i$.

7. Numerical Illustration

Consider the following 4-dimensional multi-objective transportation problem given below:

$$c^1_{I_1,I_2,1,1} = \begin{bmatrix} 4 & 10 & 11 \\ 1 & 9 & 6 \\ 3 & 5 & 7 \end{bmatrix} c^1_{I_1,I_2,1,1} = \begin{bmatrix} 4 & 10 & 11 \\ 1 & 9 & 6 \\ 3 & 5 & 7 \end{bmatrix} c^1_{I_1,I_2,2,1} = \begin{bmatrix} 8 & 6 & 7 \\ 10 & 9 & 2 \\ 3 & 3 & 11 \end{bmatrix} c^1_{I_1,I_2,2,2} = \begin{bmatrix} 8 & 6 & 9 \\ 7 & 9 & 2 \\ 3 & 4 & 10 \end{bmatrix}$$

$$c^2_{I_1,I_2,1,1} = \begin{bmatrix} 10 & 25 & 26 \\ 17 & 25 & 28 \\ 19 & 21 & 28 \end{bmatrix} c^2_{I_1,I_2,1,1} = \begin{bmatrix} 20 & 26 & 27 \\ 17 & 25 & 21 \\ 19 & 15 & 26 \end{bmatrix}$$

$$c^2_{I_1,I_2,2,1} = \begin{bmatrix} 20 & 22 & 18 \\ 26 & 25 & 18 \\ 19 & 19 & 27 \end{bmatrix} c^2_{I_1,I_2,2,2} = \begin{bmatrix} 20 & 22 & 25 \\ 23 & 25 & 21 \\ 19 & 20 & 26 \end{bmatrix}$$

$$\boldsymbol{a}_{\boldsymbol{I_1}}(\mathbf{1}) = \begin{bmatrix} 29 \\ 11 \\ 10 \end{bmatrix}, \boldsymbol{a}_{\boldsymbol{I_2}}(\mathbf{2}) = \begin{bmatrix} 18 \\ 18 \\ 14 \end{bmatrix}, \boldsymbol{a}_{\boldsymbol{I_3}}(\mathbf{3}) = \begin{bmatrix} 34 \\ 16 \end{bmatrix}, \boldsymbol{a}_{\boldsymbol{I_4}}(\mathbf{4}) = \begin{bmatrix} 30 \\ 20 \end{bmatrix}$$

with the following optimal solutions:

Primal:

$$x_{1,1,1,1} = 18,\ \ x_{1,2,2,1} = 4,\ \ x_{1,2,2,2} = 4,\ \ x_{1,3,2,1} = 3,\ \ x_{2,3,1,2} = 6,\ \ x_{2,3,2,1} = 5,\ \ x_{3,2,1,2} = 10.$$

Dual:

$$u^1_1(1) = 7,\ \ u^1_2(1) = 2,\ \ u^1_3(1) = 2,\ \ u^1_1(2) = -7,\ \ u^1_2(2) = -1,\ \ u^1_3(2) = 0,$$

$$u^1_1(3) = 4,\ \ u^1_2(3) = 0,\ \ u^1_1(4) = 0,\ \ u^1_2(4) = 0$$

$$u^2_1(1) = 18,\ \ u^2_2(1) = 18,\ \ u^2_3(1) = 8,\ \ u^2_1(2) = -11,\ \ u^2_2(2) = 4,\ \ u^2_3(2) = 0,$$

$$u^2_1(3) = 3,\ \ u^2_2(3) = 0,\ \ u^2_1(4) = 0,\ \ u^2_2(4) = 0$$

$$Z^1(\boldsymbol{a}_{\boldsymbol{I}}(\boldsymbol{k}), C^1) = 237,\ \ Z^2(\boldsymbol{a}_{\boldsymbol{I}}(\boldsymbol{k}), C^2) = 776$$

When we check the sufficient condition for the existence of paradoxical solution with $u^L_p(1) + u^L_q(2) + u^L_r(3) + u^L_s(4) < 0$ and $(p, q, r, s) \notin B$, we observe that for Z^1, a paradox occurs in cells (2,1,1,1), (2,1,1,2), (2,1,2,1), (2,1,2,2), (3,1,1,1), (3,1,1,2), (3,1,2,1), (3,1,2,2). For Z^2, a paradox

occurs in cells (3,1,2,1) and (3,1,2,2). Hence Z^1, Z^2 the paradox commonly in the cells (3,1,2,1) and (3,1,2,2).

Applying step 1: The cost flow pair is $(Z_0, F_0) = \{(237, 50), (776, 50)\}$ corresponding to the initial optimal solution$X_0 = \{x_{1,1,1,1} = 18,\ x_{1,2,2,1} = 4,\ x_{1,2,2,2} = 4,\ x_{1,3,2,1} = 3,\ x_{2,3,1,2} = 6,\ x_{2,3,2,1} = 5,\ x_{3,2,1,2} = 5\}$.

Step 2: Fix $i = 1$.

Step 3: Check the sign of $u_p^L(1) + u_q^L(2) + u_r^L(3) + u_s^L(4) < 0$ for $(p, q, r, s) \notin B$, for the non-basic cell(3,1,2,1) we obtain $u_3^1(1) + u_1^1(2) + u_2^1(3) + u_1^1(4) = 2 + (-7) + 0 + 0 = -5 < 0$ and $u_3^2(1) + u_1^2(2) + u_2^2(3) + u_1^2(4) = 8 + (-11) + 0 + 0 = -3 < 0$, and for the non-basic cell (3,1,2,2), we obtain $u_3^1(1) + u_1^1(2) + u_2^1(3) + u_2^1(4) = 2 + (-7) + 0 + 0 = -5 < 0$ and $u_3^2(1) + u_1^2(2) + u_2^2(3) + u_2^2(4) = 8 + (-11) + 0 + 0 = -3 < 0$.

Step 4: Hence consider increasing the total shipment by 1 unit at each constraint for the cell we have:

$$\boldsymbol{a}_{I_1}(\mathbf{1}) = \begin{bmatrix} 29 \\ 11 \\ 10+1 \end{bmatrix}, \boldsymbol{a}_{I_2}(\mathbf{2}) = \begin{bmatrix} 18+1 \\ 18 \\ 14 \end{bmatrix}, \boldsymbol{a}_{I_3}(\mathbf{3}) = \begin{bmatrix} 34 \\ 16+1 \end{bmatrix}, \boldsymbol{a}_{I_4}(\mathbf{4}) = \begin{bmatrix} 30+1 \\ 20 \end{bmatrix}$$

and the new optimal solution is $X_1 = \{x_{1,1,1,1} = 19,\ x_{1,2,2,1} = 2,\ x_{1,2,2,2} = 5,\ x_{1,3,2,1} = 3,\ x_{2,3,1,2} = 4,\ x_{2,3,2,1} = 7,\ x_{3,2,1,2} = 11\}$ for which $(Z_1, F_1) = \{(232, 51), (773, 51)\}$. It means the new optimal value is lower by 5 units for Z^1 and 3 units for Z^2 than before increasing the total shipment.

Step 5: $(Z_1, F_1) = \{(232, 51), (773, 51)\}$.

Step 6: Fix $i = 1 + 1$.

Step 7: Repeat step 3, so we have $u_3^1(1) + u_1^1(2) + u_2^1(3) + u_1^1(4) = 2 + (-7) + 0 + 0 = -5 < 0$ and $u_3^2(1) + u_1^2(2) + u_2^2(3) + u_1^2(4) = 8 + (-11) + 0 + 0 = -3 < 0$ for non-basic cell (3,1,2,1), $u_3^1(1) + u_1^1(2) + u_2^1(3) + u_1^1(4) = 2 + (-7) + 0 + 0 = -5 < 0$ and $u_3^2(1) + u_1^2(2) + u_2^2(3) + u_2^2(4) = 8 + (-11) + 0 + 0 = -3 < 0$ for non-basic cell (3,1,2,2).

Increase the total shipment by 1 unit at each constraints for the cell (3,1,2,1) we have

$$\boldsymbol{a}_{I_1}(\mathbf{1}) = \begin{bmatrix} 29 \\ 11 \\ 11+1 \end{bmatrix}, \boldsymbol{a}_{I_2}(\mathbf{2}) = \begin{bmatrix} 19+1 \\ 18 \\ 14 \end{bmatrix}, \boldsymbol{a}_{I_3}(\mathbf{3}) = \begin{bmatrix} 34 \\ 17+1 \end{bmatrix}, \boldsymbol{a}_{I_4}(\mathbf{4}) = \begin{bmatrix} 31+1 \\ 20 \end{bmatrix}$$

and the new optimal solution is $X_2 = \{x_{1,1,1,1} = 20,\ x_{1,2,2,2} = 6,\ x_{1,3,2,1} = 3,\ x_{2,3,1,2} = 2,\ x_{2,3,2,1} = 9,\ x_{3,2,1,2} = 12\}$ for which $(Z_2, F_2) = \{(227, 52), (770, 52)\}$. It means the new optimal value is lower by 5 units for Z^1 and 3 units for Z^2 than before increase the total transshipment.

The new dual solution is:

$$u_1^1(1) = 7,\ u_2^1(1) = 2,\ u_3^1(1) = 2,\ u_1^1(2) = -7,\ u_2^1(2) = -1,\ u_3^1(2) = 0,$$

$$u_1^1(3) = 4,\ u_2^1(3) = 0,\ u_1^1(4) = 0,\ u_2^1(4) = 0$$

$$u_1^2(1) = 21,\ u_2^2(1) = 21,\ u_3^2(1) = 14,\ u_1^2(2) = -8,\ u_2^2(2) = 1,\ u_3^2(2) = 0,$$

$$u_1^2(3) = 0,\ u_2^2(3) = 0,\ u_1^2(4) = -3,\ u_2^2(4) = 0$$

When we check the sufficient condition for the existence of paradoxical solution with $u_p^L(1) + u_q^L(2) + u_r^L(3) + u_s^L(4) < 0$ and $(p, q, r, s) \notin B$, we observe that for Z^1, a paradox occurs in cells (2,1,1,1), (2,1,1,2), (2,1,2,1), (2,1,2,2), (3,1,1,1), (3,1,1,2), (3,1,2,1), (3,1,2,2). For Z^2, there aren't any dual variables that satisfy$u_p^2(1) + u_q^2(2) + u_r^2(3) + u_s^2(4) < 0$. So the iteration stops with $(Z_*, F_*) = (Z_2, F_2) = \{(227, 52), (770, 52)\}$.

Applying step 8: The best paradoxical pair is $(Z_*, F_*) = (Z_2, F_2) = \{(227, 52), (770, 52)\}$ corresponding to the optimal solution $X_* = X_2 = \{x_{1,1,1,1} = 20,\ x_{1,2,2,2} = 6,\ x_{1,3,2,1} = 3,\ x_{2,3,1,2} = 2,\ x_{2,3,2,1} = 9,\ x_{3,2,1,2} = 12\}$.

8. Conclusion

In this paper, the sufficient condition for the occurrence paradox of the *d*-dimension multi-objective transportation problem is established through it's primal and dual. A new algorithm is developed to solve its paradoxical solution with step by step procedure to find the best paradoxical pair.

Acknowledgments

This paper is part of a research that was supported by Direktorat Riset dan Pengabdian Masyarakat, Direktorat Jenderal Penguatan Riset dan Pengembangan Kementerian Riset, Teknologi, dan Pendidikan Tinggi Republik Indonesia No. 3/E1/KP.PTNBH/2019. We are very grateful.

References

[1] Siswanto 2006 *Operations Research Jilid 1* (Jakarta: Erlangga)
[2] Storøy S 2007 The Transportation Paradox Revisited. Retrieved from http://www.optimization-online.org/DB_HTML/2007/09/1763.html.
[3] Charnes A, Klingman D 1971 The more-for-less paradox in the distribution model *Cahiers du Centre d'Etudes de Recherche Operationalle* **13**: 11-22
[4] Szwarc W 1971 The Transportation Paradox *Naval Research Logistics Quarterly* **18**(2): 185-202
[5] Basu M, Archaya D, Das A 2012 The Algorithm of Finding All Paradoxical Pairs in A Linear Transportation Problem *Discrete Mathematics Algorithms and Applications* **4**(4): 1250049-1-1250049-9
[6] Das A, Archaya D, Basu M 2015 More-for-Less Paradox in A Solid Transportation Problem *Journal of Information and Computing Science* **10**(4): 271-276
[7] Kautsar MMA, Silalahi BP, Guritman S 2018 Paradox In a *d*-Dimensional Transportation Problem *International Journal of Pure and Applied Mathematics* **118**(3): 547-557
[8] Porchelvi R, Anitha M 2017 Paradox in A Linear Multi Objective Transportation Problem *Annals of Pure and Applied Mathematics* **15**(2): 185-192
[9] Desylvia SN, Buono A, Silalahi BP 2017 Modeling Text Independent Speaker Identification with Vector Quantization *Telkomnika* **15**(1): 322-327
[10] Krisnawijaya NN, Herdiyeni Y, Silalahi BP 2017 Parallel technique for medicinal plant identification system using fuzzy local binary pattern *Journal of ICT Research and Applications* **11**(1): 77-90
[11] Mayyani H, Silalahi BP, Aman A 2017 Frequency determination of bus rapid transit (BRT) applied on service system of trans mataram metro bus to minimize the operational cost *International Journal of Engineering and Management Research* (IJEMR) **7**(6): 134-140
[12] Saifudin MA, Silalahi BP, Sitanggang IS 2015 Star Catalog Generation for Satellite Attitude Navigation Using Density Based Clustering *Journal of Computer Science* **11**(12): 1082-1089
[13] Silalahi BP 2014 Sharper analysis of upper bound for the iteration complexity of an interior-point method using primal-dual full-Newton step algorithm *Far East Journal of Mathematical Sciences* **95**(1): 69-80
[14] Silalahi BP 2019 Evaluation of interior-point method in scilab *IOP Conference Series: Earth and Environmental Science* **299**(1): 012040
[15] Silalahi BP, Bukhari F, Aman A, Khatizah E, Fahlevi NA 2019 Comparison of Interior Point Method Execution Time in Solving Linear Optimization Problems using MATHEMATICA and SCILAB *International Journal of Statistics and Economics* **20**(4): 74-81
[16] Silalahi BP, Dewi MS 2014 Comparison of sensitivity analysis on linear optimization using optimal partition and optimal basis (in the simplex method) at some cases *IndoMS International Conference on Mathematics and Its Applications*, pages 82–90
[17] Silalahi BP, Laila R, Sitanggang IS 2017 A combination method for solving nonlinear equations *IOP Conference Series: Materials Science and Engineering* **166**(1): 012011
[18] Silalahi BP, Wungguli D, Guritman S 2015 Steepest descent method with new step sizes *World*

Academy of Science, Engineering and Technology, International Journal of Mathematical, Computational, Physical, Electrical and Computer Engineering **9**(7): 378–384
[19] Wihartiko FD, Buono A, Silalahi BP 2017 Integer programming model for optimizing bus timetable using genetic algorithm *IOP Conference Series: Materials Science and Engineering* **166**(1): 012016
[20] Chvatal V 1983 *Linear Programming* (New York (US): W.H.Freeman and Company)

INTERNATIONAL PROCEEDING
The 2nd International Conference on Science and Technology (ICST)
ISBN: 978-602-5830-19-8, June 2020

Identity graph of cyclic group

A Adrianda and Yanita*

Department of Mathematics, Faculty of Mathematics and Natural Sciences, Andalas University-Kampus Unand Limau Manis Padang 25163 Indonesia

*E-mail: yanita@sci.unand.ac.id

Abstract. This paper discusses about identity graph and identity subgraph in finite cyclic group. It's presented that identity graph for n is prime, odd and even. It's shown that identity graph of this group formed by $(p-1)/2$ complete graphs K_3 while n is prime and odd, and for n is even, the identity graph of this group formed by $(p-2)/2$ complete graphs K_3 and single K_2.

1. Introduction

At this time being, study of algebraic structures by graph associated with group become interesting result. This can be indicated by the existence of several articles related to the study of graphs and groups. The study can be a graph of a group or group properties on a graph), see [1-5].

Let G be a group with identity $\mathbf{1}$. There are many different ways to describe graph of group, for instance, based on elements of Gor based on subgroup of G. The graph in [1] associated with the center of a non abelian group G, i.e let $Z(G)$ be a center of G, the vertex of graph G is the elements in G which are not center elements in G. In [2], it's introduced graph of group based on subgroup and the graph namely the non-cyclic graph of group. This graph associated with group by cyclicity of subgroup. In [3], it's study about structure for center graph of group; that is graph obtained from center of group; and condition of the graph is regular or biregular. Meanwhile, in [4] and [5], study about graph from semigroup.

In this paper, it's refered [6] to define a graph from group. It's associated graph τ_G with group G (called identity graph of G) as follows: Let G be a group with identity $\mathbf{1}$. Graph τ_G from G is describe with use elements of G as set vertexs of G and the edge xy is defined: if $x, y = \mathbf{1}$. Thus, set edges of G is elements of G which are pairs that produce identity element.

The organize of this paper as follows: In Section 2, it's introduced a lot of basic concepts and notations of group and graph theory which will be used in Section 3. In Section 3, it's given properties of τ_G with G is cyclic group. It's presented for cyclic group with n order, where n is prime and even.

2. Preliminaries

We refered [7-9] and [10,11] for group and graph consept, respectively. Let G be a group with identity $\mathbf{1}$. The number of elements of G is called its order and denoted by $o(G)$. The order of an element g in a group G is the smallest positive integer n such that $g^n = \mathbf{1}$. If no such integer exists, then g has infinite order. The order of an element g is denoted by $o(g)$.

If g is an element of a group G, it's defined g^n for integer $n > 0$ inductively by $g^1 = g$ and

$g^n = g^{g-1}g$. Then we defined $g^0 = \mathbf{1}$ and $g^{-n} = (g^{-1})^n$ for $n > 0$. It's known that with the ordinary rules of exponents apply: $g^{m+n} = g^m g^n$ and $g^{mn} = (g^m)^n$ for all integers m and n. If the underlying group is abelian and addtive notation is being used, these formulas read $(m+n)g = mg + ng$ and $(mn)g = n(mg)$.

A *cyclic group* G is a group with an element g such that every element in G is a power of g. The element g is called a *generator* of group, and the group is said to be generated by g. Let G is a cyclic group, then usually simbolized by $G = \{g^i | i \in \mathbb{Z}\}$ or $G = \langle g | g^i = \mathbf{1} \rangle$ or $G = \langle g \rangle$.

Proposition 2.1 [7] *Each cyclic group G is isomorphic either to the additive group $\mathbb{Z}$ of integer or to the additive group $\mathbb{Z}/m\mathbb{Z}$ of integers modulo m for some positive integer m.*

Proposition 2.2 [7] *Any subgroup of cyclic group is cyclic.*

Theorem 2.3 [8] *Let G be a group with identity element* $\mathbf{1}$ *and $a \in G$.*
1. *If $a^m = \mathbf{1}$, for some $m \neq 0$, then $o(a)|m$.*
2. *If $a^m = \mathbf{1}$, then for each i, $a^i = a^{r(i)}$, $1 \leq i \leq m$, where $r(i) = i \bmod m$.*
3. *$G = \langle a \rangle$ has m order iff $o(a) = m$.*

A graph τ is an ordered pair $V(\tau)$, $E(\tau)$ consisting of set $V(\tau)$ of vertices and a set $E(\tau)$, disjoint from $V(\tau)$, of edges, together with an incidence function ι_τ that associates with each edge of Gan unordered pair of (not necessarily distinc) vertices with each edge of G. If e is an edge and u and v are vertices such that $\iota_\tau(e) = \{u, v\}$, then e is said to join u and v, and the vertices u u and v are called the ends of e. It's allow the possibility that there are multiple edges with the same associated pair of vertices and two distinct edge e and e' it can be the case that $\iota_\tau(e) = \iota_\tau(e')$. It's also allow loops, that is, edges whose associated vertics are the same. Graphs without loops or multiple edges are *simple graphs*. Graphs which have no edges is called *null graphs*. In this paper we use *complete graph* on $n$vertices, that is graph has exactly one edge joining each pair distinct vertices, is denoted K_n; and *finite graph*, that is if both its vertex set and edge set are finite.

Example 2.4 Let $\tau = (V(\tau), E(\tau))$, where $V(\tau) = \{u, v, w, x, y\}$ and $E(\tau) = \{a, b, c, d, e, f, g, h\}$ and ι_τ is defined by (for notational simplicity, we write uv for unordered pair $\{u, v\}$)

$$\iota_\tau(a) = uv,\ \iota_\tau(b) = uu,\ \iota_\tau(c) = vw,\ \iota_\tau(d) = wx,\ \iota_\tau(e) = vx,\ \iota_\tau(f) = wx,\ \iota_\tau(h) = xy$$

Example 2.5 Let $\sigma = (V(\sigma), E(\sigma))$ where $V(\sigma) = \{v_0, v_1, v_2, v_3, v_4, v_5\}$ and $E(\sigma) = \{e_1, e_2, e_3, e_4, e_5, e_5, e_6, e_7, e_8, e_9, e_{10}\}$ and ι_σ is defined by $\iota_\sigma(e_1) = v_1v_2$, $\iota_\sigma(e_2) = v_2v_3$, $\iota_\sigma(e_3) = v_3v_4$, $\iota_\sigma(e_4) = v_4v_5$, $\iota_\sigma(e_5) = v_5v_1$, $\iota_\sigma(e_6) = v_0v_1$, $\iota_\sigma(e_7) = v_0v_2$, $\iota_\sigma(e_8) = v_0v_3$, $\iota_\sigma(e_9) = v_0v_4$, $\iota_\sigma(e_{10}) = v_0v_5$.

Graphs are so named because they can be represented graphically, and it is this graphical representation which helps us understand many of their properties. Each vertex is indicated by a point, and each edge by a line joining the points representing its ends. Diagram of τ and σ is shown in Figure 2.1.

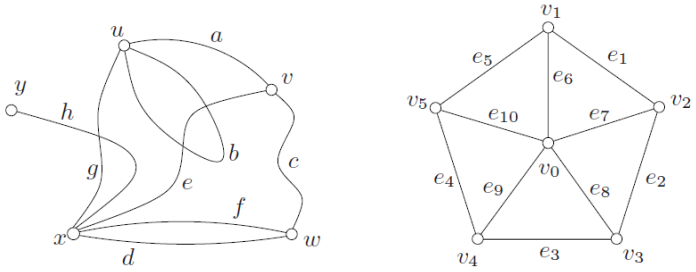

τ σ

Figure 2.1 Graph of τ and σ

Graph ρ is called a subgraph of graph τ if $V(\rho) \subseteq V(\tau)$, $E(\rho) \subseteq E(\tau)$ and function ι_ρ is restriction of ι_τ to $E(\rho)$. We then say that τ contains ρ or that ρ is contained in τ, and write $\tau \supseteq \rho$ or $\rho \subseteq \tau$, respectively. Note that the null graph is subgraph of every graph.

3. Graph τ_G of Cyclic Group

We give definition graph of group as defined by [6].

Definition 3.1 *Let G be a group with identity element $\mathbf{1}$. Graph τ_G associated with G, is graph which describe as follows: elements of $V(\tau)$ are elements of G and elements of $E(\tau)$ are two elements x, y in G are adjacent or can be joined by edge if $xy = \mathbf{1}$. Graph τ_G is called identity graph of G.*

Based on the definition, it's clear that graph τ_G consists of complete graph K_3 and K_2. The following is given an example graph of a cyclic group in Definition 3.1.

Example 3.2 Let $G = \langle g | g^6 = \mathbf{1} \rangle$ be a cyclic group of order $of 6$ under multiplication and identity element of G is $\mathbf{1}$. The graph τ_G of group G is

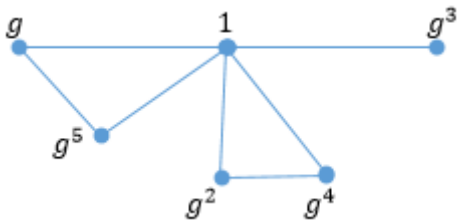

From this graph we know that $g.g^5 = \mathbf{1}$, $g^2.g^4 = \mathbf{1}$, $g^3.g^3 = '1$, dan $\mathbf{1}.\mathbf{1} = \mathbf{1}$.

Definition 3.3 *Let G be a group with identity element $\mathbf{1}$, H be a subgroup of G, then the identity graph for the subgroup H is known as the identity special subgrap of G (special identity subgrap of G).*

Note that to describe graph of subgroup same as Definition 3.1.

Example 3.4 Let $G = \langle g | g^8 = \mathbf{1} \rangle$ be a cyclic group of order 8 under multiplication and identity element of G is $\mathbf{1}$. Subgroups of G are $H_1 = \{\mathbf{1}\}$, $H_2 = \{\mathbf{1}, g^4\}$, $H_3 = \{\mathbf{1}, g^2, g^4, g^6\}$, and $H_4 = G$. Special identity subgraph of H_1, H_2, H_3 and H_4 as follows:

- Special identity subgraph of H_1 consist a vertex:

- Special identity subgraph of H_2 is

- Special identity subgraph of H_3 is

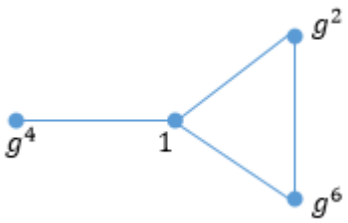

- Special identity subgraph of H_4 is

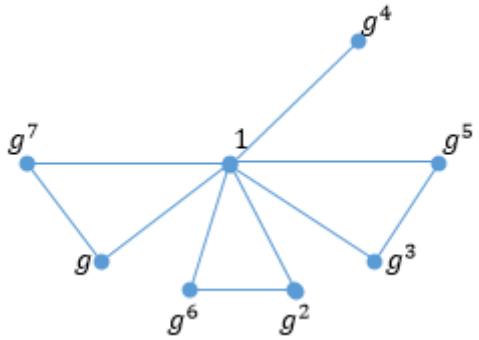

Since graph τ_G of cyclic group only consists graph K_3 (and K_2), so we need the properties for G when n is prime, odd and even.

Theorem 3.5 *Let $G = \langle g \,|g^p = \mathbf{1}\rangle$ be a cyclic group of order p, where $p > 2$ and p is prime. Then identity graph τ_G consists $(p-1)/2$ complete graphs K_3.*

Proof.
Since $o(G) = p$ and p is prime, so we have for $g^i \in G$ where $1 \le i \le p-1$, there is unique $g^{p-i} \in G$ such that $g^i.g^{p-i} = \mathbf{1}$. And then there is no $g^i \in G$ where $1 \le i \le p-1$, such that $g^i.g^i = \mathbf{1}$. We claim that identity graph τ_G has $(p-1)/2$ complete graphs K_3 and we proven case with $|K_3| < (p-1)/2$ complete graphs K_3 and $|K_3| > (p-1)/2$ complete graphs K_3.

a. If $|K_3| < (p-1)/2$, then there is number of pairs $g^i g^{p-i} = \mathbf{1}$ less than $(p-1)/2$. We have $o(G) = |g^i| + |g^{p-i}| + |g^p| < (p-1)/2 + (p-1)/2 + 1 = p$. This contradiction.
b. If $|K_3| > (p-1)/2$, then there is number of pairs $g^i g^{p-i} = \mathbf{1}$ large than $(p-1)/2$. We have $o(G) = |g^i| + |g^{p-i}| + |g^p| > (p-1)/2 + (p-1)/2 + 1 = p$. This contradiction.

Based on a. and b., identity graph τ_G consists $(p-1)/2$ complete graphs K_3. ■

Theorem 3.5 *Let $G = \langle g \,|g^p = \mathbf{1}\rangle$ be a cyclic group of order p, where p is prime. Then G has special identity subgraphs of $\{\mathbf{1}\}$ and G.*

Proof.
Since $o(G) = p$ and p is prime, based on Lagrange's Theorem[1], group G has two subgroups, that is $\{1\}$ and G. This compete the proof.
■

Theorem 3.6 *Let $G = \langle g \,|g^n = \mathbf{1}\rangle$ be a cyclic group of order n, where n is odd. Then identity graph τ_G consists $(n-1)/2$ complete graphs K_3.*

Proof.
Since $o(G) = n$ and n is odd.

1. If n is prime, use Theorem 3.5
2. If n is not prime, for arbitrary $g^i \in G$ where $1 \le i \le n-1$, there is unique $g^{n-i} \in G$ such that $g^i g^{p-i} = \mathbf{1}$ and $(g^i)^{-1} = g^{p-i}$.

We claim identity graph τ_G consists $(n-1)/2$ complete graphs K_3.

a. If $|K_3| < (n-1)/2$, then there is number of pairs $g^i g^{p-i} = \mathbf{1}$ less than $(n-1)/2$. We have $o(G) = |g^i| + |g^{n-i}| + |g^n| < (n-1)/2 + (n-1)/2 + 1 = n$. This contradiction.

[1] Lagrange's Theorem [9]: *Let G be a group of order n and H a subgroup of G of order m. Then m is a divisor of n.*

b. If $|K_3| > (n-1)/2$, then there is number of pairs $g^i g^{n-i} = \mathbf{1}$ large than $(n-1)/2$. We have $o(G) = |g^i| + |g^{n-i}| + |g^n| > (n-1)/2 + (n-1)/2 + 1 = n$. This contradiction.

Based on a. and b., identity graph τ_G consists $(n-1)/2$ complete graphs K_3. ■

Theorem 3.7 *Let* $G = \langle g \,|g^n = \mathbf{1}\rangle$ *be a cyclic group of order n, where n is even. Then identity graph* τ_G *consists* $(n-2)/2$ *complete graphs* K_3 *and one complete graph* K_2.

Proof.

Since $o(G) = n$ and n is even, for arbitrary $g^i \in G$ where $1 \le i \le n-1$, there is unique $g^{n-i} \in G$ such that $g^i g^{n-i} = \mathbf{1}$ and there is $g^i = g^{n/2} \in G$ and $(g^i)^{-1} = g^i$. Thus, identity graph τ_G consists exactly one complete graph K_2. Claim that identity graph τ_G consists $(n-2)/2$ complete graphs K_3 with number of pairs $g^i g^{n-i} = \mathbf{1}$ with $i \neq n/2$ and one complete graph K_2.

a. If $|K_3| < (n-1)/2$, then there is number of pairs $g^i g^{n-i} = \mathbf{1}$ less than $(n-2)/2$. We have $o(G) = |g^i| + |g^{n-i}| + |g^n| + |g^{n/2}| < (n-2)/2 + (n-2)/2 + 1 + 1 = n$. This contradiction.

b. If $|K_3| > (n-1)/2$, then there is number of pairs $g^i g^{n-i} = \mathbf{1}$ large than $(n-2)/2$. We have $o(G) = |g^i| + |g^{n-i}| + |g^n| + |g^{n/2}| > (n-2)/2 + (n-2)/2 + 1 + 1 = n$. This contradiction.

Based on a. and b., identity graph τ_G consists $(n-2)/2$ complete graphs K_3 and one complete graph K_2. ■

References

[1] Abdollahi A, Akbari S, and Maimani H R 2006 Non-commuting graph of group. *Journal of Algebra*, Vol. 298 No. 2 pp. 468-492.

[2] Abdollahi A and Hassanabadi A M 2007 Noncyclic graph of agroup. *Communications in Algebra*, Vol. 35 no. 7 pp. 2057–2081.

[3] Balakrishnan P, Sattanathan M and Kala R 2011 The center graph of a group. *South Asian Journal ofMathematics* Vol. 1 no. 1 pp. 21-28.

[4] Chakrabarty I, Ghosh S and Sen M K 2009 Undirected power graphs of semigroups. *Semigroup Forum*, Vol. 78 no. 3 pp. 410– 426.

[5] Kelarev A V and Quinn S J 2002 Directed graph and combinatorial properties of semigroup. *Journal of Algebra* Vol. 251 pp 16-26.

[6] Kandasamy W B V and Smaradanche F 2009 *Group As Graph* (Romania: Editura Cu Art)

[7] Knap A W 2006 *Basic Algebra* (New York: Birkh¨auser)

[8] Galian J A 2010 *Contemporary Abstract Algebra* Seventh Edition (USA: Brooks/Cole, Cengage Learning)

[9] Roth R L 2001 A History of Lagrange's Theorem on Group. *Mathematics Magazine*, Vol. 74. No.2: pp 99-108

[10] Meier J 2008 *Group, Graph and Trees: An Introduction to the Geometry of Infinite Group.* London Mathematical Society Student Text 73. (New York: Cambridge University)

[11] Bondy J A and Murty U S R 2008 *Graph Theory* (New York: Springer)

INTERNATIONAL PROCEEDING
The 2nd International Conference on Science and Technology (ICST)
ISBN: 978-602-5830-19-8, June 2020

Linear Programming Model for Parallelogram-Shaped Parking Lot

I Hasbiyati[1*], W Putri[2], and M D HGamal[1]
[1]Dapartment of Mathematics, University of Riau, Pekanbaru, Indonesia.
[2]Students Master of Mathematics, Faculty of Mathematics and natural sciences, University of Riau, Pekanbaru, Indonesia.

*E-mail: ihdahasbiyati@gmail.com

Abstract. Parking is an important element in a transportation system. The parking lot has size of highly influential with the capacity of the vehicle. Therefore, it takes a parking design that can accommodate the optimal number of vehicles. Thus, design of the parking lot to be more on notice in order to having an efficient design, safe and optimal. A parking space with an efficient design will result in higher capacities. Many factors affect the design of the parking lot, as the number of vehicles which is stored, vehicle type, parking corner, the circulatory system in the parking lot, the size of the vehicle and form of the parking lot itself. This article discusses the model of the car vehicle parking lot shaped-parallelogram with the corner of the parking $30^{\circ}, 45^{\circ}, 60^{\circ}, 75^{\circ}, 90^{\circ}$. The optimal solution is obtained with linear programming. The calculation results using LINDO show a parallelogram-shaped parking lot with a parking angle of 60 degrees more optimal

1. Introduction

Parking lots are the most important element in a transportation system. Parking land is a specified location as a place to stop vehicles that are not temporary to carry out activities in a certain period of time based on statements from *Transportation Department* [2]. Parking lots have a very influential size with a vehicle's capacity. Every vehicle on the parking lot has different sizes, such as the size of the vehicle type of car and the type of motorbike will have a different size on the parking lot itself. Therefore, parking design is needed that can accommodate the optimal number of vehicles. Parking lot design in addition to providing optimal capacity also provides security and efficiency for vehicles that will be parked in order to produce higher vehicle capacity.

In the design of parking lots, many factors influence the creation of designs that will produce optimal results, including the number of vehicles accommodated, type of vehicle, parking angle, cyclic system in the parking lot, vehicle size and the shape of the parking lot itself. The forms of parking lots vary, including square, rectangular, equilateral triangles, equilateral triangles, circles, and irregular sides adjusting to available land. The parking angles used for parking lots include 30, 45, 60, 75 and 90 degrees.

Abdel Fatah and Taha [1] in 2014 designed a parking form with a rectangular shape and with three possible parking rows and possible angles. In 2019, Ihda [3] began his research on transportation issues. Furthermore, the development is carried out on parking lot with parallelogram landforms. Further development was carried out by Ihda [4] in 2019 with landforms, which discussed the

optimization of parking lots using the concept of large areas on land in the form of parallelograms and right triangles. Discussions were held for car vehicles.

Development for parking lots continues by discussing the optimization of parking lots with a different form from the discussion of Abdelfatah and Taha [1], namely the form of a parallelogram for car vehicles.

2. Materials and Methods

2.1. Parking area

Parking space is the land that is designated for parking vehicles. Parking lots generally use vacant land, roads, and fields. However, there are also parking lots located in buildings and also lands that are not controlled by the government. Therefore, parking lots must follow the land form that is already available. The forms of parking lots can be rectangular, square, triangular, rhombic, parallelogram, circular to irregular shapes. With various forms, of course, the amount of tamping of the vehicle also varies. If the available land is large, the number of vehicles that will be parked is more. A good parking lot is a parking lot that optimizes the land without remaining to accommodate more vehicles and the cyclic in the parking lot runs safely, comfortably and efficiently. To get an efficient parking area there are certainly many factors that influence it. Among them are parking corners and parking designs. The above statement is based from *Transportation Department* [2].

2.2. Parking Angle

There are various angles that will be used in parking the vehicle, including the angles of 30, 45, 60, 75, and 90 degrees. These angles will adjust the shape of the parking lot. The 90 degree angle is the parking angle in a perpendicular manner, one vehicle is side by side with the other vehicle. Usually, the vehicle faces perpendicular to the hallway, road, sidewalk, or wall and parking is usually used in the parking building. Furthermore, parking by means of an attack, or at the angles of 30, 45, 60 and 75. Parking by means of this attack is the easiest way, because it will be easier for vehicles in and out.

2.3. Parking Design

A good parking design will produce optimal results. Usually, parking designs follow the form of available land. However, parking design is made so that it can produce optimal and efficient tamping power. Here the design to be used is a parallelogram-shaped design.

2.4 Linear Programming

Linear programming is one of the methods used for mathematical models. The aim is to look for optimal results. The Linear Program states the use of certain mathematical techniques to get the best possibilities for problems involving limited resources. Linear programs are a way to solve the problem of allocating limited resources between activities that compete with the best possible way. Linear programming is a technique that helps make decisions in allocating resources (machinery, labor, money, time, warehouse capacity, and raw materials). Linear programming is a broad use of mathematical model techniques designed to help managers plan and make decisions in allocating resources, based on Lieberman, Taha and Winston [5] [7] [8].

Linear programming is a problem that involves planning activities to get optimal results, that is, results that reach those determined with the best goals (according to mathematical models) among all feasible alternatives. Issues that are resolved include problems in daily life that are of particular concern such as economic, social, military, industry and so on. A linear program consists of a mathematical model with an objective function and several constraints. The objective function is an equation to optimize the problem. Furthermore, the constraints of the problem have limitations. The limiting function of an equation is usually in the form of an equation equal to (=) or the inequality ≤ and ≥. Linear programs can be completed using the graphical method, the simplex method to using software such as LINDO, LINGO, EXCEL SOLVER and other supporting software.

2.5 LINDO

LINDO (Linear Inertive Discreate Optimizer) is software that can be used to solve linear programming problems. The working principle of LINDO is to enter data, complete and assess the truth and feasibility of the data based on its completion. According to *Linus Scharge* [6], the calculation used in Lindo is basically using the simplex method. Whereas to solve zero-one linear integer programming problem, the external software uses the Branch and Bound method.Futhermore, to determine the optimal value by using an IDO, several steps are needed, namely:

• Determine mathematical models based on real data
• Determine the formulation of the program for Lindo
• Read the results of reports produced by Lindo

The main use of the LINDO program is to find solutions to linear problems quickly and enter data in the form of formulas in linear form. Lindo provides many benefits and convenience in solving optimization and minimization problems.

3. Results and Discussion

Given design and the size of parallelogram-shaped parking lots as follows:

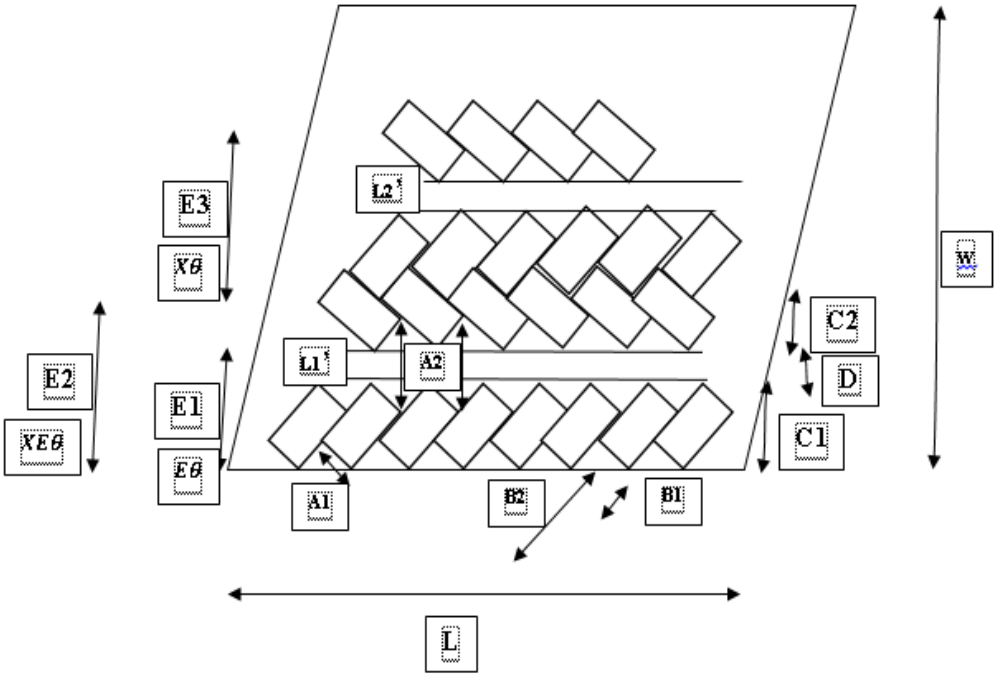

Figure 1. Parking lot design in the form of parallelogram.

Caption Figure 1.
A1 = vehicle width
A2 = vehicle width when attacking
B1 = vehicle length
B2 = the length of the vehicle when it is attacking
C1 = vehicle length from wall to end of the vehicle
C2 = the length of the vehicle from the roadside to the end of the vehicle
D = length of road in the parking lot (entrance and exit of the vehicle)
L = land width

W = length of land
E1 = the length of the outer land
E2 = full length of the outer land
E3 = length of land inside.
XEθ = full number of outer rows
Xθ = number of rows inside
Nθ = number of internal vehicles
NEθ = full number of outer vehicles

The following are the sizes from each corner.
Previous:

$E1 = C1 + D$

$E2 = C1 + D + C2$

$E3 = 2 * C2 + D$

$L1' = L - 2D$

$L2' = L1' - 2D$

Table 1. Dimension table of parking space units

	30°	45°	60°	75°	90°
A1	2.50	2.50	2.50	2.50	2.50
A2	5.00	3.54	2.89	2.59	2.50
B1	5.00	5.00	5.00	5.00	5.00
B2	9.33	7.50	6.44	5.67	5.00
C1	4.67	5.30	5.58	5.48	5.00
C2	3.58	4.42	4.96	5.15	5.00
D	3.50	3.75	4.50	6.00	7.00
E1	8.17	9.05	10.08	11.48	12.00
E2	11.75	13.47	15.04	16.63	17.00
E3	10.66	12.59	14.42	16.30	17.00
L1’	78	77.5	76	73	71
L2’	71	70	67	61	57

From the design above, the mathematical model is as follows:
Objective function:

$$\text{Max Z} = \sum_{\theta=30,45,60,75,90} NE\theta + N\theta$$

Constraints:

$E2\ XE\theta + E3\ X\theta \leq W$

$A2\ N\theta - (L1' + L2')\ X\theta \leq 0$

$A2\ NE\theta - L\ XE\theta - L1'XE\theta - L2'XE\theta \leq 0$

$$\sum_{\theta=30,45,60,75,90} XE\theta \leq 2$$

$XE\theta \geq 0$

$X\theta \geq 0$

$NE\theta \geq 0$

$$N\theta \geq 0$$

Then, to determine the optimal results, the existing measurements are then substituted into the model. So that it is obtained:

Purpose function

$$\text{Max Z} = NE30 + NE45 + NE60 + NE75 + NE90 + N30 + N45 + N60 + N75 + N90$$

Constraint:

$$11.75\,XE30 + 13.47\,XE45 + 15.04\,XE60 + 16.63\,XE75 + 17.00\,XE90 + 10.66\,X30 + 12.59\,X45 + 14.42\,X60 + 16.30\,X75 + 17.00\,X90 \leq 120$$

$$5.00\,N30 - 149\,X30 \leq 0$$
$$3.54\,N45 - 147.5\,X45 \leq 0$$
$$2.89\,N60 - 143\,X60 \leq 0$$
$$2.59\,N75 - 134\,X75 \leq 0$$
$$2.50\,N90 - 128\,X90 \leq 0$$
$$5.00\,N30 - 85\,XE30 - 78\,XE30 - 71XE30 \leq 0$$
$$3.54\,N45 - 85\,XE45 - 77.5\,XE45 - 70\,XE45 \leq 0$$
$$2.89\,N60 - 85\,XE60 - 76\,XE60 - 67\,XE60 \leq 0$$
$$2.59\,N75 - 85\,XE75 - 73\,XE75 - 61\,XE75 \leq 0$$
$$2.50\,N90 - 85\,XE90 - 71\,XE90 - 57\,XE90 \leq 0$$
$$XE30 + XE45 + XE60 + XE75 + XE90 \leq 2$$
$$XE30, XE45, XE60, XE75, XE90, X30, X45, X60, X75, X90, NE30, NE45, NE60, NE75, NE90, N30, N45, N60, N75, N90 \geq 0$$

The next step is to calculate using LINDO. And the results obtained are as follows:

LP OPTIMUM FOUND AT STEP 14

OBJECTIVE FUNCTION VALUE

1) 466.8860

VARIABLE	VALUE	REDUCED COST
NE30	0.000000	0.000000
NE45	0.000000	0.000000
NE60	158.333328	0.000000
NE75	0.000000	0.000000
NE90	0.000000	0.000000
N30	0.000000	0.000000
N45	0.000000	0.000000
N60	308.552612	0.000000
N75	0.000000	0.081074
N90	0.000000	0.000000
XE30	0.000000	21.077320
XE45	0.000000	8.101384
XE60	2.000000	0.000000
XE75	0.000000	0.066625
XE90	0.000000	0.692235
X30	0.000000	6.778857
X45	0.000000	1.534818
X60	6.235784	0.000000
X75	0.000000	0.000000
X90	0.000000	7.134013

From the results of LINDO, it is known that the objective function value shows 466.8860 or the optimal result is 466 vehicles. With NE60 = 158.333328 or the number of full outer vehicles which are 158 vehicles, and N60 = 308.552612 which means the number of inner vehicles is 308 vehicles. Then, XE60 = 2.0000 means that the number of full outer rows is 2 rows and X60 = 6.235784 means that there are 6 rows of vehicles inside.

4. Conclusion

From the above research it can be concluded that the parking lot is in the form of a square with the calculation using LINDO and linear programming methods resulting in a more optimal parking angle of 60 degrees.

.

Acknowledgement

Thank you to the author, addressed to Mrs. Ihda Hasbiyati and Mr. M. D. H. Gamal who gave their energy, thought and time to guide the smooth writing of this article. As well as, to the LPPM University of Riau who has funded the process of the success of writing this article.

References

[1] Abdelfatah A S and Taha M A, 2014 Parking Capacity Optimization Using Linear Programming. *Journal of Traffic and Logistics Engineering* 3(2): 176-181.

[2] Director General of Indonesian Land Transportation 1996 *Organizing Parking Facilities* (Jakarta:Dapartemen Perhubungan).

[3] Hasbiyati I 2019 Analysis of Multi-Stage Stochastic Optimization Model for Stochastic Transportation Problems. *Journal of Transportation Systems, MAT Journals*, 4 (2019): 21-25.

[4] Hasbiyati I, Putri W, Adnan A, Ahriyati and Hasriati 2019 Parking Lot Optimization in Parallelogram Using the Concept Area of Rectangular and Right Triangle. *Pure and Applied Mathematics Journal* SciencePG 8 (2019): 77-82.

[5] Hillier F S and Lieberman G J 2005 *Introduction to Operation Research* (New York: McGraw-Hill Companies)

[6] Scharge L E 1991 *LINDO: An Optimization Modeling System* (San Francisco, CA: Scientific Press)

[7] Taha H A 2007 *Operations Research An Introduction, Eighth Edition* (New Jersey: Person Prentice Hall)

[8] Winston W L 2004 *Operation Research Applications and Algorithms* (USA: Thomson Learning)

INTERNATIONAL PROCEEDING
The 2nd International Conference on Science and Technology (ICST)
ISBN: 978-602-5830-19-8, June 2020

A Note on the Partition Dimension of Subdivided-Thorn Graphs

N Narwen, L Yulianti*, S Y Fadillah, K Al Azizu
[1] Department of Mathematics, Faculty of Mathematics and Natural Science, University of Andalas, Kampus UNAND Limau Manis Padang, Indonesia

*Email: lyra@sci.unand.ac.id (corresponding author)

Abstract. Let $G = (V,E)$ be a connected graph and $S \subseteq V(G)$. For some vertex $v \in V(G)$ and some ordered k-partition $\Pi = \{S_1,S_2,...,S_k\}$, the representation of v with respect to Π is the k-vector $r(v|\Pi) = (d(v,S_1),d(v,S_2),...,d(v,S_k))$ where $d(v,S_i)$ denotes the distance between v and S_t for $t \in \{1,2,...,k\}$. The k-partition Π is said to be resolving if for every two vertices $u,v \in V(G)$, their representation are different, i.e $r(u|\Pi) \neq r(v|\Pi)$. The minimum k for which there is a resolving k-partition of $V(G)$ is called the partition dimension of G, denoted by $pd(G)$. Let $V(G) = \{x_1,x_2, ...,x_n\}$ and let $l_1,l_2, ...,l_n$ be non-negative integers, $l_i \geq 1$ for $i \in \{1,2,...,n\}$. The thorn of G, with parameters $l_1,l_2, ...,l_n$ is new graph obtained by attaching l_i vertices of degree one to vertex x_i, denoted by $Th(G,l_1,l_2,...,l_n)$ for $i \in \{1,2,...,n\}$. The subdivided-thorn graph is constructed by subdividing every l_i leaves of the thorn graph of G into a path on y_i vertices, denoted by $TD(G,l_1(y1),l_2(y_2),...,l_n(y_n))$. In this paper, the partition dimension of the thorn graph and the subdivided-thorn graph for $G = K_n$ and $G = C_3 \times P_2$ were determined. Next, the upper bound of the partition dimension of the thorn graph and subdivided-thorn graph for arbitrary connected graph G on n vertices are obtained.

1. Introduction

Let $G = (V,E)$ be an arbitrary connected graph. Chartrand et al. [1] gave the definition of partition dimension as follows. Let u and v be two vertices in $V(G)$. The distance $d(u,v)$ is the length of the shortest path between u and v in G. For an ordered set $\Pi = \{S_1,S_2, ...,S_k\}$ of vertices in a connected graph G and a vertex v of G, the k-vector $r(v|\Pi) = (d(v,S_1),d(v,S_2),...,d(v,S_k))$ is the representation of v with respect to Π. The notation $d(v,S_t)$ is defined as the distance between v and S_t, $d(v,S_t) = min\{d(v,x)| x \in S_t\}$ for $t \in \{1,2,...,k\}$. If $r(u|\Pi) \neq r(v|\Pi)$ for every two vertices u and v in $V(G)$, then the ordered set Π is called the resolving k-partition. The minimum k for which there is a resolving k-partition of $V(G)$ is called the partition dimension of G, denoted by $pd(G)$.

Chartrand et al. [1] determined the partition dimension of some classes of tree, i.e double stars and caterpillar. Moreover, Chartrand et al. [2] stated the characterizations of graphs on n vertices having partition dimension 2, $n - 1$ or n. Tomescu [3] gave the characterizations of graphs on n vertices having partition dimension $n - 2$. Next, Darmaji [4] found the partition dimension of firecracker graph, banana tree, multipartite graph, and complete bipartite minus matching.

Chartrand et al. [1] gave the necessary condition in partitioning the set of vertices of G as follows.

Lemma 1 [1]
Suppose that Π is the resolving partition of V(G) and u, v $\in$V(G). If d(u,w) = d(v,w) for every vertex w $\in$V(G) \ {u,v} then u and v belong to different class of Π.

Wang et al. [5] defined the thorn of an arbitrary connected graph G with $V(G) = \{x_1, x_2, ..., x_n\}$ as follows. The thorn of G, denoted by $Th(G,l_1,l_2, ..., l_n)$ is constructed by adding l_i leaves, $l_i \geq 1$, to x_i in G, for every $i \in \{1,2,...,n\}$. Next, Yulianti et al. [6] constructed the subdivided-thorn graph, denoted by $TD(G,l_1(y1),l_2(y_2),...,l_n(y_n))$ by subdividing every l_i leaves of the thorn graph of G into a path on y_i vertices and determined the metric dimension of $TD(G,l_1(y1),l_2(y_2),...,l_n(y_n))$ for $G = K_n$. This paper concerns about the partition dimension of thorn graph and the subdivided-thorn graph of complete graph K_n on n vertices and spinner graph, i.e the Cartesian product of C_3 and P_2, denoted by $A = C_3 \times P_2$. For arbitrary connected graph G, the upper bound of partition dimension of thorn and subdivided-thorn of G are also obtained.

2. Partition Dimension of Thorn Graphs

Theorem 2 gives the partition dimension of thorn of complete graph K_n, denoted by $H_1 = Th(K_n,l_1,l_2,..., l_n)$, where $l_j \geq 1$ for $1 \leq j \leq n$. Next, Theorem 3 gives the partition dimension of thorn of spinner graph A, denoted by $H_2 = Th(A,l_1,l_2,l_3,l_4,l_5,l_6)$, with $l_k \geq 1$, for $1 \leq k \leq 6$. Graphs H_1 and H_2 are given in Figure 1.

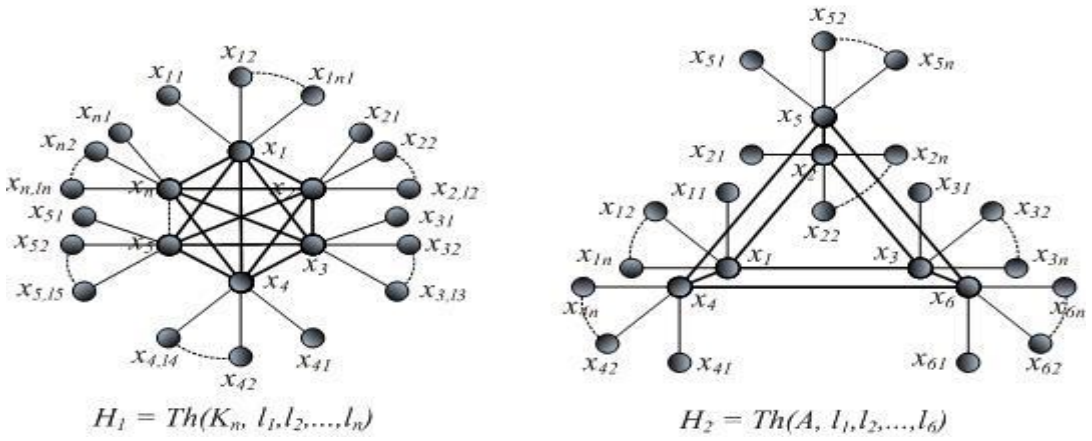

Figure 1. Graph H_1 and H_2

Theorem 2.
Let K_n be the complete graph on n vertices. Let $H_1 = Th(K_n,l_1,l_2,..., l_n)$, where $l_j \geq 1$ for $1 \leq j \leq n$. Denote $l_{max} = max\{l_j | 1 \leq j \leq n\}$. Then

$$pd(H_1) = \begin{cases} n & , l_{max} \leq n, \\ l_{max} & , l_{max} > n. \end{cases}$$

Proof. The vertex set of H_1 is $V(H_1) = \{v_i \mid 1 \leq i \leq n\} \cup \{v_{ij} \mid 1 \leq i \leq n, 1 \leq j \leq l_i\}$, while the edge set of H_1 is $E(H_1) = \{v_iv_k \mid 1 \leq i,k \leq n, i \neq k\} \cup \{v_iv_{ij} \mid 1 \leq i \leq n, 1 \leq j \leq l_i\}$. Consider the following cases.

Case 1. $l_{max} \leq n$.
Let $\Pi_1 = \{S_1,S_2,...,S_n\}$ be the resolving partition of H_1, where $v_i \in S_i$ for all i, $1 \leq i \leq n$. From Lemma 1, vertices v_{ij} and v_{it}, for $1 \leq j,t \leq l_i$ and $1 \leq i \leq n$, belong to different class of partition. Because $l_i \leq l_{max} \leq n$ then it is clear that $pd(H_1) = |\Pi_1| \leq n$.

Next, let $\Pi_2 = \{S_1,S_2,...,S_{n-1}\}$ be the resolving partition of H_1. Then some vertices v_i and v_j, for $1 \leq i,j \leq n$ must be in the same partition class. This contradicts the condition in Lemma 1, because $r(v_i|\Pi_2) = r(v_j|\Pi_2)$. Thus, Π_2 is not the resolving partition of H_1. Therefore, $pd(H_1) \geq n$.

Case 2. $l_{max} > n$.
Consider $\Pi_3 = \{S_1,S_2,..., S_{l_{max}}\}$. Without loss of generalities, let v_1 be the vertex in K_n having $l_1 = l_{max}$ leaves. Therefore, $v_{1k} \in S_k$ for $1 \leq k \leq l_{max}$. Other vertices in H_1 were placed in different partition such that their representations are different. From Lemma 1, there are at least l_{max} classes of partition. Thus, $pd(H_1) = l_{max}$. ■

Theorem 3.
Let $A = C_3 \times P_2$ be the spinner graph on 6 vertices. Let $H_2 = Th(A,l_1,l_2,l_3,l_4,l_5,l_6)$, with $l_k \geq 1$, for $1 \leq k \leq 6$. Denote $l^*_{max} = max\{l_k | 1 \leq k \leq 6\}$. The partition dimension of H_2 is as follows.

$$pd(H_2) = \begin{cases} 4 & , \ l^*_{max} = 1 \text{ or } l^*_{max} = 2, \\ 5 & , \ l^*_{max} = 3, \\ 6 & , \ l^*_{max} = 4 \text{ or } l^*_{max} = 5, \\ l^*_{max} & , \ l^*_{max} \geq 6. \end{cases}$$

Proof. The vertex set of H_2 is $V(H_2) = \{x_k \mid 1 \leq k \leq 6\} \cup \{x_{kt} \mid 1 \leq k \leq 6, 1 \leq t \leq l_k\}$ and the edge set of H_2 is $E(H_2) = \{x_1x_2,x_2x_3,x_1x_3,x_4x_5,x_4x_6,x_5x_6\} \cup \{x_1x_4,x_2x_5,x_3x_6\} \cup \{x_kx_{kt} \mid 1 \leq k \leq 6, 1 \leq t \leq l_k\}$. Consider the following cases.

Case 1. $l^*_{max} = 1$ or $l^*_{max} = 2$.
(a) For $l^*_{max} = 1$.
Let $\Pi_4 = \{S_1,S_2,S_3,S_4\}$ be the resolving partition of H_2 where $S_1 = \{x_k \mid 1 \leq k \leq 6\} \cup \{x_{11},x_{21},x_{31}\}$, $S_2 = \{x_{41}\}$, $S_3 = \{x_{51}\}$, and $S_4 = \{x_{61}\}$. The representations of x_p and x_q, for $1 \leq p,q \leq 6$ are different because $d(x_p,S_j) \neq d(x_q,S_j)$ for $1 \leq p,q \leq 6$ and some j, $2 \leq j \leq 4$. With the similar reason, the representation of x_{11}, x_{21} and x_{31} are different. Next, because $d(x_{a1},S_j) = d(x_a,S_j)+1$ for some j, $2 \leq j \leq 4$, then the representation of x_a and x_{a1}, for $a = 1,2,3$ are different. Because $r(u|\Pi_4) \neq r(v|\Pi_4)$ for every $u,v \in V(H_2)$ then Π_4 is the resolving partition of H_2. Therefore, $pd(H_2) \leq 4$.

Next, suppose that there is some resolving partition $\Pi_5 = \{S_1,S_2,S_3\}$. From its definition, H_2 contains some C_3. If one of x_{11},x_{21},x_{31} belongs to the same partition with x_{41},x_{51},x_{61}, then there are at least two vertices with the same representations. Thus, $pd(H_2) \geq 4$.

(b) For $l^*_{max} = 2$.
Let $\Pi_6 = \{S_1,S_2,S_3,S_4\}$ be the resolving partition of H_2 where $S_1 = \{x_k \mid 1 \leq k \leq 6\} \cup \{x_{11},x_{21},x_{31},x_{61}\}$, $S_2 = \{x_{k2} \mid 1 \leq k \leq 6\}$, $S_3 = \{x_{41}\}$, and $S_4 = \{x_{51}\}$. With similar reason with Case 1(a), the representations of x_p and x_q, for $1 \leq p,q \leq 6$ are different. The representation of x_{11},x_{21},x_{31} and x_{61} are also different. The

representation of x_b and x_{b1}, for $b= 1,2,3,6$ are different, because $d(x_{b1},S_j) = d(x_b,S_j)+1$ for some j, $2 \leq j \leq 4$. Then it is clear that Π_6 is the resolving partition of H_2. Therefore, $pd(H_2) \leq 4$.

Next, let $\Pi_7= \{S_1,S_2,S_3\}$ be the resolving partition of H_2. With similar reason with Case 1(a), from Lemma 1, the vertices x_{41},x_{51} and x_{61} must be in different partition. The vertices x_{41} and x_{42}, or x_{51} and x_{52} must be in different partition also. Therefore, $pd(H_2) \geq 4$.

Case 2. $l^*_{max} = 3$.

Let $\Pi_8 = \{S_1,S_2,S_3,S_4,S_5\}$ be the resolving partition of H_2 where $S_1 = \{x_k \mid 1 \leq k \leq 6\} \cup \{x_{11},x_{21},x_{31},x_{61}\}$, $S_2 = \{x_{k2} \mid 1 \leq k \leq 6\}$, $S_3 = \{x_{k3} \mid 1 \leq k \leq 6\}$, $S_4 = \{x_{41}\}$, and $S_5 = \{x_{51}\}$. Similar with Case 1(a), the representations of x_p and x_q, for $1 \leq p,q \leq 6$ are different. The representation of x_{11}, x_{21}, x_{31} and x_{61} are different. Next, because $d(x_{c1},S_j) = d(x_c,S_j)+1$ for some j, $2 \leq j \leq 4$, then the representation of x_c and x_{c1}, for $c = 1,2,3,6$ are different. Therefore, because every vertex has different representation, it is clear that $pd(H_2) \leq 5$.

Next, suppose that there is some resolving partition $\Pi_9 = \{S_1,S_2,S_3,S_4\}$. From Lemma 1, x_{41},x_{51} and x_{61} must be in different partition. The vertices x_{41}, x_{42}, and x_{43}, or x_{51}, x_{52}, and x_{53} must be in different partition also. Therefore, $pd(H_2) \geq 5$.

Case 3. $l^*_{max} = 4$ or $l^*_{max} = 5$.

(a) *For* $l^*_{max} = 4$.

Let $\Pi_{10} = \{S_1,S_2,S_3,S_4,S_5,S_6\}$ be the resolving partition with $S_1 = \{x_k \mid 1 \leq k \leq 6\} \cup \{x_{11},x_{21},x_{31},x_{61}\}$, $S_2 = \{x_{k2} \mid 1 \leq k \leq 6\}$, $S_3 = \{x_{k3} \mid 1 \leq k \leq 6\}$, $S_4 = \{x_{k4} \mid 1 \leq k \leq 6\}$, $S_5 = \{x_{41}\}$, and $S_6 = \{x_{51}\}$. Using this partition, it can be easily shown that every vertex of H_2 has different representation, and we have that $pd(H_2) \leq 6$.

Next, suppose that there is some resolving partition $\Pi_{11} = \{S_1,S_2,S_3,S_4,S_5\}$. From Lemma 1, x_{41}, x_{51} and x_{61} must be in different partition. The vertices x_{41},x_{42},x_{43}, and x_{44}, or x_{51},x_{52},x_{53} and x_{54} must be in different partition also. Therefore, $pd(H_2) \geq 6$.

(b) *For* $l^*_{max} = 5$.

Let $\Pi_{12} = \{S_1,S_2,S_3,S_4,S_5,S_6\}$ be the resolving partition with $S_1 = \{x_1,x_{11},x_{21},x_{31},x_{61}\}$, $S_2 = \{x_2\} \cup \{x_{k2} \mid 1 \leq k \leq 6\}$, $S_3 = \{x_3\} \cup \{x_{k3} \mid 1 \leq k \leq 6\}$, $S_4 = \{x_4\} \cup \{x_{k4} \mid 1 \leq k \leq 6\}$, $S_5 = \{x_5\} \cup \{x_{k5} \mid 1 \leq k \leq 6\}$, and $S_6 = \{x_6,x_{51}\}$. With similar reason with Case 1(a), all vertices in S_1,S_2,S_3,S_4 and S_5 have different representations. The representation of x_6 and x_{51} are different because $d(x_6,S_1) \neq d(x_{51},S_1)$. Therefore, Π_{12} is the resolving partition and $pd(H_2) \leq 6$.

Next, suppose that there is some resolving partition $\Pi_{13} = \{S_1,S_2,S_3,S_4,S_5\}$. From Lemma 1, x_{41}, x_{51} and x_{61} must be in different partition. The vertices $x_{41},x_{42},x_{43},x_{44}$ and x_{45}, or $x_{51},x_{52},x_{53},x_{54}$ and x_{55} must be in different partition also. Therefore, $pd(H_2) \geq 6$.

Case 4. $l^*_{max} \geq 6$.

Let $z = l^*_{max}$ and $\Pi_{14} = \{S_1,S_2,...,S_z\}$ be the resolving partition with $S_w = \{x_w,x_{kw} \mid 1 \leq k \leq 6\}$ for $1 \leq w \leq 6$, and $S_t = \{x_{kt} \mid 1 \leq k \leq 6\}$ for $7 \leq t \leq z$. It is easy to see that for some k, $1 \leq k \leq 6$, the vertices x_{kp} and

x_{kq}, where $1 \le p,q \le z$ are in different partitions. Therefore, every vertex has different representation, and we have $pd(H_2) \le z$.

Next, if $\Pi_{15} = \{S_1, S_2,...,S_{z-1}\}$ be the resolving partition, it is clear that there will be at least two vertices, namely x_{kp} and x_{kq}, for some k, $1 \le k \le 6$, and $1 \le p,q \le z$, in the same partition. It contradicts Lemma 1. Therefore, $pd(H_2) \ge z$. ■

3. The Partition Dimension of Subdivided-Thorn Graph

The subdivided-thorn graph, denoted by $TD(G,l_1(y1),l_2(y_2),..., l_n(y_n))$ is constructed by subdividing every l_i leaves of the thorn graph of G into a path on y_i vertices. The examples of subdivided-thorn graphs are given in Figure 2.

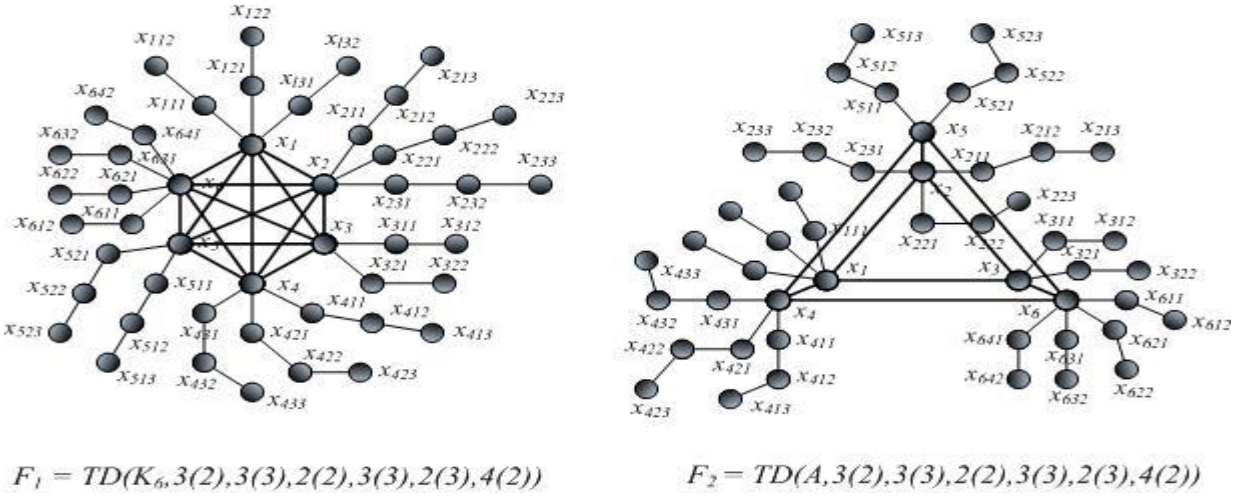

Figure 2. Graph F_1 and F_2

Theorem 4 gives the partition dimension of subdivided-thorn of complete graph K_n, denoted by $F_1 = TD(K_n,l_1(y_1),l_2(y_2),..., l_n(y_n))$, where $l_j \ge 1$ for $1 \le j \le n$. Moreover, Theorem 5 gives the partition dimension of subdivided-thorn of spinner graph A, denoted by $F_2 = TD(A,l_1(y_1),l_2(y_2),..., l_6(y_6))$, with $l_k \ge 1$, for $1 \le k \le 6$.

Theorem 4.
Let K_n be the complete graph on n vertices. Let $F_1 = TD(K_n,l_1(y_1),l_2(y_2),..., l_n(y_n))$, where $l_i, y_i \ge 1$ for $1 \le i \le n$. Denote $l_{max} = max\{l_i | 1 \le i \le n\}$. Then

$$pd(F_1) = \begin{cases} n & , l_{max} \le n, \\ l_{max} & , l_{max} > n. \end{cases}$$

Proof. Define the vertex set and edge set of F_1 as $V(F_1) = \{v_i | 1 \le i \le n\} \cup \{v_{ijk} | 1 \le i \le n,\ 1 \le j \le l_i,\ 1 \le p \le y_i\}$, and $E(F_1) = \{v_iv_k \mid 1 \le i,k \le n,\ i \ne k\} \cup \{v_iv_{ij1} | 1 \le i \le n,\ 1 \le j \le l_i\} \cup \{v_{ijs}\ v_{ij(s+1)} | 1 \le i \le n,\ 1 \le j \le l_i,\ 1 \le s \le y_i - 1\}$. Similar with Theorem 2, consider the following cases.

Case 1. $l_{max} \le n$.

Let $\Pi_{16} = \{S_1,S_2,...,S_n\}$ be the resolving partition of F_1, where $v_i \in S_i$ for all i, $1 \le i \le n$. From Lemma 1, vertices v_{ijp} and v_{itp}, for $1 \le i \le n$, $1 \le j,t \le l_i$, and $1 \le p \le y_i$ belong to different class of partition. Because $l_i \le l_{max} \le n$ then $pd(F_1) = |\Pi_{16}| \le n$. For the lower bound, the proof is similar to the proof of Case 1 in Theorem 2.

Case 2. $l_{max} > n$.
Consider $\Pi_{17} = \{S_1,S_2, ..., S_{l_{max}}\}$. Similar to the proof of Case 2 in Theorem 2, let v_1 be the vertex in K_n having $l_1 = l_{max}$ leaves. Therefore, $v_{1zp} \in S_k$ for $1 \le z \le l_{max}$ and $1 \le p \le y_i$. Other vertices in F_1 were placed in different partition such that their representations are different. Thus, it is clear that there are at least l_{max} classes of partition, and therefore $pd(F_1) = l_{max}$. ■

Theorem 5.
Let $A = C_3 \times P_2$ be the spinner graph on 6 vertices. Let $F_2 = TD(A, l_1(y_1),l_2(y_2),..., l_6(y_6))$, with $l_t \ge 1$, for $1 \le k \le 6$. Denote $l^*_{max} = max\{l_k | 1 \le k \le 6\}$. The partition dimension of F_2 is as follows.

$$pd(F_2) = \begin{cases} 4 & , \ l^*_{max} = 1 \text{ or } l^*_{max} = 2, \\ 5 & , \ l^*_{max} = 3, \\ 6 & , \ l^*_{max} = 4 \text{ or } l^*_{max} = 5, \\ l^*_{max} & , \ l^*_{max} \ge 6. \end{cases}$$

Proof.
Define the vertex and edge sets of F_2 as $V(F_2) = \{x_k \mid 1 \le k \le 6\} \cup \{v_{ktj} \mid 1 \le k \le 6, 1 \le t \le l_k, 1 \le j \le y_k\}$, and $E(F_2) = \{x_1x_2,x_2x_3,x_1x_3,x_4x_5,x_4x_6,x_5x_6\} \cup \{x_1x_4,x_2x_5,x_3x_6\} \cup \{x_kx_{kt1} | 1 \le k \le 6, 1 \le t \le l_k\} \cup \{x_{ktq}x_{kt(q+1)} | 1 \le k \le 6, 1 \le t \le l_k, 1 \le q \le y_k - 1\}$. Similar with the proof of Theorem 3, consider the following cases.

Case 1. $l^*_{max} = 1$ or $l^*_{max} = 2$.
Without loss of generalities, let $l^*_{max} = 2$. Define $\Pi_{18} = \{S_1,S_2,S_3,S_4\}$ as the resolving partition of F_2 with $S_1 = \{x_k \mid 1 \le k \le 6\} \cup \{x_{11a} \mid 1 \le a \le y_1\} \cup \{x_{21b} | 1 \le b \le y_2\} \cup \{x_{31c} \mid 1 \le c \le y_3\} \cup \{x_{61f} \mid 1 \le f \le y_6\}$, $S_2 = \{x_{12a} | 1 \le a \le y_1\} \cup \{x_{22b} | 1 \le b \le y_2\} \cup \{x_{32c} | 1 \le c \le y_3\} \cup \{x_{42d} | 1 \le d \le y_4\} \cup \{x_{52e} | 1 \le e \le y_5\} \cup \{x_{62f} \mid 1 \le f \le y_6\}$, $S_3 = \{x_{41d} | 1 \le d \le y_4\}$, and $S_4 = \{x_{51e} | 1 \le e \le y_5\}$. Because $d(x_{kwu},S_w) \ne d(x_{kwv},S_w)$ for $1 \le k \le 6$, $1 \le w \le 2$ and $1 \le u,v \le y_k$, then it is clear that $r(x_{kwu} | \Pi_{18}) \ne r(x_{kwv} | \Pi_{18})$. Because every vertex have different representation, then $pd(F_2) \le 4$. Proof for the lower bound is similar with Case 1 in Theorem 3.

Case 2. $l^*_{max} = 3$.
Let $\Pi_{19} = \{S_1,S_2,S_3,S_4,S_5\}$ be the resolving partition of F_2 where $S_1 = \{x_k \mid 1 \le k \le 6\} \cup \{x_{11a} \mid 1 \le a \le y_1\} \cup \{x_{21b} | 1 \le b \le y_2\} \cup \{x_{31c} \mid 1 \le c \le y_3\} \cup \{x_{61f} \mid 1 \le f \le y_6\}$, $S_2 = \{x_{12a} | 1 \le a \le y_1\} \cup \{x_{22b} | 1 \le b \le y_2\} \cup \{x_{32c} \mid 1 \le c \le y_3\} \cup \{x_{42d} \mid 1 \le d \le y_4\} \cup \{x_{52e} \mid 1 \le e \le y_5\} \cup \{x_{62f} | 1 \le f \le y_6\}$, $S_3 = \{x_{13a} | 1 \le a \le y_1\} \cup \{x_{23b} | 1 \le b \le y_2\} \cup \{x_{33c} | 1 \le c \le y_3\} \cup \{x_{43d} | 1 \le d \le y_4\} \cup \{x_{53e} | 1 \le e \le y_5\} \cup \{x_{63f} | 1 \le f \le y_6\}$, $S_4 = \{x_{41d} | 1 \le d \le y_4\}$, and $S_5 = \{x_{51e} | 1 \le e \le y_5\}$. By defining this partition, every vertex has different partition. Then $pd(F_2) \le 5$. Proof for the lower bound is similar with Case 2 in Theorem 3.
Case 3. $l^*_{max} = 4$ or $l^*_{max} = 5$.
Without loss of generalities, let $l^*_{max} = 5$. Let $\Pi_{20} = \{S_1,S_2,S_3,S_4,S_5,S_6\}$ be the resolving partition of F_2 where $S_1 = \{x_1\} \cup \{x_{11a} | 1 \le a \le y_1\} \cup \{x_{21b} | 1 \le b \le y_2\} \cup \{x_{31c} | 1 \le c \le y_3\} \cup \{x_{51e} | 1 \le e \le y_5\} \cup \{x_{61f} | 1 \le f \le y_6\}$, $S_2 = \{x_2\} \cup \{x_{12a} | 1 \le a \le y_1\} \cup \{x_{22b} | 1 \le b \le y_2\} \cup \{x_{32c} | 1 \le c \le y_3\} \cup \{x_{42d} | 1 \le d \le y_4\} \cup \{x_{52e} | 1 \le e \le y_5\} \cup \{x_{62f} | 1 \le f \le y_6\}$, $S_3 = \{x_3\} \cup \{x_{13a} | 1 \le a \le y_1\} \cup \{x_{23b} | 1 \le b \le y_2\} \cup \{x_{33c} | 1 \le c \le y_3\} \cup \{x_{43d} | 1 \le d \le$

$y_4\}\cup\{x_{53e}|1 \le e \le y_5\}\cup\{x_{63f}|1 \le f \le y_6\}$, $S_4 = \{x_4\}\cup\{x_{14a}|1 \le a \le y_1\}\cup\{x_{24b}|1 \le b \le y_2\}\cup\{x_{34c}|1 \le c \le y_3\}\cup\{x_{44d}|1 \le d \le y_4\}\cup\{x_{54e}|1 \le e \le y_5\}\cup\{x_{64f}|1 \le f \le y_6\}$, $S_5 = \{x_5\}\cup\{x_{15a}|1 \le a \le y_1\}\cup\{x_{25b}|1 \le b \le y_2\}\cup\{x_{35c}|1 \le c \le y_3\}\cup\{x_{45d}|1 \le d \le y_4\}\cup\{x_{55e}|1 \le e \le y_5\}\cup\{x_{65f}|1 \le f \le y_6\}$, $S_6 = \{x_6\}\cup\{x_{41d}|1 \le d \le y_4\}$. By defining this partition, every vertex has different partition. Then $pd(F_2) \le 5$. Proof for the lower bound is similar with Case 3 in Theorem 3.

Case 4. $l^*_{max} \ge 6$.
Let $z = l^*_{max}$. Let $\Pi_{21} = \{S_1,S_2,...,S_z\}$ be the resolving partition of F_2 where S_1, S_2, S_3, S_4 and S_5 are the partition class in Case 3. Define $S_g = \{x_g\}\cup\{x_{1ga}|1 \le a \le y_1\}\cup\{x_{2gb}|1 \le b \le y_2\}\cup\{x_{3gc}|1 \le c \le y_3\}\cup\{x_{4gd}|1 \le d \le y_4\}\cup\{x_{5ge}|1 \le e \le y_5\}\cup\{x_{6gf}|1 \le f \le y_6\}$, for $6 \le g \le z$. By defining this partition, every vertex has different partition. Then $pd(F_2) \le z$. Proof for the lower bound is similar with Case 4 in Theorem 3. ■

4. Conclusion

This paper discusses about the partition dimension of thorn and subdivided-thorn of complete graph and spinner graphs. As the conclusion, in the following conjecture, the upper bound of the partition dimension of thorn and subdivided-thorn of an arbitrary connected graph G on n vertices are given.

Conjecture 6.
Let G be an arbitrary connected graph on $n \ge 2$ vertices. Let $H = Th(G,l_1,l_2,...,l_n)$ be the thorn of G and $F = TD(G,l_1(y_1),l_2(y_2),..., l_n(y_n))$ be the subdivided-thorn of G. Denote $l_{max} = max\{l_i \mid 1 \le i \le n\}$. The partition dimension of H and F, denoted by $pd(H)$ and $pd(F)$ are as follows.

$$pd(F) = pd(H) = \begin{cases} \le |V(G)| & , \ l_{max} \le |V(G)|, \\ l_{max} & , \ l_{max} > |V(G)|. \end{cases}$$

Acknowledgement
This paper was partially supported by the Hibah BOPTN Skim Riset Dasar from Andalas University, Indonesia.

References

[1] Chartrand G, Salehi E, Zhang P 2000 The Partition Dimension of Graph. *A equations Math* 59: 45-54
[2] Chartrand G, Zhang P, Salehi E, 1998 On The Partition Dimension of Graph. Congressus Numerantium **130**: 157-160
[3] Tomescu I 2008 Discrepancies between metric dimension and partition dimension of a connected graph. *Discrete Mathematics* **308**: 5026-5031
[4] Darmaji 2011 Dimensi Partisi Graf Multipartit dan Graf Hasil Korona, *Disertasi S3*, unpublished, Program Studi Pascasarjana Institut Teknologi Bandung
[5] Wang Z P, Zou Y T, Lin H Y, Wang Z T 2009 Graham's pebbling conjecture on product of thorn graphs of complete graphs. *Discrete Mathematics* **309**: 3431-3435
[6] Yulianti L, Narwen, Hariyani S 2019 On The Metric Dimension of Thorn-subdivided Graphs. *accepted for publication in Indonesian Journal of Combinatorics*

INTERNATIONAL PROCEEDING
The 2nd International Conference on Science and Technology (ICST)
ISBN: 978-602-5830-19-8, June 2020

The Numerical Solution by Modified Adomian Decomposition Method for General Wave Equation

J A Putra, M A Ridzi, Hafnani, and R Zuhra*
Department of Mathematics, Faculty of Mathematics and Natural Sciences, Syiah Kuala University, 23111 Banda Aceh, Indonesia

*E-mail: rahmazuhra@unsyiah.ac.id

Abstract. The Adomian decomposition method and its modification are great methods used to solve a nonlinear equation in calculus of variations. Many researchers work in this method to solve problems in mathematics, physics, biology, and chemistry. In this paper, we apply modified Adomian decomposition method for wave equation problem. Then, we compare the result to exact solution and ordinary Adomian decomposition method. By using software *MATLAB*, we also plot the numerical solution to this problem.

1. Introduction

Most scientific problems arising in applied mathematics formed as a nonlinear differential equation. Calculus of variations as a branch of mathematics has been intimately connected with the theory of differential equations that can be solved and gave the desired optimal solution. Later, many methods have been used to find solutions of the problem for example direct method, Walsh series method, Legendre wavelets method, rationalized iteration method, Chebychev polynomials method and Adomian decomposition method [1].

The Adomian decomposition method (ADM) was firstly introduced by George Adomian in 1981[2]. This technique is based on the representation of a solution to a functional equation as a series of functions. Each term of the series is obtained from a polynomial generated by a power series expansion of an analytic function. Although the abstract formulation of the Adomian method is very simple, the calculations of the polynomials and the verification of convergence of the function series in specific situations are usually a difficult task [3]. Furthermore, the main advantage of this method is that it can be applied directly to all types of differential and integral equations, linear or non-linear, homogeneous or inhomogeneous, with constant or variable coefficients. Another important advantage is that the method is capable of greatly reducing the size of computational work while still maintaining high accuracy of the numerical solution [4]. The ADM decomposes a solution into an infinite series that converges rapidly to the exact solution. The non-linear problems are solved easily and elegantly without linearizing the problem by using ADM. It also avoids linearization, perturbation and discretization unlike other classical techniques [4]

The ADM has led to several modifications on the method made by various researchers in an attempt to improve the accuracy or expand the application of the original method. Adomian and Rach introduced modified Adomian polynomials which converge slightly faster than the original or classical Adomian polynomials and are convenient for computer generation [5]. The modified polynomials are defined using a differencing method. The first few terms of the modified Adomian polynomials

generated are identical to the original Adomian polynomials, but higher order terms do exhibit differences. In addition to the classical and modified Adomian polynomials, Adomian also introduced accelerated Adomian polynomials [5, 6]. These Adomian polynomials provide faster convergence; however, they are less convenient computationally [5]. Then, proposed modifications to the standard ADM can be as simple as the following; Wazwaz presented a reliable modification of the ADM [7]. The modified ADM proposed by Wazwaz divides the original function into two parts, one assigned to the initial term of the series and the other to the second term. All remaining terms of the recursive relationship are defined as previously, but the modification results in a different series being generated. This method has been shown to be computationally efficient; however, it does not always minimize the size of calculations needed and even requires much more calculations than the standard ADM. The success of the modified method depends mainly on the proper choice of the parts into which to divide the original function [7].

Many researchers have worked in this method, see [8, 9]. In this paper, we focus on vibrations, which is general wave equation problem. We apply the modified Adomian decomposition method for wave equation problem. Then, we compare the result to exact solution and ordinary Adomian decomposition method. By using software *MATLAB*, we also plot the numerical solution to this problem.

2. Modified Adomian Decomposition Method

First of all, we review the Adomian Decomposition Method (ADM). First, we consider a differential equation

$$F\big(u(t)\big) = g(t),$$

where *F* represents a general nonlinear ordinary or partial differential operator including both linear and nonlinear terms. Linear terms are decomposed into *L* + *R*, where *L* is invertible and is taken as the highest order derivative, and R is the remainder of the linear operator. Thus the equation may be written as

$$Lu + Nu + Ru = g, \tag{1}$$

where *Nu* represents the nonlinear terms. Solving for *Lu*, we obtain

$$Lu = g - Ru - Nu. \tag{2}$$

Operating on both sides of eq. (2) with L^{-1} we have,

$$L^{-1}Lu = L^{-1}g - L^{-1}Ru - L^{-1}Nu. \tag{3}$$

The decomposition method represents the solution $u(x, t)$ as a series of this form,

$$u(x,t) = \sum_{n=0}^{\infty} u_n\ (x,t). \tag{4}$$

The nonlinear term *Nu* is decomposed as

$$Nu = \sum_{n=0}^{\infty} A_n\ . \tag{5}$$

Substitution equation (4) and equation (5) into equation (3) we obtain,

$$\sum_{n=0}^{\infty} u_n\ (x,t) = \varphi_0 + L^{-1}g(x) - L^{-1}R\sum_{n=0}^{\infty} u_n - L^{-1}\sum_{n=0}^{\infty} A_n, \tag{6}$$

where,

$$\varphi_0 = \begin{cases} u(0), & if\ L = \frac{d}{dx}, \\ u(0) + xu'(0), & if\ L = \frac{d^2}{dx^2}, \\ \vdots & \\ u(0) + xu'(0) + \frac{x^2}{2!}u''(0) + \cdots + \frac{x^n}{n!}u^{(n)}(0), & if\ L = \frac{d^{n+1}}{dx^{n+1}}. \end{cases} \tag{7}$$

Therefore

$$\begin{cases} u_0 = \varphi_0 + L^{-1}g(x), \\ u_1 = -L^{-1}Ru_0 - L^{-1}A_0, \\ \vdots \\ u_{n+1} = -L^{-1}Ru_n - L^{-1}A_n,\ n \geq 0. \end{cases} \tag{8}$$

where A_n are the Adomian polynomials generated for each nonlinearity so that A_0 depends only on u_0, A_1 depends only on u_0 and u_1, A_2 depends only on u_0, u_1 and u_2 and etc. The Adomian polynomials are obtained from the formula

$$A_n = \frac{1}{n!}\frac{d^n}{d\alpha^n}[N(\sum_{n=0}^{\infty}\alpha^n u_n)]_{\alpha=0}, n = 0,1,2,\cdots. \quad (9)$$

So, the practical solution for the n terms approximation is

$$\sigma_n = \sum_{i=0}^{\infty} u_i,$$

where

$$u(x,t) = \lim_{n\to\infty}\sigma_n(x,t) = \sum_{i=0}^{\infty} u_i\,(x,t). \quad (10)$$

Now, we present the modification by Wazwaz and Al-sayed [10]. They presented a reliable modification of the Adomian decomposition method. As we know the ADM suggests that the zeroth component u_0 usually defined by function $f = \varphi + L^{-1} g$. But the modified decomposition method proposed by Wazwaz was established based on the assumption that the function f can be divided into two parts one assigned to the initial term of the series and the other to the second term [7]. All remaining terms of the recursive relationship are defined as previously, but the modification results in a different series being generated. This method has been shown to be computationally efficient; however, it does not always minimize the size of calculations needed. The success of the modified method depends mainly on the proper choice of the parts into which to divide the original function. Under this assumption, we set $f = f_0 + f_1$. Based on this, we formulate the modified recursive relation as follows:

$$\begin{cases} u_0(x) = f_0, \\ u_1(x) = f_1 - L^{-1}Ru_0 - L^{-1}A_0, \\ \vdots \\ u_{n+1}(x) = -L^{-1}Ru_n - L^{-1}A_n,\ n \geq 0. \end{cases} \quad (11)$$

Although this variation in the formation of u_0 and u_1 is slight, however it plays a major role in accelerating the convergence of the solution and in minimizing the size of calculations. Furthermore, there is no need sometimes to evaluate the so-called Adomian polynomials required for nonlinear operators. Then, by proper selection of the function f_0 and f_1, the exact solution u may be obtained by using very few iterations, and sometimes by evaluating only two components. The success of this modification depends only on the choice of f_0 and f_1, and this can be made through trials, which are the only criteria that can be applied so far.

3. Results and Discussions

In this section, we discuss our research results. As has been mentioned, we investigate the performance of the Modified Adomian decomposition method in solving the general wave equation of the second-order ordinary differential equations involving source terms. Now, we consider the system as follows

$$\begin{aligned} &u_{tt} = C^2 u_{xx},\ \ 0 < x < L, t > 0, \\ &u(0,t) = 0,\ \ u(l,t) = 0,\ t \geq 0, \\ &u(x,0) = f(x),\ \ u_t(x,0) = g(x). \end{aligned} \quad (12)$$

where $u = u(x, t)$ is a function that depends on position of x and time t. Variable C^2 is a constant related to velocity of wave propagation. The limit value indicates the endpoint of the wave which is a fixed value. The initial condition indicates the position and initial velocity at time $t = 0$. Now, we define the differential operators as follows

$$L_t = \frac{\partial^2}{\partial t}, L_x = \frac{\partial^2}{\partial x}. \quad (13)$$

Then one-dimensional wave equation can write as

$$L_t u(x,t) = C^2 L_x u(x,t). \tag{14}$$

Assume the inverse operator in equation (13) exists, so that

$$L_t^{-1}(.) = \int_0^t \int_0^t (.)dt\,dt \;;\; L_x^{-1}(.) = \int_0^x \int_0^x (.)dx\,dx. \tag{15}$$

Hence,

$$\begin{aligned} L_t^{-1}L_t u(x,t) &= \int_0^t \int_0^t \left(\frac{\partial^2}{\partial t^2}u(x,t)\right) dt\,dt \\ &= \int_0^t \left(\frac{\partial}{\partial t}u(x,t)\right)\Big|_0^t dt \\ &= \int_0^t \left(\frac{\partial}{\partial t}u(x,t) - \frac{\partial}{\partial t}u(x,0)\right) dt \\ &= \left[u(x,t) - t \times \frac{\partial}{\partial t}u(x,0)\right]\Big|_0^t \\ &= \left[u(x,t) - t\,\frac{\partial}{\partial t}u(x,0)\right] - \left[u(x,0) - 0 \times \frac{\partial}{\partial t}u(x,0)\right] \\ &= u(x,t) - t\,\frac{\partial}{\partial t}u(x,0) - u(x,0) \end{aligned}$$

$$\therefore\; L_t^{-1}L_t u(x,t) = u(x,t) - t\,u_t(x,0) - u(x,0) \tag{16}$$

Now, we apply L_t^{-1} in equation (13) that is

$$\begin{aligned} L_t^{-1}L_t u(x,t) &= C^2 L_t^{-1}(L_x u(x,t)) \\ u(x,t) - t\,u_t(x,0) - u(x,0) &= C^2 L_t^{-1}(L_x u(x,t)) \\ u(x,t) &= u(x,0) + t\,u_t(x,0)\,C^2 L_t^{-1}(L_x u(x,t)) \\ u(x,t) &= f(x) + t\,g(x)\,C^2 L_t^{-1}(L_x u(x,t)) \end{aligned} \tag{17}$$

From equation (17) we have $f_0 = f(x)$ and $f_1 = t\,g(x)$. By Modified Adomian Decomposition Method (MAMT) we obtain

$$\begin{cases} u_0(x,t) = f(x) \\ u_1(x,t) = tg(x) + L_t^{-1}(L_x u_0(x,t)) \\ u_{n+1}(x,t) = L_t^{-1}(L_x u_n(x,t)),\;\; n \geq 0 \end{cases}. \tag{18}$$

Then, we find $u_0(x,t)$, $u_1(x,t)$, $u_2(x,t)$, etc as follows:

$$\begin{cases} u_0(x,t) = f(x) \\ u_1(x,t) = tg(x) + C^2 L_t^{-1}(L_x f(x)) = t\,g(x) + C^2\left(\frac{t^2}{2!}f''(x)\right) \\ u_2(x,t) = C^2 L_t^{-1}\big(L_x u_1(x,t)\big) = C^2\,\frac{t^3}{3!}g''(x) + C^4\left(\frac{t^4}{4!}f^{(4)}(x)\right) \\ u_3(x,t) = C^2 L_t^{-1}\big(L_x u_2(x,t)\big) = C^4\,\frac{t^5}{5!}g^{(4)}(x) + C^6\left(\frac{t^6}{6!}f^{(6)}(x)\right) \\ u_4(x,t) = C^2 L_t^{-1}\big(L_x u_3(x,t)\big) = C^6\,\frac{t^7}{7!}g^{(6)}(x) + C^8\left(\frac{t^8}{8!}f^{(8)}(x)\right) \\ \vdots \\ \vdots \end{cases}. \tag{19}$$

Afterward, we get the infinite series

$$\sum_{n=1}^{\infty} u_n(x,t) = \sum_{n=0}^{\infty} C^{2n} \frac{t^{2n+1}}{(2n+1)!} g^{(2n)}(x) + C^{2(n+1)} \left(\frac{t^{2(n+1)}}{2(n+1)!} f^{(2(n+1))}(x) \right). \quad (20)$$

From MADM, we have

$$\sum_{n=0}^{\infty} u_n(x,t). \quad (21)$$

So from equation (20), (21) and $u_0(x,t) = f(x)$, we obtain:

$$\sum_{n=0}^{\infty} u_n(x,t) = f(x) + \sum_{n=1}^{\infty} u_n(x,t) \quad (22)$$

Thus, we gain infinite series from equation (22) that is the solution of the one-dimensional wave equation. The solution obtained for equation (22) is an exact solution. However, to determine a numerical solution, we have to take finite element. Therefore, numerical solutions can be expressed as

$$u(x,t) \approx u_0(x,t) + \sum_{n=1}^{k} u_n(x,t), \quad (23)$$

where k is a positive integer. By following the steps above, we can make a program by MATLAB code that attached in supplementary data. For example, we take the wave equation

$$u_{tt} - 4u_{xx} = 0, \quad (24)$$

where $u(x,0) = 1 + \sin(x)$ dan $u_t(x,0) = 0$.

The exact solution for equation (24) is

$$u(x,t) = 1 + \sin(x)\cos(2t). \quad (25)$$

Furthermore, we obtain the numerical solution for Modified Adomian Decomposition Method (MADM) by using MATLAB program. The results can we get in the following figure.

```
=====================================================
Menyelesaikan persamaan gelombang
U_tt - 4U_xx = 0
.............(1)
U(x,0) = 1+sin(x)
.............(2)
U_t(x,0) = 0
.............(3)
Menggunakan metode adomian

 misalkan L_tt adalah operator
L_tt = d^2/dt^2; L_tt^-1 = int[int[(.)dt]^t_0 dt]^t_0

didapat
L_tt^-1 = U(x,t)- U(x,0) - int[U_t(x,0)dt]
        = U(x,t) - 1+sin(x) - 0

 U(x,t) = Ltt^-1(4 Uxx) + 1+sin(x) + 0

 Dengan menggunakan metode adomian dekomposisi modifikasi

 U_0(x,t)=f(x)
 U_1(x,t)=t*g(x)+L_t^-1(LxU0(x,t))
 U_n+1 (x,t) = L_t^-1(LxUn(x,t))

=====================================================
U_1(x,t) = (-2)*t^2*sin(x)

U_2(x,t) = (2*t^4*sin(x))/3

U_3(x,t) = -(4*t^6*sin(x))/45

U_4(x,t) = (2*t^8*sin(x))/315

U_5(x,t) = -(4*t^10*sin(x))/14175

U_6(x,t) = (4*t^12*sin(x))/467775

U_7(x,t) = -(8*t^14*sin(x))/42567525

U_8(x,t) = (2*t^16*sin(x))/638512875

U_9(x,t) = -(4*t^18*sin(x))/97692469875

U_10(x,t) = (4*t^20*sin(x))/9280784638125
```

Figure 1. The output of solution for example problem

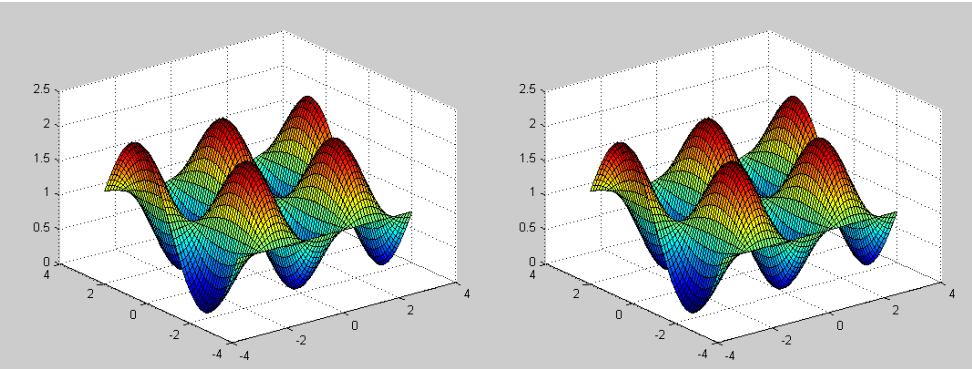

Figure 2. The solution in graphic for the exact solution and MADM solution

From Figure 2, we can be seen that the graph for the exact solution is the same as the MADM solution. Then, the results of numerical solutions at several points is shown in the following table.

Table 1. The numerical solution for three method

t	*x*	Exact solution	ADM	MADM	ADM error	MADM error
0	0	1.000000000000000	1.000000000000000	1.000000000000000	0.000000000000000	0.000000000000000
0	1	1.841470984807890	1.841470984807890	1.841470984807890	0.000000000000000	0.000000000000000
0	2	1.909297426825680	1.909297426825680	1.909297426825680	0.000000000000000	0.000000000000000
0	3	1.141120008059860	1.141120008059860	1.141120008059860	0.000000000000000	0.000000000000000
1	0	1.000000000000000	1.000000000000000	1.000000000000000	0.000000000000000	0.000000000000000
1	1	0.649824511625985	0.649824511625985	0.649824511625985	0.000000000000000	0.000000000000000
1	2	0.621598752346035	0.621598752346035	0.621598752346035	0.000000000000000	0.000000000000000
1	3	0.941273355072378	0.941273355072378	0.941273355072378	0.000000000000000	0.000000000000000
2	0	1.000000000000000	1.000000000000000	1.000000000000000	0.000000000000000	0.000000000000000
2	1	0.449977858638497	0.449977858638496	0.449977858638496	0.000000000000001	0.000000000000001
2	2	0.405643537487696	0.405643537487695	0.405643537487695	0.000000000000001	0.000000000000001
2	3	0.907757806955446	0.907757806955446	0.907757806955446	0.000000000000000	0.000000000000000
3	0	1.000000000000000	1.000000000000000	1.000000000000000	0.000000000000000	0.000000000000000
3	1	1.807955436690960	1.807955436690940	1.807955436690970	0.000000000000020	0.000000000000010
3	2	1.873080370965650	1.873080370965620	1.873080370965650	0.000000000000030	0.000000000000000
3	3	1.135499238590940	1.135499238590940	1.135499238590940	0.000000000000000	0.000000000000000

Besides, another result is the numerical solution is very close to the exact solution, whereas the error is 0 for certain point. However, it happens only for a certain radius. For example, if we take $x = 7$ and $t = 7$, then we get the exact solution is 1.0898 while the MADM solution is 699.3 by taken 10 terms. In the other case, if take 20 terms, both of solution generate 1.0904 with error 0.01. Thus, we conclude that more terms are used, the greater the radius of convergence of the solution.

4. Conclusion

We have presented how the Modified Adomian Decomposition Method (MADM) is applied when it is used to solve second order-ordinary differential equations involving source terms. Our computational

treatment of the source term is indeed effective to obtain accurate solutions to the problems. The solutions obtained from MADM can be expressed in numeric form by taking finite terms and we get the graph for the exact solution is the same as the MADM solution. For further research, we suggest to determining the converging radius of the MADM solution.

Acknowledgement
The authors would like to thanks to financial support received from Department of Mathematics, Faculty of Mathematics and Natural Sciences, Syiah Kuala University, Banda Aceh, Indonesia.

References

[5] Saadatmandi A and Dehghan M 2008 *The numerical solution of problems in calculus of variation using Chebychev finite difference method*, Physics letters A 372(**2008**) 4037-4040.
[6] Adomian G 1988 *A Review of the Decomposition Method in Applied Mathematics* J Math Anal Appl 135: 501-544.
[7] Cano J A S 2011 *Adomian Decomposition Method for a Class of Nonlinear Problems*, ISRN Applied Mathematics (**2011**) Article ID 709753, 10 pages.
[8] Nhawu G, Mafuta P and Mushanyu J 2016 *The Adomian Decomposition Method for Eigenvalue Problems*, Journal of Applied & computational mathematics (**5)** 2 pages.
[9] Adomian G and Rach R 1996 *Modified Adomian Polynomials*, Mathematical and Computer Modelling, 24(**11**):39-46.
[10] Rach R 2008 *A new definition of the Adomian polynomials*, Kybernetes, (**37**) 910-955.
[11] Wazwaz A M 1999 *A Reliable Modification of Adomian Decomposition Method*, Applied Mathematics Computation, (**102**) 77-86.
[12] Mungkasi S and Ekaputra I M W 2018 IJCAET & ISAMPE 2017 *Adomian decomposition method for solving initial value problems in vibration models* Matec Web Of Conferences 159 02007.
[13] Mungkasi S and Wiryanto L H 2016 On the relevance of a variational iteration method for solving the shallow water equations *AIP Conference Proceedings* **1707** 050010.
[14] Wazwaz A M and El-Sayed S M 2001 *A new Modification of the Adomian Decomposition Method for linear and nonlinear operator*, Appl. Math. Comput. (**122**) 393 - 405.
[15] Mustafa I 2005 *On Numerical Solution of One-Dimensional Non-Linear Burger's Equation and Convergence of the Decomposition Method* Appl Math Comput 170: 76-85.
[16] Marasi H R, Nikbakht M 2011 *The Adomian Decomposition Method for Boundary Eigenvalue Problems* Australian Journal of Basic and Applied Sciences 5: 2106-2111.

Supplementary data

```
%adomian decompotition A
clc
clear

syms x t
c=input('Masukkan Konstanta kecepatan gelombang (c): ');
f=input('Masukkan fungsi U(x,0)                    : ','s');
g=input('Masukkan fungsi Ut(x,0)                   : ','s');
k=input('masukkan banyak nya suku dari adomian     : ');

in = int(g);
iin = char(in);

%% awal L
fprintf('\n=====================================================\n')
fprintf('Menyelesaikan persamaan gelombang \nU_tt - %dU_xx = 0\n',c^2);
fprintf('.............(1)\nU(x,0) = '); disp(f);
fprintf('.............(2)\nU_t(x,0) = '); disp(g);
fprintf('.............(3)\n');
fprintf('Menggunakan metode adomian \n\n misalkan L_tt adalah operator\n');
fprintf('L_tt = d^2/dt^2; L_tt^-1 = int[int[(.)dt]^t_0 dt]^t_0 \n\n')
fprintf('didapat \nL_tt^-1 = U(x,t)- U(x,0) - int[U_t(x,0)dt]\n');
fprintf('\t\t= U(x,t) - '); disp([f,' - ',iin]);
fprintf('\n U(x,t) = Ltt^-1(%d Uxx) + ',c^2); disp([f,' + ',iin]);
fprintf('\n Dengan menggunakan metode adomian dekomposisi modifikasi \n');
fprintf('\n U_0(x,t)=f(x)\n U_1(x,t)=t*g(x)+L_t^-1(LxU0(x,t))\n');
fprintf(' U_n+1 (x,t) = L_t^-1(LxUn(x,t))\n');
fprintf('\n=====================================================\n')
%% coding adomian decomposisiton F
sum = 0;
for i = 1:k
sl = 2*(i-1);
s2 = 2*i-1;

Uixt = c^sl*(t^s2/factorial(s2))*diff(g,sl)+ ...
       c^(sl+2)*(t^(s2+1)/factorial(s2+1))*diff(f,sl+2);
fprintf('U_%d(x,t) = ',i);disp(Uixt)
sum = sum + Uixt;
end
U = inline(sum+f);

fprintf('sehingga solusi dengan adomian adalah\n');
fprintf('U(x,t) = '); disp(sum+f);

fprintf('\n=====================================================\n')
%% ploting image  A
fprintf('tampilkan plot ? (Y/N) : ');
pp = input(' : ','s');
lol = inline('1+sin(x)*cos(2*t)');
if pp == 'Y' || pp == 'y'
    n = input('masukkan batasan grid : ');
    [t,x] = meshgrid(-n:0.1:n);
    Z = U(t,x);
    u = inline('1+sin(x)*cos(2*t)');
    z = u(t,x);
    figure(1)
    surf(t,x,Z)
    figure(2)
    surf(t,x,z)
end
```

Gambar coding program adomian dekomposisi

INTERNATIONAL PROCEEDING
The 2nd International Conference on Science and Technology (ICST)
ISBN: 978-602-5830-19-8, June 2020

On the Rainbow Connection Number and Strong Rainbow Connection Number of Generalized Triangle-Ladder Graph

LYulianti*, N Narwen, S Fitrianda and K Al Azizu

[1] Department of Mathematics, Faculty of Mathematics and Natural Science, University of Andalas, Kampus UNAND Limau Manis Padang, Indonesia

*Email: lyra@sci.unand.ac.id (corresponding author)

Abstract. Let $G = (V,E)$ be a non-trivial connected graph. The rainbow coloring (respectively, strong rainbow coloring) $c: E(G) \rightarrow \{1,2,...,k\}$ is defined as the edge-coloring of G such as for every pair of vertices $u,v \in V(G)$, there is some rainbow (respectively, rainbow geodesic) (u,v)-path, whose edges all have different colors. The rainbow connection number (respectively, strong rainbow connection number) of G, denoted by $rc(G)$ (respectively, $src(G)$), is the smallest k such that G has the rainbow coloring (respectively, strong rainbow coloring). This paper concerns about the determination of rainbow connection number and the strong rainbow connection number of the generalized triangle-ladder graph Tr_n, denoted by $rc(Tr_n)$ and $src(Tr_n)$, for $n \geq 2$.

1. Introduction

The concept of the rainbow connection number was first introduced by Chartrand et al [1]. Let $G = (V,E)$ be a non-trivial connected graph on n vertices. Consider an edge-coloring $c: E(G) \rightarrow \{1,2,...,k\}$, $k \in N$, where adjacent edges may be colored the same. Let u and v be some arbitrary vertices in G. A (u,v)-path in G is defined as rainbow (u,v)-path if every edge in the path are colored differently. Graph G is rainbow connected with respect to c if G contains rainbow (u,v)-path for every two vertices u and v in G. If G is rainbow connected then the edge-coloring is called a rainbow coloring of G. The rainbow connection number of G, denotes by $rc(G)$, is defined as the minimum number of colors needed such that G rainbow connected.

Chartrand et al [1] gave a similar concept of strong rainbow coloring as follows. Let c be a rainbow coloring of a connected graph G. Let u and v be some arbitrary vertices in G. A rainbow (u,v)-path in G is defined as rainbow (u,v)-geodesic if the length of the path is $d(u,v)$, where $d(u,v)$ denotes the distance between u and v. Graph G is strongly rainbow connected under the edge-coloring if G contains a rainbow (u,v)-geodesic for every two vertices u and v in G. If G is strongly rainbow connected then c is called a strong rainbow coloring of G. The strong rainbow connection number of G, denotes by $src(G)$, is defined as the minimum number of colors given such that G is strong rainbow connected. By these definition, it is clear that $rc(G) \leq src(G)$ for every connected graph G.

Chartrand et al [1] stated that since every coloring that assigns different colors to the edges of a connected graph is both a rainbow coloring and a strong rainbow coloring, thus every connected graph is rainbow connected and strongly rainbow connected, with respect to some coloring of the edges of G. Therefore, the rainbow connection and strong rainbow connection are defined for every connected

graph G. Next, for every connected G on n vertices and m edges, with $diam(G) = max\{d(u,v) \mid u,v \in V(G)\}$, it can be seen that

$$diam(G) \leq rc(G) \leq src(G) \leq m. \qquad (1)$$

Chartrand et al [1] gave the characterizations of connected graphs G with some specified values of $rc(G)$ and $src(G)$ as follows. Let G be a non-trivial connected graph on n vertices and m edges. Then (1) $rc(G) = 1$ if and only if G is a complete graph, (2) $rc(G) = 2$ if and only if $src(G) = 2$, (3) $rc(G) = m$ if and only if G is a tree.

The exact values of the rainbow connection number and the strong rainbow connection for some other connected graphs have been obtained by Chartrand et al. [1], namely for path, cycle, wheel, complete graph, complete bipartite graph, and complete multipartite graph. Next, Sy et al. [2] obtained the rainbow connection number and the strong rainbow connection of the fan graph and the sun graph. Furthermore, there are some results regarding the determination of rainbow connection numbers and strong rainbow connections for graphs constructed from Cartesian product, amalgamation and corona operations of several simple graphs. These results are summarized in a survey by Li, Shi and Sun [3], as well as in a book by Li and Sun [4].

Let L_n be a triangle ladder graph on n vertices, $n \geq 2$. The diamond graph Br_n, for $n \geq 2$, is constructed by adding one vertex, namely v, that adjacent to all vertices in the first row of L_n. In [5] Shulhany and Salman determined the rainbow connection number and strong rainbow connection number of Br_n for $n \geq 2$ in Theorem 1 and Theorem 2 as follows.

Theorem 1 [5]
Let Br_n be a diamond graph on 2n vertices, for $n \geq 2$. The rainbow connection of Br_n is $rc(Br_n) = diam(Br_n)$.

Theorem 2 [5]
Let Br_n be a diamond graph on 2n vertices, for $n \geq 2$. The strong rainbow connection of Br_n is

$$src(Br_n) = \begin{cases} rc(Br_n), & 2 \leq n \leq 5, \\ \left\lceil \frac{n}{3} \right\rceil + 2, & n \geq 6. \end{cases}$$

Shulhany and Salman [5] using (1) to determine the lower bound of $src(Br_n)$ and $rc(Br_n)$, i.e $diam(Br_n) \leq rc(Br_n) \leq src(Br_n)$. Next, some edge coloring using $diam(Br_n)$ color were constructed to find the upper bound of $rc(Br_n)$. For finding the upper bound of $src(Br_n)$, the edge coloring using $rc(Br_n)$ colors for $2 \leq n \leq 5$ and $\left\lceil \frac{n}{3} \right\rceil + 2$ for $n \geq 6$ colors were constructed.

Next, some new graph is constructed from the diamond graph, namely the generalized triangle ladder graph, denoted by Tr_n for $n \geq 2$. In this paper, the rainbow connection number and strong rainbow connection of the generalized triangle ladder graph Tr_n are determined for $n \geq 2$.

2. The Rainbow Connection and Strong Rainbow Connection Number of Tr_n for $n \geq 2$

Let L_n and Br_n be a triangle ladder graph on n vertices and a diamond graph, for $n \geq 2$ respectively. The generalized triangle ladder graph Tr_n is constructed from Br_n by the following procedure. First, one corresponding triangle ladder graph was added on the top of Br_n, the ladder was defined as the second row. Next, one corresponding triangle ladder graph was added on the top of the second row; and was defined as the third row. The process continued until the n^{th} row. Graph L_n, Br_n, and Tr_n for $n \geq 2$ are given in Figure 1.

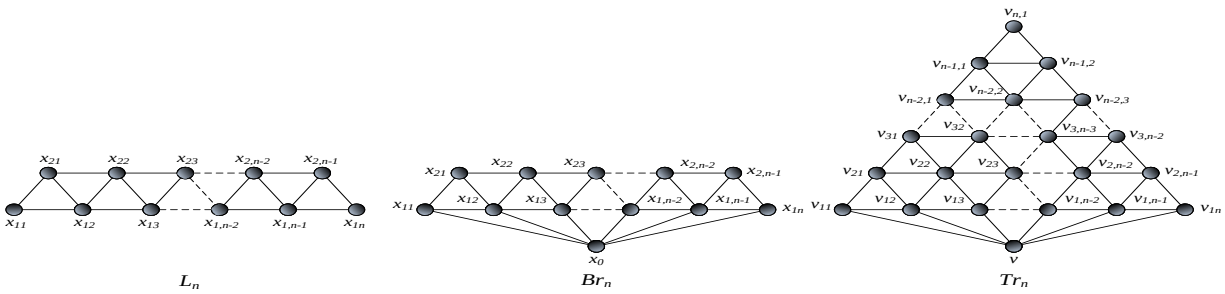

Figure 1. Triangle Ladder L_n, Diamond Br_n and Generalized Triangle Ladder Tr_n for $n \geq 2$

Let Tr_n be a generalized triangle ladder graph with vertex set and edge set for $n \geq 2$ as follows.

$$\begin{aligned} V(Tr_n) &= \{v\} \cup \{v_{ij} \mid 1 \leq i \leq n, 1 \leq j \leq n-i+1\}, \\ E(Tr_n) &= \{vv_{1j} \mid 1 \leq j \leq n\} \cup \{v_{ik}v_{i(k+1)} \mid 1 \leq i \leq n-1, 1 \leq k \leq n-i\} \\ &\quad \cup \{v_{ki}v_{(k+1)i} \mid 1 \leq i \leq n-1, 1 \leq k \leq n-i\}, \\ &\quad \cup \{v_{it}v_{(i+1)(t-1)} \mid 1 \leq t \leq n-i+1\}. \end{aligned}$$

It is clear that $|V(Tr_n)| = 1 + \frac{n(n+1)}{2}$, $|E(Tr_n)| = n + \frac{3n(n-1)}{2}$ and $diam(Tr_n) = n$ for $n \geq 2$.

The rainbow connection number and strong rainbow connection number of Tr_n for $n \geq 2$ were given in Theorem 3 and Theorem 4 as follows.

Theorem 3 *Let Tr_n be a generalized triangle ladder graph and $n \geq 2$. The rainbow connection number and the strong rainbow connection number of Tr_n is as follows.*

$$rc(Tr_n) = diam(Tr_n) = n.$$

Proof. Consider the following cases.

From (1), it is clear that $rc(Tr_n) \geq diam(Tr_n) = n.$ In order to show that $rc(Tr_n) \leq n$, consider the following cases.

Case 1. For $n = 2$ or n = 3,

Define the edge-coloring $c_1: E(Tr_n) \rightarrow \{1,2,3\}$ as follows.

$$\begin{aligned} c_1(vv_{1j}) &= j, & 1 \leq j \leq n, \\ c_1(v_{ik}v_{i(k+1)}) &= k, & 1 \leq i \leq n-1, 1 \leq k \leq n-i \\ c_1(v_{ki}v_{(k+1)i}) &= k+1, & 1 \leq i \leq n-1, 1 \leq k \leq n-i, \\ c_1(v_{12}v_{21}) &= i+1. & 1 \leq i \leq n-1, 2 \leq t \leq n-i+1. \end{aligned}$$

It is easy to check that for every two vertices x and y in $V(Tr_2)$, there is some (x,y)-rainbow path.

Case 2. For $n \geq 4$

Construct the edge-coloring $c_2: E(Tr_n) \rightarrow \{1,2,\ldots, n\}$ as follows.

$$
\begin{aligned}
c_2(vv_{11}) &= 1, \\
c_2(vv_{1s}) &= n-(s-2), && 2 \le s \le n-1, \\
c_2(vv_{1n}) &= 4, \\
c_2(v_{ki}v_{(k+1)i}) &= k+1, && 1 \le i \le n-1, 1 \le k \le n-i, \\
c_2(v_{it}v_{(i+1)(t-1}) &= i+1, && 1 \le i \le n-1, 2 \le t \le n-i+1, \\
c_2(v_{ik}v_{i(k+1)}) &= [1,n] - \bigcup_{i=1}^{n-1} c_2(v_{i1}v_{(i+1)1}), && 1 \le i \le n-1, 1 \le k \le n-i.
\end{aligned}
$$

It can easily checked that by this edge coloring, there is some rainbow *(x,y)*-path for every two vertices *x* and *y* in Tr_n with $d(x,y) \ge 2$. For example, choose $x = v$ and $y = v_{ik}$, for some $1 \le i \le n-1$ and $1 \le k \le n-i$. Then the rainbow *(x,y)*-path is $v,v_{1k},v_{2k}, \ldots,v_{(i-1)k},v_k$. If $x = v_{ki}$ and $y = v_{ik}$, then the rainbow *(x,y)*-path is $v_{ki},v_{(k+1)(i-1)},v_{(k+2)(i-2)},\ldots,v_{(i-2)(k+2)},v_{(i-1)(k+1)},v_{ik}$. If $x = v_{ik}$ and $y = v_{pq}$, for some $1 \le i,p \le n-1$ and $1 \le k \le n-i$, $1 \le q \le n-p$, then the path is $v_{ik},v_{(i+1)k},v_{(i+2)k},\ldots,v_{(p-1)k},v_{pk},v_{p(k+1)},\ldots,v_{p(q-1)},v_{pq}$. It implies that $rc(Tr_n) \le n$ for $n \ge 2$. ■

Theorem 4 *Let Tr_n be a generalized triangle ladder graph and $n \ge 2$. The strong rainbow connection number of Tr_n is $src(Tr_n) = n$.*

Proof. From (1), $src(Tr_n) \ge rc(Tr_n) = n$. To show that $src(Tr_n) \le n$, consider the following cases.

Case 1. For $n = 2$ or $n = 3$.

Define the edge coloring $c_2: E(Tr_n) \to \{1,2,3\}$ as follows.

$$
\begin{aligned}
c_3(vv_{1p}) &= p, && 1 \le p \le n, \\
c_3(v_{ik}v_{i(k+1)}) &= k, && 1 \le i \le n-1, 1 \le k \le n-i, \\
c_3(v_{ki}v_{(k+1)i}) &= k+1, && 1 \le i \le n-1, 1 \le k \le n-i, \\
c_3(v_{it}v_{(i+1)(t-1)}) &= i+1, && 1 \le i \le n-1, 2 \le t \le n-i+1.
\end{aligned}
$$

Case 2. For $4 \le n \le 6$.

The edge-coloring $c_4: E(Tr_n) \to \{1,2,\ldots, 6\}$ is as follows.

$$
\begin{aligned}
c_4(vv_{11}) &= 1, \\
c_4(vv_{1s}) &= n-(s-2), && 2 \le s \le n-1, \\
c_4(vv_{1n}) &= 4, \\
c_4(v_{ki}v_{(k+1)i}) &= k+1, && 1 \le i \le n-1, 1 \le k \le n-i, \\
c_4(v_{it}v_{(i+1)(t-1}) &= i+1, && 1 \le i \le n-1, 2 \le t \le n-i+1, \\
c_4(v_{ik}v_{i(k+1)}) &= [1,n] - \bigcup_{i=1}^{n-1} c_4(v_{i1}v_{(i+1)1}), && 1 \le i \le n-1, 1 \le k \le n-i.
\end{aligned}
$$

Case 3. For $n \ge 7$.

$$
\begin{aligned}
c_5(vv_{1p}) &= p, && 1 \le p \le n, \\
c_5(v_{ik}v_{i(k+1)}) &= k, && 1 \le i \le n-1, 1 \le k \le n-i, \\
c_5(v_{ki}v_{(k+1)i}) &= k+1, && 1 \le i \le n-1, 1 \le k \le n-i, \\
c_5(v_{it}v_{(i+1)(t-1)}) &= (i+t+m) \bmod n, && m = i-1, 1 \le i \le n-1, 2 \le t \le n-i+1.
\end{aligned}
$$

Next, it will be shown that by this edge coloring, there is some rainbow geodesic *(x,y)*-path for every two vertices *x* and *y* in Tr_n for $n \geq 2$. If $x = v$ and $y = v_{ik}$, for some $1 \leq i \leq n-1$ and $1 \leq k \leq n-i$, then the rainbow geodesic *(x,y)*-path is $v,v_{1n},v_{2(n-1)},v_{3(n-2)},\ldots,v_{(i-2)(k+2)},v_{(i-1)(k+1)},v_{ik}$. If $x = v_{ki}$ and $y = v_{ik}$, then the path is $v_{ki},v_{(k+1)(i-1)},v_{(k+2)(i-2)},\ldots,v_{(i-2)(k+2)},v_{(i-1)(k+1)},v_{ik}$. If $x = v_{ik}$ and $y = v_{pq}$, for some $1 \leq i,p \leq n-1$ and $1 \leq k \leq n-i$, $1 \leq q \leq n-p$, then the path is $v_{ik},v_{(i-1)(k+1)},v_{(i-1)(k+2)},v_{(i-2)(k+3)},v_{(i-2)(k+4)}\ldots,v_{(p+1)(q-3)},v_{(p+1)(q-2)},v_{p(q-1)},v_{pq}$. Similar with Theorem 3.1, by defining this edge coloring, for every two vertices *x* and *y* in Tr_n there is some rainbow geodesic *(x,y)*-path. Thus, $src(Tr_n) \leq n$. ■

The rainbow and strong rainbow coloring of the generalized triangle ladder graph Tr_7 were given in Figure 2.

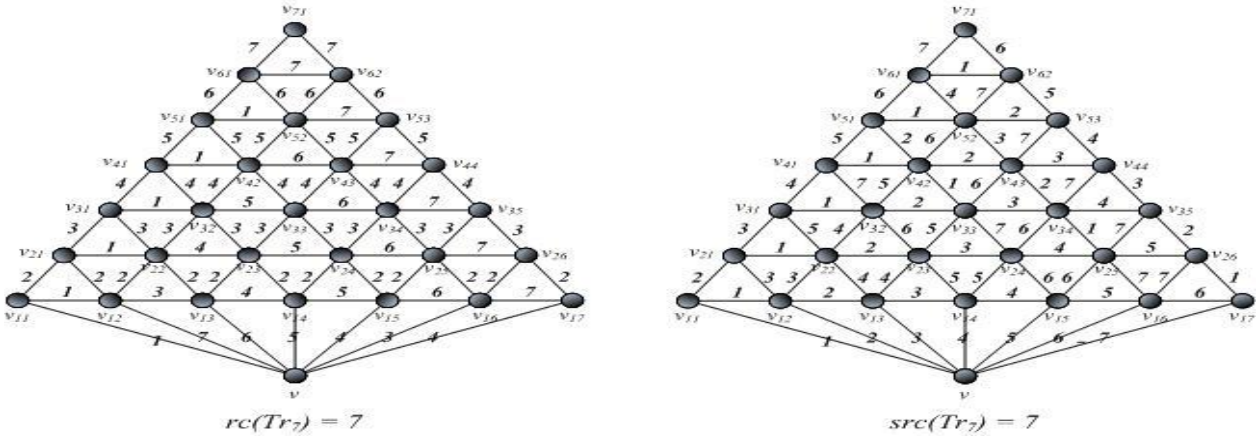

Figure 2. $rc(Tr_7) = 7$ and $src(Tr_7) = 7$

3. Conclusion

In this paper, the rainbow connection number and strong rainbow connection number of the generalized triangle ladder graph were determined. It is found that the exact number of $rc(Tr_n)$ and $src(Tr_n)$ equal the diameter of Tr_n.

Acknowledgement

This research was partially funded by Hibah Penelitian Pengembangan Sains Dasar dan Matematika-Skim Riset Dasar 2018 from Faculty of Mathematics and Natural Sciences, Andalas University, Indonesia.

References

[1] Chartrand G, Johns G L, McKeon K A and Zhang P 2008 Rainbow Connection in Graphs. *Math. Bohem* **133**: 85–98

[2] Syafrizal, Histamedika G, Yulianti L 2013 The Rainbow Connection Number of fan and sun. *Applied Mathematical Sciences* **7**(64) : 3155–3159

[3] Li X and Sun Y F 201, *Rainbow Connection of Graphs* (New York: Springer Brief in Mathematics, Springer)

[4] Li X, Sun Y F and Shi Y T 2013 Rainbow Connection of Graphs: A Survey. *Graph and Combinatorics* **29**(1): 1–38

[5] Shulhany M A, Salman A N M 2015 Bilangan Terhubung Pelangi Graf Berlian. *Prosiding Seminar Nasional Matematika dan Pendidikan Matematika* UMS **1**: 916–924

INTERNATIONAL PROCEEDING
The 2nd International Conference on Science and Technology (ICST)
ISBN: 978-602-5830-19-8, June 2020

Numerical studies of free convection process in Sabang Bay using 2d non-hydrostatic model

T Iskandar[1], M Ikhwan[2], Y Haditiar[2], and S Rizal[2,3,*]

[1]Department of Mathematics, Faculty of Mathematics and Natural Sciences, Universitas Syiah Kuala, Banda Aceh, 23111, Indonesia.
[2]Graduate School of Mathematics and Applied Science, Universitas Syiah Kuala, Banda Aceh, 23111, Indonesia.
[3]Department of Marine Science, Faculty of Marine and Fisheries, Universitas Syiah Kuala, Banda Aceh, 23111, Indonesia.

[*]Email: syamsul.rizal@unsyiah.net

Abstract. Sabang Bay has steep topography, most of its area has a depth of more than 100 meters. This study aims to study the effect of heat release in the regions that have the deep sea on density dynamics. 2D non-hydrostatic models are used for free convection simulation in Sabang Bay. Ocean slice models are formed by taking a transverse line from the open sea in the bay of Sabang and the path that extends to the deepest coast of Sabang Bay. Based on the simulation results, changes in density begin with an increase in density in areas with shallow depth and leave low-density in areas with high depth. Convection cells start to sink after 35 minutes of simulation with a vertical velocity of 0.0042 m/s on the surface and stop dropping at a depth of 360 meters. Areas with high depth indicate falling speeds after about 3 hours of simulation, but in the surface layer area shows density stability. In general, the deep sea area is not affected by the convection process, and the surface area is well-mixed after 3 hours of simulation.

1. Introduction

Sabang Bay has a depth of up to 340 meters at the map coordinates about 5.75°-5.82° N and 95.3833°-95.3458° E[1]. With insignificant depth, Sabang bay is strongly influenced by the surrounding oceans such as the Indian Ocean, the Andaman Sea, and the Malacca Strait[2], [3]. Sea surface temperature (SST) is a physical property that can be affected by the oceans around Sabang bay. Previous research has reported that there has been an increase in SST in the Andaman sea[4]. The results of the study indicate that mass coral bleaching events in the Andaman Sea occur when there is an increase in SST in a short period or a small increase in a long time due to El Niño or La Niña events on a large scale every ten years. Obviously, it was a threat to the Sabang bay as the area contribute income Sabang City area as a tourist destination.

Not only the influence that is carried from the surrounding sea, the impact of convection dramatically affects the temperature of the sea both the bottom and the surface. Low density at higher altitudes means a decrease in convection[5], [6]. It indicates that at the surface of the water the density of water is smaller than the density on the seabed caused by forced convection. This convection is required in maintaining the climate on earth[7], [8]as heat fluctuations in high latitude areas with annual average SST will be much higher and seasonal cycles will be dramatically reduced[9]. Free

convection is a way to stabilize the ocean temperature again after the forced convection. The free convection process occurs in the surface of the ocean surface with the division of layers such as the thermal boundary layer, free convection layer, and the layer with N_{th} uniform buoyancy loss [10]. The value of N is the stratification which is also known as the frequency of stability [11].

This study explains the effects of the release of heat on sea deep density dynamics. Sabang Bay was chosen because it has heat effects from the Andaman Sea and the Indian Ocean, in latitude with high heat flux, and the influence of heat affects ecosystems and economic activities.

2. Materials and Methods

Bathymetry data obtained from the data Shuttle Radar Topography Mission with 30 minutes resolution SRTM30[12]. The coordinate of bathymetry is 5.85°-5.95°N and 95.2°-95.33° E as map in Figure 1.

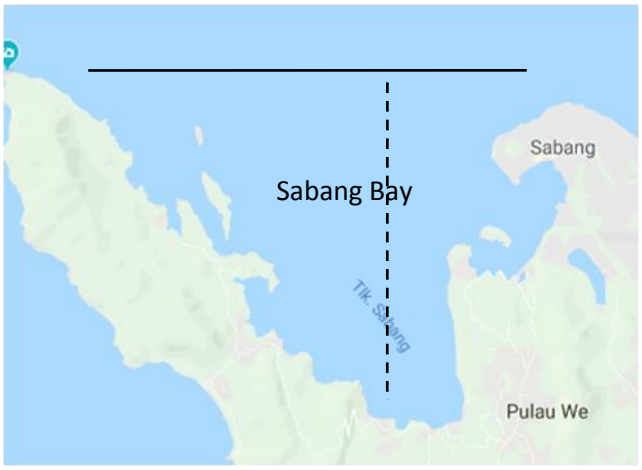

Figure 1. Domain of research (straight line as zonal vertical slice and dash line as a meridional vertical slice)

Bathymetry data is used as the seabed boundary of the area given the free convection effect. The distribution of stratification based on frequency stability follows the formula[11]:

$$\rho(z) = \rho_0 \left(1 + \frac{N^2}{g}|z|\right) \quad (1)$$

Where $\rho(z)$ is the layer with N_{th} uniform buoyancy loss, ρ_0 is density at sea surface, g is gravity, z is depth in meters and N is stability frequency.

This study used the Navier-Stoke equation to obtain a numerical solution for horizontal velocity u and w. The system of differential equations used is [11]:

$$\frac{\partial u}{\partial t} + u\frac{\partial u}{\partial x} + w\frac{\partial u}{\partial z} = -\frac{1}{\rho_0}\frac{\partial (p+q)}{\partial x} + \text{Diff}\,(u) \quad (2)$$

$$\frac{\partial w}{\partial t} + u\frac{\partial w}{\partial x} + w\frac{\partial w}{\partial z} = -\frac{1}{\rho_0}\frac{\partial q}{\partial z} + \text{Diff}\,(w) \qquad (3)$$

where u and w are currents velocity in zonal and vertical term, ρ is sea water density, η is sea level elevation, and h is total depth added to sea elevation. The parameters used are f as the Coriolis parameter, pas a hydrostatic pressure and q as a non-hydrostatic pressure.

The solution to the Navier-Stokes equation can be solved by following the algorithm as follows:

Algorithm 1

1. Separate the pressure into several parts.
2. Execute momentum Equation (2) and (3)
3. Use finite different scheme.
4. Use SOR for iteration.
5. Determine the boundary conditions for the bathymetry variable.
6. Determine the value of the stability criteria.

Stability criteria are achieved with Δt that determined using formula[11]:

$$\Delta t \leq \frac{\Delta x}{\sqrt{g h_{max}}} \qquad (4)$$

3. Results and Discussion

This study took two vertical slices from the Sabang bay domain. For zonal vertical slice, the grid formed is 99x32 with a maximum depth of 490 meters. Zonal vertical slice stretches for 14.5 Km. The simulation runs for 6 hours and produces a current and density profile that can be seen in Figure 2.

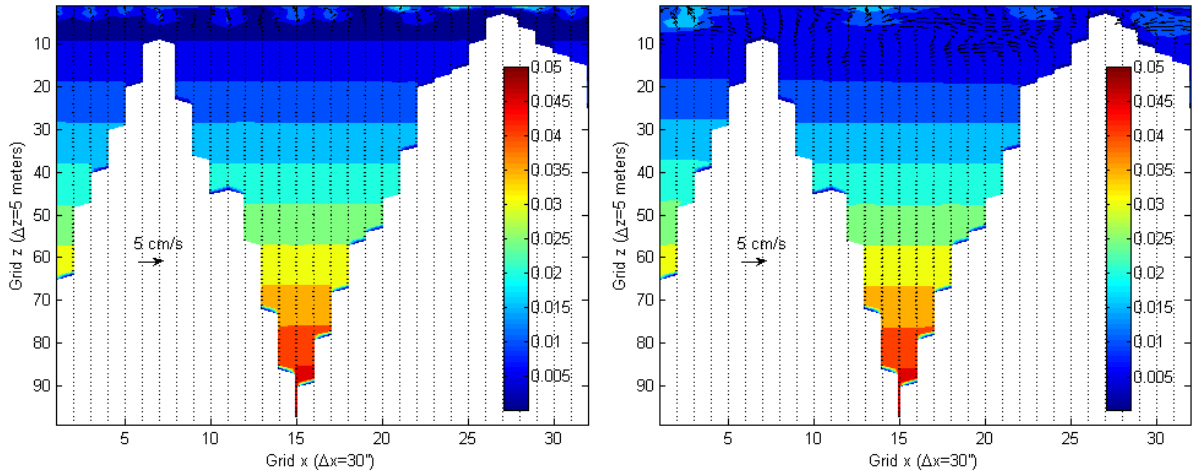

(a) 1 hour simulation

(b) 2 hours simulation

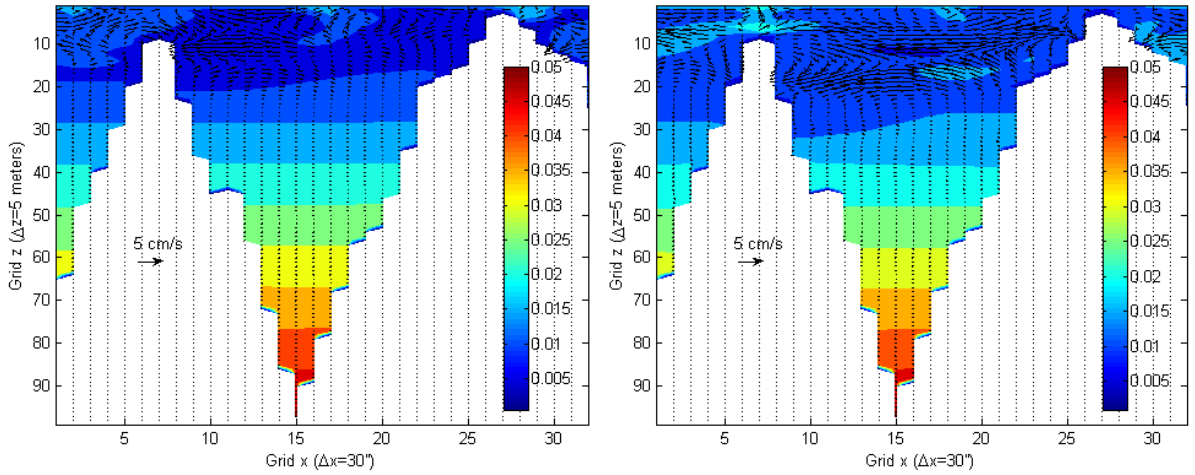

(c) 3 hours simulation (d) 6 hours simulation

Figure 2. Profile of free convection in zonal vertical slice

At the start of the simulation, both horizontal and vertical velocity indicates a value of 0 or without initial velocity. The stratification of the layers is still visible with little disturbance at the top layer. In the first hour, the surface layer undergoes cooling marked by changes in surface density. Some of these surface cells begin to sink when they reach 35 minutes of simulation. The segment that undergoes a cooling and sinking process is at a depth of 0 - 50 meters. Horizontal current velocity has not been seen, but the vertical velocity is clearly visible in the sinking cell with speed 0.0042 m/s.

The convection process continues until it reaches the third layer (based on the colour of the segment). During the two-hour simulation, horizontal and vertical velocity emerged due to the momentum caused by the gulf base. On the right seafloor, the sinking cell has reached the bottom, then reflected the mass of water. The disturbance is seen from the quivering form that moves away from the sea floor. In the middle of the domain, small disturbances are seen as biases from disturbances on both sides, left and right. The third colour layer begins to mix with the layers that experience convection and the current velocity starts to look diverse.

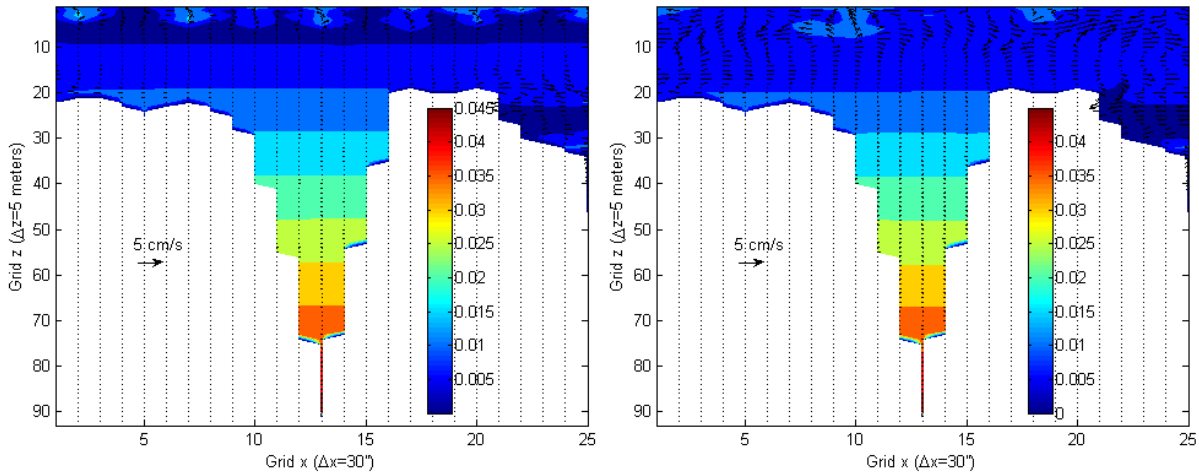

(a) 1 hour simulation (b) 2 hours simulation

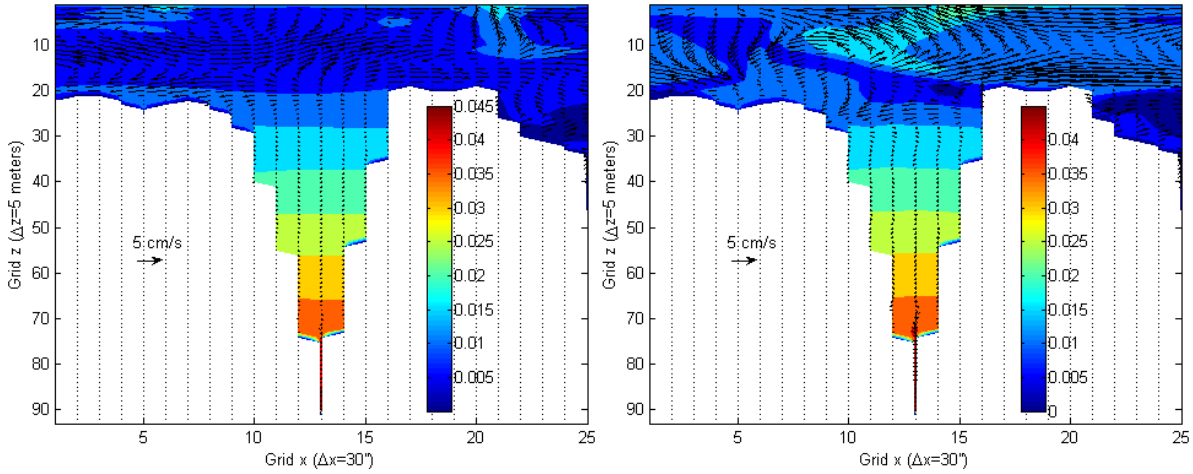

(c) 3 hours simulation (d) 6 hours simulation

Figure 3. Profile of free convection in meridional vertical slice

The simulation has been running for 3 hours and seen stratification began to decrease. The third layer starts to thin so that it can be said that the first three layers have reached stability. Vertical current velocity continues to sink to a depth of 140 meters. Layers with a depth greater than 150 meters experience only a small amount of interference, not even disturbed at all at the very base. After the simulation runs for more than 3 hours, steady conditions can be seen in layers 0 - 150 meters. Even though it looks like the convection is only in the surface layer, but, if it is seen only from the vertical velocity, there are several cells of water mass sinking to a depth of 360 meters.

The second vertical slice has 93x25 grids. This domain is 11.7 Km long starting from the beach to the middle of the bay. The depth observed was 470 meters with conditions in the form of a small trough in the middle of the domain. like the first case, the second domain was also simulated for six hours. The result of free convection from this domain is in Figure 3.

Vertical current velocity is different from the previous case. The effect of the seabed on the momentum of the mass of water has been seen in one hour of simulation. In general, physical phenomena that are generated are the same as zonal vertical slices, the occurrence of vertical current velocity and the beginning of the presence of water cells that were sunk due to the cooling process. The condition of the seabed in the second domain has a very sharp slope. It causes the momentum generated is also different. In the two-hour simulation, the vertical and horizontal currents have seen very solid. The first and second layers are even thoroughly mixed and begin to see a slight mass of water with a density like the third layer.

Stratification in the three-hour simulation has been reduced. With a domain form such as a trough, the vertical and horizontal flow velocities formed are very large. The horizontal velocity is evenly distributed on the surface layer. As in the first domain, this second domain also began to reach steady conditions at 3 hours of simulation time. Vertical and horizontal current velocities only move in layers 0-150 meters. In the middle of the domain, the cell sink reaches a depth of 360 meters. The mass of

water in 150-360 meters only moves horizontally and is very slow. Significant horizontal speeds reach 5 cm/s on the surface, while vertical velocity is only 0.0042 m/s on the surface.

4. Conclusions

Based on the simulation results, changes in density begin with an increase in density in areas with shallow depth and leave low-density in areas with high depth. Convection cells start to sink after 35 minutes of simulation with a vertical velocity of 0.0042 m/s on the surface and stop dropping at a depth of 360 meters. Areas with high depth indicate falling speeds after about 3 hours of simulation, but in the surface layer area shows density stability. Both vertical slice domains have a mass of water that is at a depth greater than 150 meters. At that depth, the mass of water only moves horizontally, and the magnitude is not significant. In general, the deep sea area is not affected by the convection process, and the surface area is well-mixed after 3 hours of simulation.

Acknowledgments

Authors would like to express gratitude to the Ministry of Research, Technology and Higher Education of Indonesia for financial assistance in term '*Penelitian Lektor Kepala*' under contract number 121/UN11.2/PP/PNPB/SP3/2019. We also thank for facility support at Ocean Modelling Laboratory Universitas Syiah Kuala during the research.

References

[1] Iskandar T, Haditiar Y, Setiawan I, Fahmi K, Muhammad M, and Rizal S 2018 Simulation of long waves in a layered Sabang waters *IOP Conf. Ser. Earth Environ. Sci.* **216**012013.

[2] Setiawan I, Alfawirsa M A, Haditiar Y, and Rizal Y 2018 Simulation of tidal hydrodynamics in Sabang Bay, Indonesia *IOP Conf. Ser. Earth Environ. Sci.* **216**012012.

[3] Seo H, Xie S P, Murtugudde R, Jochum M, and Miller A J 2009 Seasonal effects of Indian Ocean freshwater forcing in a regional coupled model *J. Clim.* **22(**24) 6577–6596.

[4] Koad P, Jaroensutasinee M, and Jaroensutasinee K 2012 Sea Surface Temperature Trends in the Gulf of Thailand and the Andaman Sea *2012 Oceans - Yeosu* 1–8.

[5] Doherty R E and Carter E S 1924 Effect of Altitude on Temperature Rise*J.A.I.E.E* **43(**12) 824–843.

[6] Hoggard M J, Winterbourne J, Czarnota K, and White N 2017 Oceanic residual depth measurements, the plate cooling model, and global dynamic topography*J. Geophys. Res. Solid Earth* **122(**3) 2328–2372.

[7] D. S. Abbot and E. Tziperman 2008 Sea ice, high-latitude convection, and equable climates*Geophys. Res. Lett.* **35** 1–5.

[8] Cheon W G and Gordon A LOpen-ocean polynyas and deep convection in the Southern Ocean*Sci. Rep.* **9(**1) 1–9.

[9] Nuijens L and Siebesma A P 2019 Boundary Layer Clouds and Convection over Subtropical Oceans in our Current and in a Warmer Climate*Curr. Clim. Chang. Reports* **5(**2) 80–94.

[10] Marshal J and Schott F 1999 Open-ocean convection: observations, theory, and models*Rev. Geophys.* **37(**1) 1–64.

[11] Kämpf J 2010 *Advanced Ocean Modelling Using Open Source Software*. Berlin, Heidelberg: Springer Berlin Heidelberg.

[12] Haditiar Y, Rizal S and Abdullah F 2017 Current simulation in the Malacca Strait and part of South China Sea due to wind*12th Int. Conf. Math. Stat. Their Appl. ICMSA 2016 Conjunction with 6th Annu. Int. Conf. Syiah Kuala Univ.*, 47–50.

INTERNATIONAL PROCEEDING
The 2nd International Conference on Science and Technology (ICST)
ISBN: 978-602-5830-19-8, June 2020

The simulation of free convection in the shallow waters of Krueng Raba Bay, Aceh

T Iskandar[1], M Ikhwan[2], Y Haditiar[2], and S Rizal[2,3,*]

[1]Department of Mathematics, Faculty of Mathematics and Natural Sciences, Universitas Syiah Kuala, Banda Aceh, 23111, Indonesia.
[2]Graduate School of Mathematics and Applied Science, Universitas Syiah Kuala, Banda Aceh, 23111, Indonesia.
[3]Department of Marine Science, Faculty of Marine and Fisheries, Universitas Syiah Kuala, Banda Aceh, 23111, Indonesia.

[*]Email: syamsul.rizal@unsyiah.net

Abstract. Krueng Raba Bay is flanked by two busy coastal tourism areas on the west coast of Aceh. The bay is also filled with activities of cement factories and fishers so that this place has high economic activity. This article aims to observe and simulate the process of releasing heat from shallow water and full of human activities. Simulation is designed by vertical slice cases with varying density values based on stability frequency. The vertical current velocity or upwelling starts to strengthen in the sill area at two hours simulation. The lighter fluid moves upwards, looking for a gap between the denser fluid on the surface with a maximum speed of 0.03 m/s. The speed of upwelling and downwelling at four and five hours is quite strong and almost the same. However, after 6 hours of the simulation, the downwelling speed was reduced quite quickly while the upwelling speed was still the same.

1. Introduction

The Indian Ocean has a significant role for the west coast of the island of Sumatra. The effect of the entry of fresh water from the river discharge into the Indian Ocean increases the upper sea stratification and rises the SST near the mouth of the river where the power of freshwater is the largest[1].The simulation revealed the seasonal effect of salinity on oceanic vertical density stratification related to changes in sea surface temperature (SST), surface wind, and precipitation. One of the bays directly adjacent to the Indian Ocean is Krueng Raba Bay in the waters of Aceh Besar[2].

Krueng Raba Bay is an open beach area and slightly protrudes into the mainland. This bay is influenced by the Indian Ocean in the west and Aceh waters [3][4].This area is crowded with tourists starting from the white sand beach in the north to the middle of the domain. Economic activities run very densely in this area. To the south of the coast, there is one cement factory that carries cargo by sea transportation. This dense activity is a significant disturbance for the free convection process. The base and surface of the bay determine the momentum and velocity of the vertical current. Also, the convective process increases surface roughness under free convection conditions[5], [6].

The convection process produces the boundary layer convergence [7]. Boundary layer convergence occurs due to a layer that is continually changing due to convection both current velocity and density. In the case of fluid convection, some boundary layers can occur in thick layers but will be completely mixed in thin layers[8].

2. Materials and Methods

Bathymetry data obtained from the data Shuttle Radar Topography Mission with 15 minutes resolution SRTM15[9]. The coordinate of bathymetry is 5.43°-5.5°N and 95.2°-95.25° E as map in Figure 1.

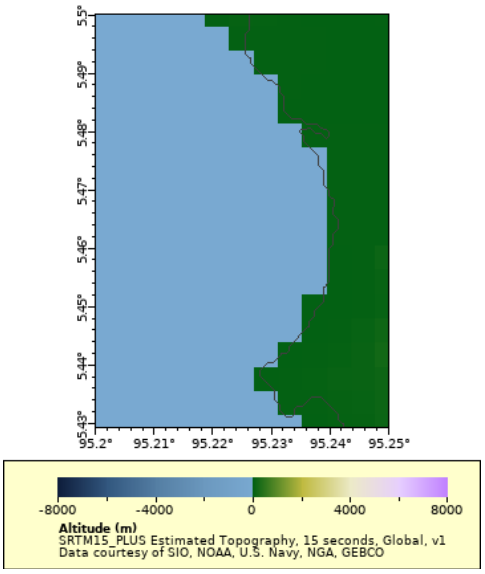

Figure 1. Domain of research

Bathymetry data is used as the seabed boundary of the area given the free convection effect. The distribution of stratification based on frequency stability follows the formula[10]:

$$\rho(z) = \rho_0 \left(1 + \frac{N^2}{g}|z|\right) \quad (1)$$

where $\rho(z)$ is the layer with N_{th} uniform buoyancy loss, ρ_0 is density at sea surface, g is gravity, z is depth in meters and N is stability frequency.

This study used the Navier-Stoke equation to obtain a numerical solution for horizontal velocity u and w. Non-hydrostatic model can be used to solve Navier-Stokes equation[10]. Momentum and energy were written as nonlinear differential equations under appropriate similarity transformations [11]. The system of differential equations used is [11]:

$$\frac{\partial u}{\partial t} + u\frac{\partial u}{\partial x} + w\frac{\partial u}{\partial z} = -\frac{1}{\rho_0}\frac{\partial (p+q)}{\partial x} + \text{Diff}\,(u) \quad (2)$$

$$\frac{\partial w}{\partial t} + u\frac{\partial w}{\partial x} + w\frac{\partial w}{\partial z} = -\frac{1}{\rho_0}\frac{\partial q}{\partial z} + \text{Diff}\,(w) \quad (3)$$

where u and w are currents velocity in a zonal and vertical term, ρ is sea water density, η is sea level elevation, and h is total depth added to sea elevation. The parameters used are f as the Coriolis parameter, p as a hydrostatic pressure and q as a non-hydrostatic pressure.

Parameterization of free convection over the ocean is quite crucial for the atmosphere, so the value of flux and surface density must be observed [12]. The treatment of this study is to provide a surface parameter $\rho_0 = 1021$ kg/m^3, heat flux of 600 Watt/m^2, and specific heat capacity is 4000 J/(Kg Kelvin). The initial vertical and horizontal current velocity are set to 0 m/s, and the speed that rise can be said as a speed caused by differences in density.

3. Results and Discussion

Simulation results can be seen in the following Figure 2:

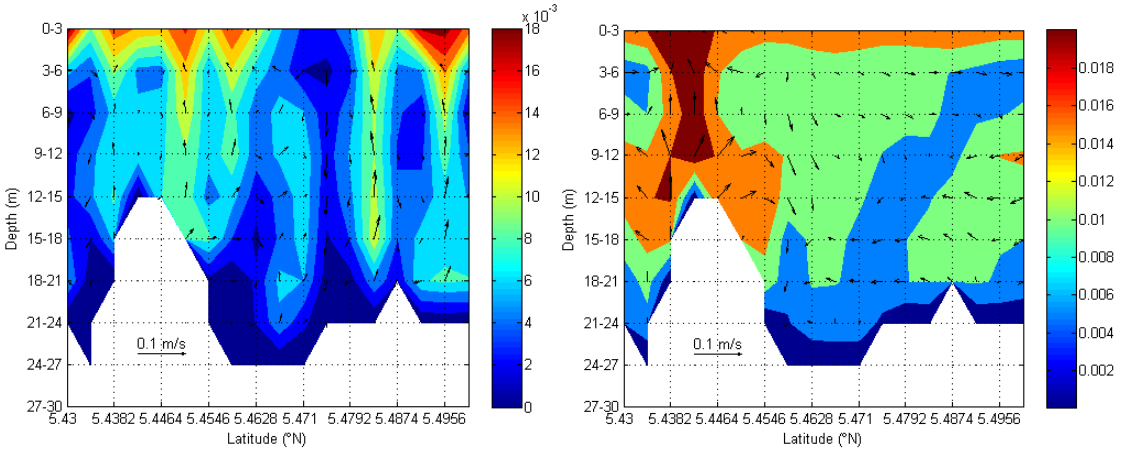

(a) 1 hour simulation (b) 2 hours simulation

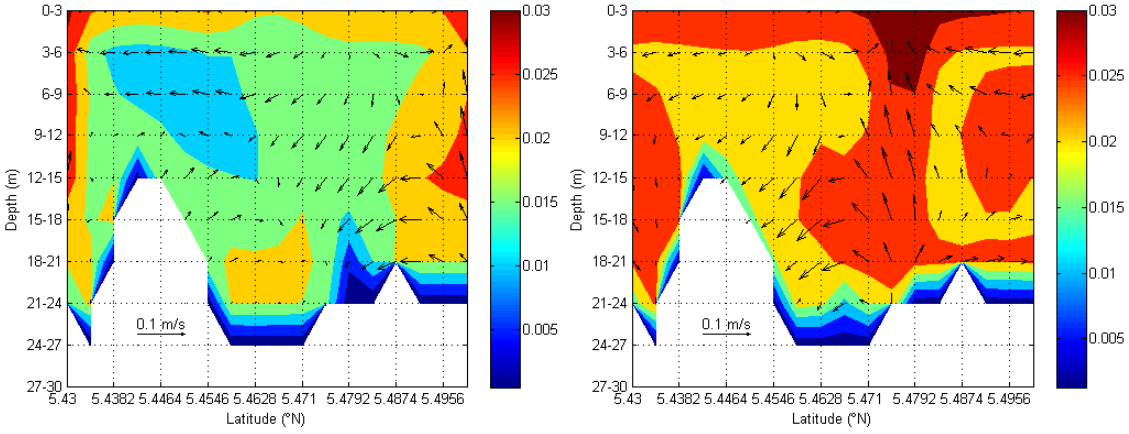

(c) 3 hours simulation (d) 4 hours simulation

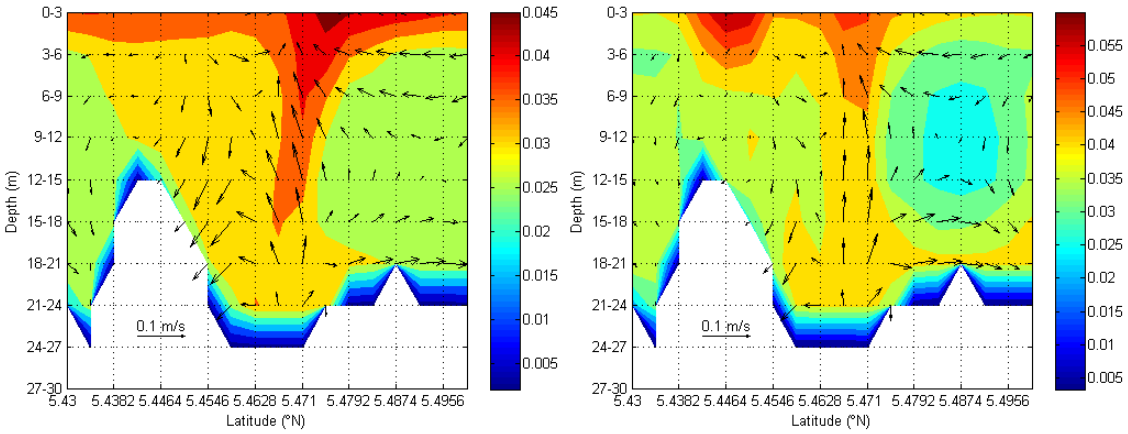

(e) 5 hours simulation (f) 6 hours simulation

Figure 2. Profile of free convection in a meridional vertical slice

Meridionally, heat loss takes place gradually and starts at the surface layer, which is characterized by a high density in the surface layer compared to the lower layer. Figure 2 shows the current profile and density of the loss energy 600 W/m2 in all fluid columns.

In the first five minutes, fluid in the surface layer between 0-6 meters experienced stronger and heavier stratification while the lower layer was lighter and mixed well. This condition then causes interference with the vertical current after 35 minutes and horizontal current after 45 minutes. At 1 hour simulation, the light and heavy density have begun to mix. This is followed by vertical turbulence.

At two hours of simulation, the vertical current velocity or upwelling starts to strengthen in the sill area (around 5.44 oN) where the lighter fluid moves upwards, looking for a gap between the denser fluid on the surface with a maximum speed of 0.03 m/s — examples of internal wave and sill interactions in the ocean. Upwelling in the sill region after 3 hours of simulation is followed by the emergence of lightly clarified density. Also, when this disturbance originates from the east, the domain begins to form.

At four and five hours of simulation, current disturbances from the east contribute to downwelling and upwelling on the right side of the sill (5.4546 - 5.4792 ^{o}N). The speed of upwelling and downwelling at that time is quite strong and almost the same. However, after 6 hours of the simulation, the downwelling speed was reduced quite quickly while the upwelling speed was still the same. In the upwelling zone (5,4628-5,471 ^{o}N), the density is greater than that of the sill or the surrounding part. Based on the simulation results for 6 hours, current and density conditions have not reached stability, where the upwelling is still formed, and the density layer on the surface is still higher than the part under the sea.

4. Conclusions

In the first hour of simulation, the vertical current velocity shows that water mass that has a higher density in the southern region of the bay is characterized by mass of sinking water. In the middle of the bay, the current speed is enlarged, which means that the mass of water has a low density. The

northern part of the bay does not show significant changes in density or vertical current velocity. The vertical current velocity or upwelling starts to strengthen in the sill area at two hours simulation. The lighter fluid moves upwards, looking for a gap between the denser fluid on the surface with a maximum speed of 0.03 m/s. The speed of upwelling and downwelling at four and five hours is quite strong and almost the same. However, after 6 hours of the simulation, the downwelling speed was reduced quite quickly while the upwelling speed was still the same.

Acknowledgments
Authors would like to express gratitude to the Ministry of Research, Technology and Higher Education of Indonesia for financial assistance in the term '*Penelitian Lektor Kepala*' under contract number 121/UN11.2/PP/PNPB/SP3/2019. We also thank for facility support at Ocean Modelling Laboratory Universitas Syiah Kuala during the research.

References

[1] Seo H, Xie S P, Murtugudde R, Jochum M, and Miller A J 2009 Seasonal effects of Indian Ocean freshwater forcing in a regional coupled model *J. Clim.* **22(**24) 6577–6596.
[2] Setiawan I, Yuni S M, Purnawan S, Ilhamsyah Y, and Wafdan R 2019 Simulation of two-dimensional currents to the depth and suspended sediment concentration in Aceh Besar Waters *IOP Conf. Ser. Earth Environ. Sci.* **284** 012026.
[3] Rizal S, Setiawan I, Boihaki B, Haditiar Y, Iskandar T, and Sugianto S 2018 Simulation of current using a two-dimensional numerical model in the Aceh Barat Daya waters, Indonesia *IOP Conf. Ser. Earth Environ. Sci.* **216(**1) 0–5.
[4] Irham M, Miswar E, Ilhamsyah Y, and Setiawan I 2018 The northern tidal dynamic of Aceh waters: A 3D numerical model in *IOP Conference Series: Materials Science and Engineering* **352(**1).
[5] Huang C 2010 Sea surface roughness and drag coefficient under free convection conditions in *Latest Trends on Theoretical and Applied Mechanics, Fluid Mechanics and Heat & Mass Transfer* 121–127.
[6] Huang C 2009 Parameterization of the roughness length over the sea in forced and free convection *Environ. Fluid Mech.* **9(**3), 359–366.
[7] Beare R J and Cullen M J P 2019 A Simple Model of a Balanced Boundary Layer Coupled to a Large-Scale Convective Circulation *J. Atmos. Sci.***76(**3) 837–849.
[8] Zhou X, Dong B, Li W, and Chen C 2019 A 3D thermal LB model on non-orthogonal grid and its application for natural convection in irregular domains *Int. J. Heat Mass Transf.* **136** 223–234.
[9] Haditiar Y, Rizal S, and Abdullah F 2017 Current simulation in the Malacca Strait and part of South China Sea due to wind *12th Int. Conf. Math. Stat. Their Appl. ICMSA 2016 Conjunction with 6th Annu. Int. Conf. Syiah Kuala Univ.*pp. 47–50.
[10] Kämpf J 2010 *Advanced Ocean Modelling Using Open Source Software*. Berlin, Heidelberg: Springer Berlin Heidelberg.
[11] Farooq U and Xu H 2014 Free convection nanofluid flow in the stagnation-point region of a three-dimensional body *Sci. World J.*
[12] A. C. M. Beljaars 1995 The parametrization of surface fluxes in large-scale models under free convection *Q. J. R. Meteorol. Soc.* **121** (522) 255–270.

INTERNATIONAL PROCEEDING
The 2nd International Conference on Science and Technology (ICST)
ISBN: 978-602-5830-19-8, June 2020

Box-Jenkins Box-Jenkins Modelling to Forecast Monthly Rainfall in Bengkulu City and Accuracy using MAPE

H Fransiska*, P Novianti, and D Agustina

Dept. of Statistics, University of Bengkulu

*E-mail: hfransiska@unib.ac.id

Abstract. Rainfall in Bengkulu city is very fluctuating and high so knowledge of future monthly rainfall information is important to study. In this research, based on historical data, the monthly rainfall was forecasted by Box-Jenkins model. Monthly rainfall in Bengkulu city since January 2011 to December 2017 were used for modeling and forecasting. Stages of analysis is split data into two, data for modeling dan data for validation, then modeling data were analyzed using Box-Jenkins method. Box-Jenkins procedure contains three main stages to build the best model, that stages is model identification (stationarity test, model identification), model estimation (estimation parameter models) and model checking, it is used for determining the best model for certain time series data then the best model used for forecasting. Based on the analysis results, the best Box-Jenkins model is ARIMA (2,0,2). After obtaining the best model, that it used for forecasting 4 periods and MAPE accuracy is 31,33%.

1. Introduction

Bengkulu is a province with high rainfall and a very moist area. The intensity of rainfall is very large, so it means very dangerous because it has a bad impact on the life activities as can cause floods, landslides that it has a negative effect on various sectors such as agriculture, tourism, and transportation. This makes information about rainfall forecasting in Bengkulu city very important to know. Based on historical data, univariate time series data, forecasting about rainfall in Bengkulu city can used Box-Jenkins modeling approach. The best model is based on AIC and SBC information criteria, while the accuracy of model is based on MAPE values.

The non-stationary time series model for univariate time series data is Autoregressive Integrated Moving Average order (p, d, q) or ARIMA (p, d, q) where p is the order of the autoregressive parameter, d is the quantity stating the differencing process whose become this model is stationary, and q is the order of the moving average parameter. This model has been originated from the Autoregressive model (AR (p)), the Moving Average model (MA(q)) and the combination of the AR(p) and MA(q), the ARMA (p,q) models.

In the case where seasonal components are included in this model, then the model is called the SARIMA (p,d,q)(P,D,Q)^s model [4]. The generalized form of SARIMA (p,d,q)(P,D,Q)^s model can be written as [1] :

$$\phi_p(B)\Phi_P(B^s)(1-B)^d(1-B^S)^D Z_t = \theta_q(B)\Theta_Q(B^s)\alpha_t$$

with

$$\phi_p(B) = 1 - \phi_1 B - \phi_2 B^2 - \cdots - \phi_p B^p$$
$$\Phi_P(B^S) = 1 - \Phi_1 B - \Phi_2 B^2 - \cdots - \Phi_P B^{PS}$$
$$\theta_q(B) = 1 - \theta_1 B - \theta_2 B^2 - \cdots - \theta_q B^q$$
$$\Theta_Q(B^s) = 1 - \Theta_1 B - \Theta_2 B^2 - \cdots - \Theta_Q B^{QS}$$

where Φ and φ = autoregressive (AR) parameters of seasonal and non-seasonal components, respectively; Θ and θ = moving average (MA) parameters of seasonal and non-seasonal components, respectively; B = backward shift operator, d and D = The non-seasonal and seasonal order of differences, respectively; α_t = an independently distributed random variable; P and p = the orders of the AR components; Q and q = the orders of MA components; D and d are difference terms, and usually abbreviated as SARIMA (p,d,q)(P,D,Q)^S [5].

When there is non-seasonal effect, a SARIMA model reduces to pure ARIMA (p,d,q) and when the time series dataset is stationary a pure ARIMA reduces to ARMA(p,q) [4]. The first requirement for ARIMA modeling is that the time series data to be modeled are either stationary or can be transformed into stationary. Therefore, the letter 'I' (Integrated) means that the first order difference is applied in order to stationarize given time series. First order differencing requires that there is a need to find between observations in two successive months. In case that there is a time series with trends, seasonal pattern and short time correlations a Seasonal ARIMA (SARIMA) model can be used. Besides three main components present in ARIMA model, there is a need for seasonal differencing in order to make a seasonal time series stationary [3].

The stages of modeling by the Box-Jenkins method: (1) Model identification. The first step for model identification is the test of the dataset stationarity. For this purpose, graphical methods: sample autocorrelation function (ACF) and sample partial autocorrelation functions (PACF) were used. Moreover, unit root test has been made using Augmented Dickey–Fuller (ADF) at 0.5 significance level (α = 0.05) for mean stationarity [5] and Box-Cox plot for test of variance stationarity. Transform dataset using the Box-Cox transformation method if the dataset nonstationarity in variance and differencing data if the dataset nonstationarity in mean. During model identification, a type (seasonal or non-seasonal) and order (p, q, P, Q) of model parameters were determined on the basis of an ACF plot [5]. (2) Model estimation. Parameter estimation used conditional maximum likelihood called the conditional sum of squares method. Estimating the parameters model used t test or looking at the p-value, we used SAS. (3) Diagnostic checking, The autocorrelation check of residuals was applied to test white noise (autocorrelation) of model. Whether the ACF check of residual values at various lags were settled within tolerance interval at 95% confidence limits was evaluated or p-value > 0.5 significance level (α = 0.05), residuals is white noise. Next, Test of normality residuals used Kolmogorov-smirnov test. Residuals is normal if p-value > 0.5 significance level. If a selected model fails in diagnostic check it is necessary to repeat the whole procedure again. The next steps is overfitting, Overfitting is the one technique that can be used for diagnostic checking is overfitting. Having identified what is believed to be a correct model, we actually fit a more elaborate one. This puts the identified model in jeopardy because the more elaborate model

contains additional parameters covering feared directions of discrepancy. Careful thought should be given to the question of how the model should be augmented [1].

As a final step for modeling, forecast precision was evaluated against performance measures: Akaike information criteria (AIC) and SBC. These information criteria are designed to deal with the fit of the nonlinear models and to account for the number of the parameters in the model as well. They consist of the natural log of the Mean Squared Error (MSE) and a penalty for the number of parameters being estimated [3]. Common procedure often involves estimating the largest model for which it is assumed to correctly capture the dynamics of a time series and then decreasing its size (dropping the lags) until the minimum value of AIC and SBC [3]. Next the best model will be used for forecasting dan calculate the accuracy of forecasting models obtained based on MAPE values.

The best model is a model having the lowest AIC and SBC for dataset forecasting. The formula AIC and SBC is:

$$AIC(M) = n\ ln\ \hat{\sigma}_a^2 + 2M$$
$$SBC(M) = n\ ln\ \hat{\sigma}_a^2 + M \ln n$$

where:

M = Number of parameters in the model
$\hat{\sigma}_a^2$ = Maximum likelihood estimator of σ_a^2
n = Number of observations.

The forecasting accuracy model used *Mean Absolute Percentage Error* (MAPE). This criterion can show how big the forecast error is. The Formula MAPE is [2]:

$$MAPE = \frac{\sum_{t=1}^{n} \left| \frac{Z_t - \hat{Z}_t}{Z_t} \right|}{n} \times 100\%$$

The best forecast is a model having the smallest MAPE.

2. Materials and Methods

The object of this research is Bengkulu City. The variable used is the monthly rainfall in Bengkulu City (Published:Bengkulukota.bps.go.id). The stages of this research include the following activities:

1. Data collection
   In this study, the data to be used is the monthly rainfall in January, 2011-December, 2017. The data source is BMKG Stasiun Klimatologi Kelas I Pulau Bai, published in Bengkulukota.bps.go.id.
2. Data Exploration
   The purpose of data exploration is a general description of the monthly rainfall data in Bengkulu City.
3. Modeling used the Box-Jenkins method
   Building the monthly rainfall model in Bengkulu city used the Box-Jenkins method with procedure: model identification (stationarity test, model identification), model estimation (estimation parameter models) and model checking (model diagnostic checking, overfitting).
4. Selection of the Best Model

From the steps above, if there are several ARIMA models that meet the parameter significance test and meet the residual assumptions (white noise and normality), the best model will be chosen based on the AIC and SBC criteria.

5. Forecasting
   The best model will be used for forecasting 4 periods. Furthermore, its accuracy will be measured using MAPE criteria using data validation and data forecasting.

3. Results and Discussion

The monthly rainfall in Bengkulu City can be seen in Figure 1:

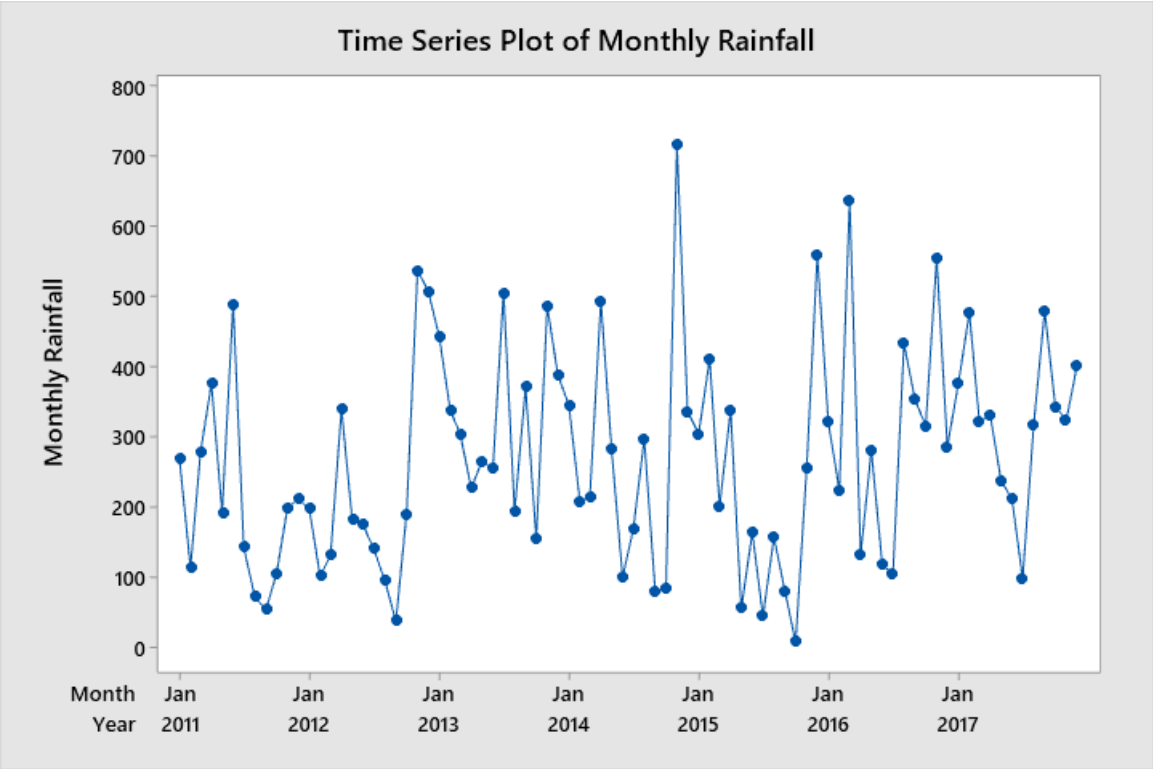

Figure 1. Time series of Monthly Rainfall in Bengkulu city (January, 2011-December, 2017)- Raw Data

If seen the pattern of monthly rainfall in Bengkulu City is very fluctuated every month, and it can be seen that the minimum monthly rainfall in October 2015 was 7 mm and the largest in November 2014 was 717 mm.

3.1. Model Identification

The stationarity test is the first step in modeling with the Box-Jenkins method. The test of stationarity used Box-Cox plot for variance stationarity and ADF test for mean stationarity for modeling data. Box-Cox plot that this data is non stationary in variance so this data has to be transformed. The transformation used "x^2" transformation. This picture is box-cox plot for monthly rainfall data.

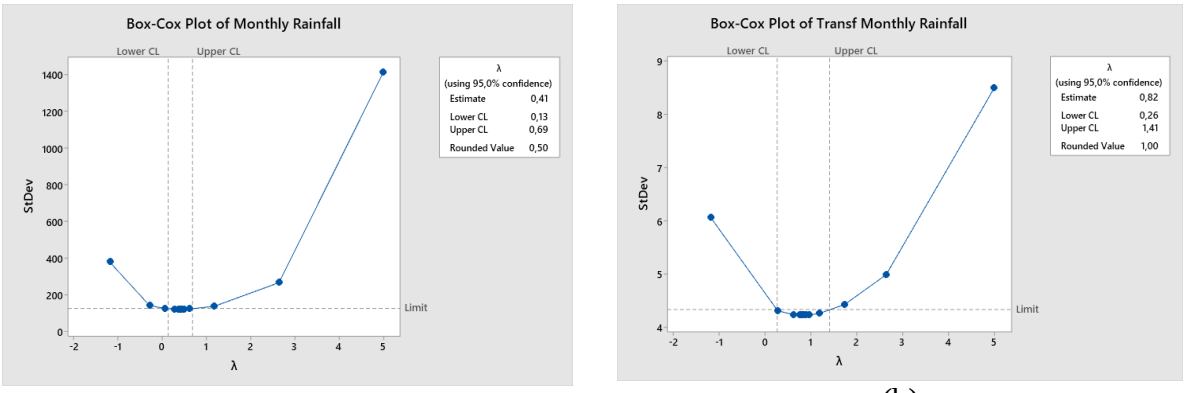

(a) (b)

Figure 2. (a) Box-Cox plot of monthly rainfall (modelling) data and (b) Box-Cox plot of transformation monthly rainfall (modelling) data

After transformation, stationary test again, and it is found that the monthly rainfall dataset stationary in mean. The ACF and PACF plots:

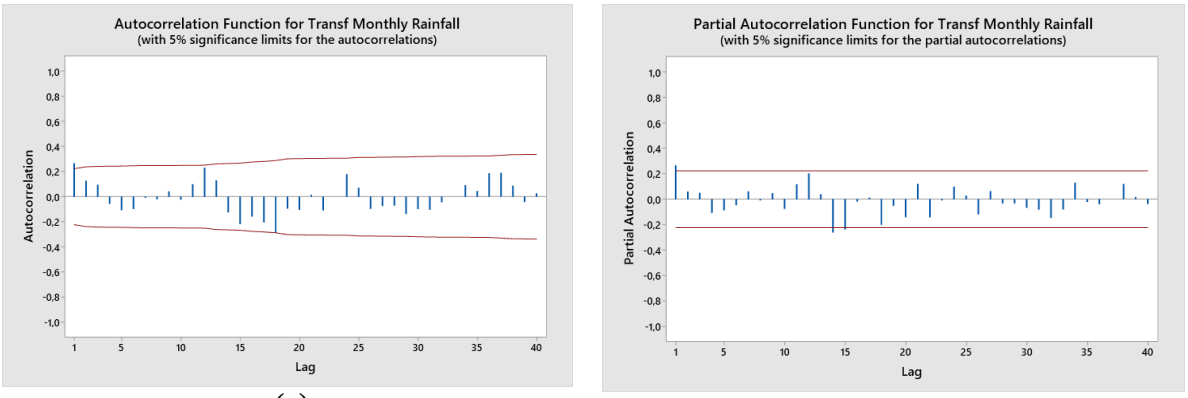

(a) (b)

Figure 2. (a) ACF Plot and (b) PACF plot for Transformation Monthly Rainfall

Based on the ACF plot (Figure 2, a), it can be seen that the non-seasonal was significant in lag-1. Based on the PACF plot (Figure 2,b), it can be seen that lag was significant in lag-1 lag-14, and lag-15. The initial models are ARIMA(1,0,0), ARIMA(0,0,1) and ARIMA(1,0,1) was identified as initial models. The initial model only that because the temporary model must be based on parsimony principle, the model must be as simple as possible. That means the model has few parameters so the model is more stable.

3.2. Parameter Estimation

Next, parameter estimation for all initial models used the conditional sum of squares method, obtained:

Table 1. Final Estimates of Parameters for ARIMA (1,0,0)

Type	Coef	SE Coef	T-Value	P-Value
AR 1	0,267	0,109	2,44	0,017
Constant	11,364	0,534	21,28	0,000
Mean	15,498	0,728		

Based on table 1, ARIMA(1,0,0) significant (alpha 5%).

Table 2. Final Estimates of Parameters for ARIMA (0,0,1)

Type	Coef	SE Coef	T-Value	P-Value
MA 1	-0,241	0,111	-2,18	0,032
Constant	15,500	0,666	23,28	0,000
Mean	15,500	0,666		

Based on table 2, ARIMA(0,0,1) significant (alpha 5%).

Table 3. Final Estimates of Parameters for ARIMA (1,0,1)

Type	Coef	SE Coef	T-Value	P-Value
AR 1	0,466	0,364	1,28	0,205
MA 1	0,214	0,403	0,53	0,596
Constant	8,278	0,421	19,64	0,000
Mean	15,489	0,789		

Based on table 2, ARIMA(1,0,1) not significant (alpha 5%). If this model no include constant term in model, the final estimate of parameter for ARIMA (1,0,1):

Table 4. Final Estimates of Parameters for ARIMA (1,0,1) no include constant term

Type	Coef	SE Coef	T-Value	P-Value
AR 1	0,999965	0,000758	1320,04	0,000
MA 1	0,9812	0,0440	22,32	0,000

Based on Table 1, only two models was significant: ARIMA (1,0,0), ARIMA (0,0,1) and ARIMA (1,0,1) no include constant term..

3.3. Diagnostic checking

From the plots of residual ACF and PACF, all residual values at various lags were settled within tolerance interval at 95% confidence limits. This means each residual is very small relative to its standard error and shows the existence of no significant correlation between residuals. As a result, the residuals obtained from the model are white noise or independent (Tadesse and Dinka, 2017). the next step, the diagnostic model checking (only for significant models).

Table 5. Diagnostic Checking

Model	Residual (White Noise)	Residual (Normal)	Information
ARIMA(1,0,1)	×	√	Bad Model
ARIMA(0,0,1)	×	√	Bad model
ARIMA(1,0,1) no include constant term	√	√	Good model

3.4. Selection of the Best Model

For know the best model, we used outomatic ARIMA Forecasting (Eviews program). The best model is ARIMA(2,0,2) with AIC 24,518.

Table 6. Output outomatic ARIMA Forecasting

Automatic ARIMA Forecasting
Selected dependent variable: (MONTHLY_RAINFALL^2-1)/2
Date: 06/07/20 Time: 18:05
Sample: 1 80
Included observations: 80
Forecast length: 0

Number of estimated ARMA models: 25
Number of non-converged estimations: 0
Selected ARMA model: (2,2)
AIC value: 24.518246969

And The finals estimates of parameters for ARIMA (2,0,2) model is

Table 4. Final Estimates of Parameters for ARIMA (2,0,2) no include constant term

Type	Coef	SE Coef	T-Value	P-Value
AR 1	1,600	0,102	15,66	0,000
AR 2	-0,600	0,102	-5,86	0,000
MA 1	1,22617	0,00007	18685,93	0,000
MA 2	-0,2432	0,0431	-5,64	0,000

3.5. Forecasting

A historical, validation and prediction (forecast) plot for monthly rainfall (time series dataset) using ARIMA (2,0,2) model is shown in Table 7.

Figure 3. Validation data and forecasting for monthly rainfall in Bengkulu City in 4 periods.

Month	Real	Forecast	MAPE
01/09/2017	480	259,7512	0,46
01/10/2017	343	259,6546	0,24
01/11/2017	324	259,7931	0,20
01/12/2017	402	260,0737	0,35
			31,33

The performance of the best ARIMA model was evaluated by comparison of validation data and forecasting data. The accuracy criteria is MAPE 31.33%. It means this model quite valid.

4. Conclusions

In this study, we proposed the best Box-Jenkins model for forecasting monthly rainfall in Bengkulu city if we used univariate time series data. The result of Box-Jenkins modeling indicates that the ARIMA (2,0,2) is the best modeling the monthly rainfall in Bengkulu. This model was selected for monthly rainfall forecasting for its minimum values of AIC, SBC and

MAPE criteria. In addition to its best performance, the pattern of the out of sample forecast monthly rainfall is similar with that of the observed mean monthly rainfall plot. Consequently, the selected model is appropriate for monthly rainfall forecasting. This method can be a decision support tool for government consideration.

Acknowledgements

Thank you, the authors say thank you for the Faculty of Mathematics and Natural Sciences who have helped finance contract number 1845/UN30.12/HK/2018.

References

[1] Box, G.E.P., Jenkins, G.M. and Reinsel, G.C. 2008. *Time Series Analysis. Forecasting and control: Fourth edition*. A John Wiley and Sons, Inc., Publication. Hoboken, New Jersey.

[2] Hillmer, S. C. and Wei, W. W. S. 1991. *Time Series Analysis: Univariate and Multivariate Methods*. *Journal of the American Statistical Association*.Vol. 86, No. 413 pp. 245-246.

[3] Milenković, M. *et al.* 2018. *SARIMA Modelling Approach for Railway Passenger Flow Forecasting. Journal Transport*. Vol 33 No 5.

[4] Suhartono. 2011. *Time Series Forecasting by using Seasonal Autoregressive Integrated Moving Average: Subset, Multiplicative or Additive Model*. *Journal of Mathematics and Statistics*. Vol. 7 pp. 20-27.

[5] Tadesse, K. B. and Dinka, M. O. 2017. *Application of SARIMA Model to Forecasting Monthly Flows in Waterval River, South Africa*. *Journal of Water and Land Development*. Vol 35 pp. 229-236.

INTERNATIONAL PROCEEDING
The 2nd International Conference on Science and Technology (ICST)
ISBN: 978-602-5830-19-8, June 2020

The Application of INGARCH Model for Time Series Count Data in Predicting Monthly Rainy Days (Case study: Rainfall Data of Pulau Baai Climatology Station in Bengkulu City)

P Novianti [1*], D S Rini[1], I Sriliana[1], A Anwar[2]
[1] Department of Statistics, Faculty of Mathematics and Natural Sciences, University of Bengkulu, Indonesia
[2] Pulau Baai Climatology Station, Meteorological Climatological and Geophysical Agency, Bengkulu, Indonesia

*E-mail: pie_novianti@unib.ac.id

Abstract. This study will provide an overview of count time series analysis. The aim of this research is to apply the count time series analysis in predicting the number of monthly rainy days. The data in this study are the number of days of rain in one month based on count data been observed from January 2008 to December 2017. Data are sourced from Pulau Baai Climatology Station, Bengkulu City, Indonesia. The method used in this research is Integer-valued GARCH (INGARCH) model. To measure of fit model is used AIC and BIC. The result of research is the best model to be applied in the modeling of the number of monthly rainy days is INGARCH(1,11) model.

1. Introduction

Time series data is data with a variable collected based on time. This data can be used to predict or forecast future events using time series analysis. Time series analysis such as AR, MA, ARIMA, ARCH, and GARCH are widely applied in time series modeling. However these models are suitable for continuous data. In fact, discrete-valued time series can be found in many cases, usually as counting result of events or objects.

Modelling time series of count data problems have attracted considerable attention of many researchers in recent decade. Some modeling time series of counts have built, for example, INAR model [1&2], INGARCH [3], GLARMA [4], and GINAR. These models should have the assumption that the observations are nonnegative integers and they should capture suitably the dependence among observations.

INGARCH (integer-valued generalized autoregressive conditional heteroscedastic) model proposed by Ferland et al. is useful model to solve count time series data. This approach adopts the method of the classical GARCH Model. Under the Poisson distribution, Heinen (2003) have constructed an autoregressive conditional Poisson model for count time series analysis. Both of these methods can only deal with overdispersion in time series of counts [5].

Some progress in INGARCH model have done and reviewed in many papers. Fokianos (2010) proposed intervention in INGARCH process. For solving underdispersion problem, some methods are introduced [6]. Zhu (2011) proposed a negative INGARCH (p,q) model that can deal with

overdispersion and potential extreme observations simultaneously [7]. Zhu (2012) presented count time series model with COM-Poisson INGARCH models [8&9].

Rainfall is one of the elements in climate and weather that is closely related to time. Rainfall history from time to time is also a time series data. The amounts of daily, weekly and monthly rainfall are forms of continuous time series data, while if the data collected are in the form of a number of rainy days in one week, one month or year, then the data can be classified as count time series data. By using a count time series analysis approach, the researcher will apply INGARCH model to predict the rainfall forecasting model and use the AIC and BIC information criteria to determine the best prediction model of the number monthly rainy day in Bengkulu.

2. Materials and Methods

2.1. Mechanism of data collecting and processing

The data used in this study are the number of rainy days in one month. Time series data in the form of count data were observed from January 2008 to December 2017. Data are sourced from Pulau Baai Climatology Station, Bengkulu City, Indonesia.

The steps of research carried out in applying this INGARCH model are:

1. Collecting data
2. Describing data statistics
3. Hypothesis testing of stationarity.
4. Modeling data in the form of INGARCH models
5. Choosing the best INGARCH model based on AIC and BIC

2.2. INGARCH model

The most comment INGARCH model is Poisson INGARCH model. This model is assumed to come from Poisson distribution. A Poisson INGARCH(p,q) model is defined to count time series data $\{X_t\}_{t\in Z}$ as follows:

$$\begin{cases} X_t|F_{t-1}\sim Poisson(\lambda_t); \forall t \in Z \\ \lambda_t = \gamma_0 + \sum_{i=1}^{q}\gamma_i X_{t-i} + \sum_{j=1}^{p}\delta_j\lambda_{t-j} \end{cases} \quad (1)$$

Where $\gamma_0 > 0, \gamma_i \geq 0, \delta_j \geq 0, i = 1,2,\dots,q, j = 1,2,\dots,p, p \geq 1, q \geq 1$ [3].

A Poisson INGARCH(p,q) model has the conditional mean that is equal to the conditional variance. Both of these features depend on the past values of the series as well as on its own past values. INGARCH model useful for count data imitate the classical GARCH model which is suitable for continuous data.

Poisson distribution in equation (1) has mean defined as follows:

$$\mu = \frac{\gamma_0}{\sum_{j=1}^{p}\delta_j + \sum_{i=1}^{q}\gamma_i}$$

Consequently, the parameters γ_i and δ_j, $i = 1,2,\dots,q$, $j = 1,2,\dots,p$ of the non-negative integer-valued process $\{X_t\}_{t\in Z}$ satisfy the necessarily the condition $\sum_{j=1}^{p}\delta_j + \sum_{i=1}^{q}\gamma_i < 0$.

For simplicity, the focus INGARCH model is in the special INGARCH (1,1) model. INGARCH (1,1) model has identical covariance structure as the ARMA(1,1) model. The equation (1) for INGARCH (1,1) can be written:

$$\begin{cases} X_t|F_{t-1}\sim Poisson(\lambda_t); \forall t \in Z \\ \lambda_t = \gamma_0 + \gamma_1 X_{t-1} + \delta_1\lambda_{t-1} \end{cases} \quad (2)$$

In this model, the parameters will be assumed that $\gamma_1 + \delta_1 < 1$.

The expected value, variance and autocovariance function of the INGARCH(1,1) model are given by

$$\mu = \frac{\gamma_0}{1-(\gamma_1+\delta_1)}$$
$$Var = \frac{\mu(1-(\gamma_1+\delta_1)^2+\gamma_1^2)}{1-(\gamma_1+\delta_1)^2}$$
$$\gamma(r) = \frac{\gamma_1\big(1-\delta_1(\gamma_1+\delta_1)\big)(\gamma_1+\delta_1)^{r-1}\mu}{1-(\gamma_1+\delta_1)^2}, \forall r \geq 1$$

2.3. Parameter Estimation

The estimation procedure of INGARCH (1,1) model parameters is using maximum likelihood estimation. The conditional likelihood function of the observed data $X_1, \dots, X_n$ conditionally on the pre-sample values, is given by

$$L(\Theta) = \prod_{t=1}^{n} \frac{e^{-\lambda_t}\lambda_t^{X_t}}{X_t!}$$

Where

$$\Theta = \big(\gamma_0, \gamma_1, \dots, \gamma_q, \delta_0, \delta_1, \dots, \delta_p\big)' = \big(\theta_0, \dots, \theta_{p+q}\big)'$$

$\boldsymbol{\Theta}$ is the vector of unknown parameters and the estimations cannot be found analytically by the likelihood function. However, to result the optimal value of $\boldsymbol{\Theta}$ can be solved by numerical optimization methods. Therefore, likelihood function can be transformed to log-likelihood function:

$$\ln L(\Theta) = \sum_{t=1}^{n} [X_t \ln \lambda_t - \lambda_t - \ln(X_t!)] = \sum_{t=1}^{n} l_t(\Theta)$$

By neglecting the term $\ln(X_t!)$ in $l_t(\Theta)$, it can be derived the first derivatives of $l_t(\Theta)$ with respect to $\theta_i = 0,1, \dots, p+q$ as follow:

$$\frac{\partial l_t}{\partial \theta_i} = \left(\frac{\partial \lambda_t}{\partial \theta_i}\right)\left(\frac{X_t}{\lambda_t} - 1\right)$$

and the second derivatives:

$$\frac{\partial^2 l_t}{\partial \theta_i \partial \theta_j} = \left(\frac{\partial^2 \lambda_t}{\partial \theta_i \partial \theta_j}\right)\left(\frac{X_t}{\lambda_t} - 1\right) - \frac{X_t}{\lambda_t^2}\frac{\partial \lambda_t}{\partial \theta_i}\frac{\partial \lambda_t}{\partial \theta_j}$$

For $0 \leq i, j \leq p+q$. Moreover it can result

$$\lambda_t = \gamma_0 + \sum_{i=1}^{q} \gamma_i X_{t-i} + \sum_{j=1}^{p} \delta_j \lambda_{t-j};$$
$$\frac{\partial \lambda_t}{\partial \gamma_0} = 1 + \sum_{j=1}^{p} \delta_j \frac{\partial \lambda_{t-j}}{\partial \gamma_0}$$
$$\frac{\partial \lambda_t}{\partial \gamma_i} = X_{t-i} + \sum_{j=1}^{p} \delta_j \frac{\partial \lambda_{t-j}}{\partial \gamma_i}, i = 1,2, \dots, q;$$
$$\frac{\partial \lambda_t}{\partial \delta_i} = \lambda_{t-i} + \sum_{k=1}^{p} \delta_k \frac{\partial \lambda_{t-j}}{\partial \delta_i}, j = 1,2, \dots, p;$$

2.4. Model Selection

In determining a forecasting model, an evaluation of the model is carried out. A method of evaluating forecasting models that can be used is information criteria. The information criterion is a criterion for assessing the quality of the model using a statistical model of a parameter. Akaike Information Criteria (AIC) and Bayesian Information Criteria (BIC) are included in the information criteria. The model with the lowest value of the respective information criterion is preferable.

Assume that the statistical parameter model M is used in the data. Akaike Information Criticism (AIC) is defined as:

$$AIC = -2\log L(\theta) + 2M$$

Akaike (1973) in [10] has developed an extension of the minimum Bayesian AIC procedure, which is called the Bayes (BIC) information criterion, which takes from

$$BIC = -2\log L(\theta) + \log L(n)\, M$$

3. Results and Discussion

This study consists of the number of monthly rainy days recorded in Pulau Baai climatology station Bengkulu. Using the R program package, the distribution of data frequency and the statistics are presented in the following figure and table:

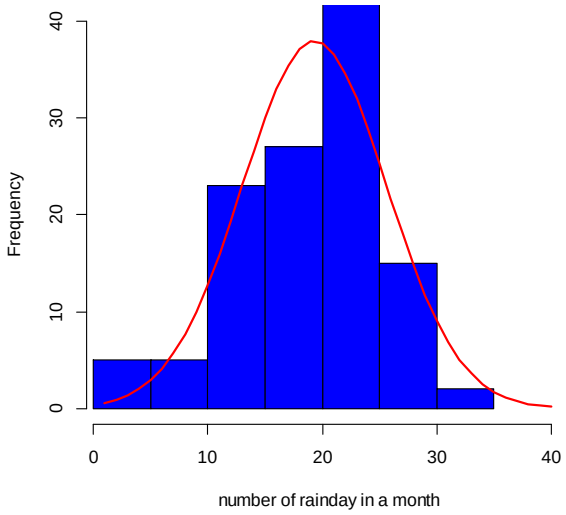

Figure 1. Histogram of the number of Monthly Rainy Days in Pulau Baai Climatology Station, Bengkulu

Table 1. Statistics of the number of monthly rainy days in Pulau Baai climatology station, Bengkulu.

Statistic	Values
N	120
Minimum	1
Maximum	31
Mean	19.32
Standard Deviation	6.31
Skewness	-0.5589
Kurtosis	3,02

Table 1 describes the statistics of the number of rainy days in one month from January 2008 to December 2017 in Pulau Baai Climatology Station, Bengkulu City. The total of data is 120 months. The table shows that the minimum rain day in one month is 3 days and the maximum value is 31 days indicating that in one month there is rain every day. The average rainy day is 19.32 days with a standard deviation of 6.19 days. It means that Kota Bengkulu has relatively high rainfall intensity. The distribution of the time series data can be displayed as follow:

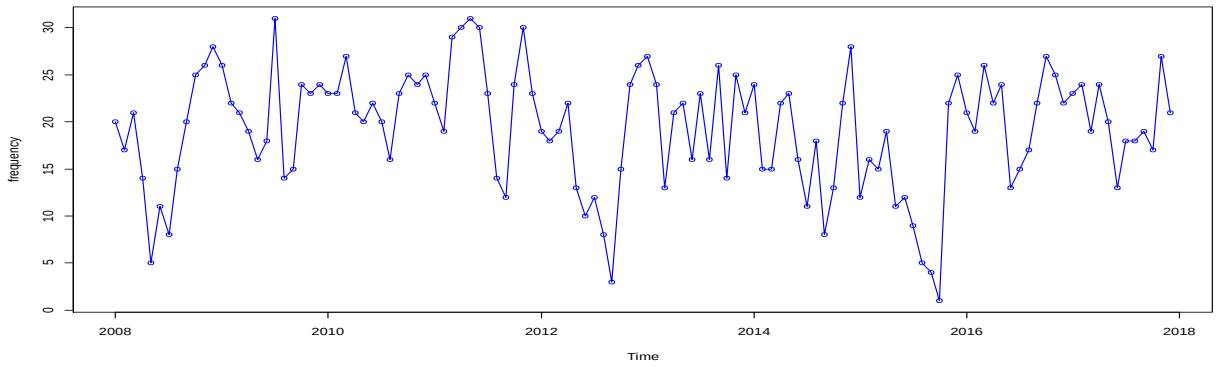

Figure 2. Number of monthly rainy days from January 2008 to the end of December 2017

Figure 2 depicts the time series of the number of monthly rainy days in Bengkulu from year 2008 to 2017. This picture represents constant moving data around the average, meaning that it does not rise continuously or does not go down continuously. Therefore, it can be assumed that the monthly rainy day around the Pulau Baai Climatology Station in that period is stationary. To further ensure this assumption, stationary test will be conducted using ACF and PACF plots as well as dickey fuller test.

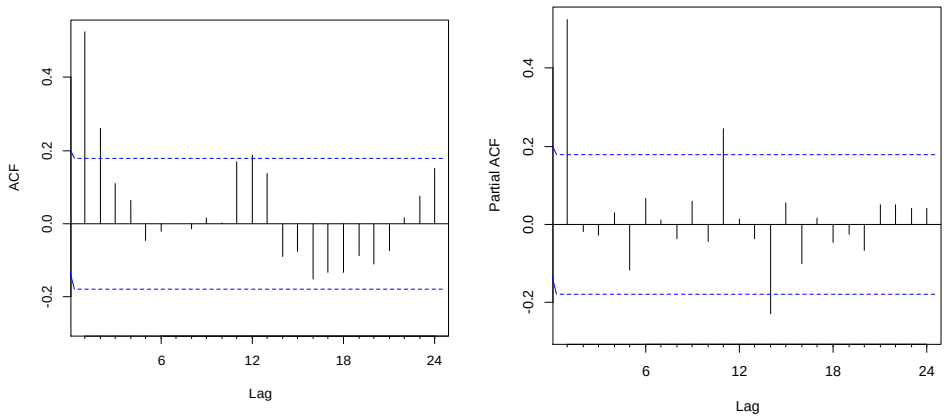

(a) (b)

Figure 3. ACF and PACF of the number of monthly rainy days

In the correlogram method, to see the stationary or not data, it can be seen through the Partial Autocorrelation Function (PACF) value and the autocorrelation function (ACF) value. The series is said to be stationary if the value is close to zero at time lag 2 or time lag 3. Displayed in Figure 3 the ACF value at lag 2 and lag 3 goes to zero and is worth below 0 in lag 5, while on PACF, the value is below zero in lag 2. Stationary testing based on the ADF unit root test also states that at level 95% the data has been stationary, evidenced by the ADF static value (-5.8435) and p-value <5%. In conclusion, the ADF unit root test supports the conclusion that data is stationary.

Regarding to ACF and PACF graphs in figure 3, six INGARCH models are chosen. Those are INGARCH(1,1), INGARCH (1,11), INGARCH(1,12), INGARCH(2,1), INGARCH(2,11) and

INGARCH (2,12). The next step is choosing the best time series model. Model selection assessments are using the smallest AIC and BIC value criteria presented in Table 2.

Table 2. Parameter values and criterion values of the chosen models

Model	γ_0	γ_i	δ_j	AIC	BIC
INGARCH(1,1)	8.89	0.538	1.76×10^{-9}	751.991	760.1996
INGARCH(1,11)	4.20	0.53	0.25	747.2402 *	755.4488*
INGARCH(1,12)	8.6456	0.5336	0.0167	751.9604	760. 169
INGARCH(2,1)	0.141	0.268	$3.19\ x\ 10^{-6}$	808.2722	816.4808
INGARCH(2,11)	2.740	0.261	0.596	801.4052	809.6138
INGARCH (2,12)	0.142	0.26	$7.71\ x\ 10^{-10}$	808.2585	816.4671

*) the smallest value

From Table 2, for the number of monthly rainy days, the INGARCH(1,11) model results the smallest AIC and BIC value, 747.2402 and 755.4488 respectively. As shown in Table 2, INGARCH(1,11) is selected for best model of the number of monthly rainy days. Accordingly, the fitted model for the number of rainy days in month t is given by:

$$\lambda_t = 4.20 + 0.53X_{t-1} + 0.25\lambda_{t-1}$$

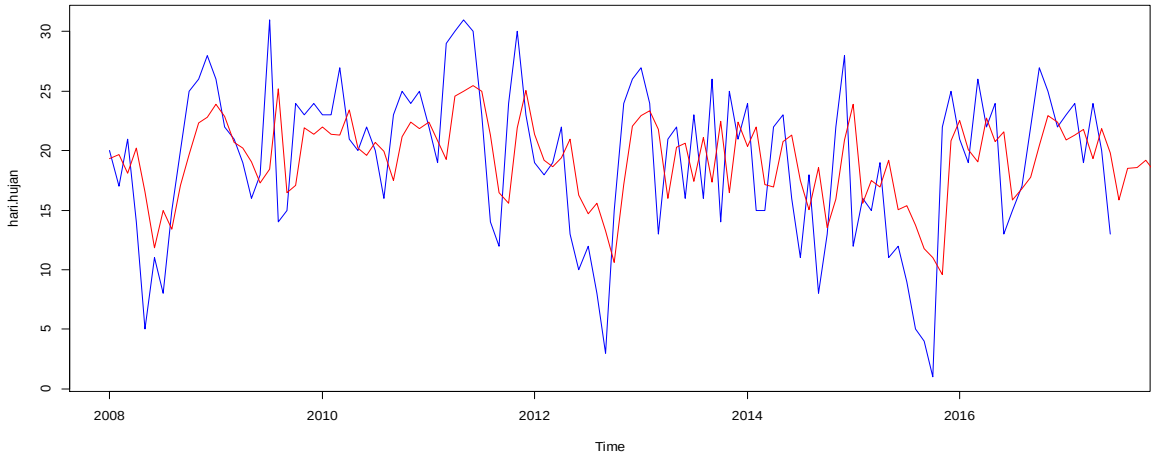

Figure 4. Fitted Values (blue) and predicted values (red) According to the INGARCH(1,11) Model

4. Conclusion

From the results and discussion concluded that the best model that can be used is INGARCH(1,11) model. The parameters are estimated by the maximum likelihood estimation method and yield the results $\gamma_0 = 4.20$, $\gamma_1 = 0.53$ and $\delta_j = 0.25$. For the next research, INGARCH with others conditional distribution, such as Negative Binomial, Generalized Poisson, and Double Poisson can be performed and compared with Poisson INGARCH model. Furthermore, count time series approach like INAR, GLARMA and GINAR can be applied to build the number of monthly rainy days model.

Acknowledgement
This work was supported by Research Projects ***Penelitian Pembinaan***, University of Bengkulu and Ministry of Research, Technology, and Higher Education of Republic Indonesia.

References

[1] Al-Osh M and Alzaid A 1987 First-order integer-valued autoregressive (INAR(1)) process *Journal of Time Series Analysis* Vol 8: 261-275
[2] Al-zaid A, and Al-Osh M 1988 First-order integer-valued autoregressive (INAR(1)) process: distributional and regression properties *Statistica Neerlandica* Vol. 42: 53-61
[3] Ferland R A, Latour A, and Oraichi D 2006 Integer-valued GARCH Process *Journal of Time Series Analysis* Vol 27 (6): 923-942
[4] Davis R, Dunsmuir W, and Streett S 2003 Observation-Driven Models for Poisson Counts *Biometrika*, Vol 90(4): 777–790
[5] Heinen A 2003 Modeling time series count data: an autoregressive conditional Poisson model *CORE Discussion paper* 2003/62, Université catholique de Louvain
[6] Fokianos K, and Fried R 2010 Interventions in INGARCH processes, *Journal of Time Series Analysis* Vol 31: 210–225
[7] Zhu F, 2011 A negative binomial integer-valued GARCH model *Journal of Time series analysis* Vol 32: 54-67
[8] Zhu F, 2012 Modeling overdispersed or underdispersed count data with generalized Poisson integer-valued GARCH models *Journal of Mathematical Analysis and Applications* Vol 389: 58-71
[9] Zhu F, 2012 Modelling Time Series of counts with COM-Poisson INGARCH models *Mathematical and Computer Modelling* Vol 56: 191-203
[10] Agustini R, Hajarisman N, Sunendiari S, 2018 Kriteria Pemilihan Model Peramalan Terbaik Berdasarkan Kriteria Informasi *Prosiding Statistika* Vol. 4(1): 57-65

INTERNATIONAL PROCEEDING
The 2nd International Conference on Science and Technology (ICST)
ISBN: 978-602-5830-19-8, June 2020

The Pricing of Premium of Endowment Insurance under Stochastic Interest Rate Vasicek with Weibull Mortality Laws

S Yosmar*, P Nurhidayah, and F Faisal

Department of Mathematics, Bengkulu University, Indonesia

*E-mail: siskayosmar@unib.ac.id

Abstract. Life insurance could minimize the risk of financial loss of someone caused by the death of family members. Insurances have an agreement called with a policy which organizes the amount of insurance premium. Determining of a net single premium for endowment insurance using Weibull mortality law and interest rate counts using the stochastic interest rate of Vasicek Models. The result is the pricing of premium under Vasicek interest rate with Weibull mortality law cheaper than constant interest rates.

1. Introduction

Human life is an asset that can bring income. This asset faces risks such as death, illness and disability caused by accidents. One way to manage risk is to transfer risk to an insurance company. According to RI Law No. 40 of 2014 explained that insurance is an agreement between two parties, the insurer and the insured whereby insurer binding to someone, by receiving a premium as a form of reimbursement due to loss, damage, defect which may be experienced as an event that is not certain in the future.

There are several types of insurance offered, among others: life insurance, health, vehicle, property, education, business and so on. Life insurance is an insurance service that is used as a form of protection against financial losses due to the death of family members who intended as a form of anticipation for families left behind Life insurance can be divided into two traditional and unit-linked insurance. Traditional insurance consists of term insurance, pure endowment insurance, and endowment insurance [1].

Each insurer has an agreement in the form of a policy where the policyholder can choose the payment method either single premium or periodic premium. This research used premium single premium payment is made once at the beginning of all the insurance policies. Basically premiums are influenced by three factors: mortality factors, interest rates, and fees. Premium pays attention to the third factor called gross premiums whereas premiums are only concerned with mortality and interest rate factor called net premiums. This research used net single premium.

Mortality is a person's chances of a certain age that will die in a given period of time. Usually the value of mortality can be seen in mortality tables but in this research developed with Weibull distribution. Another thing that affects the amount of the premium is the interest rate, the usual premium calculation using deterministic interest rate. This research used a stochastic interest rate Vasicek models. Based on previous studies, researchers developed a life insurance premium calculation using a stochastic interest rate Vasicek model which the person's life chances values calculated using the Weibull distribution.

2. Literature review

2.1. Survival function

Survival functions are defined by $s(x)$ which is often used to determine the chance that someone aged x will live or die at an interval of time.

$$F_X(x) = P(X \le x) \qquad x \ge 0 \tag{1}$$

in general, the life insurance function of life insurance can be stated with

$$\begin{aligned} s(x) &= P(X > x) \qquad x \ge 0 \\ &= 1 - F_X(x) \end{aligned} \tag{2}$$

2.2. Lifetime opportunity

Probability distribution function the rest of life is stated as follows: $F_{T(x)}(t)$

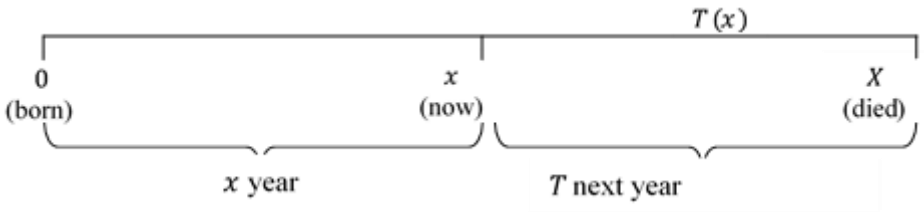

Figure 1 Residual lifetime opportunity

$$F_{T(x)}(t) = (P(T(x) \le t) \tag{3}$$

${}_tq_x$ states as an opportunity for someone who is x years old to die in the next year or dies until the age $(x + t)$ of the year

$${}_tq_x = 1 - \frac{s(x+t)}{s(x)} \tag{4}$$

${}_tp_x$ which states the aged person's x year will live up to t year again or will live to age $(x + t)$ year,

$${}_tp_x = \frac{s(x+t)}{s(x)} \tag{5}$$

2.3. Force of mortality

Equation of density function of distribution of the rest of life probability that used for the calculation of the premium, which can generally be expressed as:

$$f_{T(x)}(x) = {}_tp_x \mu(x+t) \tag{6}$$

where

${}_tp_x$ = probability of someone aged x years will live to $(x + t)$ years.

$\mu(x+t)$ = force of mortality someone at the age of $(x + t)$ years.

2.4. Weibull distribution

Weibull distribution was introduced by a Swedish physicist in 1939. Waloddi Weibull density function of the Weibull distribution probability :

$$f(x;\theta,\beta)=\begin{cases}\dfrac{\beta}{\theta^{\beta}}x^{\beta-1}e^{-\left(\frac{x}{\theta}\right)^{\beta}}, & x\geq 0\\ 0 \quad , \quad x \quad others\end{cases} \tag{7}$$

Cumulative distribution function :

$$F(x;\theta,\beta)=\begin{cases}1-e^{-\left(\frac{x}{\theta}\right)^{\beta}}, & x\geq 0\\ 0 \quad , \quad x \quad others\end{cases} \tag{8}$$

2.5. Mortality Weibull **[2]**

Survival function for the Weibull distribution $s(x)$

$$\begin{aligned} s(x) &= 1-F_X(x)\\ s(x) &= \exp\left[-\left(\frac{x}{\theta}\right)^{\beta}\right] \end{aligned} \tag{9}$$

Mortality rate equation for the Weibull distribution

$$\mu(x) = \frac{\beta(x)^{\beta-1}}{\theta^{\beta}} \tag{10}$$

$$\mu(x+s) = \frac{\beta(x+s)^{\alpha-1}}{\theta^{\beta}} \quad k>0 \tag{11}$$

Life probability ${}_tp_x$ the Weibull distribution

$${}_tp_x = \exp\left[-\left(\frac{(x+t)^{\beta}-x^{\beta}}{\theta^{\beta}}\right)\right] \tag{12}$$

*2.6. Integral Ito***[3]**

Stochastic integral theory was first introduced by the Japanese mathematician Kiyoshi Ito in 1946. The stochastic integral theory arose because the Riemann integral can not be used in defining the stochastic integral function. The following is Ito equation.

$$dY_t = \frac{\partial f}{\partial t}(t,X_t)dt+\frac{\partial f}{\partial x}(t,X_t)dX_t+\frac{1}{2}\frac{\partial^2 f}{\partial x^2}(t,X_t)\cdot(dX_t)^2 \tag{13}$$

2.7. The rate of interest **[4]**

δ referred to as the acceleration rate (force of interest).

$$\delta = \lim_{k\to\infty} i^{(k)} \qquad = \ln(1+i) \tag{14}$$

Using these equations when multiplied by an exponential function to both sides of the obtained

$$v = e^{-\delta} \tag{15}$$

2.8. Vasicek interest rate

Vasicek is a stochastic model of the earliest of short-term interest rates. The Vasicek interest rate model is a model that predicts the movements of the interest rate for the next time to see previous interest rate. The following differential equation model of Vasicek:

$$dx_t = \alpha(\theta - x_t)dt + \sigma dW_t \tag{16}$$

2.9. Endowments

Endowment insurance is the combination of a term life insurance with a pure endowment,

$$\overline{A}_{x:\overline{n}|} = \int_0^n e^{-\delta t}\, {}_t p_x \mu\,(x+t)dt + \int_n^\infty e^{-\delta t}\, {}_t p_x \mu(x+t)dt \tag{17}$$

3. Results and discussions

3.1. Vasicek Interest Rate Model

Vasicek interest rate on time *t* symbolized by x_t, based on **[5]** the x_t equation is given as follows:

$$x_t = \theta(1-e^{-\alpha(t-s)}) + x_s e^{-\alpha(t-s)} + \sigma e^{-\alpha t}\int_s^t e^{\alpha u} dW_u \tag{18}$$

Parameter estimation for $\alpha, \theta,$ dan σ in equation (19) is done by searching $\theta, b,$ and δ which has been assumed and further estimate using OLS (Ordinary Least Square).

$$\hat{\theta} = \frac{\sum_{i=1}^{n}\left[x_i - \hat{b}x_{i-1}\right]}{n(1-\hat{b})} \tag{19}$$

$$\hat{b} = \frac{n\sum_{i=1}^{n} x_i x_{i-1} - \sum_{i=1}^{n} x_i \sum_{i=1}^{n} x_{i-1}}{n\sum_{i=1}^{n} x_{i-1}^{\,2} - \left(\sum_{i=1}^{n} x_{i-1}\right)^2} \tag{20}$$

$$\hat{\delta}^2 = \frac{1}{n}\sum_{i=1}^{n}\left[x_i - \hat{b}\,x_{i-1} - \hat{\theta}\left(1-\hat{b}\right)\right]^2 \tag{21}$$

$$\alpha = \frac{-\ln(b)}{\Delta t} \tag{22}$$

$$\sigma = \frac{\delta}{\sqrt{\frac{\left(b^2-1\right)\Delta t}{2\ln(b)}}} \tag{23}$$

3.2. Single Premium of Endowment Insurance Under Vasicek Interest Rate with Weibull Mortality

A single premium of endowment insurance under Vasicek interest rate with Weibull mortality obtained by substituting equation Mortality Weibull and Vasicek interest rate on endowment insurance.

$$\overline{A}_{x:\overline{n}|Vasicek} = \int_0^n e^{-\left[\ln(1+(\theta(1-e^{-\alpha(t-s)})+x_s e^{-\alpha(t-s)}+\sigma e^{-\alpha t}\int_s^t e^{\alpha u}dW_u))t\right]} e^{\left[-\left(\frac{(x+t)^\beta - x^\beta}{\vartheta^\beta}\right)\right]}\left(\frac{\beta(x+t)^{\beta-1}}{\vartheta^\beta}\right)dt$$

$$+e^{-\left[\ln(1+(\theta(1-e^{-\alpha(t-s)})+x_s e^{-\alpha(t-s)}+\sigma e^{-\alpha t}\int_s^t e^{\alpha u}dW_u))t\right]} e^{\left[-\left(\frac{(x+t)^\beta - x^\beta}{\vartheta^\beta}\right)\right]} \quad (24)$$

3.3. Example of application

In January 2016, a 30-year-old Mr. Damar interested in following the life insurance program with benefits Rp 100.000.000. The interest rate used is the interest rate refers to the interest rate of the Central Bank of the Republic of Indonesia (BI rate) with the last interest rate at 7.25% in January 2016.

3.4. Calculation of Single Premium of Endowment Insurance Under Vasicek Interest Rate with Weibull Mortality

In this issue, it is known that Mr. Damar's age ($x = 30$), Vasicek interest rate is 7.7354179%. Furthermore, the interest rate can be searched single premium of endowment insurance under Vasicek interest rate with Weibull mortality. Based on previous research that has been done by **[6]** using a nonlinear least square method is obtained parameter Weibull distribution is $\beta = 7.151$ and $\theta = 80.096$ here is the calculation of premiums of endowment insurance under Vasicek interest rate with Weibull mortality:

Table 1. Calculation of Single Premium of Endowment Insurance Under Vasicek Interest Rate with Weibull Mortality

Time period (year)	Single Premiums of Endowment Insurance (Rupiah)
10	46,229,819
15	31,563,073
20	21,714,237
25	15,166,529
30	10,884,777
35	8,156,982
40	6,487,126
45	5,523,671
50	5,013,521
60	4,679,942
70	4,643,649
80	4,642,548

3.5. Calculation of Single Premium Endowment Insurance Weibull Mortality with Interest Rate Constant

In this issue, it is known that Mr. Damar's age ($x = 30$), constant interest rate refers to the interest rate of the BI rate in January 2016 amounted to 7.25%. Furthermore, it can be sought single premium of endowment insurance with Weibull Mortality and constant interest rate

$$\begin{aligned}\delta &= \ln(1+x_t)\\ &= \ln(1+0.0725)\\ &= 0.069992\end{aligned}$$

Table 2. Calculation of Single Premium of Endowment Insurance with Weibull Mortality and interest rate constant

Time period (year)	Single Premiums of Endowment Insurance (Rupiah)
10	49,756,590
15	35,236,168
20	25,135,764
25	18,192,039
30	13,511,029
35	10,452,188
40	8,546,363
45	7,439,719
50	6,858,979
60	6,495,222
70	6,460,586
80	6,459,746

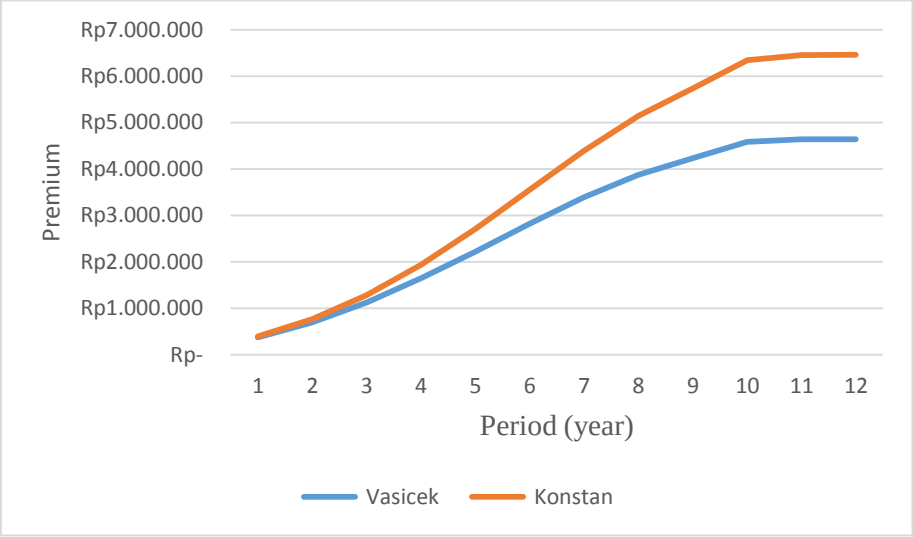

Figure 1. Calculation of single premium endowment insurance with Weibull Mortality between Vasicek interest rate and interest rate constant

According to the table and figure above shows that the single premium of endowment insurance with Weibull Mortality and Vasicek interest rates tend to be lower than the interest rate constant. Figure 1 show how changes in premiums following the stochastic interest rate movements. Single premium using Vasicek interest rates tend to go down, this happens because there is a stochastic element in the calculation so that the movement of single premiums following the movement of interest rates.

4. Conclusion

Based on the results and discussion of the research that has been done, then the conclusion can be drawn:

1. Single premium endowment life insurance using Weibull Mortality law and Vasicek interest rate

$$\overline{A}_{x:\overline{n}|Vasicek} = \int_0^n e^{-\left[\ln(1+(\theta(1-e^{-\alpha(t-s)})+x_s e^{-\alpha(t-s)}+\sigma e^{-\alpha t}\int_s^t e^{\alpha u}dW_u))t\right]} e^{\left[-\left(\frac{(x+t)^\beta - x^\beta}{\vartheta^\beta}\right)\right]}\left(\frac{\beta(x+t)^{\beta-1}}{\vartheta^\beta}\right)dt$$

$$+e^{-\left[\ln(1+(\theta(1-e^{-\alpha(t-s)})+x_s e^{-\alpha(t-s)}+\sigma e^{-\alpha t}\int_s^t e^{\alpha u}dW_u))t\right]} e^{\left[-\left(\frac{(x+t)^\beta - x^\beta}{\vartheta^\beta}\right)\right]}$$

2. Calculation of single premium life insurance using Weibull Mortality law and Vasicek interest rate will change, because the calculations are stochastic elements that premium rate changes with changes in interest rates.
3. Single premium insurance using Weibull Mortality law and Vasicek interest rates tend to be cheaper than using a constant interest rate

References

[1] Bowers N L, Geerber H U, Hickman J C, Jones D A, & Nesbitt 1997 *Actuarial Mathematics* Second Ed, Illinois: The Society of Actuaria

[2] Hoppa R D and Vaupel, J W 2002 *Paleodemography* Cambridge University Press New York

[3] Oksendal B 2003 *Stochastic Differential Equations* Spinger Germany.

[4] Kellison S G 2009 *The Theory of Interest* Third Edition McGraw-Hill America.

[5] Brigo et al. 2007 A Stochastic Processes Toolkit for Risk Management, *Journal of Risk Management*. JLE G32, C13, C15, C16., AMS 60H10, 60J60, 60J75, 65C05, 65c20, 91B70. Accessed on 13 january 2018 https://arxiv.org/pdf/0812.4210.pdf

[6] Hardiyanti, N P U 2015 Penentuan Premi Asuransi Jiwa Berjangka berdasarkan Life Tabel Amerika Serikat dan Hukum mortalita yang berdistribusi Gompertz dan Weibull, Skripsi, Fakultas Matematika dan Ilmu Pengetahuan Alam Universitas Lampung, Bandar Lampung. Accessed on 24 February 2018 http://repository.unila.ac.id

INTERNATIONAL PROCEEDING
The 2nd International Conference on Science and Technology (ICST)
ISBN: 978-602-5830-19-8, June 2020

The Valuing Employee Stock Options (ESO) Under Dilution Effect by Using Trinomial Multilevel Monte Carlo

Suherman*, H Maulana, and Jazwinarti
Mathematics Department, Faculty of Mathematics and Natural Sciences
Universitas Negeri Padang

*E-mail: suherman@fipa.unp.ac.id

Abstract: Employee Stock Option (ESO) is a type of call options which granted to employees of a company for free as a form of compensation to its employees. ESO entitles employees to buy shares of the company within a period of time and a certain vesting period. ESO has a difference with the usual options traded, so this is what distinguishes it calculated from the other types of options. In this paper will be used the CRR binomial method (Cox-Ross-Rubinstein) in calculating the fair value of ESO, which applied in several models, which are popular models and the new model. The models are SFAS 123 (R) model, and the Hull-White model, as well as new models that dilution model where in this model has taken into account the dilution effect. The dilution effect will be reflected right after the exercise, which decreases the outstanding stock price. Then the results of this model will be compared with the SFAS 123 (R) model, and the Hull-White model. At the end of this paper, it will also be shown the influence of several specific parameters to the ESO's value. The observed parameters are volatility parameter, interest rate, dividends, and employee's forfeiture rate.

1. Preliminary

Option is a form of financial derivative in the form of an agreement between two parties, namely the party that issues the option (writer) with the option buyer (holder), where a holder is given the right (not obligation) to buy or sell an asset to the writer at a certain price (strike price) and the specified maturity time. Based on the rights held by option owners, the options are divided into two types of options, both options are: Call option is an option that gives the right (not obligation) to the holder to buy an asset from the writer at a certain price (strike price, exercise price) and at a specified time (expiry date, maturity time). Put option is an option that gives the right (not obligation) to the holder to sell an asset to the writer at a certain price (strike price/exercise price) and at a specified time (expiry date/maturity time). Payoff of an option at maturity is:

$Call = C = Max\{S(T) - K, 0\}$
and
$Put = P = Max\{K - S(T), 0\}$

where T represents the maturity time, S (T) is the stock price at maturity, K is the strike price, C is the call option, and P is the put option [4].

One form of option commonly used is Employee Stock Options (ESO). Employee stock options are a type of call option that is different from options that can be traded in the option market, where this option is given free by a company (writer) to a certain group of employees in the company as a form of incentive. ESO is one form of incentives given by companies in addition to salaries, bonuses, benefits, insurance, and others. The source of the shares from ESO offered can be the issuance of new shares and can also be from shares bought back (shares bought back by the company) from the old shareholders. So ESO is one of the company's strategies in providing incentives to its employees in the form of stock-based compensation. The amount of compensation is related to determining the fair value of ESO, which according to PSAK No. 53 is determined by the option pricing model including the Black-Scholes formula or the Binomial method.

The purpose of the employee stock option itself is to harmonize the wishes of the company, employees, and shareholders. For companies, the purpose of providing ESO includes:

a. By providing ESO, it is hoped that it can stimulate and motivate employee morale to be more optimal, so that it can improve the performance of the company, which in turn makes the company's stock price rise / improve.
b. In an effort for the company to retain superior and outstanding employees, because ESO is an incentive for employees who excel in a company.
c. To foster a sense of belonging and sense of responsibility from an employee towards the company.

While for employees themselves, with the increase in the company's stock price, profits will be obtained from a large payoff when exercising ESO. For shareholders, the provision of ESO will have an impact on a large increase in dividends if the share price rises. The meaning of employees here is not only ordinary workers, but also includes members of the board of directors and commissioners. Meanwhile for ESO recipients themselves, it can be carried out thoroughly to all employees without a selection process, or even through selection, carried out based on positions or other criteria that are more qualitative, depending on the purpose of ESO.

In general, employee stock options (ESO) have some differences with options traded in the usual option market. This difference distinguishes ESO from other options in its calculations [8]. Among the special features that are the differences are:

a. A call option issued by a company for the shares of the company itself.
b. It has a vesting period, during which the option cannot be implemented (excised). If the employee leaves the company either voluntarily or not during the waiting period, the option becomes null and void. But if the employee leaves the company after the waiting period, the option can be implemented immediately (early exercise) if the stock market price is in-the-money, but the option cannot be implemented if the stock market price is out-of-the-money.
c. Employees are not allowed to sell their ESO (change hands). So if the employee wants to immediately realize ESO in cash, then the employee must sell the shares he will get. This situation encourages ESO to be implemented faster before the maturity period (early exercise). This is possible because ESO can be carried out at any time, starting after the waiting period ends to maturity.

d. Generally, ESO has a long maturity period (several years) and usually 10 years.
This paper will use the assumption that ESO can change hands / ignore special features in c above.

The value of ESO is calculated so that companies that use ESO as a form of incentive for their employees can prepare / reserve funds for the ESO needs, which are valued at fair value. This is done so that when ESO is exercised, the company is ready with the funds reserved. In this paper, the ESO value will be determined using 3, of which two are often used models, namely the SFAS 123 (R) model, and the Hull-White model. Then the results obtained in this model will be compared with the Dilution model where in this model dilution factors (decreasing stock prices) have been calculated. Next will be seen the influence of certain parameters on the price of ESO. In this paper the number of employees leaving the company is modeled as a Poisson process at a rate ofλ. So the opportunity for an employee to leave the company is given by$(1 - e^{-\lambda\Delta t})$.

2. Models

In this paper, the Binomial CRR method (Cox, Ross, Rubienstein) will be used in determining the fair value of options. According to Cox, Ross, and Rubinstein for values u and d and p can be used:

$$u \approx e^{\sigma\sqrt{\Delta t}}, \quad d = \frac{1}{u} = \frac{1}{e^{\sigma\sqrt{\Delta t}}} = e^{-\sigma\sqrt{\Delta t}}, \qquad p = \frac{e^{r\Delta t} - d}{u - d}$$

Let at $t_0 = 0$ the stock price is S_0, so by binomial model, the stock price at $t_1 = 1.\Delta t$is given by$S_0 u$ or$S_0 d$.Then at t_2 the stock price can be one of$S_0 d^2, S_0 ud$or$S_0 u^2$. By the recurrent way, at $t_j = j, \Delta t$ will be there exist$j + 1$stock prices which are given by:

$$S_{i,j} = S_0 u^i d^{j-i}, \;\; i = 0,1,2, \dots, j$$

where $S_{i,j}$is the stock price at $t_j$and already happened$i$times the increament of stock price and also $j - i$ times the decrement. At the maturity time$t_M = M.\Delta t = T$there is M +1 stock price : $\{S_{i,M}\}_{i=0,1,\dots,M}$.To determine the value of the share price in the binomial tree, a calculation is carried out with a backward motion, while to determine the option value, the calculation is carried out by forward.

2.1. SFAS 123 (R) Model

Based on the Statement of Financial Accounting Standard No. 123 (revised 2004) issued by Financial Accounting Standards Boards (FASB) regarding Share-Based Payments (SFAS 123R), better known as stock-based payments, stated that all entities must recognize that employee stock option payments are based on fair value.

Under the SFAS 123 (R) rule for calculating the fair value of ESO the Black-Scholes formula is used or by using the Binomial method. This is because the binomial method is more flexible than the B-S formulation. Besides that, the binomial method is also convergent towards the B-S formulation and is also able to combine the characteristics and special features of ESO.

In this calculation using the SFAS 123 (R) model, for the expiration of ESO, the life expectancy of the option is used. The expectation of the lifetime of each node in the binomial tree is not necessarily the same. This is because there is a possibility not to exercise on a particular node because it depends on the position of the option at that time. The following describes the life expectancy calculation of the options:

Suppose there is subinterval N during the lifetime of ESO, with T being the maturity time so that for each interval the length is equal to$\Delta t = \frac{T}{N}$. Let $E_{i,j}$be the expected value of life time at $j\Delta t$at node-$i\ th$, where$j = 0,1,2, \dots, N$ and$i = 0,1,2, \dots, j, v$is the end of vesting time and D is dividend. For expected lifetime when the due time, given by$E_{i,N} = 0$, dan $p = \frac{e^{(r-D)\Delta t} - d}{u-d}$.While for other vertices$(0 \leq j \leq N-1)$, must meet the following criteria:
During the waiting period, namely$j\Delta t < v$:

- Life expectancy for each increase i, given by:
  $p \times E_{i+1,j+1}$
- Life expectancy for each reduction i, given by:
  $(1-p) \times E_{i,j+1}$
  So we have
  $E_{i,j} = p \times E_{i+1,j+1} + (1-p) \times E_{i,j+1} + \Delta t$

Along the period after vesting time$j\Delta t \geq v$

- If the option is exercised, then the amount of life expectancy is$E_{i,j} = 0$.
- If the option is held, then the life expectancy is large
  - If employees leave the company with a chance of $1 - e^{-\lambda\Delta t}$hence the magnitude of the life expectancy of the option becomes
    $E_{i,j} = \left(1 - e^{-\lambda\Delta t}\right)0 = 0$
  - If employees stay in the company with opportunities$e^{-\lambda\Delta t}$, then the expected life span of the option is obtained:
    $E_{i,j} = e^{-\lambda\Delta t}(p \times E_{i+1,j+1} + (1-p) \times E_{i,j+1} + \Delta t)$

  So for the criteria of time after the waiting period ends, the life expectancy is given by:
  $E_{i,j} = \left(1 - e^{-\lambda\Delta t}\right).0 + e^{-\lambda\Delta t}(p \times E_{i+1,j+1} + (1-p) \times E_{i,j+1} + \Delta t)$

For the overall large expectation of the lifetime of the option is$E_{0,0}$.

Next to obtain the ESO value using the SFAS 123 (R) model, and then the value of the European call option is calculated first using the binomial CRR method, where for the maturity time it is used$E_{0,0}$obtained by the above method, with the interest rate r, and for strike price K.

Furthermore, after obtaining the European call option value, then the ESO value is determined with the SFAS 123 (R) model as follows:

$$C^{SFAS\ 123\ (R)} = \left(e^{-\lambda}\right)^{v} \times C^{T=expected\ life}$$

Where $C^{SFAS\ 123\ (R)}$state the size of ESO using the SFAS 123 (R), $C^{T=expected\ life}$states the magnitude of the European call option value with time to maturity$E_{0,0}$obtained as above, and multiplied by$\left(e^{-\lambda}\right)^{v}$, where $e^{-\lambda}$is an opportunity for employees to remain in the company during the waiting period [7]. In this model, the weakness is not counting the rate of employees leaving the company after the waiting period.

2.2. Hull-WhiteModel

In this model, the opportunity for employees to leave the company has been calculated after the waiting period. Explicitly this model combines the early exercise strategy by assuming that in the period after the waiting period ends until the maturity time, the option will be implemented if the stock price is at least equal to the multiple of M of the strike price.$(S_{i,j} \geq MK)$[6].

At any short time interval of Δt during the period of the waiting period, the opportunity for employees to leave the company is stated by$1 - e^{-\lambda\Delta t}$, with$\lambda$is the rate of employees leaving the company annually. While after the waiting period, in the short interval Δt, there is an opportunity for employees to leave the company, namely$1 - e^{-\lambda\Delta t}$. In this situation, an employee will immediately analyze his options if the share price is in-the-money. But if the stock price is out-of-the-money then that option will not be exercised.

Let there exist N partitions along the lifetime of ESO, where T is the maturity time thus the length of every interval is stated by $\Delta t = \frac{T}{N}$. Let $S_{i,j}$ and $C_{i,j}$ are shares price and option price respectively at $j\Delta t$ on the node i-th, with $j = 0,1,2,\dots,N$ and $i = 0,1,2,\dots,j$, v is the end of vesting time, r is risk free interest rate, D is dividend and K is *strike price*. The stocks price for every node is obtained by using forward method with Binomial CRR Model that is $S_0 u^i d^{j-i}$ and $u = e^{\sigma\sqrt{\Delta t}}, d = e^{-\sigma\sqrt{\Delta t}}, p = \frac{e^{(r-D)\Delta t} - d}{u-d}$, while the options price is counted by using backward method and start at the maturity time ($j = N$). The option's price at maturity time is given by the intrinsic value $C_{i,N} = max\{S_{i,N} - K, 0\}$, and for the other nodes ($0 \leq j \leq N-1$), should be satisfy the following criterions:

Along the vesting time$j.\Delta t < v$:

- If the employees leave the company with probability $1 - e^{-\lambda\Delta t}$ then the option will be forfeited and the value become 0.
- If the employee keeping stay in the company with probability $e^{-\lambda\Delta t}$ then the option price can be obtained from $e^{-\lambda\Delta t}e^{-r\Delta t}\left(pC_{i+1,j+1} + (1-p)C_{i,j+1}\right)$.
  Furthermore the option's price along the vesting period is the sum of both points above,
  $C_{i,j} = 0 + e^{-\lambda\Delta t}e^{-r\Delta t}\left(pC_{i+1,j+1} + (1-p)C_{i,j+1}\right)$
  $= e^{-\lambda\Delta t}e^{-r\Delta t}\left(pC_{i+1,j+1} + (1-p)C_{i,j+1}\right)$

Along the period after vesting time$j\Delta t \geq v$

- If the stock price is greater or equal to the criteria for the exercise strategy($S_{i,j} \geq MK$), then the option will be exported. If employees leave the company with opportunities$1 - e^{-\lambda\Delta t}$,so the option's price:
  $\left(1 - e^{-\lambda\Delta t}\right)(S_{i,j} - K)$. But if the employee stays in the company with opportunities$e^{-\lambda\Delta t}$, so the option's price is $e^{-\lambda\Delta t}\left(S_{i,j} - K\right)$.Thus the option price for this criterion is fulfilled by:
  $C_{i,j} = \left(1 - e^{-\lambda\Delta t}\right).\left(S_{i,j} - K\right) + e^{-\lambda\Delta t}.\left(S_{i,j} - K\right)$
  $= S_{i,j} - K$
- When the stock price is smaller than the exercise criteria ($S_{i,j} < MK$), if employees leave the the company with opportunities$1 - e^{-\lambda\Delta t}$,so option's price is given by $\left(1 - e^{-\lambda\Delta t}\right)\max\{S_{i,j} - K, 0\}$.But if the employee stays in the company with opportunities$e^{-\lambda\Delta t}$,so the option's price:
  $e^{-\lambda\Delta t}e^{-r\Delta t}\left(pC_{i+1,j+1} + (1-p)C_{i,j+1}\right)$. So the option price for this criterion is:
  $C_{i,j} = \left(1 - e^{-\lambda\Delta t}\right) max\{S_{i,j} - K, 0\} + e^{-\lambda\Delta t}e^{-r\Delta t}\left(pC_{i+1,j+1} + (1-p)C_{i,j+1}\right)$

The ESO's price is stated by $C_{0,0}$.

2.3. Dilution Model

Employee stock options (ESO) can be implemented in 2 ways, namely by issuing new shares and through bidding or repurchasing existing shares that are outstanding. However, the implementation of ESO through the issuance of new shares is more complicated and must go through procedures and a long time. So that the provision of ESO is usually done in the second way, namely the company provides shares to ESO by buying old shares in circulation..

Giving employee stock options (ESO) is basically giving compensation to employees in buying company shares. In this case, the employee should buy the company's shares for S (the price that applies in the market) but with the ESO program, the employee is compensated for buying the company's shares for K, so that the employee receives compensation from the company for (S-K). When ESO is exercised, the exercise price is definitely lower than the stock price in the market. Exercise prices whose value is lower than this stock price will cause a decrease in the value of the existing shares. Decreasing the value of shares compared to the value of shares at first is called dilution. Dilution is a decrease in stock price returns due to an exercised option [2].

In previous models, the dilution effect was not taken into account in determining the ESO value, but this dilution effect should not be ignored if in large numbers. If the number of ESO given is small, the dilution effect will not be clearly seen in the ESO value. But for the number of ESO given in large quantities, there will be a significant/large difference caused by the effect of dilution. So that for a large number of ESO his dilution effect cannot be ignored as in table 1 below.

Suppose that many shares circulating before ESO are ω, and many ESO provided by the company are θ. It is assumed that one ESO states the right to buy one share at a K strike price and no option is excreted at the same time. Then the price of shares that have been diluted after exporting θ ESO is:

$$\frac{S_{i.j}\omega + K\theta}{\omega + \theta}$$

In the above equation, the price of the outstanding stock (ω) before the option exercised is $S_{i.j}\omega$ and the stock price of ESO (θ) which is excreted is Kθ. Furthermore, after ESO was exercised, the number of shares outstanding was many shares before the exercise was added with a lot of shares from exporting ESO, namely ω + θ. So that the stock price after experiencing a dilution is obtained from the sum of the prices of all outstanding shares (shares before the exercise plus shares from the EXCISE ESO) are divided by many shares outstanding after ESO exercise [5].

The following shows the effect of dilution effects with several variations in the percentage of ESO given to employees. Given:

$S = 50;\ K = 50; r = 5\%; T = 10\ years\ ; v = 1 - 8\ years; D = 1\%; \lambda = 0.03; \sigma = 30\%;\ \omega = 25000000$

Table 1. ESO Price based on number of ESO

α / v	4%	2%	1%	0.4%	0.1%	0.08%	0.05%	0.03%	Without Dilution
1	19.4710	19.8528	20.0493	20.1691	20.2296	20.2336	20.2397	20.2438	20.2498
2	19.2389	19.6161	19.8103	19.9287	19.9885	19.9925	19.9984	20.0024	20.0084
3	18.9401	19.3115	19.5027	19.6192	19.6780	19.6819	19.6878	19.6918	19.6977
4	18.5922	18.9567	19.1444	19.2588	19.3166	19.3204	19.3262	19.3301	19.3359
5	18.2062	18.5632	18.7469	18.8590	18.9155	18.9193	18.9250	18.9287	18.9344

6	17.7895	18.1383	18.3179	18.4274	18.4826	18.4863	18.4918	18.4955	18.5011
7	17.3475	17.6877	17.8628	17.9695	18.0234	18.0270	18.0324	18.0360	18.0414
8	16.8845	17.2156	17.3860	17.4899	17.5423	17.5458	17.5511	17.5546	17.5599

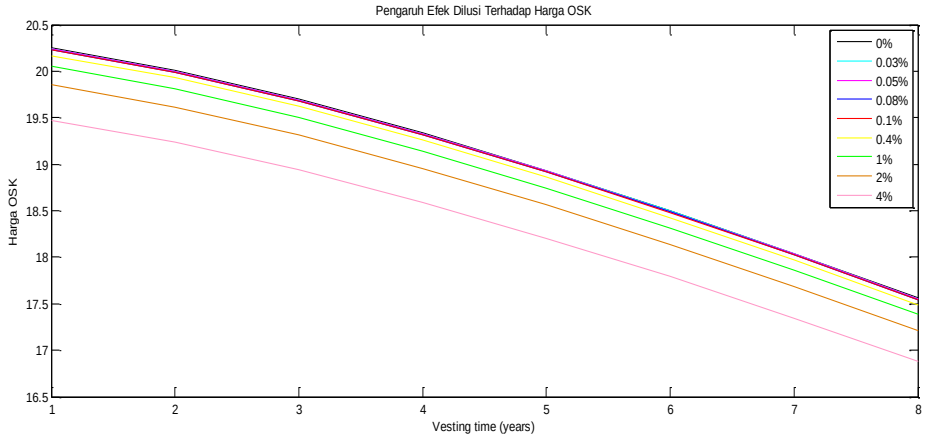

Figure 1. The Graph of ESO Price based on number of ESO

where α states the percentage of ESO given to employees, θ states that a lot of ESO is given to employees and V states the waiting period (years). The following is given the conversion of α value into:

α (%)	0%	0.03%	0.05%	0.08%	0.1%	0.4%	1%	2%	4%
θ	0	7500	12500	20000	25000	100000	250000	500000	1000000

Suppose there are sub-interval N during the lifetime of ESO, with T being the maturity time so that for each interval the length is equal to$\Delta t = \frac{T}{N}$. Let$S_{i,j}$and$C_{i,j}$successively states the stock price, and the option price at $j\Delta t$ at the i-th node, with$j = 0,1,2,\dots,N$and$i = 0,1,2,\dots,j,v$is the end of vesting time, $r$is risk free interest rate, D is dividend, $K$is*strike price*, $\omega$is a lot of shares outstanding before ESO diercercise and θ is the number of ESO given. For the stock price, each node is obtained by going forward using the binomial CRR method, namely$S_0 u^i d^{j-i}$ and$u = e^{\sigma\sqrt{\Delta t}}, d = e^{-\sigma\sqrt{\Delta t}}, p = \frac{e^{(r-D)\Delta t} - d}{u-d}$, while for the option price itself, it is calculated by backward motion which starts with calculating the option price at maturity, ie $(j = N)$. For option value when due, given by intrinsic value that is equal to$C_{i,N} = max\left\{\frac{S_{i,N}\,\omega + K\theta}{\omega+\theta} - K, 0\right\}; j = 0,1,\dots,N$. While for other nodes$(0 \le j \le N-1)$, should be met along the vesting time$j\Delta t < v$:

- If employees leave the company with opportunities as big as$1 - e^{-\lambda\Delta t}$, so the option's price is 0.
- If employees keep stay in the company with opportunities as big as$e^{-\lambda\Delta t}$so the option's price is $e^{-\lambda\Delta t} e^{-r\Delta t}\left(pC_{i+1,j+1} + (1-p)C_{i,j+1}\right)$.
  So that the option price during the waiting period is obtained from the sum of the two points above, namely:
  $C_{i,j} = 0 + e^{-\lambda\Delta t} e^{-r\Delta t}\left(pC_{i+1,j+1} + (1-p)C_{i,j+1}\right)$
  $= e^{-\lambda\Delta t} e^{-r\Delta t}\left(pC_{i+1,j+1} + (1-p)C_{i,j+1}\right)$

Along the period after vesting time$j.\Delta t \geq v$

- For the criterion$\frac{S_{i,j}\,\omega+K\theta}{\omega+\theta} - K > e^{-r\Delta t}\left(pC_{i+1,j+1} + (1-p)C_{i,j+1}\right)$then the option will be exercised with the option price for this criterion fulfilled by:

$$C_{i,j} = \left(1 - e^{-\lambda\Delta t}\right).\left(\frac{S_{i.j}\omega + K\theta}{\omega+\theta} - K\right) + e^{-\lambda\Delta t}.\left(\frac{S_{i.j}\omega + K\theta}{\omega+\theta} - K\right)$$
$$= \frac{S_{i,j}\,\omega + K\theta}{\omega+\theta} - K$$

- For the criterion $\frac{S_{i,j}\,\omega+K\theta}{\omega+\theta} - K \leq e^{-r\Delta t}\left(pC_{i+1,j+1} + (1-p)C_{i,j+1}\right)$the provisions apply if the employee leaves the company, then the option price is given by$\left(1 - e^{-\lambda\Delta t}\right).max\left\{\frac{S_{i.j}\omega+K\theta}{\omega+\theta} - K, 0\right\}$.But if the employee stays in the company, then the option price is given by $e^{-\lambda\Delta t}e^{-r\Delta t}\left(pC_{i+1,j+1} + (1-p)C_{i,j+1}\right)$, so the option price for this criterion is:

$$C_{i,j} = \left(1 - e^{-\lambda\Delta t}\right).\max\left\{\frac{S_{i.j}\omega + K\theta}{\omega+\theta} - K, 0\right\} + e^{-\lambda\Delta t}e^{-r\Delta t}\left(pC_{i+1,j+1} + (1-p)C_{i,j+1}\right)$$

For ESO prices alone will be given by$C_{0,0}$.

3. Result

Before looking at how the ESO values under the SFAS 123 (R), Hull-White, and Dilusi models are first reviewed how changes to the life expectancy of options in the SFAS 123 (R) model under certain parameters.

Table 2. The effect of Vesting time to Expected life $S = 50;\ K = 50; r = 5\%; T = 10\ years$; $D = 1\%;\ \lambda = 0.03;\ \sigma = 30\%;$

Vesting Time	*Expected Life*
1	2.3760
2	3.6468
3	4.7185
4	5.6772

Table 3. The effect of T to Expected life $S = 50;\ K = 50; r = 5\%; v = 3\ years;$ $D = 1\%;\ \lambda = 0.03;\ \sigma = 30\%;$

Maturity time	*Expected Life*
9	4.5670
10	4.7185
11	4.8958
12	5.2106

Table 4. The effect of volatility to Expected life $S = 50;\ K = 50; r = 5\%; T = 10\ years$; $v = 3\ years$; $D = 1\%;\ \lambda = 0.03;$

Volatility (σ)	*Expected Life*
10%	3.5324
20%	4.3770
30%	4.7185
40%	5.2867

Table 5. The effect of exit rate to Expected life, $S = 50;\ K = 50; r = 5\%; T = 10\ years\ \ v = 3\ years$; $D = 1\%$; $\sigma = 30\%;$

Exit Rate (λ)	*Expected Life*
0.01	4.8239
0.02	4.7701
0.03	4.7185
0.04	4.6692

Table 6. The effect of interest rate to Expected life $S = 50;\ K = 50; T = 10\ tahun$; $v = 3\ tahun;$ $D = 1\%;\ \lambda = 0.03;\ \sigma = 30\%;$

Interest Rate (r)	*Expected Life*

4%	4.8701
5%	4.7185
6%	4.5733
7%	4.4350

From the results obtained in the tables above, it can be seen that the waiting period, maturity time, and volatility have a positive correlation with the expected lifetime. The greater the value of these parameters, the greater the expected life span of the option. But on the contrary for the interest rate parameters and the rate of employees leaving the company. These parameters are negatively correlated with the expected lifetime of the option. So that if the value of this parameter increases then the expected life span of the option will decrease. This is because when the interest rate and the employee's rate increase, it will indicate that ESO will be exercised as soon as possible.

Furthermore, for the ESO value under the SFAS 123 (R), Hull-White, and Dilution models, it can be seen from the following cases: For example, a problem with determining the value of employee stock options (ESO) is known:

$$S = 50;\ K = 50; r = 5\%; T = 10\ years\ ; v = 1 - 8\ years; D = 1\%\ \lambda = 0.03; \sigma = 30\%;\ \omega = 2500;\ \theta = 50$$

Vesting time	SFAS 123 (R) Model	Hull-White Model	Dilution Model
1	10.6106	6.5788	16.8408
2	12.8838	9.3414	16.6428
3	14.3053	11.2914	16.3862
4	15.2335	12.7612	16.0867
5	15.8537	13.8927	15.7539
6	16.2397	14.7665	15.3944
7	16.4803	15.4354	15.0129
8	16.5700	15.9367	14.6131

Table 7. ESO price by using SFAS 123 (R), Hull-White, and Dilution Model

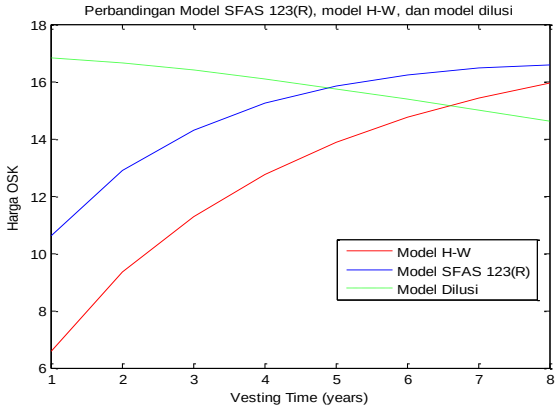

Figure 2. The graph of ESO price by using SFAS 123 (R), Hull-White, and Dilution Model

From the results in table 9 above, it can be seen that the value of employee stock options (ESO) is calculated using the SFAS 123 (R) model and the Hull-White model increases for each vesting time increase. The increase in the value of options that occur in this model is quite large. As for the value of employee stock options (ESO) with calculations using the Dilution model has decreased, although not too significant for each increase in vesting time. In figure 2, if we compare the ESO value graph using the Dilution model with the SFAS 123

(R) model, and the Hull-White model, for the Hull-White model and SFAS 123 (R) model, ESO prices increase for each increase in the waiting period sharply, but on the contrary in the Dilution model there is a decrease in ESO value, this is because the Dilution factor/dilution effect has been calculated so that there will be a decrease in option prices while in the SFAS 123 (R) and Hull-White models this dilution effect is not taken into account . The decline in the Dilution model is not too large, or in other words the Dilution model has a low sensitivity to changes in the waiting period. While the SFAS 123 (R) and Hull-White models this dilution effect is not taken into account. For a small amount, the effect of dilution will not be too visible, but on the contrary when for a large number of ESO, the dilution effect will increase. Therefore, dilution effects should not be ignored when calculating ESO values.

Now, we are doing an approximation by using the trinomial method which is combined with Multilevel Monte Carlo. This method is predicted van be better and produced an accurate result than the other methods before.

4. Conclusion

From the results obtained in the previous section, it can be concluded that:

1. The value of employee stock options (ESO) calculated using a dilution model has decreased even though it is not too significant for each vesting time, which is due to the influence of dilution factors, but for SFAS 123 (R) models and models Hull-White, ESO prices have increased for each increase in the waiting period.
2. Our research today to solve the same case by using trinomial multilevel Monte Carlo is predicted will be better and more accurate than the method before.

References

[1] Dewan Standar Akuntansi Keuangan 2010 *Pembayaran Berbasis Saham no. 53 (R)* (Ikatan Akuntan Indonesia)

[2] Dewan Standar Akuntansi Keuangan 2010 *Pernyataan Standar Akuntansi Keuangan (PSAK) no. 56 (R)* (Ikatan Akuntan Indonesia)

[3] FAS 123 (R) 2006 *Share-Based Payment : A Multidisciplinary Approach* (Price Water House Coopers)

[4] Higham J Desmond 2004 *An Introduction to Financial Valuation Mathematics, Stochastics and Computation* (New York : Cambridge University Press)

[5] Hull J and White A 2004 Accounting of Employee Stock Options: A Practical Approach to Handling The Valuation Issues (*Journal of Derivatives Accounting*) 1(1): 3-9.

[6] Hull J, and White A 2004 How to Value Employee Stock Options. *Financial Analysts Journal* 60: 114-119.

[7] Liao F Y, Lyuu Y D 2008 An Expanded Model For The Valuation of Employee Stock Options. *The Journal of Futures Markets* 8(29): 713-735.

[8] Rubinstein M 1995 On The Accounting Valuation of Employee Stock Options. *Journal of Derivatives* 3: 8-24.

[9] Sidarto K A 2009 PenentuanHarga Opsi Saham Karyawan dengan Metode Binomial. *Indonesian Journal of Banking and Finance* 1(1)

[10] Telaumbanua, Faoso F 2000 *Opsi Saham Karyawan. Bisnis Indonesia. Edisi 29* (PT. Jurnalindo Aksara Grafika)

INTERNATIONAL PROCEEDING
The 2nd International Conference on Science and Technology (ICST)
ISBN: 978-602-5830-19-8, June 2020

The Properties of Matrix in Group from Kronecker Product on The Representation of Quaternion Group Using Partitioned Matrix

N N Bakar[1], Yanita[2*], M R Helmi[3], and Ahsan[4]

Department of Mathematics, Faculty of Mathematics and Natural Sciences, Andalas University-Kampus Unand Limau Manis Padang 25163 Indonesia

E-mail: yanita@sci.unand.ac.id

Abstract. This paper discusses about the properties of matrices which are element of a group derived from the application of Kronecker product to the representation of the quaternion group (this group is called by author with *Kronecker quaternion group*). The properties the new matrix that constructed by matrices from the Kronecker quaternion group as submatrix in partitioned matrix are discussed based on transpose and determinant matrix. It's known that the construction of the partitioned matrix implies that product of partitioned matrix and the transpose of the matraix is commute.

Keyword: *partitioned matrix, transpose matrix, determinant matrix*

1. Introduction

In this paper, $\mathcal{G}$ denotes a finite non-abelian group with 32 orders. Group $\mathcal{G}$ was obtained by applying Kronecker product on the representation quaternion group. Thus, the elements of $\mathcal{G}$ are 4×4 matrices [1]. There are some specific properties of these matrices, that is:

a. Symmetric matrix (20 symmetric matrices).
b. Non-symmetric matrix (12 non-symmetric matrices)
c. For every $A \in \mathcal{G}$, $A^T = A^{-1}$ (orthogonal matrix)
d. For every $A \in \mathcal{G}$, $|A| = 1$.
e. For every $A \in \mathcal{G}$, $AA^T = A^T A$.
f. For every $A, B \in \mathcal{G}$, $AB^T = A^T B$ A and B non-symmetric matrix.

Let A is an arbitrary $m \times n$ matrix. A matrix A can be divided or partitioned into submatrices by drawing horizontal or vertical lines between various of its rows or columns, in this case the matrix is called a partitioned matrix. Meanwhile, a submatrix of a matrix A is a matrix that can be obtained by striking out rows and/or columns of A [2].

In this paper, we construct a new matrix that entries are matrices in $\mathcal{G}$. Thus, the new matrix can be seen as a partitioned matrix. New matrix properties are arranged in the form of matrix partitions, where the submatrices are matrices derived from [1], using some properties in the partitioned matrices related to transpose (in Part 2: Theorems 2.1, 2.2, 2.3, and 2.4) and the determinant matrix (in Section 3: Theorems 3.3, 3.4 and 3.5).

2. Properties Matrix From G related to Transpose Matrix

It's known that if A is symmetric matrix, then the product $A^TA = AA^T$. Thus the properties given below are in the following theorems for non-symmetric matrix. We refer [3] and [4], to show the following theorems:

Theorem 2.1
Let $\mathbf{A} = \begin{bmatrix} U & \mathbf{0} \\ V & W \end{bmatrix}$ and $\mathbf{B} = \begin{bmatrix} U & V \\ \mathbf{0} & W \end{bmatrix}$ where U, V, W non-symmetric matrices in $\mathcal{G}$ and $\mathbf{0}$ is a 4×4 zero matrix. Then $\mathbf{A}^T\mathbf{A} = \mathbf{B}\mathbf{B}^T$.
Proof.
Noted that $\mathbf{A}^T = \begin{bmatrix} U^T & V^T \\ \mathbf{0} & W^T \end{bmatrix}$ and $\mathbf{B}^T = \begin{bmatrix} U^T & \mathbf{0} \\ V^T & W^T \end{bmatrix}$. Based on e. and f. in Section 1, we have

$$\mathbf{A}^T\mathbf{A} = \begin{bmatrix} U^TU + V^TV & V^TW \\ W^TV & W^TW \end{bmatrix}$$
$$= \begin{bmatrix} UU^T + VV^T & VW^T \\ WV^T & WW^T \end{bmatrix}$$
$$= \mathbf{B}\mathbf{B}^T$$

■

Theorem 2.2
Let $\mathbf{A} = \begin{bmatrix} U & V \\ W & X \end{bmatrix}$ where U, V, W, X are non-symmetric matrices in $\mathcal{G}$. Then $\mathbf{A}\mathbf{A}^T = \mathbf{A}^T\mathbf{A}$.

Proof.
Noted that $\mathbf{A}^T = \begin{bmatrix} U^T & V^T \\ V^T & X^T \end{bmatrix}$. Based on e. and f. in Section 1, we have

$$\mathbf{A}\mathbf{A}^T = \begin{bmatrix} UU^T + V^TW & UV^T + VX^T \\ WU^T + XW^T & WV^T + XX^T \end{bmatrix}$$
$$= \begin{bmatrix} U^TU + V^TW & U^TV + V^TX \\ W^TU + X^TW & W^TV + X^TX \end{bmatrix}$$
$$= \mathbf{A}^T\mathbf{A}$$

■

In general we have the following theorem:

Theorem 2.3
Let

$$\mathcal{A} = \begin{bmatrix} A_{11} & \mathbf{0} & \mathbf{0} & \cdots & \mathbf{0} & \mathbf{0} \\ A_{21} & A_{22} & \mathbf{0} & \cdots & \mathbf{0} & \mathbf{0} \\ A_{31} & A_{32} & A_{33} & \cdots & \vdots & \vdots \\ \vdots & \vdots & \vdots & \cdots & \mathbf{0} & \mathbf{0} \\ A_{(n-1)1} & A_{(n-1)2} & A_{(n-1)3} & \cdots & A_{(n-1)(n-1)} & \mathbf{0} \\ A_{n1} & A_{n2} & A_{n3} & \cdots & A_{n(n-1)} & A_{nn} \end{bmatrix}$$

and

$$\mathcal{B} = \begin{bmatrix} A_{11} & A_{21} & A_{31} & \cdots & A_{(n-1)1} & A_{n1} \\ \mathbf{0} & A_{22} & A_{32} & \cdots & A_{(n-1)2} & A_{n2} \\ \mathbf{0} & \mathbf{0} & A_{33} & \cdots & A_{(n-1)3} & A_{n3} \\ \vdots & \vdots & \vdots & \ddots & \vdots & \vdots \\ \mathbf{0} & \mathbf{0} & \mathbf{0} & \ddots & A_{(n-1)(n-1)} & A_{n(n-1)} \\ \mathbf{0} & \mathbf{0} & \mathbf{0} & \cdots & \mathbf{0} & A_{nn} \end{bmatrix}$$

where $A_{ij} \in \mathcal{G}$ and A_{ij} non-symmetric matrix and $\mathbf{0}$ is an 4×4 zero matrix. Then $\mathsf{A}^T\mathsf{A} = \mathsf{B}\mathsf{B}^T$.

Theorem 2.4

Let $\mathsf{A} = \begin{bmatrix} A_{11} & A_{12} & \cdots & A_{1n} \\ A_{21} & A_{22} & \cdots & A_{2n} \\ \vdots & \vdots & \ddots & \vdots \\ A_{n1} & A_{n2} & \cdots & A_{nn} \end{bmatrix}$ where $A_{ij} \in \mathcal{G}$ and A_{ij} non symmetric matrix. Then $\mathsf{A}\mathsf{A}^T = \mathsf{A}^T\mathsf{A}$.

Proof of Theorem 2.3 and 2.4 are analogues with proof of Theorem 2.1 and 2.2 respectively.

3. Properties Matrix from G Related to Determinant Matrix

Noted that, if an $n \times n$ matrix $A = [a_{ij}]$ is (upper or lower) triangular then the determinant of a triangular matrix equals the product of its diagonal elements. Furthermore, we have the following properties:

Theorem 3.1 [4]

Let P be an $m \times m$ matrix, Q be an $n \times m$ matrix and R an $n \times n$ matrix. Then,

$$\begin{vmatrix} P & \mathbf{0} \\ Q & R \end{vmatrix} = \begin{vmatrix} R & Q \\ \mathbf{0} & P \end{vmatrix} = |P||R|.$$

■

The repeated application of Theorem 3.1 leads to the following formulas for the determinant of an arbitrary (square) upper or lower block-triangular matrix (with square diagonal blocks):

$$\begin{vmatrix} A_{11} & \mathbf{0} & \mathbf{0} & \cdots & \mathbf{0} & \mathbf{0} \\ A_{21} & A_{22} & \mathbf{0} & \cdots & \mathbf{0} & \mathbf{0} \\ A_{31} & A_{32} & A_{33} & \ddots & \vdots & \vdots \\ \vdots & \vdots & \vdots & \ddots & \mathbf{0} & \mathbf{0} \\ A_{(n-1)1} & A_{(n-1)2} & A_{(n-1)3} & \cdots & A_{(n-1)(n-1)} & \mathbf{0} \\ A_{n1} & A_{n2} & A_{n3} & \cdots & A_{n(n-1)} & A_{nn} \end{vmatrix} = |A_{11}||A_{22}||A_{33}| \ldots \left|A_{(n-1)(n-1)}\right||A_{nn}|$$

and

$$\begin{vmatrix} B_{11} & B_{12} & B_{13} & \cdots & B_{1(n-1)} & B_{1n} \\ \mathbf{0} & B_{22} & B_{23} & \cdots & B_{2(n-1)} & B_{2n} \\ \mathbf{0} & \mathbf{0} & B_{33} & \cdots & B_{3(n-1)} & B_{3n} \\ \vdots & \vdots & \vdots & \ddots & \vdots & \vdots \\ \mathbf{0} & \mathbf{0} & \mathbf{0} & \ddots & B_{(n-1)(n-1)} & B_{(n-1)n} \\ \mathbf{0} & \mathbf{0} & \mathbf{0} & \cdots & \mathbf{0} & B_{nn} \end{vmatrix} = |B_{11}||B_{22}||B_{33}| \ldots \left|B_{(n-1)(n-1)}\right||B_{nn}|$$

The following theorems give formulas for the determinant of a partitioned matrix:

Theorem 3.2 [4]
Let P an $m \times m$ matrix, Q an $n \times m$ matrix, R an $n \times n$ matrix and S an $m \times n$. If P is nonsingular, then

$$\begin{vmatrix} P & S \\ Q & R \end{vmatrix} = \begin{vmatrix} R & Q \\ S & P \end{vmatrix} = |P||R - QP^{-1}S|.$$

■

We continue with the matrix from group $\mathcal{G}$. Based on Theorem 3.1 and 3.2, we have the following theorems:

Theorem 3.3
Let $\mathbf{A} = \begin{bmatrix} U & \mathbf{0} \\ V & W \end{bmatrix}$ and $\mathbf{B} = \begin{bmatrix} U & V \\ \mathbf{0} & W \end{bmatrix}$, where $U, V, W \in \mathsf{G}$ and $\mathbf{0}$ is a 4×4 zero matrix. Then $|\mathbf{A}| = |\mathbf{B}| = 1$.
Proof.

$$\begin{aligned} &|\mathbf{A}| = |\mathbf{B}| \\ &= \begin{vmatrix} U & \mathbf{0} \\ V & W \end{vmatrix} \\ &= \begin{vmatrix} U & V \\ \mathbf{0} & W \end{vmatrix} \\ &= |U||W| \\ &= 1. \end{aligned}$$

■

In general, we have

Theorem 3.4
Let Let $\mathsf{A} = \begin{bmatrix} A_{11} & \mathbf{0} & \mathbf{0} & \cdots & \mathbf{0} & \mathbf{0} \\ A_{21} & A_{22} & \mathbf{0} & \cdots & \mathbf{0} & \mathbf{0} \\ A_{31} & A_{32} & A_{33} & \ddots & \vdots & \vdots \\ \vdots & \vdots & \vdots & \ddots & \mathbf{0} & \mathbf{0} \\ A_{(n-1)1} & A_{(n-1)2} & A_{(n-1)3} & \cdots & A_{(n-1)(n-1)} & \mathbf{0} \\ A_{n1} & A_{n2} & A_{n3} & \cdots & A_{n(n-1)} & A_{nn} \end{bmatrix}$ where $A_{ij} \in \mathcal{G}$ and A_{ij} non-symmetric matrix and $\mathbf{0}$ is an 4×4 zero matrix and

$\mathsf{B} = \begin{bmatrix} B_{11} & B_{12} & B_{13} & \cdots & B_{1(n-1)} & B_{1n} \\ \mathbf{0} & B_{22} & B_{23} & \cdots & B_{2(n-1)} & B_{2n} \\ \mathbf{0} & \mathbf{0} & B_{33} & \cdots & B_{3(n-1)} & B_{3n} \\ \vdots & \vdots & \vdots & \ddots & \vdots & \vdots \\ \mathbf{0} & \mathbf{0} & \mathbf{0} & \ddots & B_{(n-1)(n-1)} & B_{(n-1)n} \\ \mathbf{0} & \mathbf{0} & \mathbf{0} & \cdots & \mathbf{0} & B_{nn} \end{bmatrix}$ where $B_{ij} \in \mathcal{G}$ and B_{ij} non-symmetric matrix and $\mathbf{0}$ is an 4×4 zero matrix. Then $|\mathsf{A}| = 1$ and $|\mathsf{B}| = 1$

Proof.

$$|\mathcal{A}| = \begin{vmatrix} A_{11} & \mathbf{0} & \mathbf{0} & \cdots & \mathbf{0} & \mathbf{0} \\ A_{21} & A_{22} & \mathbf{0} & \cdots & \mathbf{0} & \mathbf{0} \\ A_{31} & A_{32} & A_{33} & \ddots & \vdots & \vdots \\ \vdots & \vdots & \vdots & \ddots & \mathbf{0} & \mathbf{0} \\ A_{(n-1)1} & A_{(n-1)2} & A_{(n-1)3} & \cdots & A_{(n-1)(n-1)} & \mathbf{0} \\ A_{n1} & A_{n2} & A_{n3} & \cdots & A_{n(n-1)} & A_{nn} \end{vmatrix} = |A_{11}||A_{22}||A_{33}| \dots \left|A_{(n-1)(n-1)}\right||A_{nn}|$$

$= 1$

and

$$|\mathsf{B}| = \begin{vmatrix} B_{11} & B_{12} & B_{13} & \cdots & B_{1(n-1)} & B_{1n} \\ \mathbf{0} & B_{22} & B_{23} & \cdots & B_{2(n-1)} & B_{2n} \\ \mathbf{0} & \mathbf{0} & B_{33} & \cdots & B_{3(n-1)} & B_{3n} \\ \vdots & \vdots & \vdots & \ddots & \vdots & \vdots \\ \mathbf{0} & \mathbf{0} & \mathbf{0} & \ddots & B_{(n-1)(n-1)} & B_{(n-1)n} \\ \mathbf{0} & \mathbf{0} & \mathbf{0} & \cdots & \mathbf{0} & B_{nn} \end{vmatrix} = |B_{11}||B_{22}||B_{33}| \dots \left|B_{(n-1)(n-1)}\right||B_{nn}|$$

$= 1$

Theorem 3.5

Let $\mathbf{A} = \begin{bmatrix} U & V \\ W & X \end{bmatrix}$ where U, V, W, X are non-symmetric matrices in $\mathcal{G}$. Then

$$|\mathbf{A}| = \begin{vmatrix} U & V \\ W & X \end{vmatrix} = |X - WU^T V|$$

Proof.

Since all of matrices in G are nonsingular, so we have U is nonsingular. We can apply Theorem 3.2 and 3.3 to prove this theorem.

Consider that

$\begin{bmatrix} U & V \\ W & X \end{bmatrix} = \begin{bmatrix} I & \mathbf{0} \\ WU^{-1} & X - WU^{-1}V \end{bmatrix} \begin{bmatrix} U & V \\ \mathbf{0} & I \end{bmatrix}$, thus

$$|\mathbf{A}| = \begin{vmatrix} U & V \\ W & X \end{vmatrix}$$
$$= \left| \begin{bmatrix} I & \mathbf{0} \\ WU^{-1} & X - WU^{-1}V \end{bmatrix} \begin{bmatrix} U & V \\ \mathbf{0} & I \end{bmatrix} \right|$$
$$= \begin{vmatrix} I & \mathbf{0} \\ WU^{-1} & X - WU^{-1}V \end{vmatrix} \begin{vmatrix} U & V \\ \mathbf{0} & I \end{vmatrix}$$
$$= |I||X - WU^{-1}V||U||I|$$
$$= |X - WU^{-1}V||U|$$
$$= |U||X - WU^{-1}V|$$
$$= |X - WU^{-1}V|$$
$$= |X - WU^T V|$$

■

Acknowledgement

This work supported by BOPTN Grand Andalas University 2018

References

[1] Yanita Y, Helmi M R and Zakiya A M 2018 Solvability group from Kronecker product on the representation of quaternion group. *Asian Journal of Scientifics Research.* 2 (12): 293-297.

[2] Piziak R And Odell P L 2007 *Matrix Theory*: *From Generalized Inverses to Jordan Form.* (New York: Chapman & Hall/CRCX)

[3] Wang K, and Davis P J 1986 Group matrices for the quaternion and Generalized Dihedral Groups. *Computers and Mathematics with Applications*, 5-6(12B): 1297-1301.
[4] J Harville D A 1997 *Matrix Algebra from a Statiscian's Perspective* (New York Springer-Verlag)

INTERNATIONAL PROCEEDING
The 2nd International Conference on Science and Technology (ICST)
ISBN: 978-602-5830-19-8, June 2020

The Poverty Modeling in Bengkulu Province using Geographically Weighted Logistic Regression

D S Rini*, I Sriliana, H Fransiska
Department of Statistics, University of Bengkulu, Bengkulu, Indonesia

*Email: dyah.setyorini@unib.ac.id

Abstract. This study aims to model poverty in Bengkulu Province and analyze the factors that influence it. The method used in this study is Geographically Weighted Logistic Regression (GWLR) with Kernel Adaptive Bisquare Weighting functions. The data are obtained from the Central Bureau of Statistics of Bengkulu Province (Susenas and Podes 2014). Modeling with the GWLR produces a local model in Bengkulu Province. Based on this research, number of education facilities is affecting poverty in 103 municipalities in Bengkulu Province, while in the other 10 municipalities, poverty is influenced by number of families without electricity, number of education facilities, number of health facilities, number of JAMKESMAS recipients, and number of SKTM.

1. Introduction

Poverty is a problem faced in developing countries, including Indonesia. The Central Bureau of Statistics (BPS) defines that poverty is seen as an economic inability to fulfill food and non-food needs that is measured by expenditure. Poor people are residents who have an average monthly per capita expenditure below the poverty line. In September 2017, the number of poor people in Indonesia reached 26,58 million people (10,12 percent). The percentage of poor people in urban areas is 7,26 percent. While the percentage of poor people in rural areas is 13,47 percent [1].

The percentage of poor people in Indonesia varies for each region. This difference is caused by inequality between regions in Indonesia. The largest percentage of poor people is in Maluku and Papua Island, which is 21,23 percent, while the lowest percentage of poor people is on Kalimantan Island, which is 6,18 percent. The percentage of poor people on Sumatra Island in September 2017 was 10,44 percent (5,97 million people) with a total poor population in Indonesia of 26,58 million people. In other words, Sumatra Island is an island that still has many poor people.

Bengkulu Province is a province located on the island of Sumatra. Bengkulu Province ranks seventh as the poorest province in Indonesia in September 2017 based on the percentage of poor people, which is 15,59 percent. The percentage of poor people in Bengkulu Province from year to year is high. The poverty rate in Bengkulu Province also tends to be static. If there is a decrease in the poverty rate, the decline includes slow or small. Poverty that occurs in areas in Bengkulu Province also varies for each district / city, sub-district, and village, because poverty data is spatial data that varies regionally.

The diversity of poverty data that occurred in Bengkulu Province was influenced by spatial effects. Therefore, the classical method is not qualified enough to analyze the diversity that occurs.

This study will model poverty in Bengkulu Province using Geographically Weighted Logistic Regression (GWLR) and analyze the factors that influence poverty in Bengkulu Province spatially, which is based on poverty data in each subdistrict in Bengkulu Province. Different poverty indicators between regions will influence the policies given to each region in efforts to alleviate poverty.

The GWLR method is used to model data that contains spatial diversity, where the response variable used is a binary variable (eg poor and not poor) that spreads according to the binomial distribution and predictor variables are factors that are thought to affect the response variable. So the model produced for each region can be different or the same. The adaptive bisquare kernel weighters will be used as weighters in the GWLR model because Bengkulu Province has a different area for each sub-district, so it is expected that the results of the analysis will be better.

Previous research was conducted by Dwinata, namely the GWLR model with a case study of poverty modeling in East Java Province. The results show that the geographically weighted logistic regression model is better used to model poverty in East Java, where the factors that influence it are the percentage of people aged 15-55 years who can read Latin and other letters, percentage of expenditure per capita for food, and percentage of health card users [2]. Fathurahman et al used the GWLR model with a Gaussian kernel weighting to analyze the factors that influenced the district / city Public Health Development Index (IPKM) in Papua Province in 2013. The results obtained were the percentage of residents who graduated from college and the percentage of poor people [3]. Hasriana models poverty in South Sulawesi by using GWLR. The result is a factor that affects poverty is the percentage of the population with a floor area less than equal to 8 m and the percentage of households that use their own/shared latrines [4]. Albuquerque et al applied the GWLR method to find out the factors that influence credit risk based on geographical location. The results of his research prove that credit risk is influenced by factors that vary depending on each region [5]. Widyastuti, Yuniarti, and Hayati used the GWLR model in modeling the factors that influence the Human Development Index (HDI) in Kalimantan. The results of the research obtained are that each district in Kalimantan has different factors [6]

2. Materials

1. Geographically Weighted Logistic Regression (GWLR) Model

Geographically Weighted Regression (GWR) is a statistical method used to analyze data that has the effect of spatial diversity. The GWR model is a development of the classic regression model. The parameters of the GWR model are determined based on each observation area, so that each observation area has different regression parameter values. The response variable in the GWR model is predicted by a predictor variable in which each regression parameter depends on the region where the data is observed.

If the response variable data is binary data, then the GWR model and the logistic regression model are combined to form a Geographically Weighted Logistic Regression (GWLR) model. The GWLR model is stated in:

$$\pi(x_i) = \frac{\exp\left(\sum_{k=0}^{p} \beta_k(u_i, v_i) x_{ik}\right)}{1 + \exp\left(\sum_{k=0}^{p} \beta_k(u_i, v_i) x_{ik}\right)}$$

where $\pi(x_i)$ is probability of events, $0 \le \pi(x_i) \le 1$, k-th predictor variable of location (u_i, v_i), x_{ik}, and $\beta_k(u_i, v_i)$ is regression parameter of each location.

The GWLR model is a nonlinear model so that transformation of model is needed to make a linear function. The transformation used is a logit transformation from $\pi(x_j)$:

$$g(x_j) = \ln\left[\frac{\pi(x_j)}{1+\pi(x_j)}\right] = \beta_0(u_i, v_i) + \beta_1(u_i, v_i)x_{j1} + ... + \beta_p(u_i, v_i)x_{jp}$$

In the GWLR model, the parameter estimation method used is the maximum likelihood estimation. Because of the form of implicit equations, numerical iteration procedures are used, namely the weighted least squares method:

$$\beta^{(t+1)}(u_i, v_i) = \beta^{(t)}(u_i, v_i) - \mathbf{H}^{(t)^{-1}}\left(\beta^{(t)}(u_i, v_i)\right)\mathbf{g}^{(t)}\left(\beta^{(t)}(u_i, v_i)\right)$$

By repeating the iterative procedure for each of the i-th regression points, the local parameter estimator will be obtained. Iteration will stop when convergent, i.e. when it is a very small number ε, that is $\left\|\beta^{(t+1)}(u_i, v_i) - \beta^{(t)}(u_i, v_i)\right\| \le \varepsilon$. Initial estimates for parameters were obtained using logistic regression models [7].

2. Weighting Function

Brunsdon (1998) proposed the kernel bisquare function, namely:

$$w_{ij} = \begin{cases} \left[1-\left(d_{ij}/h\right)^2\right]^2, & \text{untuk } d_{ij} < h \\ 0, & \text{untuk lainnya} \end{cases}$$

This kernel bisquare function is a continuous weighting function and resembles normal up to the distance as far as h from the i-th observation area. The function is zero for the area that has a distance greater than h.

In addition to kernel bisquare functions, there are also kernel adaptive functions, which are functions that have different bandwidth for each observation area. This is caused by the ability of kernel adaptive functions that can adjust to the conditions of the observation points. If the observation points are scattered densely around the 1st observation, then the bandwidth is relatively narrower. Conversely, if the observation points have a distance that is relatively far from the first observation, then the bandwidth is wider. The functions of kernel adaptive bisquare are:

$$w_j(u_i, v_i) = \begin{cases} \left[1 - \left(\frac{d_{ij}}{\square_{i(q)}}\right)^2\right]^2, & d_{ij} \leq \square_{i(q)} \\ 0, & d_{ij} > \square_{i(q)} \end{cases}$$

where $h_{i(q)}$ is an adaptive bandwidth that specifies q as the distance of the nearest neighbor from region i [7].

Bandwidth is a balance controller between the conformity of the curve to the data and the smoothness of the data. Method used to determine the optimum bandwidth is the Cross Validation (CV) method. The optimum bandwidth is obtained when the CV value is minimum.

$$CV(h) = \sum_{i=1}^{n} \left(y_i - \hat{y}_{\neq i}(h)\right)^2$$

where $\hat{y}_{\neq i}$ is the estimator of y which observations in region i are omitted from the estimation process [7].

3. Selection of the Best Model

Akaike's Information Criterion (AIC) is one of the methods used to select the best method. AIC is used because of the complexity of the model, which is the difference in the value of observations with predictive values. The AIC value also depends on the variables in the model and the bandwidth. AIC is defined as follows:

$$AIC(h) = D(h) + 2K(h)$$

Where $D(h)$ is the model deviance with the bandwidth h and $K(h)$ is the number of parameters in the model with the bandwidth h [7]. The best model is the model with the smallest AIC value.

3. Methods

The purpose of this study is to model poverty and analyze the factors that influence poverty in Bengkulu Province using the GWLR model. The research activities included data collection, GWLR modeling, selecting the best models, and determining the factors that influence poverty. The object of this research is Bengkulu Province. The data used in this study are obtained from the Central Bureau of Statistics (Susenas and Podes 2014). The response variable (Y) used is a binary variable (0 = poor and 1 = not poor). A sub-district is categorized as poor (0) if the per capita expenditure per month in the region is smaller than the middle value per capita expenditure per month in Bengkulu Province and is categorized as not poor (1) if the opposite is true. The predictor variables were the Number of Families without Electricity (X_1), Number of Education Facilities (X_2), Number of Health Facilities (X_3), Number of JAMKESMAS Recipients (X_4), and SKTM Amount (X_5).

4. Results and Discussion

1. Multicollinearity Test

The multicollinearity test aims to find out whether or not the predictor variables contain linear or not dependency relationships. If there is a strong correlation between predictor variables, the problem of multicollinearity will emerge. One of the most popular measures to see multicollinearity between predictor variables is Variance Inflation Factor (VIF). The results of calculating the VIF value with the R program are as follows:

Table 1. VIF of Predictor Variables

Variable	VIF
X_1	1,02
X_2	2,25
X_3	2,08
X_4	1,31
X_5	1,45

Based on table 1, it can be seen that the VIF value of each predictor variable is less than 10 (<10), so that there are no multicollinearity among predictor variables.

2. Spatial Heterogeneity Test

Spatial heterogeneity test aims to see whether there are differences between one observation point and another observation point. In other words, to test whether the data used has the effect of spatial diversity or not. The test statistic used to test spatial heterogeneity is the Breusch-Pagan test. The results of spatial heterogeneity tests using the R program are presented in the following table:

Table 2. Breusch-Pagan Statistic Test

Breusch-Pagan Statistic Test	Df	p-value
19,93	5	0,0012

The results of spatial heterogeneity test in table 2 show that the value of the Breusch-Pagan test statistic is 19,93, the free degree is 5, and the p-value is 0,0012. The Chi-square value of the table at the real level of 10% is 9,23. Because the Breusch-Pagan test value is greater than the Chi-square value of the table and the p-value value is smaller than 10%, it can be concluded that there is an effect of spatial heterogeneity on poverty data in Bengkulu Province used in this study.

3. Model of Poverty in Bengkulu Province

3.1 Poverty Model in Bengkulu Province Using Logistic Regression

The first step in modeling using logistic regression is the multicollinearity test. The calculation results of VIF values in table 2 show that there is no multicollinearity between predictor variables, so that all predictor variables can be used in forming a logistic regression model. The parameter estimation of the logistic regression model using SPSS 16 program can be seen in the following table:

Table 3. Parameter Estimator of Logistic Regression

Parameter	Estimator	*Standard Error*	[Wald]^2	*Odds Ratio*
β_0	-0,004	0,413	0,000	0,996
β_1	-0,005	0,005	1,276*	0,995
β_2	-0,114	0,139	0,448	0,892
β_3	0,035	0,115	0,008	1,035
β_4	0,001	0,001	0,358	1,001
β_5	0,001	0,002	0,029	1,001

In table 4, the value of parameter estimates of each predictor variable and the Wald test statistic values are shown in each predictor variable. At the real level of 30%, the Chi-square value of the table is 1,074. Because the Wald test statistic value of the variable is 1,276 and the value is greater than the Chi-square value of the table, the variable Number of Families without Electricity has a significant effect on the poverty level of the subdistrict in Bengkulu Province. The AIC value for this logistic regression model is 166,27.

3.2 Poverty Model in Bengkulu Province Using GWLR

Table 2 shows that there are effects of spatial heterogeneity in the subdistrict poverty data in Bengkulu Province. Therefore, a GWLR model is needed to overcome the effects of spatial heterogeneity. Therefore a spatial weighting matrix is needed, namely the weighting function of kernel adaptive bisquare. The spatial weighting matrix is obtained by comparing the Euclid distance with the optimum bandwidth value from each subdistrict.

The estimated parameter of the GWLR model is obtained by substituting the weighting of each subdistrict. The calculation of parameter estimation is carried out by the R and GWR 4.0.9 program. The calculation results are presented as follows:

Table 4. Parameter Estimate of GWLR using Kernel Adaptive Bisquare Function

Parameter	Minimum	Maximum
β_0	0,009	14647522066,093
β_1	-289607613,201	-0,0049
β_2	-0,1445	12372511907,898
β_3	-5049768707,844	0,0278
β_4	-19588402,274	0,0008
β_5	-228591086,884	0,0015

The GWLR model produced in each District in Bengkulu Province is different. For example, the GWLR model produced for North Lebong has the following parameter estimation values:

Table 5. Parameter Estimate for North Lebong

Parameter	Estimate	Standar Error	W
β_0	0,010132	0,435853	0,023246
β_1	-0,004919	0,005066	-0,970974
β_2	-0,144538	0,142551	-1,013936
β_3	0,027841	0,124848	0,223004
β_4	0,000837	0,00105	0,797045
β_5	0,001576	0,002362	0,667324

So that the GWLR model for North Lebong is:

$$g(x) = 0,010132 - 0,004919X_1 - 0,144538X_2 + 0,027841X_3 + 0,000837X_4 + 0,001576X_5$$

The significant variable in North Lebong is X_2, because the value of W is greater than $Z = 0,9948$. In other words, the number of educational facilities affects poverty in North Lebong.

Based on the results of parameter estimate, subdistrict in Bengkulu Province can be divided into two groups of regions according to significant variables. The first group is the subdistrict where X_2 (the number of educational facilities) is the only significant variable. The first group consists of

103 sub-districts. Whereas the second group is the subdistrict where variable X_1, X_2, X_3, X_4, X_5 are the significant variables.

The following figure presents a map of Subdistrict areas which are categorized into two groups. The first group is the Subdistrict group where X_2 (the number of educational facilities) is the only significant variable. Whereas the second group is the Kecamatan group where variable X_1, X_2, X_3, X_4, X_5 are significant variables.

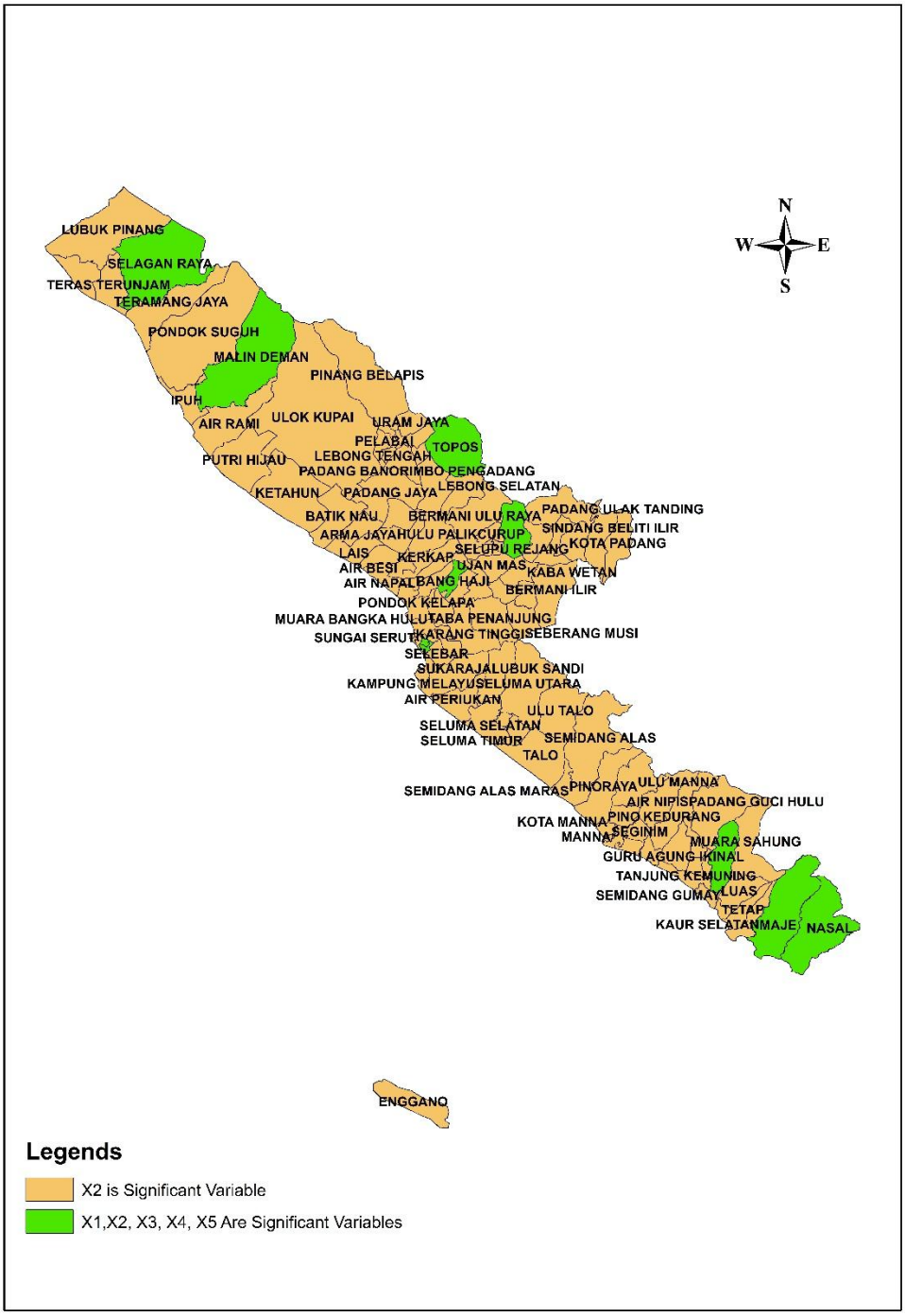

Figure 2. Poverty Model Maps of Bengkulu Province in 2014

4. Selection of the Best Models

The selection of the best model between the logistic regression model and the GWLR model can be done by comparing the AIC values of the two models. The model that has the smallest AIC value is the best model. In addition to comparing the AIC values, the best models can also be determined based on the deviance of each model. The smallest deviance model indicates that the model is the best model.

Tabel 7. AIC and Deviance of Model

Model	AIC	Deviance
Logistic Regression	166,27	154,27
GWLR	151,76	139,81

Based on table 7, it can be seen that the AIC value of the GWLR model is smaller than the AIC value of the logistic regression model, so the GWLR model is the best model. So the weighted GWLR model of the kernel adaptive bisquare function is better used in analyzing the poverty of subdistricts in Bengkulu Province.

Acknowledgement

We thank the Natural Sciences Faculty of Bengkulu University which has funded this research.

References

[1] BPS 2018 *Berita Resmi Statistik Profil Kemiskinan Provinsi Bengkulu September 2017* BPS, Bengkulu
[2] Dwinata, A. Model Regresi Logistik Terboboti Geografis (Studi Kasus: Pemodelan Kemiskinan di Provinsi Jawa Timur*). Jurnal Tesis Sekolah Pascasarjana Institut Pertanian Bogor*. 2012. Bogor
[3] Fathurahman, M., Purhadi, Sutikno, Ratnasari, V. Pemodelan Geographically Weighted Logistic Regression pada Indeks Pembangunan Kesehatan Masyarakat di Provinsi Papua. *Prosiding Seminar Nasional MIPA*. Jatinangor, 27-28 Oktober 2016.
[4] Hasriana. Pemodelan Kemiskinan menggunakan Geographically Weighted Logistic Regression dengan Fungsi Pembobot Fixed Kernel. *Jurnal Skripsi Universitas Hasanuddin*. 2016. Tidak dipublikasikan.
[5] Albuquerque, P.H.M., Medina, F.A.S., da Silva, A.R. Geographically Weighted Logistic Regression Applied to Credit Scoring Models. *Paper Presented at the XL ANDAP Congress, Costa do Sauipe, BA, Brazil, September 2016*.
[6] Widyastuti, L., Yuniarti, D., dan Hayatim, M.N. Pemodelan Faktor-faktor yang Berpengaruh terhadap Indeks Pembangunan Manusia (IPM) di Kalimantan dengan Geographically Weighted Logistic Regression (GWLR). *Jurnal Eksponensial Vol. 9 No.1*. 2018, halm 67-74.
[7] Fotheringham, A.S., Brunsdon, C., Charlton M 2002 *Geographically Weighted Regression: The Analysis of Spatially Varying Relationships*. John Wiley & Sons, Ltd., West Sussex, England.

INTERNATIONAL PROCEEDING
The 2nd International Conference on Science and Technology (ICST)
ISBN: 978-602-5830-19-8, June 2020

The Track Record of the Usage of Plant Parts as Immunomodulator Medicine by Suku Anak Dalam Bendar Bengkulu

F Lestari* and I Susanti
Lecturers of Program Studi Pendidikan Biologi, STKIP PGRI Lubuklinggau

*E-mail: Fitrinq98@gmail.com

ABSTRACT. Immunity is an essential part in living things because it maintains the body-defense system against diseases. People usually use drugs to improve the immune system. However, a long-term use of drugs may have side effects to other organs, such as heart function, respiration and many more. One of the ways to minimize the usage of drug is by boosting the immune system through traditional plants that are used for traditional medicine. One of the tribes which still use this traditional medicine is Suku Anak Dalam Bendar Bengkulu.The research aims to find out the plants and their parts that are used for immunomodulator by Suku Anak Dalam Bendar Bengkulu. The research was a qualitative research by applying observation, interview, and documentation. The results showed that there were 10 parts of plant that can be applied for immunomodulator, i.e. leaves, roots, seeds, stems, flowers, fruit, rhizomes, bark, tuber and gland secretion. In conclusion, all part of the plant can be applied for traditional medicine purposes, particularly by Suku Anak Dalam Bendar Bengkulu.

1. Introduction

Immunity is a very important system in the human body. Reduction of the system may affect our health, as our body will be easily infected by viruses, bacteria, protozoa, worms, and parasitic fungi. The presence of this disease indicates that immunity is very important as the protection of the body. If the number and function of immune cells decrease, then pathogenic microorganisms will easily cause various diseases, especially infectious diseases[1]. Substances that can help improve the function of the immune system are known as immunomodulators with their mechanisms, including 1) restoring damaged immune function (immunoreaction), improving immune system function (immunostimulation) and suppressing the immune response (immunosuppression)[2,3].

Generally, people treat infectious diseases by synthetic medicine, such as ketoprofen, aspirin, azathioprine, Cytoxan, isoprenoid, levamisole, arginine, and others. However, long-term use of these medicines can have negative effects, such as decreased platelet levels, respiratory depression, urticaria, toxic to the liver, digestive disorders, and others. Therefore, one way to minimize this negative impact is to use medicinal plants that potentially act as an immunomodulator. Some of the advantages of using medicinal plants such as easily to find, have low prices, and minimum side effects. They are easily to find in rice fields, gardens, and roadside as well as easily grow at home. One tribe in Musi Rawas Regency that still uses plants as medicine is Suku Anak Dalam Bendar Bengkulu[4].

The results of interviews with the tribal chief of Suku Anak Dalam Bendar Bengkulu revealed that this tribe still uses plants to treat infectious diseases. The usage of these plant cover: 1) leaves, roots,

and bougainvillea flowers as a vaginal discharge; 2) periwinkle leaves as a leukemia drug; 3) Alamanda leaves and flowers for antidotes and malaria drugs, etc. The habits of Suku Anak Dalam are inseparable from the behavior that has been inherited from their ancestors who are very dependent on nature[5]. However, the existence of plants used as medicine by this tribe has not been properly recorded and identified. This is proved by the fact that no reference has been found to discuss medicinal plants by this tribe either online or in printed books. Documentation of traditional knowledge in the use of plants can also be useful for subsequent generations[6]. Therefore, this research is expected to be preliminary data to find out the plant parts used by Suku Anak Dalam Bendar Bengkulu specifically as immunomodulators.

2. Research Method

The research was conducted from March to June 2019 on Suku Anak Dalam Bendar Bengkulu, STL (Suku Tengah Lakitan) Ulu Terawas, Musi Rawas Regency. This location was choosen due to several reasons, including: 1) the area potentially has diverse immunomodulatory medicinal plants. 2) people know the function of herbal medicines. 3) no data collection on immunomodulatory medicinal plants in the area.

The place of the research was also carried out at the STKIP Laboratory in PGRI Lubuklinggau to identify immunomodulatory medicinal plants obtained in the field and matched from the results of observations and interviews.

The data collected included primary and secondary source data. Data collection techniques are as follow:

a. Observation

At this stage, the researcher made direct observations and explored information from the chief and the community who used plants as immunomodulatory medicine using the observation sheet.

b. Interview

Teknik pengmpulan dilakukan dengan cara melakukan wawancara dengan kepala suku, dukun beranak, penjual jamu, dan masyarakat yang sering menggunakan tumbuhan obat.

c. Plant Documentation

Documentation is intended to obtain plant pictures directly from the place of research. After the data collection was conducted, the collected plant data was proven by the fact of its existence in the field, namely by documenting it for the identification of medicinal plants.

d. Plant Identification

Data from interviews regarding medicinal plants mentioned by the community were then identified using reference books of medicinal plants such as Flora[8]'s book and Plant Morphology[9]. Plant identification was using identification sheets. After identification, the number of medicinal plants in Suku Anak Dalam Bendar Bengkulu, Musi Rawas Regency was recapitulated.

Data analysis in this study used qualitative descriptive analysis techniques. Data from interviews were grouped according to the species of medicinal plants, the parts used, and the efficacy as well as known processing.

3. Result

The research was conducted on Suku Anak Dalam Bendar Bengkulu through purposive sampling. The result of observation and interview with the chief of the tribe, shaman and surrounding community, it was known that there are more than 41 species with 10 parts that are mostly used as medicines (Table 1).

Table 1. Parts of plant as Imunomodulatory Medicine by Suku Anak Dalam Bendar Bengkulu

No	Species Name/ Local Name	Familly	Latin Name	Useful part
1	Alamanda	Apocynaceae	*Allamanda cathartica*	Leaves, flowers
2	Avocado/*Pokad*	Lauraceae	*Persea americana*	Leaves, fruit,seed
3	Bandotan	Asteraceae	*Ageratum conyzoides*	Root, leaves
4	Bangle/*Gemelai*	Zingiberaceae	*Zingiber cassumunar*	Rhizome
5	Bangle hantu/*Gemelai atu*	Zingiberaceae	*Zingiber ottensii*	Rhizome, leaves
6	Thorn spinach	Amaranthaceae	*Amaranthus spinosus*	Whole parts
7	Belimbing wuluh	Oxalidaceae	*Averhoa bilimbi*	Fruit, flowers, leaves
8	knopflowers	Amaranthaceae	*Gomphrena globosa*	Whole parts
9	Four O'clock Flowers pukul empat	Nyctaginaceae	*Mirabilis jalava*	Root, leaves, seed
10	tahi kotokflowers	Asteraceae	*Tagetes erecta*	Leaves, flowers
11	Bougenvil	Nyctaginaceae	*Bougainvillea spectabilis*	root, flowers
12	Cabai rawit/*Cabe rawet*	Solanaceae	*Capsicum annum*	Fruit
13	Indonesian Bay leave	Myartaceae	*Syzigium polynathum*	Leaves
14	Duku	Meliaceae	*Lansium domesticum*	Seed
16	Jali/*Jelai*	Poacceae	*Coix lacryma-jobi*	Fruit, root
18	Jeruk purut/*limau porot*	Rutaceae	*Citrus hystrix*	Fruit, leaves
19	Hibiscus flower	Malvaceae	*Hibiscus rosasinensis*	Flowers
20	Kencur	Zingiberaceae	*Kaempferia galanga*	Rhizome
21	Keladi tikus	Araceae	*Typhonium flagelliforme*	Tuber
22	Lengkuas/*Laos*	Zingiberaceae	*Alpinia galanga*	Rhizome
23	Lidah mertua	Liliaceae	*Sansevieria trifasciata*	Leaves
24	Mango	Anacardiaceae	*Mangifera indica*	Leaves, fruit
25	Mangos teen	Clusiaceae	*Garcinia mangostana*	Bark, fruit
26	Mahkota dewa	Thymelaceae	*Phaletia macrocarpa*	Fruit, leaves, seed
27	Meniran	Euphorbiaceae	*Phyllanthus niruri*	Root
28	Nanas kerang	Rhizophoraceae	*Tradescantia spathacea*	Leaves
29	Nangka/*Nake*	Moraceae	*Artocarpus heterophyllus*	Fruit, seed
30	Pacar air	Balsaminaceae	*Impatiens balsamina*	Leaves, flowers
31	Pacar kuku	Lythraceae	*Lawsonia inermis*	Leaves
32	Pecut kuda	Verbenaceae	*Stachytarpheta jamaisensis*	Root, flowers, leaves
33	Petikan kebo	Euphorbiaceae	*Euphorbia hirta*	Seluruh bagian
34	Pinang	Palmae	*Areca catechu*	Seed
35	Rambutan/ *Mutan*	Sapindaceae	*Naphelium lappaceum*	Bark, fruit, leaves, seed
36	Sawo/*Hawo*	Sapotaceae	*Manilkara zapota*	Fruit, getah
37	Senduduk	Melastomataceae	*Melastoma malabathricum*	Leaves, root
38	Sirsak/*Nake belendo*	Annonaceae	*Anona muricata*	Leaves
39	Periwinkle	Apacynaseae	*Catharantthus roseus*	Leaves
40	Terong susu kerbau	Solanaceae	*Solanum mammosum*	Seed
41	Sweet Potato/*Kepar*	Euphorbiaceae	*Ipomea batatas*	Leaves, stem, tuber.

Table 1 presents that out of 41 species found, there were 10 useful parts such as leaves, root, stem, flowers, bark, seed, rhizome, fruit, tuber, and gland secretion. Leaves were the most useful part whereas the gland secretion was only used a little. Out of 41 species, the parts then were calculated in

percentage. The percentages were found by accumulating the plant parts used in each species. If one species was used more than one part, it was still accumulated in the different parts. Based on the percentage, it was found out that the most useful parts are leaves (35,6%).

Table 2. Percentage of Plant Parts Use as Imunomodulatory Medicine

No	Useful Parts	Total	Percentage (%)
1	Leaves	26	35,6
2	Root	10	13,7
3	Stem	4	5,48
4	Flowers	7	9,58
5	Bark	2	2,72
6	Seed	8	10,95
7	Rhizome	3	4,11
8	Fruit	10	13,7
9	Tuber	2	2,71
10	Gland Secretion	1	1,37
Total		**73**	**100**

Table 2 presented that the most useful part was leaves with percentage of 35,6%, followed by fruitand rootfor 13,7%. The least useful part was gland secretion with percentage 1,37%.

4. Discussion

This research found that there are some plants that the whole parts can be used as potential immunomodulator. However, in general, the most useful part was leaves with a percentage of 35.6%. This is due to leaves processing which can be done easily because it is softer texture than the other parts. Leaves play role as the central of photosynthesis, so their cells have many raw materials for secondary metabolic which can treat disease10. These compounds, such as tannins, alkaloids, essential oils, those are useful for medicinal purposes[11].

Leaves are the easier parts to use because it simply can be extracted to get the essence[12]. Leaves have high water content and as the central of photosynthetic which contain organic elements or substances which have the property of curing various diseases; as well as contain soft fibers in helping to extract (substances) that will be used as medicine[9]. It also has secondary metabolic compounds. Thus, cells in the leaves tissue have a lot of raw material for the formation of secondary metabolites that can have the potential to treat disease.

The most useful plant part was leaves [13]. This is because the use of leaves for medicinal ingredients will not harm plant because leaves are easily grows back. It may be different if the used parts are root, stem, bark wood, tuber, and rhizome, because taking them can directly kill the plants and/or make them are easier infected by fungi and bacteria. People generally use 10 plant parts as medicines including leaves, roots, seeds, stems, flowers, fruit, rhizomes, bark, tuber and gland secretion. The most useful parts are leaves with percentage 35, 6%.

A test of the phytochemical content of several local plants that were often used as raw material for medicine in Lombok Island was conducted by 14. The results showed that secondary metabolic in leaves had antibacterial properties, denatured proteins, and prevented the digestion of bacteria. These secondary metabolic compounds include flavonoids, alkaloids, steroids, tannins, saponins, anthraquinones, and terpenoids.

5. Conclusion

In conclusion, out of 41 species of plants were used by Suku Anak Dalam, there were 10 plant parts were potential can be used as an immunomodulator.

Acknowledgement
Thank you to Kemenristekdikti for the PDP research grants 2018.

References

[1] Joyce B, dan Swain 2008 *Prinsip-prinsip Sains Untuk Keperawatan* (Jakarta: Erlangga)
[2[Masihi K N 2001 Fighting infection using immunomodulatory agents. *Exp Opin Biol Ther.* 1(4): 64-73.
[3] Kayser O, Masihi K N, Kiderlen F K 2003 Review: natural products and synthetic compounds as immunomodulators. *Expret Rev Anti-infect Ther*. 1(2): 31-35.
[4] Pranata S 2014 *Herbal TOGA (Tanaman Obat Keluarga.* (Yogyakarta: Aksara Sukses)
[5] Jauhari Dkk 2012 *Jejak Peradaban Suku Anak Dalam* (Bangko: Lembaga Swadaya Masyarakat Kelompok Suku Anak Dalam) 15-17
[6] Hidayat D dan Hardiansyah G 2012 Studi Keanekaragaman Jenis Tumbuhan Obat di Kawasan IUPHHK PT. Sari Bumi Kusuma Camp Tontang Kabupaten Sintang. *Journal Biology Science* 8 (2): 61-68
[7] Riduwan M B A 2007 *Belajar Mudah Penelitian untuk Guru, Karyawan dan Peneliti Pemula*. Bandung: ALFABETA
[8] Steenis C G, Van G J 2013 *Flora untuk Sekolah di Indonesia* (Jakarta: Balai Pustaka)
[9] Tjitrosoepomo 2009 *Morfologi Tumbuhan*. (Yogyakarta: Gadjah Mada University Press)
[10] Kaunang N E and Mokosuli Y S 2017 Botanical and phytochemical constituents of veral medicinal plants from mount Klabat north Minahasa. *Jurnal Of Medicinal Plants Studies* 5 (2)
[11] Kartika T 2015 Inventarisasi Jenis-Jenis Tumbuhan Berkhasiat Obat Di Desa Tanjung Baru Petai Kecamatan Tanjung Batu Kabupaten Ogan Ilir (OI) Provinsi Sumatera Selatan. *Sainmatika*12 (1).
[12] Jalius dan Muswita 2013 Eksplorasi Pengetahuan Lokal tentang Tumbuhan Obat di Suku Batin Jambi. *Biospesies* 6 (1): 28-37
[13] Setyowati 2010 Etnofarmakologi dan Pemakaian Tanaman Obat Suku Dayak Tunjung di Kalimantan Timur. *Jurnal Media Litbang Kesehatan* 3(XX)
[14] Rohyani 2015 Kandungan Fitokimia Beberapa Jenis Tumbuhan Lokal yang Sering dimanfaatkan Sebagai Bahan Baku Obat di Pulau Lombok. *Jurnal Pros Sem Nas Masy Biodiv Indon.* 1 (1) :388-391

INTERNATIONAL PROCEEDING
The 2nd International Conference on Science and Technology (ICST)
ISBN: 978-602-5830-19-8, June 2020

Soil Nematode Inventory in South Kalimantan

A Gafur*
Department of Biology, Faculty of Mathematics and Natural Sciences
Lambung Mangkurat University

*E-mail: agafur@ulm.ac.id

Abstract. Nematodes are the most abundant and the most diverse metazoa in soils. Soil nematode diversity reflects general biodiversity in the soil and the structure of nematode community has been demonstrated to contain a high information content to asses soil conditions. Therefore, there are theoretical and practical reasons for nematode diversity inventory, particularly in areas where the diversity is predictably high but mostly unexplored. In this paper, the current status of soil nematode diversity inventory in South Kalimantan is briefly described. All available reports on soil nematode from South Kalimantan were compiled and analyzed. The nematode collection deposited at the Laboratory of Biosystematics, Department of Biology, Faculty of Mathematics and Natural Sciences, Lambung Mangkurat University were further identified. The taxonomic collection currently consists of at least 63 genera dan 79 species. Recommendations for future agenda are: (1) expansion of samplings to other districts in South Kalimantan; (2) species-level identification; and (3) development of keys; (4) skill and expertise developments. This is the first report on soil nematode biodiversity of South Kalimantan.

1. Introduction

Soils are the core components of terrestrial ecosystems that host extremely diverse biota [1] that has been estimated to be orders of magnitude higher than that of above surface world [2]. The biodiversity, in terms of assemblages of species ("functional groups") and the distribution and abundance of those organisms over space and time, strongly influence vital ecosystem processes [3]. Those "keystone" species may be less abundant, but have disproportionately strong effects on the functioning of ecological communities and ecosystems [4].

As the identity of the great majority of species in soil is still unknown [5], there is an urgent need to develop taxonomic expertise to identify soil organisms, particularly in countries where knowledge of soil biota is lacking. Identification aids should then be developed, especially for key taxa of which identification is essential to understanding the effect of loss of species to ecosystems [4].

In the soil, in addition to prokaryotes, the major components of soil biodiversity are metazoans, and nematodes are the most numerous and the richest in species of all soil metazoans [6][7]. Studies [7–10] have shown that soil nematode diversity is correlated with soil functional parameters and reflects soil functioning, and even indicative of general biodiversity in the soil [11].

Unfortunately, in most tropical countries, including Indonesia, the study of nematodes is still in early stage and nematode diversity is to a large extent still unknown [12]. On the other hand, as one of the top megacentres of biodiversity [13][14] Indonesia can be expected to harbor a high below-ground

biodiversity, including that of nematodes. Therefore, soil nematode diversity in Indonesia merits further study, particularly in the biodiversity hotspots.

This paper summarizes recent advances and future directions in soil nematode diversity study in South Kalimantan, a part of Sundaland biodiversity hotspot.

2. Current Status

In Indonesia, like in most tropical developing countries, the limited budget has led to the government's policies to give much more priority to nematodes of agricultural and health importance, instead of the much more diverse and abundant non parasitic nematodes abound in soils. Non governmental sponsors are, similarly, more interested in studies directly related to food and health securities. Furthermore, past studies on nematodes have been mainly focused on control measures against parasitic nematodes of plants, animals, and humans. Very few systematic and taxonomic studies have been carried out, mostly by researchers or graduate students working in universities or research institutions abroad.

Several reports on plant parasitic nematodes from South Kalimantan have been made. Existence of plant parasites *Ditylenchus angustus*, *Helicotylenchus caudatus*, and *Hirschmanniella oryzae* has been reported [15]. Liestiany & Fitriyanti [16] found *Meloidogyne* sp. from vegetable crops in South Kalimantan. However, no description was given and even no specimen was mentioned in the publications. Consequently, the identification could not be verified.

During a nematode ecology-focused survey Gafur [17] collected free-living as well as plant parasitic nematodes. Although no description was given, permanent slides of specimens produced from the survey were kept, allowing further examinations for proper identification and formal taxonomic publications. The specimens are currently deposited in the Nematode Collection of the Laboratory of Biosystematics, Department of Biology, Faculty of Mathematics and Natural Sciences, Lambung Mangkurat University, curated by the author. Ever since subsequent studies have contributed more descriptions, and more specimens were added to the Nematode Collection.

All permanent slides of nematode specimens so far collected were prepared by first killing and fixing nematodes in hot 4% formalin. The specimens were then transferred to pure glycerine following the rapid method of Seinhorst [18].

Until recently, 56 genera and 7 higher taxa, consisting of at least 82 species, have been reported from South Kalimantan (Table 1). In many cases identification to species could not be made, and identification was carried out only up to genus. This is usually because key characters could not be examined due to the improper condition of the specimens. Besides, specimens of juvenile stages could not be properly identified because published species descriptions are mainly based on adult characters. In fact, species identification of soil nematodes is often challenging and requires the role of specialists. It is also time consuming, especially for specimens from new localities, so that it is unsuitable for projects with very short time limits. On the other hand, identification to species is not always necessary because higher taxon and functional group approaches are usually sufficient to serve as efficient indicators of nematode diversity [19].

Table 1. Soil nematode genera and higher taxa found in South Kalimantan with specimens deposited in the Nematode Collection of FMNS Lambung Mangkurat University

	GENERA / HIGHER TAXA	NUMBER OF SPECIES	DISTRIBUTION (DISTRICT)
1	*Achromadora*	1	Banjar
2	*Acrobeles*	1	Banjar
3	*Acrobeloides*	1	Banjar
4	*Alaimus*	1	Banjar
5	*Amphidelus*	1	Banjar

	GENERA / HIGHER TAXA	NUMBER OF SPECIES	DISTRIBUTION (DISTRICT)
6	*Aphanolaimus*	1	Banjar
7	*Aphelenchoides*	1	Banjar
8	*Aphelenchus*	1	Banjarbaru
9	*Aporcelaimellus*	1	Banjarbaru
10	*Aulolaimus*	1	Banjar
11	*Axonchium*	1	Banjar
12	*Belondirella*	1	Banjar
13	*Cervidellus*	1	Banjar
14	*Chronogaster*	1	Banjar
15	*Coslenchus*	1	Banjar
16	*Criconema*	2	Banjarbaru, Barito Kuala
17	*Criconemella*	1	Tanah Laut
18	Desmodoridae	1	Banjar
19	*Ditylenchus*	1	Banjar
20	Dorylaimida	6	Banjar, Tanah Laut, Banjarbaru
21	*Dorylaimus*	1	Banjar
22	*Doryllium*	1	Barito Kuala
23	*Eudorylaimus*	1	Banjar, Banjarbaru, Barito Kuala
24	*Ecphyadophora*	1	Banjar
25	*Eucephalobus*	1	Banjar
26	*Euteratocephalus*	1	Banjar
27	*Fuscheila*	1	Banjar
28	*Helicotylenchus*	1	Tanah Laut, Banjar
29	*Hirschmanniella*	1	Banjar
30	*Iotonchus*	4	Banjar, Banjarbaru, Tanah Laut
31	*Longidorella*	1	Banjar
32	*Margaronchulus*	1	Banjarbaru
33	*Mesodorylaimus*	1	Banjar
34	*Metateratocephalus*	1	Banjar
35	Miconchinae	1	Banjar
36	Mononchida	2	Tanah Laut
37	*Mononchus*	1	Banjar
38	*Mylonchulus*	3	Banjar, Banjarbaru, Tanah Laut
39	*Nygolaimoides*	1	Banjar
40	*Paractinolaimus*	1	Banjar
41	*Paramylonchulus*	2	Banjar
42	*Paratylenchus*	1	Banjar
43	*Plectus*	1	Banjar
44	*Pratylenchus*	1	Banjarbaru, Banjar, Tanah Laut
45	*Prismatolaimus*	1	Banjar
46	*Pristionchus*	1	Banjar
47	*Prionchulus*	1	Banjar
48	*Prodesmodora*	1	Banjar
49	*Pungentus*	1	Banjar

	GENERA / HIGHER TAXA	NUMBER OF SPECIES	DISTRIBUTION (DISTRICT)
50	*Radopholus*	1	Batola
51	Rhabditida	2	Banjarbaru
52	*Rhabditonema*	1	Banjar
53	*Rhabditophanes*	1	Banjar
54	*Rhabdolaimus*	1	Banjar
55	*Rotylenchus*	1	Banjar
56	Leptonchidae	1	Banjar
57	*Telotylenchus*	1	Banjar
58	*Tobrilus*	1	Banjar
59	Tylenchidae	6	Banjar, Banjarbaru
60	*Tylencholaimus*	1	Banjar
61	*Tylenchorhynchus*	1	Banjar, Banjarbaru
62	*Wilsonema*	1	Banjar
63	*Xiphinema*	1	Banjar, Banjarbaru

Sources: [17,20–27].

3. Future Direction

Four kinds of development can be recommended: (1) expansion of samplings to other districts in South Kalimantan; (2) species-level identification; and (3) development of keys; (4) skill and expertise developments.

Specimens deposited in the nematode collection so far came from 4 out of the 13 districts in the Province of South Kalimantan. Expectedly, with more districts covered more species will be collected and identified. Even more specimens of the same species from different localities will improve data on intraspecific variability and, in turn, species descriptions.

Despite that identification to species level is not always necessary in estimating nematode diversity [19], the real picture of nematode biodiversity will never be obtained without proper species identification. In addition, the role of nematodes in soil ecosystem processes will never be appropriately understood without species-level discrimination [28]. Cryptic species with delicate morphological differences have been shown to exist among soil nematodes, and those of plant parasitic species are of particular importance for the development of effective and efficient control measures as well as early warning systems of potential pest attack. Therefore, efforts should be made to reach species-level identification of all specimens in the collection. Resampling in the recorded localities may thus have to be carried out to obtain more and/or better specimens.

Identification aid in the form of keys will have to be developed to help non-specialists and occasional workers. Keys to species, genera, and higher taxa all have their own potential use and users. With growing number of entries covered with more specimens collected, a more flexible and easy-to-revise key is desirable. Therefore, a polytomous, computer-based, interactive key is preferable over a traditional dichotomous one. Nowadays, online keys are much more accessible than printed guides.

Over the past few decades, DNA technology has led to revolutionary approaches to taxonomy. Because of the many potential combinations in only a few hundred base pairs, DNA sequences can be useful not only in phylogenetic analysis but also in identification. It has even been proposed that DNA should be given a central or mandatory role in defining and identifying species [29,30]. Therefore, DNA sample and its sequence should be taken from newly collected nematodes.

Another scheme on making use of the nematode collection and the to be developed keys is a training on nematode identification. This will produce skilled workers for routine identification of

nematodes. Training for students will hopefully also develop interest among them in nematode taxonomy, as an answer to the notion of the lack of interest in taxonomy among young scientists and of the acute decline in taxonomical expertise in nematology [31,32].

4. Conclusion

Surveys on soil nematodes in the Province of South Kalimantan since 2005 have led to a taxonomic collection of nematodes hosted by the Laboratory of Biosystematics, Department of Biology, Faculty of Mathematics and Natural Sciences, Lambung Mangkurat University. The collection currently comprises specimens of at least 79 species of 63 genera, all mounted in glycerin as permanent slides. Four agenda can be recommended for future development. Because only some districts in the province have been sampled, with expansion of samplings to other districts in South Kalimantan more taxa will be covered. Species-level identification of all, or at least most, specimens is needed to obtain a better understanding of nematode diversity in the region and to allow more accurate use of nematofauna as bioindicator of soil conditions. To help non specialists in identification, keys to species are urgently needed. Finally, interest and expertise in nematode biodiversity must be developed by providing trainings for students and young scientists.

Acknowledgements

The author wishes to thank his students for depositing specimens from their nematode surveys in the Laboratory of Biosystematics, Department of Biology, Faculty of Mathematics and Natural Sciences, Lambung Mangkurat University. The heads of the Laboratory of Biosystematics and the Department of Biology is acknowledged for allowing establishment of a taxonomic collection of nematodes in the laboratory.

References

[1] Coleman D C, Whitman W B 2005 Linking species richness, biodiversity and ecosystem function in soil systems. *Pedobiologia (Jena)* **49**, 479–497.
[2] Heywood VH, Watson RT 1995 *Global biodiversity assessment*. Cambridge University Press Cambridge.
[3] Adams GA, Wall DH 2000 Biodiversity above and below the surface of soils and sediments: linkages and implications for global change. *Bioscience* **50**, 1043–1048.
[4] Power ME *et al.* 1996 Challenges in the quest for keystones: identifying keystone species is difficult—but essential to understanding how loss of species will affect ecosystems. *Bioscience* **46**, 609–620.
[5] 2005 *Handbook of the convention on biological diversity Including its Cartagena Protocol on Biosafety*. Montreal, Canada.
[6] Sohlenius B 1980 Abundance, biomass and contribution to energy flow by soil nematodes in terrestrial ecosystems. *Oikos* , 186–194.
[7] Hodda M, Peters L, Traunspurger W 2009 Nematode diversity in terrestrial, freshwater aquatic and marine systems. *Nematodes as Environ. Indic. CAB Int.* , 45–93.
[8] Freckman DW 1988 Bacterivorous nematodes and organic-matter decomposition. *Agric. Ecosyst. Environ.* **24**, 195–217.
[9] Bongers T, Bongers M 1998 Functional diversity of nematodes. *Appl. Soil Ecol.* **10**, 239–251. (doi:10.1016/S0929-1393(98)00123-1)
[10] Ekschmitt K *et al* 2001 Nematode community structure as indicator of soil functioning in European grassland soils. *Eur. J. Soil Biol.* **37**, 263–268.
[11] Yeates GW, Bongers T 1999 Nematode diversity in agroecosystems. In *Invertebrate Biodiversity as Bioindicators of Sustainable Landscapes*, pp. 113–135. Elsevier.
[12] Boag B, Yeates GW. 1998 Soil nematode biodiversity in terrestrial ecosystems. *Biodivers.*

Conserv. **7**, 617–630.
[13] Mittermeier RA, Myers N, Gil PR, Mittermeier CG. 1999 Hotspots. *Earths Biol. richest Most Endanger. Terr. ecoregions. Cemex SA y Agrup. Sierra Madre, SC* **431**.
[14] Myers N 2000 Mittermeier R a, Mittermeier CG, da Fonseca G a, Kent J. *Biodivers. hotspots Conserv. priorities. Nat.* **403**, 853–858.
[15] 2000 *Daftar Organisme Pengganggu Tumbuhan Potensial yang Dilaporkan telah Terdapat di Dalam Wilayah Republik Indonesia*. Jakarta: Puskara.
[16] Liestiany E, Fitriyanti D 2009 Keragaman Nematoda Parasit Tanaman pada Pertanaman Sayuran di Kalimantan Selatan. *Entomol. Kalimantan* **3**, 32–38.
[17] Gafur A 2006 Struktur Komunitas Nematoda Tanah Gambut Tropis dari Kalimantan Selatan. In *Seminar Nasional Biologi, Universitas Negeri Semarang*, pp. 78–87.
[18] Seinhorst JW 1959 A rapid method for the transfer of nematodes from fixative to anhydrous glycerin. *Nematologica* **4**, 67–69.
[19] Bhusal DR, Kallimanis AS, Tsiafouli MA, Sgardelis SP. 2014 Higher taxa vs. functional guilds vs. trophic groups as indicators of soil nematode diversity and community structure. *Ecol. Indic.* **41**, 25–29.
[20] Adhany R 2017 Identifikasi Nematoda di Lahan Perkebunan Buah Naga (Hylocereus costaricencis) Kabupaten Banjar dan Banjarbaru Kalimantan Selatan. Universitas Lambung Mangkurat.
[21] Halisah N 2018 Identifikasi Nematoda pada Tanah Tanaman Jagung (Zea mays) di Kabupaten Tanah Laut. Universitas Lambung Mangkurat.
[22] Aisyah S 2018 Identifikasi Nematoda pada Lahan Perkebunan Singkong (Manihot esculenta) di Kabupaten Banjar Kalimantan Selatan. Universitas Lambung Mangkurat.
[23] Novianita D 2018 Nematoda Tanah pada Perkebunan Durian (Durio zibethinus Murr.) di Banjarbaru, Kalimantan Selatan. Universitas Lambung Mangkurat.
[24] Nurbaiti 2017 Identifikasi Nematoda di Perkebunan Rambutan (Nephelium lappaceum L.) di Kabupaten Barito Kuala dan Kabupaten Banjar Kalimantan Selatan. Universitas Lambung Mangkurat.
[25] Gampung AO 2018 Nematoda pada Rizosfer Tanaman Karet (Hevea brasiliensis) di Kabupaten Banjar, Kalimantan Selatan. Universitas Lambung Mangkurat.
[26] Yogaswara DA 2016 Identifikasi Nematoda Rizosfer Pisang di Kabupaten Tanah Laut. Universitas Lambung Mangkurat.
[27] Nurdahlia S, Muhamat M, Gafur A 2017 Nematoda Mononchid dari Kebun Jeruk di Kabupaten Banjar, Kalimantan Selatan. *Bioscientiae* **13**.
[28] Yeates GW 2003 Nematodes as soil indicators: functional and biodiversity aspects. *Biol. Fertil. Soils* **37**, 199–210. (doi:DOI 10.1007/s00374-003-0586-5)
[29] Hebert PDN, Cywinska A, Ball SL, Dewaard JR. 2003 Biological identifications through DNA barcodes. *Proc. R. Soc. London. Ser. B Biol. Sci.* **270**, 313–321.
[30] Tautz D, Arctander P, Minelli A, Thomas RH, Vogler AP. 2003 A plea for DNA taxonomy. *Trends Ecol. Evol.* **18**, 70–74.
[31] Coomans A 2000 Nematode systematics: past, present and future. *Nematology* **2**, 3–7.
[32] Coomans A 2002 Present status and future of nematode systematics. *Nematology* **4**, 573–582.

INTERNATIONAL PROCEEDING
The 2nd International Conference on Science and Technology (ICST)
ISBN: 978-602-5830-19-8, June 2020

Bellucia pentamera Naudin Potency as a Natural resource of Medicine; Change its Status From Invasive to Useful plant

H Marisa[1] and Salni[2*]
[1]Laboratory of Plant Ecology, Sriwijaya University, Km 32, Indralaya, South Sumatra, 30662
[2]Laboratory of Biotechnology and genetics, Sriwijaya University Km 32, Indralaya, South Sumatra, 30662

*E-mail address: salnibasir@yahoo.com

Abstract. A Regulation from Indonesian Ministry for Environmental and Forestry, number P.94/MENLHK/SETJEN/KUM.1/12/2016 categorizes *Bellucia pentamera* Naudin is characterized as an invasive plant, that need a strict management and control. However, many recent studies show this species has many useful as source of traditional medicine recipes. characters that indicate the new status of *Bellucia pentamera* as useful medicinal plant. Green-immature fruit of Bellucia pentamera contains 2.210 mg/100 g of vitamin C, while the yellow-ripening one has higher, up to 3.500 mg/100 g of. Vitamin C is generally known as an effective threat for many symptoms. Therefore, it could be consider to put *Bellucia pentamera* as a potential plant for medicinal purpose. Organoleptic test of fruits sauté, found 60 % respondents said the fruit sauté is generally taste as sauté, and 40 % of them said rather delicious.

1. Introduction

Bellucia pentamera (Melastomataceae) is native to South America. Renner (1986) wrote that B *pentamera* and B *grossularioides* occur from southern Mexico to Bolivia and Mato Grosso, Brazil; cover a similar latitudinal span, but not reach the Guianas.This ese species were introduced to Indonesia via Bogor Botanic Gardens in early of 20th century. (de Kok et al. 2015) reported that it became an introduced weed in Harapan rainforest, Jambi province, Sumatra, Indonesia. B *pentamera* also was reported by Kudo et al., (2014) as an invasive species in Mt. Halimun-Salak National Park and Mt. Ged-Pangrango National Park, West Java province, Indonesia. Dahlia et al., (2016) found B *pentamera* is a kind of medium tree in Baning tourism forest area, Java. B *pentamera* also could be found in West Kalimantan. Renner (1986) wrote that B *pentamera* and B *grossularioides* occur from southern Mexico to Bolivia and Mato Grosso, Brazil; cover a similar latitudinal span, but not reach the Guianas.

Muhelni et al., (2016) studied on fruit feeding butterflies at a conservation forest of oil palm plantation in West Sumatra, and reported that B *pentamera* is a species found as habitat vegetation.

Need a sentence describes the idea of this paragraph, i.e. Although B *pentamera* is mostly known as an invasive plant, recent research show it can be useful for medicinal purposes. Laboratory test of methanol-water fraction leaves extract on Eschericia *coli* and Staphylococcus *aureus* showed the inhibition growth with Minimum Inhibitory Concentration about 125 µg/ml for E *coli* and 500 µg/ml for S *aureus* (Salni and Sari, 2017), but the crude extract of aerial part of B *grossularioides* has no

effect on S *aureus*, *Candida albicans*, and C *krusei*. Furthermore, Slik (2016) wrote the usage of fresh fruits as medicinal plant on antihelmintic function against worms. It is explained that these plants are cultivated and invasive in tropical Asia.

According to Sossonik et al., (2006) in European Journal of Clinical Nutrition, vitamin C is significantly reduce the frequency of the common cold. It is mean if the fruits of B *pentamera* have vitamin C content, it could be used as natural medicine for cold cases too.

Based on the above information, it is interesting to find out information wether B *pentamera* was distributed wherever, minimally in South Sumatra province, and wether its has vitamin C content of their fruits and furthermore how the respondents response to fruit sauté.

2. Material and Methods

Investigation on spatial distribution of B *pentamera* was conducted in June-July 2017. Site visit record, student homework, and reportation of the alumnies of Biology Department, Faculty of Mathematic and Natural Science, Sriwijaya University via social media group were tabulated into table of distribution. Documentation by photograph was done too. Furthermore, the vitamin C content of green immature fruits and yellow ripening fruits were determined by titration methods at Genetics and Biotechnology Laboratory, Biology Department, Faculty of Mathematic and Natural Science, Sriwijaya University. Three volume replication were done for these measurement. Last but not least, organoleptic test was done too, to ten respondent, they were lecturer (8 persons), post graduated student (1 person) and department staff (1 person). Five categories were requested from respondents; wether B *pentamera* fruit sauted is very delicious, rather delicious, just like general sauté daily, quite not tasty or even not delicious.

3. Results and Discussion

Data collected on B *pentamera* distribution show that the plant was distributed at some residence of South Sumatra province as could be seen at the below pictures.

Figure 1. B *pentamera* seedling in Pali

Figure 2. Fruit and flower, in Indralaya

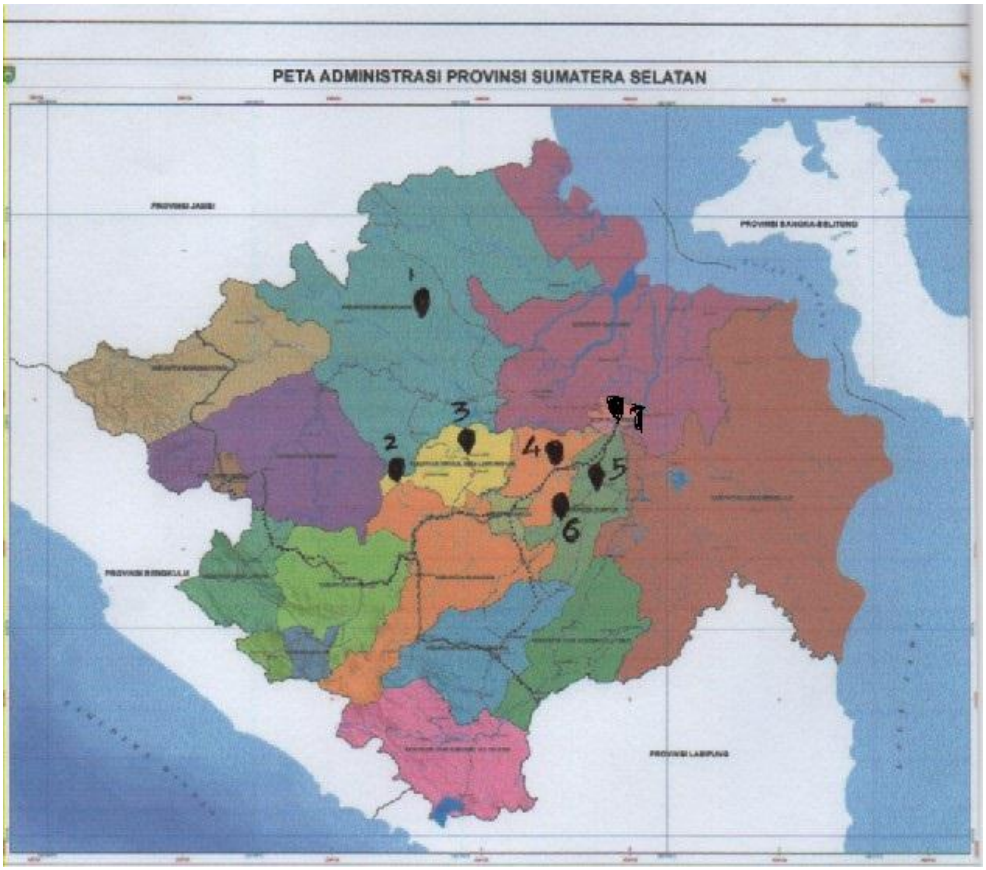

Figure 3. Map of B *pentamera* distribution in South Sumatra province.

1. Dangku forest conservation, Musi Banyuasin residence
2. Talang Ubi district, Pali residence
3. Penukal district, Pali residence
4. Gelumbang district, Muara Enim residence
5. Indralaya district, Ogan Ilir residence
6. Payaraman district, Ogan Ilir residence
7. Palembang City, around SMB II airport area

Figure 4. Fruits serve

Figure 5. B *pentamera* fruit sauté

Vitamin C content Our analysis by titration method show that green immature fruits of *B. pentamera* contains 2.210 mg/100 g of vitamin C, while the yellow ripening fruit one is up to 3.550 mg/100 g. This green-immature value was higher than than fruit of Blueberry (*Vaccinium* sp) about 1.3 mg/100 g; Fig ((*Ficus carica*) about 2 mg/100 g; Kiwano (*Cucumis metuliferus*) about 0.5 mg/100g ; Medlar (*Mespilus germanica*) about 0.3 mg/100 g; and Loquat (Eriobatrya japonica) about 1 mg/ 100 g (USDA Nutrient database cit. Anonymous, 2001). The vitamin C on the ripening ones were higher than Peach (*(Prunus persica*) about 3 mg/100 g. However, these result of vitamin C were still lower than Apple, Grape, Lemon, and Java plum and Tangerine.

Table 1. Vitamin C content of fruits (mg/100 g)

	Immature fruits	**Ripening fruits**
Vitamin C	2.210	3.550

Vitamin C is well known to significantly reduce the frequency of the common cold (Sossonik et al., 2006). As fruits of B *pentamera* have a high vitamin C content, it could be used as natural medicine for cold cases. Slik (2016) also noted that fruits of this plant were effective for antihelmintic usage.

Organoleptic test Organoleptic test found that 60 % respondents said fruit sauté of B. pentamera has general taste as a usual sauté usual, while other 40 % respondents said good taste or delicious. Most of respondents said that the taste was sour, just like "sayur asem" of Indonesian daily vegetable sauté food. Its propose to analyze the other acid content of fruit; not ascorbic acid only.

4. Conclusion

B *pentamera* is distributed around South Sumatra province, were recorded at Palembang city (around airport area), Ogan Ilir(Tanjung Lalang, Indralaya, and Tanjung Batu), Muara Enim (Talang Taling), Penukal Abab Lematang Ilir(Penukal, Talang Ubi), and Banyuasin(rambang dangku) regency. It is found 2.210 mg/100 g of green immature fruits, and 3.550 mg/100 g of yellow ripening fruit of vitamin C. At last, organoleptic test of fruits sauté, found 60 % respondents said the fruit sauté is generally taste as sauté, and 40 % of them said rather delicious.

Acknowledegement

We thank Muhammad Iqbal, Sahira Wirda, Andi Mulfa, Atia Febriana, and Rendra Bayu for distribution data of B *pentamera* trees in South Sumatra province.

References

[1] Anonymous 2016 Peraturan Mentri Lingkungan Hidup dan Kehutanan Republik Indonesia. No P.94/MENLHK/SETJEN/KUM.1/12/2016. Jakarta. p 14.

[2] Anonymous 2001 Natural food-Fruit Vitamin C Content. www.naturalhub.com/natural_food_guide_fruit_vitamin_c.htm

[3] Dahlia I and Mahanal S 2016 Pemanfaatan Potensi Hutan Wisata Baning Sebagai Sumbel Belajar Interaksi Makhluk Hidup dengan Lingkungan di SMP. *Pros. Semnas Pend. IPA Pascasarjana UM. 2016* 1: p. 873-881

[4] De K, Rogier PJ, Briggs M, Pirnanda Dafid and Girmansyah D 2015 Identifying Targets of Plant Coservation in Harapan rainforest, Sumatra. *J Tropical Conservation Science* 8 (1); 28-32

[5] Kudo Y, Mutaqien Z, Simbolon H and Eizi S 2014 Spread of Invasive Plants along Trails in Two National Parks in West Java, Indonesia. *Tropics* 23 (3); 99-110

[6] Muhelni L, Herwina H, and Dahelmi 2016 Stratificatin of Fruit Feeding Butterflies at a Conservation Forest of Oil Palm Plantation in West Sumatra, Indonesia. *J Entomology & Zoology Studies* 4 (4); 525-540

[7] Renner S S 1986 Reproductive Biology of *Bellucia* (Melastomataceae). *ACTA AMAZONICA. 16/17* p 197-208
[8] Salni and Sari Y 2017. Uji Aktifitas Antibakteri Fraksi dan Senyawa Aktif Ekstrak Daun Kardia (Bellucia pentamera Naudin) Terhadap *Escheria coli* dan *Staphylococcus aureus*. Scription. Biology Dept. Fac Mathematic and Nat Sci. Sriwijaya University. Indralaya. (unpublished).
[9] Slik, Ferry2016 *Bellucia pentamera* Naudin. Ann.Sci. Nat.ser. 3; 6;105 (1851)

INTERNATIONAL PROCEEDING
The 2nd International Conference on Science and Technology (ICST)
ISBN: 978-602-5830-19-8, June 2020

Making fish feed by farmers wife in *Nagari* Limau Gadang Pesisir Selatan District West Sumatra

Armen*, Ristiono, M Fifendy and I M Fadlan

Department of Biology, Universitas Negeri Padang, Padang 25131, Indonesia

*E-mail: armenimik@ymail.com

Abstract. Catfish farming can serve as the main effort to increase family income. Economically catfish farming is very profitable. Catfish farming is not difficult and can be done by farmers who do not usually cultivate freshwater fish. The right family member is empowered to improve the family economy through the cultivation of catfish is the farmer's wife. Farmer's wives in Limau Gadang Nagari tend not to improve the family economy, they play the role of taking care of children, doing housework and sometimes delivering food to the fields. The farmer's wife activity is only fulfilling the wife's obligation to husband in a married life. Farmers' wives are economically unproductive in improving the family economy. How to research, selected 20 poor farmer's wife then trained to make pellets. Pellet made from raw trash fish, quail feces, fine bran, and cassava. The pellet formulation is made of 4 kinds. Each formulation produces a quality pellet. Based on laboratory test produced pellet contains very good nutrition for enlargement catfish. The nutritional range of protein is 21% -35% and fat is 17% -22%. Based on the test of enlargement in the experimental pond, obtained the best pellet result influence to the weight of catfish is pellet with 40% trash fish formula, 35% quail feces, 15% fine bran, and 10% cassava. The goal to be achieved in this research is for the wife of farmers can contribute to improving the family economy. Specific targets to be achieved in this study is the wife of skilled farmers cultivate catfish, Nagari Limau Gadang population increases their living standards and TNKS in Nagari Limau Gadang free from the pressure of the population.

1. Introduction

Nagari Limau Gadang is geographically adjacent to Kerinci Seblat National Park (TNKS). Approximately 250 households have cultivated land in TNKS. Farm fields are planted with various types of plants, eg cinnamon, nutmeg, coffee, areca nut, and crops. The activities of making fields are cutting down and burning forests. As a result of logging and burning, many species of flora and fauna are threatened with extinction. Other economic activities of the people who destroy TNKS are the transporters of processed timber, taking the bark of taro, taking manau, looking for gaharu and hunting animals. Economic business activities are pressuring the area of TNKS very rapidly because the forests where they earn money to survive, without their forest can not carry on daily life. The economic activity of farming outside TNKS and planting rice in paddy fields is not sufficient to support the economy of the population. If further stimulated, conducting economic activities in the area of TNKS is not the best choice, but is escaped and forced to save the home economy.

Making a living in TNKS is high risk because the distance to pick up wood to TNKS reaches 16 km and the terrain is very dangerous. Based on interviews of researchers with 20 residents, who carry

on daily activities as transporters of processed wood, all of them say bored to the forest, but circumstances force. Conducting economic activities in the village is not sufficient to meet the needs of life.

According to the researchers, Nagari Limau Gadang residents can conduct economic activities outside TNKS if the government or concerned parties and related TNKS create a choice economic business, for example, poultry breeding and freshwater fish farming. All these efforts are very promising increase in the economy of the population.Nagari Limau Gadang is a Nagari in District IV Jurai whose inhabitants work as farmers. They only rely on rice fields and use resources to fulfill their daily needs. This situation has happened for a very long time. The economic condition of Nagari Limau Gadang residents is very poor, almost all Nagari Limau Gadang residents work as farmers in the rice fields and in the fields [1].

This study focuses on determining the right formula to make a quality catfish (pellet) feed. Pellet fish is expected to be made by the farmer's wife. The wife of farmers who are skilled to make the feed will be able to cultivate catfish. The cultivation of catfish by the farmer's wife will improve the farm household's economy. Increasing the family economy will reduce farmer visits to TNKS [1].

Women (farmers' wives) do not contribute directly to the family's income to support households. The wife of the farmer always helps the husband to do the job as a farmer. Economically, farmers 'wives do not ease the burden of husbands' earnings [2].

The activities of Nagari Limau Gadang residents to earn a living in TNKS, eg farming, hunting and gathering of natural resources will damage the ecosystem and cause disaster. As evidence of ecosystem damage TNKS Nagari Limau Gadang, there have been river floods in 1987,1997, and 2005. According to Yusran [3] damage ecosystem TNKS can be overcome by way of economic activity. One of the economic activities that can be done by the community is freshwater fish farming, because land and water resources are very supportive. Fish farming will improve people's economy so they will not enter the forest area.

Poverty can literally be said to be a state of not having enough. In various views there are three types of poverty that are often expressed are structural poverty, relative poverty and absolute poverty. Structural poverty is understood as poverty arising as a result of government policies and corporate behavior that make the poor, have little or no access to the productive economy. Relative poverty is a poverty that arises not only from the aspect of income but also living conditions in the social environment, while the absolute poverty according to Ferryal [4] is poverty measured from the level of ability to finance a minimum living in accordance with the dignity of human life.

Environmental damage is caused by many factors, especially human activities that are not friendly with the environment itself. Humans should be responsible for preserving the environment, but they are destroying the environment. They tend to take unlimited natural wealth causing damage. They do not care about the needs of future generations. Needs often encourage people to take natural resources TNKS on a large scale regardless of the impact. One of the main factors causing the destruction of the environment TNKS is poverty [4].

Many experts argue that poverty is one of the main causes of environmental destruction in TNKS. Environmental degradation caused by poor people tends to be influenced by their mindset because they are squeezed by poverty, their minds are focused only on the food they can get to survive today. It is this narrow-mindedness that drives them to plunder nature's resources without giving time for nature to renew resources [5].

Forest destruction due to poverty also occurs in the Kerinci Seblat Nagari National Park Limau Gadang. Kerinci Seblat National Park damage is estimated to have been quite severe, the damage has reached about 50 ha. Kerinci Seblat National Park damage includes flora, fauna and land.

Associated with fish farming, fish farmers have problems in getting cheap feed, because fish feed prices tend to increase. According to Sinaga [6] if farmers use factory feed material, the value can reach 70% of all cost components. One effort that can be done for successful freshwater fish cultivation is to make their own feed. Most fish feed raw materials are available in Nagari Limau

Gadang.

Based on research that researchers have done about the cultivation of tilapia as a model of economic activity options overcome the dependence of the population on TNKS. The results showed that the activity of tilapia fish farming can reduce the level of population visit to TNKS [1]. Researchers have also conducted training to make pellets for tilapia against youth and women in Nagari Limau Gadang. The results showed 95% of the participants trained to be skilled at making the feed [7]. Researchers have conducted a study on the ratio of the effect of homemade feed to factory-made feed to the weight of tilapia. The results showed no difference means the influence between homemade pellets with factory-made pellets [8]. Listening to the findings of relevant research, which once researchers do, the catfish cultivation research is very possible to improve the family economy.

Research activities conducted are to guide, train, test and compare to get the best quality pellet. The best quality pellet produced is used as feed for catfish cultivation. To understand the implementation of research it is necessary to understand about catfish and feed ingredients in need. Catfish began to be known in Indonesia around 1986, these catfish live wild in swamps, freshwater rivers, but now the cultivation has been carried out intensively. Catfish has a high nutrient content that consists of 17-37% protein, 4.8% fat, 1.2% minerals, 1.2% vitamins and 75.1% water, rapid growth, the fans are increasing due to the meat tasty and delicious [9].

In Indonesia catfish are known by some names according to their respective regional languages. In the area of West Sumatra called the fish kalang and in the area of Kalimantan called catfish [10]. Characteristics of this catfish can be seen from several parts of the body that is elongated body shape with a flat head, the mouth is at the end or terminal with 4 pairs of tentacles consisting of two nasal nasal fruit, mandibular tentacle in 2 pieces. Catfish have five fins consisting of double fins, which are paired with pectoral fins and abdominal fins, while unpaired are the dorsal fin, caudal fin and anal fin. On the pectoral fins are equipped with a gaff or spurs are non-toxic, when compared with local catfish, spurs catfish shorter and duller. The skin of catfish is not scaly, but slippery because of mucus. Body color like mud, the head to the back of brown to blackish, the stomach and the bottom of the head is more brighter [9].

One of the most crucial elements in the growth and mortality of fish is the availability of adequate feed, in addition to the existing natural feed, so to accelerate the growth of fish should be given nutritious food. Provision of nutrient feed can increase the production of fish maintenance up to three times compared with those not given nutritious food.

Nutrient feed given to fish contains at least protein, carbohydrates and fats. All three of these substances will be converted into energy that is necessary to perform its activities, but the protein contained in a feed more determine the growth of fish than carbohydrates and fats [11].

The function of nutritious food for fish is to nourish the body, replace the damaged cells, after which the remaining excess feed is used for growth. In line with Dewi's opinion, Mudjiman [12] says that the protein present in the feed is needed by the fish as a source of energy, to replace damaged cells and to grow.

Factors that need to be considered in the provision of nutrient feed for the growth of fish is the quality of feed and the amount of feed. Protein contained in the feed is a very important element for the growth of fish. Protein is derived from animal protein and vegetable protein [12]. Nutritious food that can be given for catfish is fine bran, cassava, coconut meal, fish rucah, quail feces.

The feed functions in the growth of fish. To grow the optimal fish required amount and quality of feed enough. The purpose of feeding produces meat in a short time. Provision of nutrient feed can increase fish production up to 3 times compared with that is not given nutritious food, then added by [9] that with the feeding of nutritious, fish weight gain can be 25-35% every month from the beginning.

The raw materials used to make catfish feed are many raw materials available in Nagari Limau Gadang. This raw material is mixed to feed catfish. The raw materials needed to make catfish pellets are (1) trash fish, trash fish is unused fish. Small fish and other types of fish not consumed by the community can be classified into trash fish. The dried trash fish contains 43% -50% protein. Trash fish

can be used as a source of protein to make fish feed (pellet). Trash fish contains proteins that can be standard as a source of protein for fish and poultry feed [13]. (2) quail feces, quail feces are waste from quailing cultivation layers. Quail feces contain 18-20% protein, 11-15% carbohydrate. Quail feces contained high protein and carbohydrate, then quail feces can be used as a source of protein and carbohydrates to make fish feed. The price of quail feces is much lower than other feed raw materials. If fish farmers utilize the nutrient source of quail feces, the price of feed will be lower with feed price made from other raw materials [13]. (3) Cassava is a priority raw material in this study because it is easy to obtain has never been used as a feed raw material. In addition to raw materials, cassava also serves as a glue [8]. Cassava used is a smoothing of cassava that has been boiled. The purpose of boiling is to cause sap and eliminate toxins HCN contained by cassava. In the list of foodstuff analysis issued by the Directorate of Nutrition of Dep.Kes, it is stated that the nutritional cassava is: protein 1.2%, fat 0.3%, carbohydrate 34.7%, water 63% (Rinoto, 2014). (4) fine bran is a by-product of rice milling. The selected bran has a fine texture (grain), not moist, no foul smell, and has a fresh color. Bran contains nutrients: 11.35% protein, 12.15% fat, 28.62% carbohydrate, 10.5% ash, crude fiber 24.46% and water 10.15% [12].

Economically cultivation of catfish conducted by farmer groups is quite successful, they can generate profits for 10,000 seedlings in the 2-3 month period of approximately IDR 5,000,000, if the average farmer group earnings per day IDR 66,000, -, Their income can increase if feed price is cheaper. The feed price used by the farmer group is around IDR 10,000, -, / kg, if the farmer can get the feed for around IDR 5,000, - / kg, each member of the farmer group will earn IDR 93.000, -, per day . One effort that can be done to reduce the price of feed is the farmers of catfish farmers should gather their own feed. The price of homemade food can be made IDR 5.000, -, / kg with good quality.

The right family member is empowered to improve the family economy through the cultivation of catfish is the farmer's wife. Farmers' wives in Limau Gadang Nagari tend not to improve the family economy, they play a role in taking care of the children, doing housework and sometimes delivering food to the fields and to the fields. Farmer's wife is economically unproductive improving the family economy. Generally, their activities only stay at home and only help cultivate the land at a certain time. The role of the wife can be utilized to improve the family economy. Economic activity that can be done by farmer's wife is catfish farming. Catfish farming is not complicated and can be done by the farmer's wife while taking care of the household, generally the farmers have a decent land to be used as a catfish pond [2]. The cultivation of catfish is enough to give profit. The fish farmers gain enough profit. The benefits of cultivation can still be improved if farmers can make their own feed.
Fortunately earned will reach 40-50% If using factory feed gain is only 20-25%.

Making your own fish feed does not require large funds. Price per kg can be reduced to 50%. Raw materials used are raw materials that exist around Limau Gadang, eg trash fish, quail feces, fine bran and cassava. The problems faced by the farmer's wife in catfish farming is the difficulty of getting fish seeds and making feed.

Specific objectives to be achieved in this research is for the farmer's wife can contribute to improve the family economy. Urgency of this study, if the family economy increases, then TNKS avoid the pressure of the population. Innovative findings found in the study are the right nutritional formulations to grow catfish and the skills to make their own quality feed.

2. Research Method

Poor farmer's wife as 20 people are grouped into four groups and designated as catfish farmers. They was educated and directly involved in the research. Research activities: (1) making fish feed with raw materials trash fish, quail feces, fine bran and cassava. All raw materials except cassava was dried and mashed. The cassava is boiled, then all the ingredients was put together into a dough and printed using printing equipment. Wet pellet was dried in the sun; (2). to conduct guidance evaluation and guidance to the group of farmers. If it has not succeeded, the coaching will be continue until it is complete. It performed to formulate the nutrient content of pellets and labratory test.

This activities were contudted to find a good formulation to get proteinn, carbohydrate and fat levels.. By considering the nutrient content of raw materials. To obtained the protein content of 22.92% (minimum requirement of catfish protein by 20%) in 1000 gram pellet, it took 30% trash fish, 45% quail feces, 15% fine bran, 10% cassava, with the provision of trash fish protein 40%, 20% quail stool, 12% fine bran and 1.2% cassava.

Variations of the nutritional formula are made of 4 kinds:

(a) 0% trash fish: 45% quail stool: 15% fine bran: 10% cassava
(b) 35% trash fish: 40% quail stool: 15% finely ground: 10% cassava
(c) 40% trash fish: 35% quail feces: 15% finely ground bran: 10% cassava
(d) 45% trash fish: 30% quail feces: 15% finely bran: 10% cassava

From 4 variations, the best variation will be compared to factory-made feed. The main requirements of artificial pellets should contain high nutrition, easy to process and do not contain toxic, easy to obtain, and affordable prices. How to make the feed (pellet): (1) taken trash fish, quail feces, fine bran, cassava mixed into one and stir evenly, then added with tempeh yeast as much as 125 gram. stirred; (2) paste closed, let stand one night for fermentation process well; (3) fermented paste that has been settled one night mixed with salted fish and papaya leaves that have been ground first, then stir evenly; (4) put up a pellet printer, and put the paste in. The resulting pellets cut to 1.5 cm. Pellet then dried in the sun to dry. Catfish cultivation research by farmer's wife to increase family income in Nagari Limau Gadang Subdistrict IV Jurai, stage 1 has succeeded in developing farmer's wife and make pellet. The study will continue in year II. In year II will be known the quality of standard pellets made by the farmer's wife.

Research activities that have been done are: 1) formulate the nutrient content of fish feed; 2)making formulated feed; 3) test the effect of homemade feed on catfish growth; 4) choose the best formula that will be compared to the factory-made feed; 5)test the best quality pellets in the lab.

3. Results and Discussion

In this research produced various pellet formulas, the level of cultivation and skills of farmers' wives make pellets. The percentage of farmers 'wives who understand and do not understand how to make pellets before they are educated can be seen in table 1.

Table 1. Percentage of farmers' wives who understand and do not understand in making pellets before they are educated.

No.	Activity	No. of Wife Farmers	Not Understood	% Do not Understood	Understood %	Understood
1	Make Pellet	20	20	100%	0	0%

Listening to the low percentage of wives of farmers in making feed. This is in accordance with the assertion of Armen [1]that the women of Nagari Limau Gadang, especially the farmer's wife, only help the husband work to earn a living in the fields and no other activities.

Their work only helps the husband to cultivate the fields in TNKS and cultivate the rice fields. The percentage of farmers' wives who understand and do not make pellets after being educated can be seen in table 2.

Table 2. Percentage of wives who understand and do not understand in making pellets after being educated.

No	Activity	Number of Farmers Wife	Not Understood	% Do not Understand	Understood	% Understood

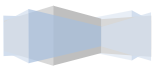

1	Making Pellet	20	3	15%	17	85%

To produce feed catfish, required raw materials containing nutrients. The necessary nutrients are proteins, fats, carbohydrates and minerals. The raw materials made into pellets are trash fish, quail stools, fine bran and cassava. The result of the pellet formulation made from raw material is 4 variation. The percentage of raw material required to make a quality pellet can be listened to in table 3.

Table 3. Percentage of raw materials for quality pellets.

No	Percentage of raw materials for quality pellets			
	Trash fish	Quail feses	Finely bran	Cassava
1.	30%	45%	15%	10%
2.	35%	40%	15%	10%
3.	40%	35%	15%	10%
4.	45%	30%	15%	10%

To make a quality pellet more precedence protein and carbohydrate nutritional content. Trash fish contains 43%-50% protein, quail feces contains 18%-20% protein and 11%-15% carbohydrate, cassava contains 1.2% protein and 34,7% carbohydrate. Fine bran contains 11,35% protein and 28,62% carbohydrates.

Pellets made from 30% trash fish, 45% quail feces, 15% fine bran and 10% cassava obtained pellet containing 22,82% protein and 17% carbohydrate. This pellet is suitable for enlarging catfish. Good pellet protein content for 20-30% catfish and 15-20% carbohydrate [14].

Based on laboratory test Pellet with good nutrition for catfish enlargement is pellet made from 40% trash fish, quail feces 35%, 15% fine bran and 10% cassava. The results of laboratory tests showed the quality of homemade pellets is standard for catfish feed because protein needed for the growth of catfish around 20-23% [7]. The results of homemade pellet laboratory tests can be seen in Table. 4

Table 4. Results of fish feed analysis.

No.Sampel	Result of analysist		
	Carbohydrates (%)	Fat (%)	Protein (%)
1	38.39	2.20	22.08
2	26.55	2.09	34.60
3	39.56	2.32	21.79
4	31.40	1.95	28.03

4. Conclusions

Based on the results of the study, it was concluded that:

1. The farmer's wife does not yet have the skills or knowledge to make catfish feed.
2. The wife of the farmer is able and skillful to make a quality catfish feed.
3. Raw materials trash fish, quail feces, fine bran and cassava can be made into high quality catfish feed.

References

[1] Armen 2014 Tilapia Fish Cultivation as a Choice Model for Economic Activities Overcoming Population Dependence on Biological Resources in Kerinci Seblat National Park (KSNP) in Nagari Limau Gadang Lumpo District IV Jurai, Pesisir Selatan Regency. *Journal of Eksakta*. Volume 2, year XV, JULY 2014.

[2] Armen 2017 Empowering Farmer's Wife Makes Catfish Feed (Pellet) In Nagari Limes Gadang. *Proceeding 2nd International Conference on Mathematics, Science, Education and Technology*.
[3] Yusran.2011. Coastal Resource Conservation in Improving the Economy of Natural Resources. [Online]: http: jujungbandung.com
[4] Ferryal, Marantha Bernard 2010 Poverty and Environmental Damage. http: maranathabernardferryal.blogspot.com/2010/04/koverty-and-damage- environment
[5] Altin, Darus 2007 Improving Community Economy through Fish Culture. [online] .http: fppb.ubb.ac.id/? Page =ubject_ubb &&id = 184
[6] Sinaga 2013 Freshwater Fish Cultivation Can Improve People's Economy. [Online]. http: hariansemarang.net
[7] Armen 2012 Making Tilapia Fish Feed in the village of Limau Gadang Lumpo District IV Jurai, Pesisir Selatan Regency . FMIPA: UNP
[8] Armen 2010 Comparison of the Effect of Giving Factory-Made Feed with Homemade Feed on the Growth of Tilapia. Journal of the exact sciences
[9] Soetomo HA Moch. 2009 Dumbo Catfish Cultivation TechniquesBandung: Sinar Baru
[10] Suyanto, S.achmatun 1996 Catfish Cultivation. Jakarta: Self-help Spreaders
[11] Dewi, Ratna. 2008. The Effect of Percentage of Artificial Feed on Growth and Survival of Carp Chef. Padang: Faculty of Fisheries, Bung Hatta University
[12] Mudjiman, Ahmad 2000 Fish Food. Jakarta: Self-help Spreaders
[13] Rinoto 2014 Making Catfish Feed from Quail Waste. Article [online]: http: notesharianrinoto.blogspot.com. accessed 27 April 2014
[14] Abadi, Iskandar.2015. How to Catfish Cultivation Guide to Livestock Success. [online] .http: // masterz- seo.blogspot.com accessed 28 April 2015

PROCEEDING

THE 2nd INTERNATIONAL CONFERENCE
ON SCIENCE AND TECHNOLOGY

2019

BKS PTN WILAYAH BARAT